DETERMINE: Novel Radar Techniques for Humanitarian Demining

Federico Lombardi

A dissertation submitted in partial fulfillment

of the requirements for the degree of

Doctor of Philosophy

of

University College London.

Department of Electronic and Electrical Engineering

University College London

November 24, 2020

To my Wife, who always supported me, whatever path I took.
To my Son, who will always support my wife, whatever path I may take.

I, Federico Lombardi, confirm that the work presented in this thesis is my own. Where information has been derived from other sources, I confirm that this has been indicated in the work.

Federico Lombardi

Abstract

Today the plague of landmines represent one of the greatest curses of modern time, killing and maiming innocent people every day. It is not easy to provide a global estimate of the problem dimension, however, reported casualties describe that the majority of the victims are civilians, with almost a half represented by children. Among all the technologies that are currently employed for landmine clearance, Ground Penetrating Radar (GPR) is one of those expected to increase the efficiency of operation, even if its high-resolution imaging capability and the possibility of detecting also non-metallic landmines are unfortunately balanced by the high sensor false alarm rate.

Most landmines may be considered as multiple layered dielectric cylinders that interact with each other to produce multiple reflections, which will be not the case for other common clutter objects. Considering that each scattering component has its own angular radiation pattern, the research has evaluated the improvements that multistatic configurations could bring to the collected information content.

Employing representative landmine models, a number of experimental campaigns have confirmed that GPR is capable of detecting the internal reflections and that the presence of such scattering components could be highlighted changing the antennas offset. In particular, results show that the information that can be extracted relevantly changes with the antenna separation, demonstrating that this approach can provide better confidence in the discrimination and recognition process.

The proposed bistatic approach aims at exploiting possible presence of internal structure beneath the target, which for landmines means the activation or detonation assemblies and possible internal material diversity, maintaining a limited acquisition effort. Such bistatic configurations are then included in a conceptual design of a highly flexible GPR system capable of searching for landmines across a large variety of terrains, at reasonably low cost and targeting operators safety.

Impact Statement

The research programme, funded by the charity Find A Better Way (http://www.findabetterway.org.uk/), has been fundamentally directed towards the experimental mapping and characterisation of landmine electromagnetic signatures, as well as developing new configurations for low-cost, accurate and efficient GPR equipment. Special focus has been placed on accurately characterising landmine signatures over a wide range of bistatic angle.

The foremost contribution of the work described in this thesis consists in the perspective of discriminating landmines based on the presence of scattering contributions generated by the internal assemblies of the target, which has demonstrated to be an effective and robust feature for target characterisation. Hence, the presented material, in addition to advancing the knowledge of what can be extracted from the GPR signature of a landmine, opens the possibility to identify targets with internal structure and discriminate the buried anomalies accordingly.

The work has resulted in some key achievements, whose impact is two-fold: firstly, results have highlighted the importance of using neutralised landmines for effectively exploiting the potential of GPR of detecting the internal structure of a target and properly characterising its signature. Secondly, the investigated features are characteristic of the target itself, and are not only source but also scenario independent. This might lead to the development of a common landmine signature database, so that the outcomes can be embedded in a range of GPR systems and made available to a wide range of demining teams.

In addition, yielding the same level of information at a lower computational cost, the suggested bistatic/multistatic approach allows the conceptualisation of a 2D GPR system with the same performance as a 3D one. This consisted of an autonomous ground based platform capable of remotely acquiring dense and regular bistatic data.

Considering that mine clearance operation is a time consuming activity, such conceptual product represents a relevant improvement, outperforming the currently employed hand-held system and possibly relieving the manufacturing cost of such a platform

No clear IP has been identified so far, but might likely emerge in the areas of detection and classification algorithms, signal analysis and processing, bistatic measurement methodologies and antenna development for radar imaging.

Acknowledgements

I would like to thank a number of people who helped me throughout the course of my PhD and contributed to make the work presented in this thesis possible.

First thanks to my supervisor Professor Hugh Griffiths for his constant support and excellent supervision during these years, ensuring successful delivery of this research. This achievement is a result of his constant encouragement and motivation.

My gratitude goes to Dr. Alessio Balleri who has genuinely collaborated for the success of the project and has given me insightful suggestions and counsels throughout the research, as well assistance for the experimental trials. A special mention for Dr. Maurizio Lualdi for his critical insight and constructive collaboration.

The work would not have been possible without the funding support of Find A Better Way, who has sponsored this project, and without the support of the Defence Academy of the UK, who has made available to us the devices employed in the project.

Finally, to my wife Carla who gave me all her unconditional support every day anytime during my PhD.

Last but not least I would like to thank my family and my older and newer friends for their precious support throughout the time of my PhD. Time flies when you're having fun.

Contents

List of Figures

List of Tables

List of Abbreviations

ABC	Absorbing Boundary Condition
ALIS	Advanced Landmine Imaging System
AN/PSS-14	Army-Navy/Portable Special Search
APL	Anti Personnel Landmine
ATL	Anti Tank Landmine
AXO	Abandoned Explosive Ordnance
BLU	Bomb Live Unit
BOR	Body Of Revolution
CCW	Convention on Certain Conventional Weapons
CMP	Common Mid Point
CO	Common Offset
CORD	Collaborative Ordnance data repository
CR	Common Receiver
CS	Common Source
CUDA	Compute Unified Device Architecture
DE	Differential Equation methods
EM	ElectroMagnetic

EOD/IEDD	Explosive ordnance/Improvised Explosive Device Disposal
ERW	Explosive Remnants of War
FAR	False Alarm Rate
FARC	Revolutionary Armed Forces of Colombia
FD	Frequency Domain methods
FDTD	Finite-Difference Time-Domain
FFT	Fast Fourier Transform
GICHD	Geneva International Centre for Humanitarian Demining
GPR	Ground Penetrating Radar
GPU	Graphics Processing Unit
HH	Horizontal Polarisation
HRW	Human Rights Watch
HSTAMIDS	Handheld Standoff Mine Detection System
ICBL	International Campaign to Ban Landmines
ICRC	International Committee of the Red Cross
IDP	Internally Displaced People
IE	Integral Equation methods
IED	Improvised Explosive Devices
IFFT	Inverse Fast Fourier Transform
IS	Islamic State
IWM	Imperial War Museum
JMU	James Madison University

JRC	Joint Research Centre
KCVO	Knight Commander of the Royal Victorian Order
MAG	Mine Advisory Group
MD	Metal Detector
MoM	Method of Moments method
MsMs	Multi-Sensor Mine-Signature
NATO	North Alliance Treaty Organisation
NGO	Non-governmental organization
NQR	Nuclear Quadropole Resonance
OBE	Order of the British Empire
PETN	Pentaerythritol tetranitrate
PHR	Physician for Human Rights
PLS	Proper Lane Sweep
PSG	Pad System for Georadar
RCS	Radar Cross Section
RDX	Research Department Explosive, cyclotrimethylenetrinitramine
SAR	Synthetic Aperture Radar
SF	Single Fold
SNR	Signal to Noise Ratio
SSA	Small Spread Approximation
SVD	Singular Value Decomposition
TD	Time Domain methods

TE	Transverse Electric field
TEM	Transverse ElectroMagnetic
TLM	Transmission Line Matrix method
TM	Transverse Magnetic field
TNA	Thermal Neutron Analysis
TNT	Trinitrotoluene
UAV	Unmanned Aerial Vehicles
UK	United Kingdom
UN	United Nations
US	United States
UXO	Unexploded Ordnance
VNA	Vector Network Analyser
VV	Vertical Polarisation
VVAF	Vietnam Veterans of America Foundation
WWI	First World War
WWII	Second World War

List of Symbols

α	Attenuation parameter
β	Phase parameter
Δf	Frequency step
Δl	Horizontal resolution

Δr	Vertical resolution
ΔT	Time window
Δt	Time step
Δx	Inline sample spacing
$\Delta x, \Delta y, \Delta z$	FDTD model cell size
Δy	Crossline sample spacing
δ	Acquisition error radius
Δ_{off}	Antenna offset sampling
$\varepsilon = \varepsilon' - j\varepsilon''$	Complex permittivity
ε_0	Permittivity of free space
ε_r	Relative permittivity
ε_{tx}, ε_{rx}	Transmitter/Receiver antenna efficiency
λ	Wavelength
μ	Magnetic permeability
μ_0	Magnetic permeability of free space
μ_r	Relative magnetic permeability
ω	Angular frequency
$\sigma = \sigma' - j\sigma''$	Complex conductivity
σ_{RCS}	Radar Cross Section
$\tan\delta = \frac{\sigma' + \omega\varepsilon''}{\omega\varepsilon' - \sigma''}$	Loss tangent
τ_p	Radar pulse width
A_{rx}	Receiver antenna effective area

B	Signal bandwidth
c	Wave velocity in free space
dl	Length of the current element
E	Electric Field
E_i	Incident electric field
E_s	Scattered electric field
f	Wave frequency
f_c	Central frequency
f_t	Transition frequency
G_{tx}, G_{rx}	Transmitter/Receiver antenna gain
H	Magnetic Field
I	Current in the element
I_{TE}, I_{TM}	Incident field strength
k	Phase constant
P_D	Probability of Detection
P_{FA}	Probability of False Alarm
P_{tx}, P_{rx}	Transmitted/Received power
r	Target distance
R_{TE}, R_{TM}	Reflected field strength
T_{TE}, T_{TM}	Transmitted field strength
v	Wave velocity
Y	Admittance

Z	Impedance
Z_0	Impedance of free space
Z_{tx}, Z_{rx}	Transmitter/Receiver coupling losses

If these adults have a problem with these other adults, then go and fight them. [...]. Don't stick a bomb somewhere you'll hurt kids and ordinary women who never did anything to you.

Dolores O'Riordan

Chapter 1

Introduction

A landmine is the perfect soldier: ever courageous, never sleeps, never misses.

P. Jefferson, 1991, [2]

Contamination by landmines and other class of explosive threats is a global issue with a significant humanitarian impact [3]. The first antipersonnel mines appeared during World War I, and after that evidences and reports of landmines usage sharply and continuously increased [4]. As a figure of merit, toward the end end of the 20^{th} century, more than 350 types of devices have been manufactured in more than 50 countries [5]. In their bare form, landmines are explosive traps activated in a variety of means, from pressure actions to electrical triggering, as well as via remote control. A landmine is essentially composed of a pressure plate, a disk on top of the device which depresses as a consequence of an external pressure and initiates the landmine detonation mechanisms, and two different explosive substances, namely the detonator (a limited amount of highly sensitive explosive) and the main charge (a highly stable mixture which is ignited by the detonator charge). All these components are enclosed in an exterior casing, primarily moulded in plastic materials to protect the internal structures from weathering effects and to complicate their detection.

Taking into considerations the available estimates, though not completely reliable, there are at least 60 countries exhibiting a form of landmine contaminations, with figures describing the number of currently buried mines greatly varying, ranging from tens to hundreds of million [6].

While military minefields are laid in a certain order and are reasonably well documented,mines laid by militias are almost never marked or mapped, and when a conflict

ends, landmines are forgotten or deliberately left in the fields, remaining active for decades, thus becoming a psychological weapon that threatens confidence in the local governments [7]. This repercussion is a consequence of the widely recognised military effectiveness of the devices, considering also the fact that they are inexpensive to produce and to deploy even in wide areas. Unfortunately, however, such battlefield advantages has given rise to the humanitarian dimension of landmine contamination, as civilians, regradless age and status, represent the principal victim of mine accidents during peacetime [8]. After-effects on social life and economics are clearly inferable: maimed people cease to be active and productive members of the society where they live, and might require continuous health care, consequently affecting the health care system of the community. Moreover, only the supposed presence of an unmarked minefield might prevent the use of productive agriculture land, thus provoking an overuse of not-affected areas, hinder infrastructure and resources development, and finally endanger the activities of humanitarian aid workers and refugees return [9].

In December 1997, the renowned *Convention on the Prohibition of the Use, Stockpiling, Production and Transfer of Anti-Personnel Mines and on Their Destruction* (often called the Ottawa Treaty) was signed by more than a hundred countries in Ottawa, Canada [10]. The Treaty caused a decrease in the number of mines that are deployed every year, as well as their stockpiling by the agreeing countries. However, thousands of hectares of lands and territories are still contaminated by landmines. With a current demining rate of approximately 200,000 anti-personnel landmines per year, mine clearance is proving to be a much slower process than was thought in the beginning [11].

Numerous techniques have been used to detect mines, and many of them have demonstrated promising results, but the majority has a low maturity level for field application.

1.1 Motivations of the work

It is well known that the metal detector, representing the principal and most advanced sensor for demining operations, suffers from relevant shortcomings, such as limited penetration performance and a high False Alarm Rate (FAR) due to the high sensitivity required to detect landmines with low metal content. According to the Geneva

International Centre for Humanitarian Demining (GICHD) there have been very few instances of completely metal-free mines, but devices containing less than 5 grams of metal, mostly belonging to the triggering mechanisms, the so-called minimum metal mines, still represent a challenging detection task [12].

Lacking of a reliable sensing technology, demining operations remain unsafe, slow and costly processes, putting the deminers at risk as well (60 casualties were recorded in 2017 among deminers [6]). Within the military framework, tools to deliberately trigger mines and clear the path do exist [13], but they can not be adopted as they stand by humanitarian clearance procedures, as they do not meet the safety standards specified by the United Nations (UN) [14].

In the last years, Ground Penetrating Radar (GPR) is emerged as a potential tool for landmine detection, thanks to its capability of successfully detecting minimum metal mines and the possibility of classifying detected objects [1]. Operationally, a high frequency and high bandwidth RF signal is emitted by a transmitter and reflected back according to dielectric variations produced from the subsurface characteristics, composition and stratigraphy. Under this principles, it can be stated that GPR can detect both the presence of a mine and the soil disturbance generated by the presence of a mine, which may be either mechanical (deployment of the mine) or hydrological (soil moisture distribution) [15].

GPR has two important features, which makes it an important sensor for landmine detection [16]. First, it is the only advanced sensor that can produce an horizontal section of the subsurface at different depths, from which it is possible to retrieve volumetric information related to the target. Potentially, high-resolution images might even allow for classification of landmines. Second, the scatter from a target signal can be used for target classification, as it covers an ultrawide bandwidth. The operational capabilities and performance of a GPR sensor consequently depends on the adopted investigation approach and the processing schemes that are adopted for enhancing the data content [17, 18].

Although Ground Penetrating Radar for landmine technology is established, it is capable of further developments to enable continued classification of evolving targets and continued reduction of the size, weight and power of equipment, at the same time to reduce the human presence and supervision [19]. In particular, GPR systems and

processing do not fully take advantage of all the target information that are carried by the reflected signal, valuable features that could be extracted to identify particular types of landmine. This would notably augment the performance of the system and its operational capability [20].

As inferable from its operational principles, GPR basically intended as a subsurface anomaly detector may potentially detect any subsurface object, from natural structures, such as rocks, roots or animal burrows, to man-made debris, such as shell casings and urban debris. Considering that these objects may constitute the vast majority of subsurface scatterers, and sometimes even the only scatterers, the false alarm rate may inevitably rise, given also the high probability of detection required by mine detection sensors.

To this, it should be added that landmines are not the only explosive hazards to civilian populations once a war ends. Devices that did not explode when intended or left over after a battle still pose a risk of detonation, essentially acting as a minefield. These include bombs, artillery shells, mortars, rockets and grenades, or cluster munitions. As well, many post-modernist conflicts have seen a surge in the replacement of conventional landmine with improvised explosive devices, unconventional explosive weapons built with non-military components and without manufacturing standard.

The principal question is, are there scattering features that can uniquely define the nature of the target and unambiguously characterise a landmine? And, would it be feasible to increase the achievable level of information without increasing the complexity of demining operations?

Theoretically, a scattering object can be completely determined based on its shape, physical dimension and dielectric permittivity properties variations [21]. All these features can be determined by resolving an inverse problem [22], but the amount of the scattered field measurements required to reduce the ill-conditionedness of the problem, as well as the implicated computational costs, almost preclude the practical realisation of this approach.

The ability to separate landmines from clutter targets is essential if a sensor is to exhibit both a high probability of detection and an acceptable false alarm rate. When a buried target is illuminated by an electromagnetic wave, energy scatters via several mechanisms, each of them containing characteristic information that is essential for

target recognition. Therefore, the key to a better target recognition lies in understanding and analysing the electromagnetic signatures of landmines.

Mines (as man-made objects) exhibit a degree of vertical and circular symmetry that is not frequent in the majority of clutter targets. From a scattering behaviour perspective, an object exhibiting these symmetry characteristics will carry unique and distinctive scattering responses in terms of bistatic angle and polarisation diversity, the analysis of which can provide valuable information for separating targets with some symmetry from subsurface objects that do not have this characteristic. In this manner, landmines can be discriminated from non-symmetric objects based on the evaluation of their scattering behaviour.

Still, given the resolution capability, a large number of false alarms can fall in this category, if one just relies on shape considerations. In addition, a large number of landmines have been moulded in irregular shape to impede a visual detection and the symmetry and regularity feature could vanish when the target is inclined, hence the shape could not be a discriminant feature. In a radar image, a symmetric target will nearly always appear symmetric, whereas an asymmetric target will often appears asymmetric.

To overcome this problem, advanced descriptors that could exploit features beyond the physical properties of the object need to be collected and extracted from the radar data in order to identify a discriminant property.

A discriminant plane can be found in the nature of the target. A landmine is a complex object, composed by a number of different assemblies and structures to allow a proper detonation and activation of the mine, thus its signature would likely differ from the one collected from a natural clutter object. The potential of GPR imaging to show the internal structure of a landmine, given the prohibitive false alarm rate, can be a significant improvement for the detection and especially the identification of buried landmines. The presence of internal scattering components in the target radar signature represents a discriminant feature, and it can be unambiguously associated with a composite objects, hardly found in the majority of clutter targets.

1.2 Research scope and methods

The approach developed in this Thesis aims at exploiting possible presence of internal structure beneath the target, which for landmines means the activation or detonation assemblies and possible internal material diversity, maintaining a limited acquisition effort. Under this perspective, the point in question is whether this family of targets could benefit from angular diversity, as few contributions have been found addressing this issue. Indisputably, identification and recognition are only possible if these reflections are detected, therefore the first consideration is that a sufficient resolution is needed in the collected data.

Three major milestones and research challenges have been identified:

- **Evidence of internal reflections from landmines**: as these contributions are hardly to be present in other targets than landmines (or generally buried man-made threats), the challenge is to be able to effectively sense these internal reflections and evaluate the level of accuracy of the GPR images. Ideally, being able to delineate the internal design of a target could fill the gap between detection and recognition, breaching also the path to target identification.
- **Bistatic signature analysis and characterisation**: as per previous considerations, each of the internal components of a landmine will have its angular scattering pattern, consequently, a change in the separation between the transmitter and the receiver could better highlight these events and bring an improved target characterisation.
- **Design of a bistatic system**: the optimum configuration is intended to be deployed in a flexible and mobile ground penetrating radar platform capable of surveying several terrain conditions. This equipment must be reasonably low cost and affordable to meet the dynamics of the humanitarian demining market and to make it effectively deployable.

Ideally, the ultimate outcome needs to be as simplest as possible, i.e. an image with only landmines positions highlighted, regardless of any physical, geometrical and environmental matters. The system architecture should not only provide a logistical progress over the current operations methodologies, but also improve the safety and reduce the hassle of the operator. Area surveying and object detection are repetitive, meticulous and painstaking steps in demining operations, reasons for which a machine-based ap-

proach, rather than a manual sensing, can provide important advances in operations quality. From a practical point of view, an autonomous solution will eliminate the need for extensive training of operators, which is a time consuming and subjected to a performance decay, and ideally allows continuous operations, handing down to the human the manual removal of the identified objects only. Even if the last step can be regarded as the only really dangerous part of manual mine clearance, it strongly relies on the performance of the area sweeping step. Finally, as GPR imaging performance depend of the data collection accuracy, the constancy of operations of an automatic solution can hardly be matched by manual surveying. The ultimate solution can be therefore identified with a reliable unmanned platform, which should have the capability to operate in complex and adverse survey envronments, with flexible locomotion features and control modes, fulfilling at the same time the operational requirements of the mounted GPR platform. Finally, its deployment and operations should be accessible even to non-expert users. Lastly, the overall cost of the equipment should not significantly exceeds, on a sensor to sensor basis, the production and deployment of current metal detector tools.

The mentioned research question and the related milestones have been addressed by analysing the GPR responses of a number of landmines characterised by different design and structure, with different environment conditions and geometry, and evaluating the information that can be extracted from the different operational mode in which GPR can be operated. For each step, a comparison to a solid replica of the target has been computed to verify the results.

An introductory evaluation has been obtained through the employment of FDTD numerical simulations, to gain a fundamental understanding of the scattering mechanisms that contribute to the overall target signature and to validate the research scope. An additional preliminary analysis has been made carrying out a series of free space measurements, with a consistent wavelength to target size ratio (compared to the subsequent field experiments) to give the off the ground signatures a meaningful value. Experimental trials have been performed in controlled conditions and using a dedicated GPR platform assembled for the purpose of the study and based on already available technology.

It is essential that properly constructed landmine models are used for test and

development, otherwise their signatures could differ from real ones. Considering that landmines are objects which are difficult to replicate, it was the first priority to obtain reliable inert (or neutralised) landmines to ensure the collection of landmine signatures as close as possible to those of a real live device. Three representative landmines, provided by the Defence Academy of the UK, have been used. These were complete with all their external and internal components and were filled with a high explosive simulant commonly used to train UK Ammunition Technical Officers.

Given the reliability of the proposed approach, in particular the employment of inert device and the controlled conditions of the trials, the collected signatures and images can constitute a preparatory basis for the development of a catalogue of landmines signature, which could benefit future works and researches. This possibility is of notable importance also for target recognition/identification algorithms, for which a large number of observations, as much accurate as possible, are needed. If one considers the large number of research institutes that are currently involved in the topic, it is obvious that the learning curve can rise faster if a reliable and consistent database is available.

1.3 Scientific innovation and perspective

The foremost novelty aspect of the work described in this Thesis consists in the perspective of discriminating landmines based on the presence of scattering contributions generated by the internal assemblies of the target. Following this direction, the main original contributions are listed below.

- Demonstration of the capability of GPR methodology of discriminating the internal structure of the target, both through a numerical prediction and employing a realistic GPR platform in controlled conditions. A thorough evaluation of this GPR potential is previously not found in the literature.
- Accurate delineation of the internal design of landmines from a series of dense 3D GPR images. The close agreement with the actual structure could pave the way for target recognition scheme, as the internal assemblies could be uniquely associated with a particular family of landmines.
- Employment of different bistatic geometries to additionally characterise the internal design of the target, including the location and spatial extension of the scattering contributions, showing that the same level of information can be ob-

tained through a more efficient survey scheme (compared to a dense and accurate 3D volume).

- Validation of the previous results varying the inclination angle of the buried target towards the surface to prove that the strategy could provide the same performance even when the symmetry of the target is not maintained.

1.4 Personal publications

The following publications have resulted from the work presented in this thesis.

Journal Papers

- **Lombardi**, F., Griffiths, H., Wright, L., Balleri, A., "Dependence of landmine radar signature on aspect angle", *IET Radar, Sonar & Navigation*, 11(6): 892-902, 06/2017.
- **Lombardi**, F., Griffiths, H., Lualdi, M., "Sparse ground penetrating radar acquisition: implication for buried landmine localization and reconstruction", *IEEE Geoscience and Remote Sensing Letters*, 16(3): 362-366, 03/2019.

Conference Papers

- Wright, L., Balleri, A., Griffiths, H., **Lombardi**, F., "Multi-perspective high range resolution profiles of landmines", *IEEE Radar Conference, 2015*, Johannesburg, South Africa, 51-55, 10/2015.
- **Lombardi**, F., Griffiths, H., Lualdi, M., "The influence of the spatial sampling in GPR surveys for the detection of landmines and IEDs", *13th European Radar Conference (EURAD)*. London, United Kingdom, 322-325, 10/2016.
- **Lombardi**, F., Griffiths, H., Balleri, A., "Influence of internal structure on landmine radar signatures", *13th European Radar Conference (EURAD)*. London, United Kingdom, 161-164, 10/2016.
- **Lombardi**, F., Griffiths, H., Balleri, A., Lualdi, M., "Preliminary results on multi offset imaging of landmines", *2017 9th International Workshop on Advanced Ground Penetrating Radar (IWAGPR)*, Edinburgh, United Kingdom, 1-6, 06/2017.
- Lameri, S., **Lombardi**, F., Bestagini, P., Lualdi, M., Tubaro, S., "Landmine detection from GPR data using convolutional neural networks", *2017 25th Eu-*

ropean Conference on Signal Processing (EUSIPCO), Kos, Greece, 508-512, 09/2017.

- **Lombardi**, F., Griffiths, H., Balleri, A., "Bistatic radar signature of buried landmines", *2017 IET International Conference on Radar Systems*, Belfast, United Kingdom, 1-6,10/2017.
- **Lombardi**, F., Griffiths, H., Balleri, A., "Landmine internal structure detection from ground penetrating radar images", *2018 IEEE Radar Conference*, Oklahoma City, United States, 1201-1206, 04/2018.
- Picetti, F., Testa, G., **Lombardi**, F., Bestagini, P., Lualdi, M., Tubaro, S., "Convolutional autoencoder for landmine detection on GPR scans", *41st International Conference on Telecommunications and Signal Processing (TSP)*, Athens, Greece, 1-4, 07/2018.

1.5 Thesis outline

The thesis is split into 7 Chapters. The Chapter following this introduction provides a detailed and comprehensive description of the landmine problem, analysed in all his facets, from its socio-economic impact to the technological challenges. Chapter 3 develops a critical review of the main publications relevant to the research context, covering the existing literature with respect to the highlighted milestones. A particular focus is put on publications covering the radar application for sensing and identifying the scattering contributions from the internal structure of landmines, including bistatic and/or multistatic and polarimetric strategies. Weaknesses and limitations of the listed contributions are also given to motivate the originality of this work.

Chapter 4 provides the analytical basis for addressed problem and the subsequent experimental section. This chapter is roughly divided in two, where the first part covers the fundamental principles governing the GPR methodology and summarises the key concepts influencing electromagnetic wave propagation from a theoretical perspective. Special attention is put on the constraints that the demining framework possesses. Discussed theory is then investigated in the second part of the Chapter, in which a series of numerical simulations involving the key variables affecting the imaging performance is developed and assessed in the light of the research objectives here described.

Chapter 5 is dedicated to the assessment of the design and the outcomes of the

experimental campaigns. The contents of this chapter includes: a set of initial measurements of the landmine signature changing the antenna orientation and target aspect angle. This dataset, acquired both in free space and in a sand pit, provides a preliminary evidence of the effects generated by the target internal structure. After highlighting some limitations related to unfavourable geometries and complex target design, and after showing that neither a 2D profile can guarantee the detection of the internal contributions, the Chapter presents the results obtained from a 3D GPR experimental campaign which demonstrate the capability of accurately delineating the internal design from a set of images, confirming the suitability of the methodology and the validity of the approach. Some limiting considerations on the acquisition constraints for producing such high resolution images are illustrated as well, underlining the required acquisition effort. Finally, two different bistatic geometries, a common receiver (CR) and a common mid point (CMP) scheme, are evaluated in the light of assessing the benefits that a variation in the antenna separation could bring for target characterisation and acquisition efficiency. A summary of the findings is appended to each section.

After a detailed overview of the logistical and economical context for a successful deployment of a landmine detection system, the results of the experimental campaigns are analysed in Chapter 6 in the light of a conceptualisation of an unmanned bistatic GPR platform. The aim of this Chapter is to provide a series of operational parameters that should be considered when designing such a platform.

The conclusion of this work and suggestions for future research are given together in Chapter 7.

Chapter 2

The landmine problem and the response of technology

Technological progress has merely provided us with more efficient means for going backwards.

A. Huxley, 1937, [23]

In the last decades landmine [1] detection has become a major topic in sensor development and research. The main reasons that have pushed and are still pushing countries for the clearance of mine-affected territories are not only injuries caused to innocent people by these remnants, but also as they prevent the usage of a significant proportion of agricultural lands, feature that represents an additional barrier to communities development especially in low-income countries [24].

Cheap and easy to use, landmines represent a highly attractive battlefield weapon, and therefore they have been used by both official armies and guerrillas, as well as during conventional and insurgency wars alike, in flagrant violation of international humanitarian law. These ”eternal sentinels” recognise no armistice and long after the fighting has ended, they still prevent a return to normality. Unlike a bomb or an artillery shell which is intended to explode approaching or hitting the target object, landmines act indiscriminately, maintaining a killing and maiming potential unless deactivated or defused. Landmines are indiscriminate as they are triggered by their victim, whether

[1] defined from United Nations (UN) protocols as ”*a munition placed under, on or near the ground or other surface area and designed to be exploded by the presence, proximity or contact of a person or vehicle*”.

military or civilian, without distinguishing between them [25].

In the five decades since the end of the Second World War, mine warfare has gained increasing importance on the battlefield. Given the range of tactical situations, terrain and types of force that used them, mines have undoubtedly been one of the most flexible weapon systems of the late twentieth century. Mines became a significant security concern after wars because little effort was made to retrieve them and clear the ground, and few (if any) records of their deployment existed. In several occasions, mines were laid nearby areas commonly frequented by civilians, such as transport and resources infrastructures, that in the end went from being elements to protect to the very victims. Returning refugees generally had no knowledge of mined areas and were especially prone to treading on them [26, 27].

That mines were not cleared by government forces at the end of conflict was the result of several factors. In general, many of the conflicts did not end in a simple manner, the security situation remained tense even after the official ceasefire. Government forces rarely saw any advantages in marking mines as these were weapons on which they significantly relied.

The presence, or the suspected presence, of buried landmines has the main consequence of making potentially usable land inaccessible, hindering farming and working activities, as well as denying development and post-war reconstruction. The return to home of refugees and displaced people is also endangered, along with putting humanitarian and supplies delivery activities at risk, with operators less prone to enter mined areas [28]. Similarily, there have been several instances of landmines specifically targeting peacekeeping forces and operations, as happened to U.S. convoys in Somalia during the United Nations intervention in Somalia [29], or in Bosnia, where mines were laid on evacuation roads to block refugees rescuing activities [30]. In Afghanistan, one of the most infested country, some territories are compeltely inaccessible to demining operators [31]. In Colombia, during the last years, FARC dissidents has repeatedly damaged and even seized demining operator vehicles and equipment, eventually causing the suspension of operations[32]. Security concerns for demining operators are affecting activities also in South Sudan, where in several occasions aid workers have been the subject of ambushes or robberies [33].

No precise figure on the total number of landmines still buried in the ground can be

determined, but it is clear that the psychological impact prevails over numbers, as it is sufficient that an area is suspected to be contaminated to make it unusable.

A comprehensive and detailed factual analysis of the landmine contamination situation is annually released by the International Campaign to Ban Landmines network, and published in their *Landmine monitor* periodical, from which some of the following figures have been extracted. As of December 2018, sixty states and territories have a reported anti-personnel mine contamination, with a further 10 countries having either suspected or residual anti-personnel mine contamination. However, it is understood that also states for which no estimate is provided are considerably contaminated. The total amount of land cleared in 2017 reached approximately 128 km^2, declined for the third year in a row although in some areas the amount of land release through survey was doubled, with at least 168,000 anti-personnel mines destroyed, figures that are possibly underestimated due to the lack in reporting from some actors (armies or even informal clearance) [6].

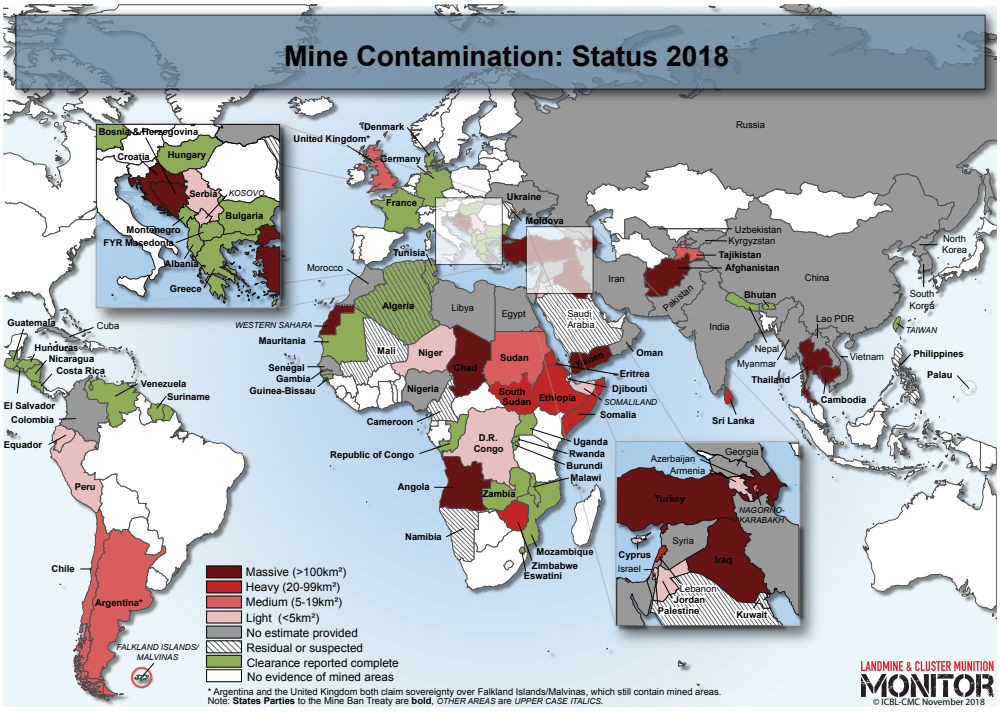

Figure 2.1: Contamination status as of December 2017. *Courtesy of icbl.org campaign.*

In the calendar year 2017, more than 7,000 people have been killed or injured by a victim-activated device, including anti-personnel and anti-vehicle landmines, improvised mines, cluster submunitions and other explosive remnants of war (Fig. 2.2), was recorded, a 25% decrease from the previous year, even if it is widely agreed that

these numbers might be underestimated due to a lack of proper reporting infrastructure [6, 34].

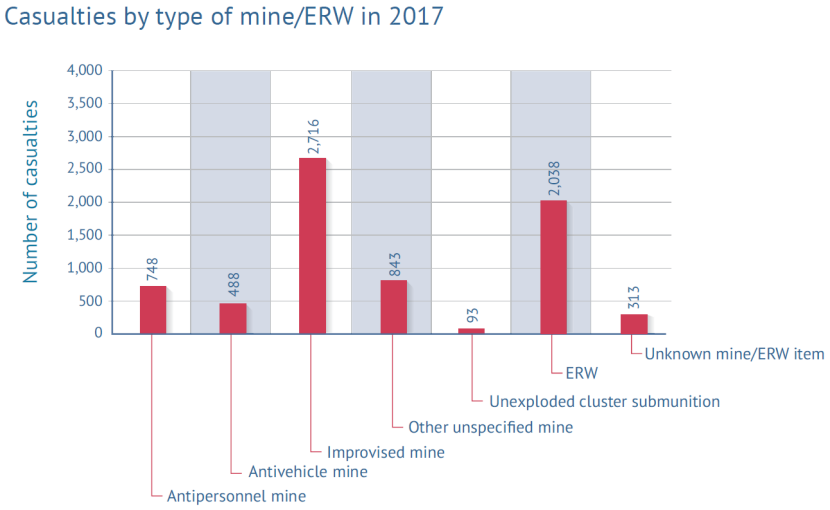

Figure 2.2: Casualties from remnants of war as of December 2017. *Courtesy of icbl.org campaign.*

Primary victims are unarmed civilians, particularly children, a casualties pattern unfortunately portraying the predominant humanitarian dimension of the problem, main features that supported the adoption of the Mine Ban Treaty: 87% of casualties were civilians in 2017 where the status was known [35]. Finally, more than the majority of the total number of casualties recorded in 2017 occurred in 35 States Parties to the Mine Ban Treaty (Fig. 2.3).

Government forces of Myanmar used anti-personnel landmines in 2017 [36], while in at least eight countries, including Yemen and Colombia, armed factions and terrorist groups have produced and used improvised landmines [32, 37]. Again, the limited amount of information does not allow a precise identification of the actual impact on such figures resulting from new use of anti-personnel mines from the already present contamination.

The existence of landmines is considered a vital socio-economic and environmental problem facing many countries exposed to their use. Unfortunately, the majority of the affected countries are among the least developed countries, for which this deadly heritage has a critical impact on communities growth and development. The contamination affects the entire post-conflict reconstruction processes, as landmines and explosive remnants restricts freedom of movements, both internally and cross-borders,

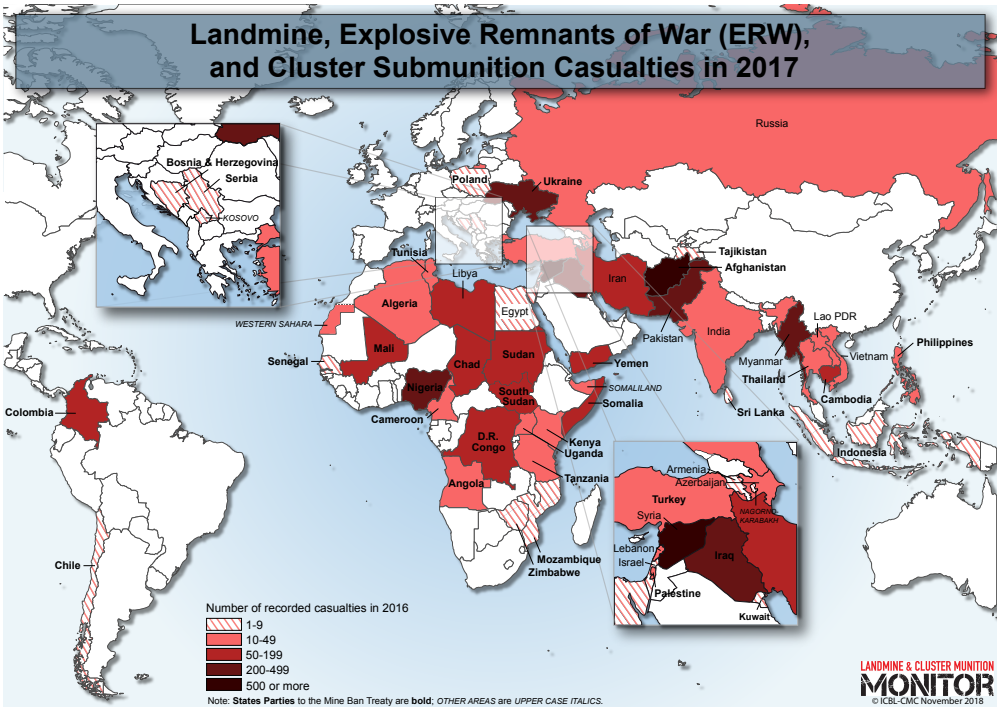

Figure 2.3: Recorded casualties as of December 2017. *Courtesy of icbl.org campaign.*

restraining infrastructure development, rehabilitation efforts and even attractiveness for foreigner investment. From an environmental perspective, such asymmetric land usage might bring major ecological repercussions, such as reduced biodiversity and chemical pollution.

The international community has responded to the threat of landmines and unexploded ordnance by spending over $5 billion on mine clearance in the last 10 years (Fig. 2.4), with the highest level of international support in a single year recorded in 2017 (more than $673 million). The overall trend is for spending to rise, with over $395 million (93% of total contribution) spent on mine clearance and risk education in 2017. Unfortunately, removing landmines requires the development of dedicated mine action programmes, including field surveys, ordnance clearance and consequently it can be easily understood that the process is significantly more expensive, up to ten times higher, than the cost of device production and deployment. However, delineating a cost–benefit evaluation of landmine clearance is contradictory, as it is complicated to assign a precise number that defines benefits such as casualties and medical costs saved, as well as community development benefits, including revenue from new production and industries or tourism incomes. Typically, a figure relating casualties reduction with respect to the proportion of cleared area and their productive value is assumed. This

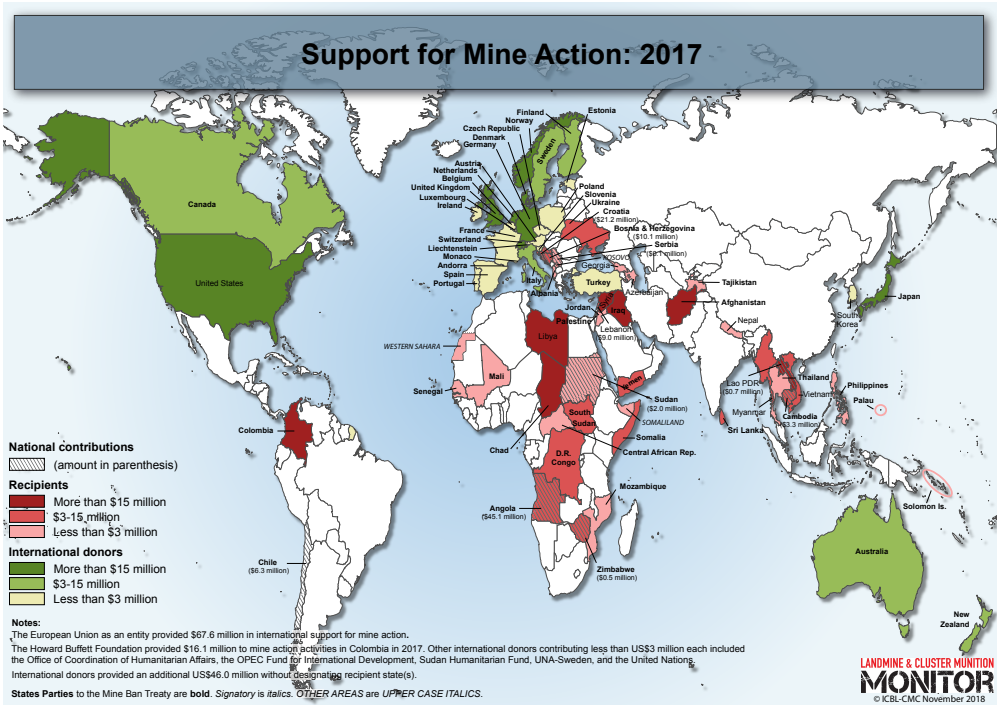

Figure 2.4: Support for mine action as of December 2017. *Courtesy of icbl.org campaign.*

estimation includes the land usage expectation, so that agricultural lands are clearly of major importance than already abandoned areas, due to the additional values brought by potential farming income, as well as considerations on the direct benefits that clearance of a particular area might bring to the community, so that transport and supplies infrastructures are critical categories, as they might reduce travel costs. As a result, the actual economic value of clearance operations is widely underestimated. For these reasons, landmine programs are initially targeted towards minefields with the greatest expected benefits and economic returns.

2.1 Evolution of mine warfare

The following section is meant to provide a compact overview of the historical milestones that have characterised the development of landmines design and to outline the evolution of the approach towards their use. A dedicated and more comprehensive breakdown can be found in [2] and [38].

Even if today landmines might span from rudimentary devices to weapons manufactured with sophisticated materials and incorporating highly technological components, they all descend from non-explosive, defensively-oriented predecessors (Fig. 2.5), such as spikes and stakes that were employed by ancient armies [2]. Therefore,

small and concealed objects with the scope of slowing the advancing enemy primarily by mean of injuring and maiming, rather than killing.

The word ”mine” is derived from the Latin word *mina* which means ”vein of ore”, originally applied to the mining activities and then borrowed by military engineers dealing with the digging of tunnels under walls of forts and castle during sieges to make them collapsing. The first use of concealed traps in a tactical defensive context to gain

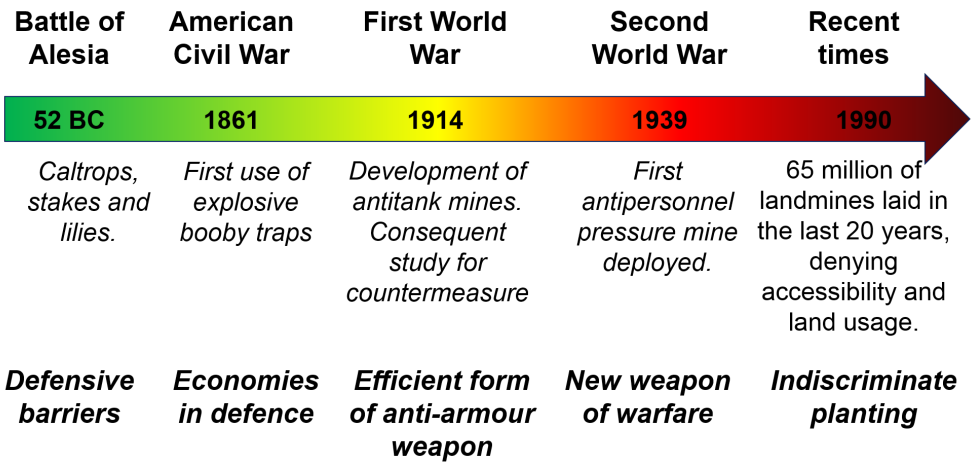

Figure 2.5: From defensive barriers to contamination: the evolution of concealed traps.

advantage on the battlefield dates back to the Siege of Alesia, in 52 B.C., when Emperor Caesar used pits, arrays of stakes and devices denominated *caltrops* to slow the advancement of the Gauls (Fig. 2.6a), a defensive strategy later replicated in some of the major battles occurred during the 14th and 15th centuries, including the First War of Scottish Independence (Battle of Bannockburn, 1314 [39]) and during the English Wars of the Roses (Battle of St. Albans, 1461 [40]), mainly to cripple cavalry. The discovery of gunpowder significantly transformed the siege warfare equipment, opening the way to the development of explosive charges, such as the *fougasse*, a buried cannon in front of a defensive position designed to scatter rocks and debris over a wide area (Fig. 2.6b). A conceptual replica of the fougasse was realised in the mid 1950s with the deployment of the extremely lethal American M18A1 anti-personnel directional fragmentation mine, better known as the ”claymore” [2].

Precursors of conventional landmines appeared in the 15th century at the Battle of Agincourt in France and in the 18th century during the American Civil War, when

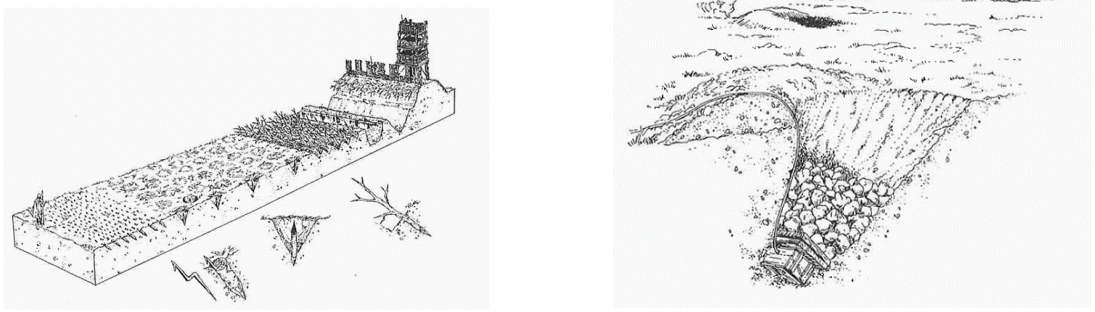

(a) Romans fortification. **(b)** American fougasse.

Figure 2.6: Landmine warfare precursors. *Taken from [2]*

the first concealed devices designed to explode on target contact, consisting of artillery shells connected to a highly sensitive percussion device, were deployed by the US Confederate Navy following the intuition of their commander Brigadier General Gabriel J. Rains (the so-called Rains mines, [41]). On May, 4th 1862, a horse rider that was scouting a road following the siege of Yorktown, VA, activated one of the earliest landmines, which had been fabricated by assembling pieces of artillery to be exploded by pulling trip wires, becoming the first victim from a pressure-operated landmine [42]. Even at that early date the use of mines were often judged as an unethical form of combat, with Union commanders General George B. McClellan and General William T. Sherman addressing them as ”murderous and barbarous” and ”not warfare, but murder”, respectively [43]. However, the ability of a highly inexpensive device in damaging the hull of a warship beyond all possible recovering had represented a very persuasive economic argument for its deployment [44]. The Civil War experience also demonstrated the longevity of the threat posed by landmines, considering that as late as 1960s, at least five devices belonging to this period were recovered in Alabama, still potentially functioning.

During the African campaign in the 1880s, the British Army often used fougasses and mines, either tripwire activated or pressure operated, commonly manufactured in the field with shells and battlefield debris. By the 20th, a countless number of regular armies started to routinely use and deploy landmines during war operations.

The development and use of the landmines became a major military strategy between 1918 and 1939. As a response to introduction of the assault tanks by the Allied

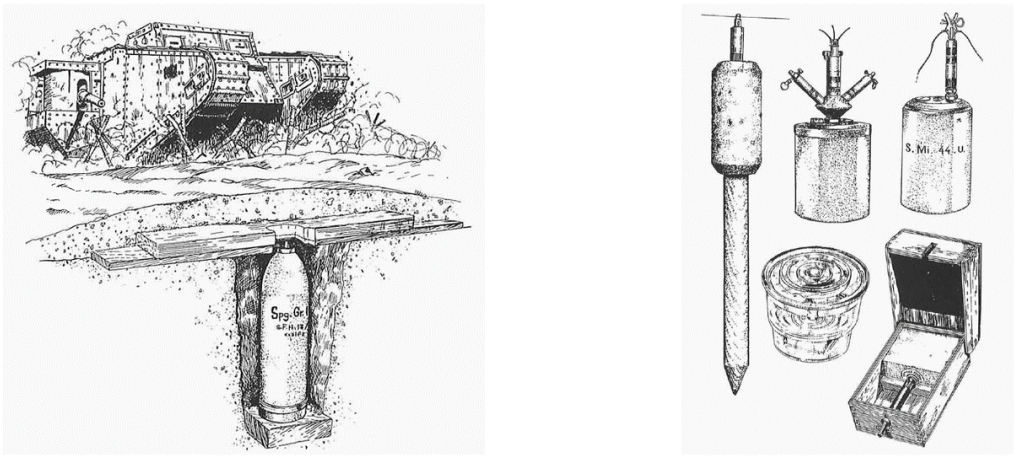

(a) Anti-tank mines from WWI. **(b)** Anti-personnel mines from WWII.

Figure 2.7: Early German landmines. *Taken from [2]*

forces and to limit their effectiveness, the Germans started to design and widely deploy mines within the First World War battlefields, initially consisting of buried artillery shells and covered with wooden boards to enhance the activation range (Fig. 2.7a).

Such devices were mainly laid in routes expected to be travelled along by the advancing enemies. To give a numerical perspective, the Germans entered the Second World War with just two models of anti-tank mines and a single anti-personnel mine, but within 5 years they manufactured sixteen additional and different types of anti-tank mines, ten anti-personnel mines (Fig. 2.7b) and a wide range of explosive traps and improvised devices [40]. Considering that from 1942 they almost constantly fought on the defensive, the significance of minefield deployment becomes increasingly important.

In early 1940 along the Franco-German border, French troops encountered a novel device which bounded out of the ground before detonating at waist height, the *Schrapnellmine*. Derived from the previously described fougasse, the S-mine was the size of a can and typically triggered by the traction of a tripwire, which activates a small explosive charge causing the buried canister to be ejected from the ground and provoking the detonation of the main charge, scattering 350 steel balls out to a range of 150 metres [38].

The first major innovation of the war was in 1942, with the introduction of the wooden-cased mine. The smaller amount of explosive that the case could contain was sufficient to leave its victim limbless but not strong enough to kill him, opening the way to the practical intention of maiming rather than killing. At the end of 1944, Ameri-

can troops first encountered metal-free mines in Lorraine, France, where in a single minefield a total of more than 12,000 mines made out of bakelite and wood was found, firstly highlighting the difficulty in detecting them with conventional metal detectors. Even if it is estimated that hundreds of million of landmines have been laid during the conflict, at this time mines were still used in a controlled manner and specifically targeted at soldiers. It was not until the 1960s that the deployment of landmines run out of control [45]. It was during the campaigns in North Africa that the Italian forces firstly developed an air-delivered, scatterable mines, the so-called AR-4 Thermos Bomb, a cylindrical-shaped bomb arming upon impact and equipped with an anti-disturbance fusing mechanism to be dropped over enemy troop concentrations or beyond enemy lines to impede its withdrawal. Nevertheless, this novel design was almost abandoned given the numerous accidents related to premature activation [46].

Developments in the production and deployment of weaponries, landmines included, accelerated in the decades following World War II, primarily as a consequence of the changing battlefield requirements, in the nature of warfare and the development of new military technologies. With the end of the open field fighting and the beginning of the Cold War, the deployment of barrier minefields became a standard activity for national border defences, not only for keeping the enemy out but also, as in the case of East Germany, designed to keep the population in [47].

Since 1960s, overcoming the initial diffidence of the Italians in the scatterable devices, the United States started to pioneer their development and consequently their widely adoption, mainly as a response of the nature and features of the Korean and particularly the Vietnamese battlefields, for which the use of traditional protective minefields was of little use to the American forces, facing an enemy in permanent movements throughout the countryside. Therefore, several sophisticated classes of air-scatterable and self-deactivating antipersonnel mines that could be deployed from both artillery, helicopter and aircrafts were introduced (Fig. 2.8), to interrupt the flow of goods, materials and men from North to South Vietnam through Laos and Cambodia [2].

The most commonly used scatterable landmines in the Vietnamese scenario were the BLU-43 and the BLU-44, weighting only 20 grams but filled with a liquid explosive capable of tearing off a foot. These were the forerunners of the Soviet PFM-1, or

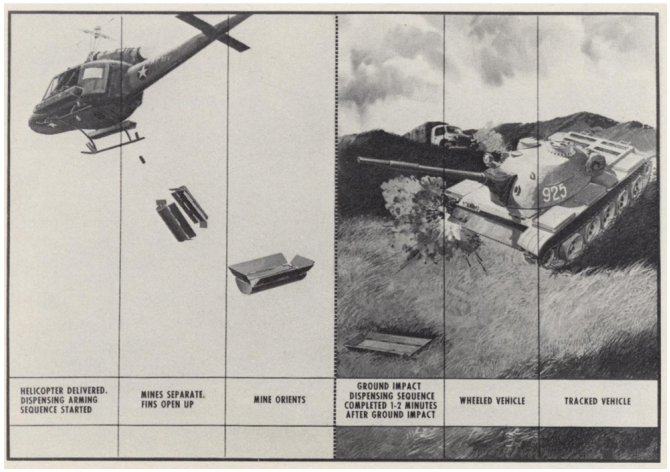

Figure 2.8: The U.S. M56 mine dispensing system. *Taken from [48]*

"butterfly" mine, used extensively in Afghanistan during the late 1970s. The downside of such effective deployment strategy, i.e. the possibility of saturating a wide area with thousands of landmines in a very short time and effort, has been that American forces repeatedly found themselves retreating across their own minefields or and maimed by American-made mines [46].

During the Cambodian conflict, minefield were intentionally deployed by government troops around the perimeter of enemy villages to accelerate their surrender, often in combination with artillery fires to cause the the enemy, mainly civilians, was forced to flee into the minefields. Examples of civilians being the primary target of landmines warfare can be found also during the Soviet-Afghan wars, where both Moscow and Kabul forces deliberately mined agricultural land and water supply infrastructures to sabotage civilians support of the Mujahideen, and in Northern Somalia, where the government Somali National Army used to lay landmines around towns, livestocks and grazing lands [49]. In both cases, there was no pretence that the widescale use of mines was directed purely at the military opposition. Landmines were used extensively throughout the conflict following the breakup of Yugoslavia (Fig. 2.9), as one of the aims of the fighting was to drive people out of their homes and keep them away, generating the so called Europe's biggest minefields [50]. As well, when Saddam Hussein's Iraqi forces occupied Kuwait, they set about encircling that country with a double ring of minefields to seal off the Kuwait City area.

In Angola, Cambodia, Ethiopia, Mozambique, Nicaragua, Iraq, Somalia, Sudan, and more recently Ukraine, Syria and along the territories occupied by the IS forces,

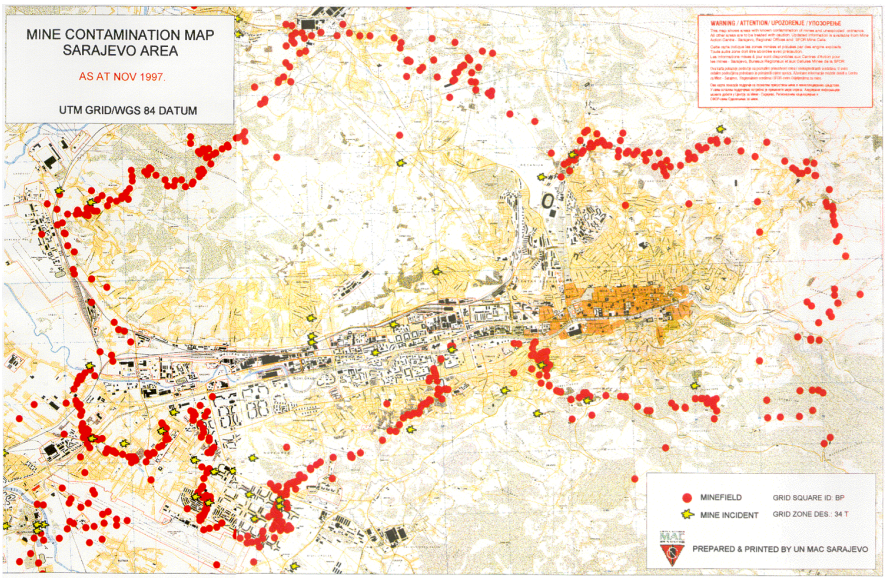

Figure 2.9: Mine contamination of the Sarajevo area in 1997. *Taken from balkansnet.org*

anti-personnel mines have been widely laid as part of a military strategy or mostly as a mean to instil fear into civilians or control their movements.

As can be inferred, mine have had a part to play at every level of conflict, in any terrain, against a variety of targets. They can be laid in advance, thus allowing the most economical use to be made of scarce engineer resources. For a fraction of the cost of a main battle tank, a mine can wreak devastating and disruptive damage upon that, as well as decimating an infantry squad as easily as a machine gun, but at lower expense. Of all the hazards of war, the mine was the most insidious and the most feared, providing a disturbing psychological dimension, as highlighted by the British officer Colonel J.M. Lambert in 1952 [2]:

> Mine warfare is an unpleasant business. It is foreign to our character to set traps cold bloodedly, or to kill a man fortnight in arrears, when you yourself are out of harm's way; and most British soldiers who have experienced it will own a rooted dislike of mine warfare in principle and practice.

and, more recently, from a letter recovered from a colombian eradication man to his commanding officer [51]:

> It's a silent killer which stalks us and threatens us, and yes, we admit it, frightens us.

2.2 The path to the global ban

Concerning international law, on August 1949 the Geneva Conventions, Fig. 2.10, were updated to reflect the changes in the nature of warfare in the previous decade. Apart from forbidding prisoners of war from employment on mine clearance duties, no specific restriction was placed on the use of mines. Even the 1980 *Convention on Prohibition or Restrictions on the Use of Certain Conventional Weapons Which May be Deemed to be Excessively Injurious and to have Indiscriminate Effects* (or CCW), did not adequately address the problem of the unique threat that mines posed to civilians, as it had two important shortcomings: it did not formally apply to internal conflicts and there was no means of implementing it.

Figure 2.10: The 1949 Geneva Convention. *Courtesy of icrc.org*

After the Vietnam War, the incapacity of landmines to prevent an offensive attack, while emphasising the injuries suffered by people, was worldwide clear and manifest. However, it was not until the early 1990s that the issue of landmines really became a matter of international attention. By that time, it was clear that thousands of civilians were victims of mines that had been laid without reference to the CCW and it was contended that mines had been used specifically to target civilians. In 1991 *Human Rights Watch* and *Physicians for Human Rights* published the first detailed study of how landmines were actually being used [52], highlighting the humanitarian dimension of the problem and the urgent need for widely agreed demining programme, aiming at safely return the land for human activities, basically different from military mine clearing techniques. October, 1992 represented the starting point of the *International Campaign to Ban Landmines* (ICBL) when a coalition of six non-governmental organisations combined their separate initiatives and harnessed popular support, sponsoring

the creation of the campaign. It must be said that none of them, *Human Rights Watch*, *Vietnam Veterans of America Foundation*, *Handicap International*, *Physicians for Human Rights*, *Medico International* and *Mines Advisory Group*, had its root within the disarmament community [53]. In 1995, the *International Committee of the Red Cross* launched its parallel supporting campaign, overcoming its political matter resistance and consequently amplifying the ICBL activities, which in the meantime had already gathered worldwide backing [54]. This led to the 1996 historic conference in Ottawa (Fig. 2.11a), that, in spite of a lack of politics consensus, was able to convey 50 governments who agreed in recognising the urgent need to ban antipersonnel landmines. Against the backdrop of the intensive campaigning was the growing involvement of Diana Spencer, Princess of Wales, who had been actively blamed the production and use of landmines, repeatedly visiting affected countries and victims, before her untimely death.

In 1997, responding to a joint invitation from the ICRC and the British demining agency HALO Trust, Princess Diana visited Angola in an effort to create a deeper global awareness of the landmines issue and made the well-known walk [55] through an active minefield (Fig. 2.11b). Such visit received an extensive media coverage, and gave the ICBL campaign a great reception boost. Her battle against landmines led also to her three-day visit to Bosnia later that August, during which she met victims who had sustained injuries from devices planted during the civil war in the 1990s [56]. However, several UK politicians censured her actions, labelling them a political position, not only charitable, thus pressing the government and trying to influence the political processes [57]. Fortunately, this dispute, which was widely covered in the news, further echoed the matter, ultimately benefitting the campaign. Lou McGrath OBE, the founder of the British organisation Mine Advisory Group, speaking on the 20th anniversary of her death, said [58]:

> Without her we couldn't have brought forward what was the fastest arms control treaty in the world.

This concerted effort culminated in 1997 with the adoption of the Ottawa Treaty, becoming a milestone in international law, at a conference in Oslo, Norway [59]. The ICBL received a further boost in October of the same year when the Nobel Peace Prize was awarded jointly to the International Campaign to Ban Landmines and its co-

ordinator Jody Williams "*for their work for the banning and clearing of anti-personnel mines*" (Fig. 2.11c) [60].

(a) The Treaty signing ceremony. The ICBL Coordinator, Jody Williams, is the first on the left. *Courtesy of canadian-landmine.org*.

(b) Princess Diana walking through a minefield. *Courtesy of halotrust.org*.

(c) Nobel Peace Prize award, Oslo, December 1997. *Courtesy of handicap-international.ca*

Figure 2.11: The Ban campaign.

The *Convention on the Prohibition of the Use, Stockpiling, Production and Transfer of Anti-Personnel Mines and on their Destruction*, shortly known as the Ottawa Treaty, made a significant effort to stop the diffusion of anti-personnel landmines worldwide, stating right at the beginning of the treaty [10] that:

1. *Each State Party undertakes never under any circumstances:*
   - *(a) To use anti-personnel mines;*
   - *(b) To develop, produce, otherwise acquire, stockpile, retain or transfer to anyone, directly or indirectly, anti-personnel mines;*
   - *(c) To assist, encourage or induce, in any way, anyone to engage in any activity prohibited to a State Party under this Convention.*
2. *Each State Party undertakes to destroy or ensure the destruction of all anti-personnel mines in accordance with the provisions of this Convention.*

In summary, the Ottawa Convention bans States Parties from using "victim-activated" explosive devices, hence excluding mines that are designed to be exploded by the presence, proximity or contact of a vehicle (i.e. anti-vehicle and anti-tank mines) and explosive devices that are remotely controlled [61]. This is the most argued issue of the Treaty, as its opponents point out that the cruel nature of landmines does not originates from whether they are anti-personnel or anti-vehicle, but from their enduring presence in the ground.

Although a triumph for popular will (to date there are 164 States Parties to the treaty plus one that has yet to ratify), 35 member states, including the United States, China and Russia (the three largest military powers) did not sign the treaty and are still are non-signatories (Fig. 2.12). The majority of non-signatories objected that anti-

personnel mines, if properly used, are defensive weapons, harming attackers only, and that their use might reduce the possibility of a war as a result of their psychological effect. Furthermore, some states felt that a ban on such weapons would compromise their national security to an unacceptable degree [2]. Presumably they believe that the humanitarian dimension lies in protecting their people from aggressors rather than from the residual effect that mines may have.

Figure 2.12: Mine Ban accomplishments as of December 2017. *Courtesy of icbl.org campaign.*

Since the Convention came into force in 1999, the use of anti-personnel mines has decreased, as well the active production of these devices. However, non-signatory States to the treaty continue to use and stockpile these landmines, and more than 82 countries have some form landmine contamination from past and ongoing conflicts. The use of anti-personnel mines by states remains a relatively rare phenomenon, even if there are confirmation of their employment by non-state armed groups in dozens of

[2]Extracted from [62]: "Even as we take this further step, the unique circumstances on the Korean Peninsula and our commitment to the defence of the Republic of Korea preclude us from changing our anti-personnel landmine policy there at this time." *US Department of State*; "A mine-free world remains our common goal. Nonetheless, our movement towards this goal has to be realistic and gradual, sustaining the necessary level of security and stability." *Statement of Russia*; "We are still obliged to maintain anti-personnel landmines as necessary for self-defence and security needs. Israel regrettably cannot commit to a total ban as they are a legitimate means for defending its borders." *Israeli Ministry of Foreign Affairs*; "As a country with long land borders, China must reserve the right to use anti-personnel mines on its territory. The Treaty addresses only the humanitarian concerns, thus China is not able to sign". *Statement of China*.

countries, due to the recent proliferation of low intensity conflicts [63, 64]. Of course, although governments may sign on to the International Campaign to Ban Landmines, terrorist groups do not conform to such [65].

In this respect the United Nations reported estimates and statistics illustrating the scale of the disaster: 120 million landmines still in the ground and a comparable number in military stockpiles, which could be eliminated after 1100 years (provided that no additional mines are planted) at a cost of more than 30 billion dollars. This means 1 landmine for every 16 children in the world. On the basis of the figures currently being promoted, the clearance of mine affected areas would be next to impossible and politically unfeasible.

Certainly, the campaign has brought a great amount of publicity to the cause (Fig. 2.13), but it has possibly distorted the size of the problem and therefore diverted the attention away from the core of the issue (the clearance of redundant minefields), making a moral issue out of a practical problem. Indisputably, the massive circulation and promotion estimates, statistics and figures on landmines and landmine victims has played a central role in efforts aimed at reaching a total legal ban on landmines but the dissemination of grossly exaggerated estimates do not serve the interests of potential victims.

(a) Pyramid of shoes in Paris, 2019. *Courtesy of sortira-paris.com.*

(b) *Lend your Leg* campaign in London, 2012. *Courtesy of article36.org.*

(c) Broken Chair monument in Geneva, 2020. *Courtesy of handicap-international.ch*

Figure 2.13: The Ban campaign public consensus.

Even if it will make no difference to a farming community whether a given square kilometre of land may be infested with one, a hundred or ten thousand mines, since the

risk of death or injury precludes its use unless cleared, and the concentration of mines may not be the prime factors determining the speed of mine clearance, since the time required for its humanitarian clearance roughly remains the same, a precise appreciation of the landmine contamination in a given territory is indispensable to evaluate and plan mine clearance programmes. [3]

2.3 Landmine classification

There are currently more than 600 different models of landmines, as well as an uncounted number of improvised mines and explosive devices made by military forces engaged in fighting (*ordata.info*).

Landmines are in the first place categorised according to the intended target, whether a person, hence addressed as anti-personnel mines (*APL*), or a vehicle, in this case anti-vehicle (*AVL*) or anti-tank mines (*ATL*). APL, whose dimensions do not typically exceed 10 or 15 cm in diameter and height, are commonly laid on the surface, shallowly buried or fixed aboce the ground, with an external casing made of plactic, metal, or other materials (such as wood or bakelite). No precise figures are disclosed on the minimum activation weight, but it can be estimated in few kilograms. They are further categorised according to the type of explosion and the mode of activation:

- **Blast** (Fig. 2.14): designed to be triggered by a pressure action, most of the time as a consequence of stepping on the mine, blast mines create a concentrated blast shock wave consisting of hot gases travelling upward at extremely high velocity. They are intended to cause serious injuries, rather than death.

- **Fragmentation**[4]: designed to project metalic shards upon detonation, typically ball bearings or metal fragments contained in the device, across a wide area, thus potentially causing fatal wounds to a large number of people. There are three basic types of fragmentation AP mines:
  i) **stake mines** (Fig. 2.15): typically concealed within vegetation, they are triggered by tripwires, and the contained metal fragments are unpredictably spread over a 360-degree arc, killing within a radius of approximately four metres (unobstructed), as well as causing severe injury up to distance of

[3] A useful essay on the landmine estimation controversy can be found in [66].
[4] Source for range: [67]

(a) Italian VS-Mk2.

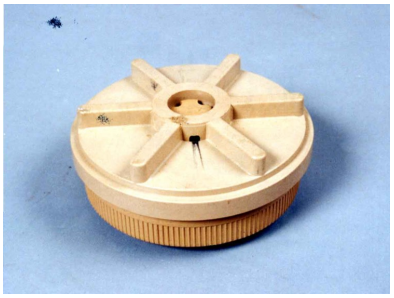

(b) Belgian PRB M409.

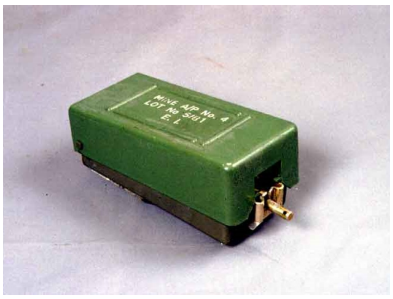

(c) Israel No. 4.

(d) Spanish P-4-B.

Figure 2.14: Examples of anti-personnel blast mines. *Courtesy of ordata.info*

(a) Chinese type 59.

(b) Soviet POMZ.

Figure 2.15: Examples of stake-mounted fragmentation mines. *Courtesy of jmu.edu*

dozens metres. Over time, stake mines may fall down, making them even more dangerous.

ii) **directional mines** (Fig. 2.16): also known as ”Claymore” type, they are designed to be positioned facing the advancing target and their detonation, either command or victim-activated, project a dense pattern of fragments in a specific direction, typically within a 60-degree horizontal arc and to a height of about two metres. Their lethal range is estimated to be around 50 metres, within which even vehicles might be at risk of being disabled or even destroyed.

iii) **bounding mines** (Fig. 2.17): similarly to the stake-mounted devices, upon

(a) US M18 Claymore (note the well-known inscriptions *FRONT TOWARDS THE ENEMY*

(b) Yugoslavian VMRUD.

Figure 2.16: Examples of directional fragmentation mines. *Courtesy of iwm.org.uk*

activation they shoot out metal fragments over a 360-degrees arc, but prior to the mine disintegration, a propelling charge lifts the mine up to a height of roughly 2 metres, consequently resulting in a lethal range of tens of metres and a range within which the mine is capable of inflicting serious injury in exceeding of 100 metres.

(a) Italian P-40.

(b) French 51/55.

Figure 2.17: Examples of bounding fragmentation mines. *Courtesy of ordata.info*

Anti-vehicle landmines, instead, are specifically designed to irreparably damage vehicles and tanks, and they can be detonated by direct pressure, by remote command, through an attached tilt rod, or even through magnetic influence sensors (Fig. 2.18). Given their purpose, AT mines are commonly found along roads and tracks, and requires a relevant weight to be activated, around 120 to 150 kg. Obviously, these devices are much larger than their anti-personnel equivalent, and contains a higher quantity of explosive charge (about 6 kg, opposed to less than 100 grams for a blast AP mine).

(a) Italian Bakelite type II. **(b)** Russian PGMDM.

(c) German T-42. **(d)** British Mk-V.

Figure 2.18: Examples of anti-vehicle landmines. *Courtesy of iwm.org.uk*

However, this does not necessarily imply that a target weighing less can safely step on them, as fuze sensitivity might degrade over time, or it can be deliberately modified to require a reduced pressure to detonate. Sometimes, anti-personnel mines have been laid on top of an anti-tank one, so that its detonation will consequently activate the deeper device. Such technique of laying these two families of landmines together in clusters is common, mainly as a way to impede the recovering of the anti-vehicle ones [68].

There are two further categories of explosive devices which eventually could have the same effects of landmines, even if their main purpose is different:

- **Explosive Remnants of War** (Fig. 2.19): according to the NATO glossary of terms, they include unexploded explosive ordnance (UXO) and abandoned explosive ordnance (AXO), and are defined as *explosive ordnance which has been primed, fuzed or otherwise prepared for action, and which has been fired, dropped, launched, projected or placed in such a manner as to constitute a hazard to operations, installations, personnel or material and remains unexploded either by malfunction or design or for any other cause [69].* The category does not include mines, because of the different primary purpose of these weapons.

(a) Unexploded shell in Libya. **(b)** Abandoned ammunition store in Iraq.

Figure 2.19: Examples of explosive remnants of war. *Courtesy of icrc.org*

- **Improvised Explosive Devices** (Fig. 2.20): dating back to the bombs made by the Irish Republican Army using explosive based on fertiliser [70], they are a type of unconventional explosive device *placed or fabricated in an improvised manner incorporating destructive, lethal, noxious, pyrotechnic or incendiary chemicals and designed to destroy, incapacitate, harass or distract [69]*. They often consist of non-military component assembled in a variety of forms.

(a) Pressure-detonated fuel container, Afghanistan 2020. **(b)** Stone camouflaged IED, Yemen 2018.

(c) Explosive soda can, Ukraine 2018 **(d)** Booby-trapped mobile phone, Yemen 2018.

Figure 2.20: Examples of improvised explosive devices. *Courtesy of iedawareness.com*

Acting *de facto* as anti-personnel landmines, IEDs account for 25% of the total casualties every year and countless more injuries [6].

2.4 Standards and Definitions

There are two principal types of mine clearance operations: military and humanitarian [14]. Military demining is conducted for a strategic advantage, i.e. the clearance of a path through a minefield, and it is about reducing risk, therefore casualties may be accepted. Normally the clearance is performed with armoured vehicles equipped with hardened roller, steel flail or similar tools capable of neutralising objects on or near the surface (Fig. 2.21).

(a) BAE Systems Terrier with mine plough.

(b) U.S. Army M1 Panther equipped with mine roller.

(c) Hydrema 910MCV with rotating shaft and flails.

Figure 2.21: Minefield breaching machines. *Courtesy of respective Owners*.

Otherwise known as minefield breaching, military mine clearance does not normally expect to achieve more than 60-75% clearance of a given mined area (up to 90% when employing explosive breaching machines).

Humanitarian mine clearance, on the other hand, aims to return land to the civilian population, with civilians being the beneficiaries of the activity. Clearance means that there is nothing dangerous left in the ground till an agreed depth. The UN statement of requirement [14] defines the clearance criteria as follows:

> The area should be cleared of mines and UXOs to a standard and depth, which is agreed to be appropriate to the residual/planned use of the land and which is achievable in terms of the resources and time available. The contractor must

> achieve at least 99.6% of the agreed standard of clearance. The target for all *UN* sponsored clearance programmes is the removal of all mines and UXOs to a depth of 130 mm.

The time spent to clear an area is not considered to be a major factor in humanitarian operations, as the safety of the clearance personnel comes first and casualties, not only directly related to the operations but also as a consequence of the clearance activities, must be avoided. In addition, another need is to strongly limit the environmental effects and the consequence on the natural resources of demining operations, so that the cleared land can return to being productive [71].

The process has the primary aim of safely returning the area to its normal use, so no explosive hazards can be left behind. It must be noted that the solutions developed for the military are generally *for* the military and cannot be used for the purposes of humanitarian demining. Military procedures cannot be employed in humanitarian operations because they cannot achieve what is defined as ”clearance”, i.e. *the identification and removal or destruction of all mine and ERW hazards from a specified area to a specific depth [72].* The techniques for breaching the minefields are not effective enough. Flails, tillers and rollers can be useful when trying to make a fast breach. Ploughs can push the mines aside, leaving them buried at unpredictable angles and burying them under piles of earth, causing further difficulties for mine clearers. Some machines are useful for breaching a single lane through a minefield in battle, but achieving close to the clearance rates demanded of humanitarian mine clearance has proved elusive [73]. The flail chain and hammers can damage munitions but very rarely detonate them. The explosive methods can be ruled out because they would be potentially polluting. Ultimately, they are also usually expensive.

The need for a systematic, 100% clearance of a contaminated land generally results in the decision to conduct manual clearance, as had been done since the Second World War, using probes (Fig. 2.22a), sniffer dogs (Fig. 2.22b) and metal detectors (Fig. 2.22c and Fig. 2.22d) [74]. It is widely acknowledged that current mine clearance techniques are extremely slow, the technology having barely advanced since the

1940s [5].

(a) Ground probing during clearance operations in Somalia.

(b) Mine Detection Dogs training in Afghanistan.

(c) Ground surveying through MD equipment in Lebanon.

(d) Demining operators in Western Sahara.

Figure 2.22: Manual demining and clearance operations. *Courtesy of unmas.org*

Most mine clearance is done manually in lanes, with one or more individuals using a mine detector and/or a metal prodder to locate each mine. Vegetation must be cleared with extreme caution, as tripwires will otherwise detonate surface-laid mines. This clearance is often done manually using hand tools such as shears and sickles, but in some case petrol strimmers can be adopted. Large machines are used to both remove the undergrowth and prepare the ground surface. Such methods are difficult, expensive, labour intensive, and not without risk (Fig. 2.23). In addition, the efficacy of manual clearance is reduced from the fact that mines are increasingly being made of plastic materials, minimising the more easily detectable metal components. Then, mined areas are often spread with metal debris creating a high false alarm rate (FAR). Even if anti-personnel landmines are commonly shallow-buried to guarantee detonation, once the mines are in place vegetation grows uncontrolled in the minefield areas. On the

[5]The first mine detector was developed in 1941 by a Polish officer, Lt. Kozacki, who escaped to Britain at the beginning of the war. He was requested the manufacture of such a device as a result of the need to move or relay minefields laid to protect Britain's beaches. The British Army was still using a version of the same device up to 1995 [2].

occasions when storms causes flooding, the vegetation traps mud and silt carried by the water, increasing the ground level [75]. In this way, mines could gradually be buried up to a metre below the surface. In addition, mines can be deliberately buried deeply to defeat conventional mine detection techniques [76].

(a) Progressive minefield clearance in Sri Lanka.

(b) Vegetation clearing activities in Colombia.

Figure 2.23: Examples of clearance activities. *Courtesy of halotrust.org*

In the age of stealth aircraft it seems ironic, if not tragic, that such primitive methods are still necessary. The efficiency of demining operations mainly depends on the environmental conditions, i.e. terrain and soil type, and weather, as well as on the methodology and technologies adopted. Field reports [77] have shown that the daily clearance rate for a single deminer lies in the range from 5 to 150 m^2, underlining the necessity of deploying suitable tools to increase these values. Demining animals, such as dogs and rats, widely employed in several territories, represent an established more cost-effective solution, capable of expanding the cleared area from 300 m^2 to 2000 m^2, always subjected to environmental conditions and survey approach. While animals exhibit excellent detection performance when used for indicating individual mine or minefield boundaries, the discrimination of devices embedded in a dense concentration remains a challenge, given also the performance inconsistency throughout operations. A detailed survey of landmine status and problem understanding can be found in [78].

Despite it has become a common figure to associate the global costs of a mine clearance programme with the extension of the cleared area, such approach still represents a relevant approximation when delineating a standard cost models. This because total costs should consider both direct expenses related to the demining operations and includes personnel, facilities, materials and equipment, as well as indirect costs, linked to planning and administration, for which it might be hard to assess their impacts on

the demining activities.

2.5 Background on Sensor Technology

Following a vicious circle, landmine design has followed, often anticipating, the evolution of countermine equipment.

If all mines exhibited a considerable metallic content, metal detectors would obviously represent the best choice for their detection. However, the widespread use of landmines containing only few grams of metal has imposed the development and deployment of more sophisticated detection technologies, attempting to detect target-related disturbances, from chemical to thermal and electrical, within its surroundings. This brings the further issue related to the interpretation of such data, which clearly is highly subjected to the environmental conditions, including soil, terrain and climate, and the possible heterogeneity in the buried objects population [79, 80].
Here lies the cornerstone: once a subsurface feature has been detected, the employed technology should be capable of recognising its signature and differentiating it from the surrounding environment. A landmine detection equipment should be as much target-agnostic as possible, i.e. it should reliably detect mines without being influenced by their shape and external casing materials, ideally being insensitive to both, the enclosed explosive substances, and should have the possibility of providing imaging information, so that the target of interest can be better distinguished from the background clutter. Along with these aspects, considering that mines can be buried at different depths, the detection system performance must not excessively drop with depth. From an operational point of view, the equipment should allow the operator to carry out the task without getting in close proximity to the device to avoid accidental triggering, and the deployed system must not constitue a logistical burden. Finally, it all has to lead to a quicker and more reliable detection accuracy. The complexity of the mine clearance framework points out the need for different types of sensors and equipment to detect and neutralise landmines [81].

Detection techniques that are in development can be grouped depending either on their operational characteristics (Fig. 2.24):

- Electromagnetic;

- Optical;
- Acoustic;
- Nuclear;
- Biological.

or on their final results:

- sensors seeing an image of the landmine through scattering;
- sensors detecting anomalies at the surface or in the soil;
- sensors detecting landmines explosive or associated chemicals.

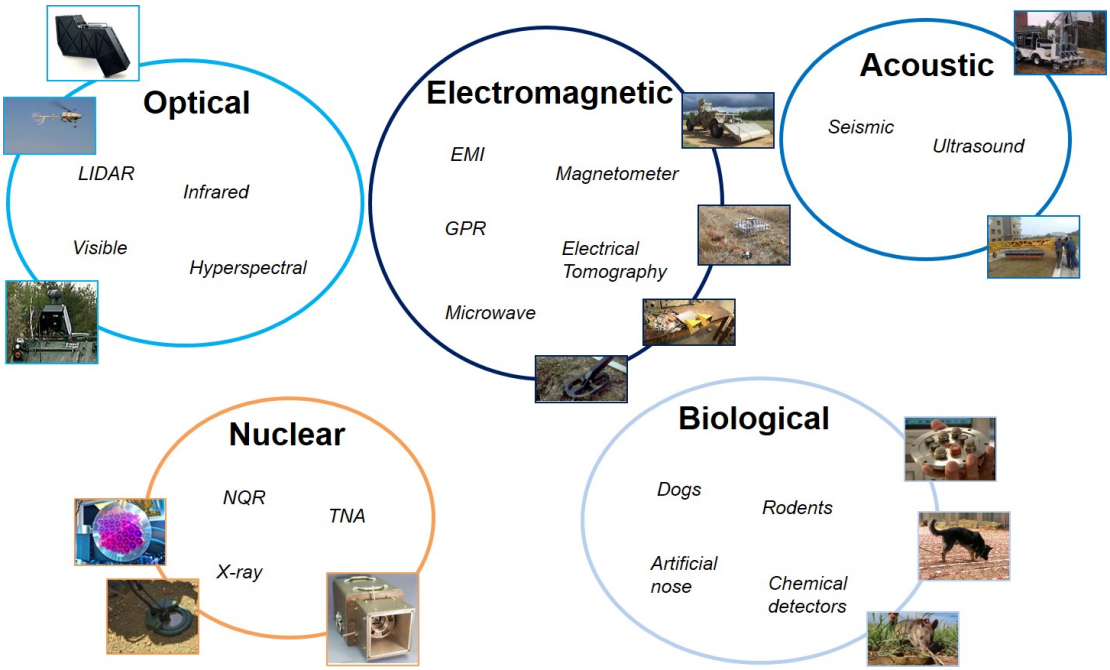

Figure 2.24: Outline of remote sensing technologies for landmine detection.

Their operational characteristics are listed in Table 2.1. Detailed descriptions and further analysis can be found in [78, 82, 83].

The key issue with any sensor for mine detection is the probability of detection (P_D, the amplitude of the signal being higher than a specified threshold whenever the target is present) and false alarm rate (P_{FA}, reflection generated by an interfering signals that is not related to any actual target but exceeding the detection threshold, thus mistakenly considered as a target) [108]. Table 2.2 shows the efficiency of different demining methods (derived from [109]).

The two quantities are strictly bounded, as a decreasing of the detection threshold could ensure a comprehensive detection, but also may lead to the detection of smaller

Table 2.1: Outline of sensors

Technology	Sensor	Operative principle	Strength	Limitations
Electro-Magnetic	Metal Detector [84]	Induction of electric currents in metal components.	Ready-to-use and lightweight. Still on the forefront of demining operations. [85]	Minimum content metal mines, metal-cluttered urban environments and mineralised soil.
	GPR [86]	Reflection of EM waves at the boundaries of dielectric contrast.	Detects all anomalies, even if non-metallic. [87]	Natural and hand-made clutter, soil conditions. Technologically complex and limited resolution.
	Electrical Tomography [88]	Determines electrical conductivity distribution.	Detects all types of mines. Suitable for wet environment. [89]	Deep buried mines. Contact required. Dry and non-conductive environments.
Electro-Optical	Hyperspectral [90]	Detects differences in material reflectivity	Discriminates different surface-laid materials from stand-off distance. [91]	Extremely variable due to changing environment, weathering can eliminate anomalies.
	Thermography [92]	Study of the temporal evolution of temperature profiles.	Detects every type of mine [93].	Significant variability. Early stage of thermal signature understanding.
Acoustic & Seismic	Seismic [94] Sensors	Response of the ground to an applied shock.	Detects all types of buried mines. Low soil moisture impact. [95]	Man made clutter and deep buried mines.
	Ultrasonic [96] Sensors	Backscattered ultrasonic wave.	Low false alarm rate and unaffected by moisture and weather. [97]	Soil condition for ultrasonic wave propagation. Heavy vegetations.
Explosive Vapour Detection	Biological [98]	Odour discriminating skills of living organism (dogs, rats and bees).	Explosives presence confirmation and material characterization. [99]	Extensive training and difficulty in maintaining continuous operations.
	Chemical [100]	Chemical identification of microscopic residues of explosive compound.	Lightweight and simple to operate. Low detection threshold. [101]	Suffers from residual vapours and chemical clutter, complexity of collecting enough explosive molecules.
Bulk Explosive Detection	NQR [102]	Resonation of the chemical bonds when subjected to RF pulse.	Very low false alarm rate (not driven by clutter). Specific for landmines [103].	Susceptibility to RF interference. Low SNR and stationary detection required.
	TNA [104]	Radiation emissions from atomic nuclei in explosives.	Low strength source radiation. Identifies the elemental content. [105]	Ground surface fluctuations. High false alarm in wet environment (sensitive to hydrogen content).
	X-ray [106]	Difference in mass densities and atomic number.	High resolution imaging capabilities. Potential lightweight and portable. [107]	Shallow penetration and sensitivity to soil topography. Long time for image generation.

Table 2.2: Probability of detection by various demining methods.

Type of asset	Assessment of quality	Probability of detection
Manual mine clearance	All mines and ERW are found to the required depth	100%
Mine detection dogs	Verification of dogs indications is conducted manually	100%
Flail and tillers	Performance is variable, very poor for some ERW	40 - 80%
Rollers	Performance depends on the ground and type of mines	0 - 40%

misleading detections, generating a high false alarms rate and slowing down the operations. The two different approaches to landmine clearance, military and humanitarian operations, can be plainly explained considering these two factors (Fig. 2.25): the first procedure follows the idea of not identifying a target as a mine unless there is an absolutely certainty that it is a mine, while for the latter a landmine is marked even if there is a low suspect on its presence.

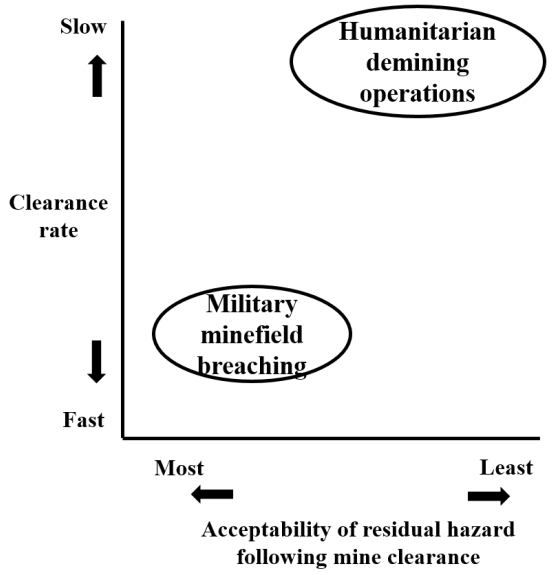

Figure 2.25: Operational mode for landmine clearance procedures.

While the detection probability is mostly dependent on the target properties and the specifications of the system, the false alarm rate instead is affected by all the surrounding objects and minefield scenario. Clutter can be either man-made, such as metal fragments, pipes or building remnants just to mention a few, and natural, such as rocks, tree roots or water ponds. Depending on the physical principle of the employed tech-

nique, the source of false alarms could be very different (Table 2.3).

Table 2.3: Common sources of false alarms for mine detection.

Detection technology	Source of false alarms
Induction	Metal scrap, natural soil conductivity and magnetisation
Radar	Natural clutter (roots, rocks) and metal debris
Acoustic	Hollow, man-made objects
Nuclear	Radio frequency interference
Optical	Man-made objects.
Biological	Explosive leakage, battlefield debris

It is therefore clear that new technologies should firstly offer a significant reduction of the false alarm rate values, widely agreed as the primary source of the slow pace of operations, while maintaining or even increasing the detection performance. In addition of being straightforward to use and operate, as many of the demining operators might not have advanced technological education and the country might have limited infrastructures for maintenance, operation, and deployment, the cost of its deployment must not also exceed the current market value of a metal detector sensor (approximately $ 5'000, [110]).

New sensors should detect low-metal mines and possibly the contained explosive substance. It is clear that no single technology has the capability to detect and recognise a variety of mines under all circumstances, as some of them are more suitable for confirmation than for primary detection. A widely acknowledged approach that could simultaneously reduce the false alarm rate and maximise the detection probability is considered the adoption of different complementary sensors and combining the retrieved information, which might lead (according to several analysis, as in [111] to a notable contraction of both the exposure time and the search rate, thus resulting in the improvement of the overall mine clerance process.

While technically feasible, very few technologies can currently meet the requirements of size, weight, manufacturability and sensitivity to be deployed within the humanitarian demining domain (Fig. 2.26). Another relevant aspect is the equipment price range, determined and bounded by the current market [111], which makes it difficult for a multi-sensor technology, regardless the number and type of combined sensors, to compete with the price level of a metal detector equipment.

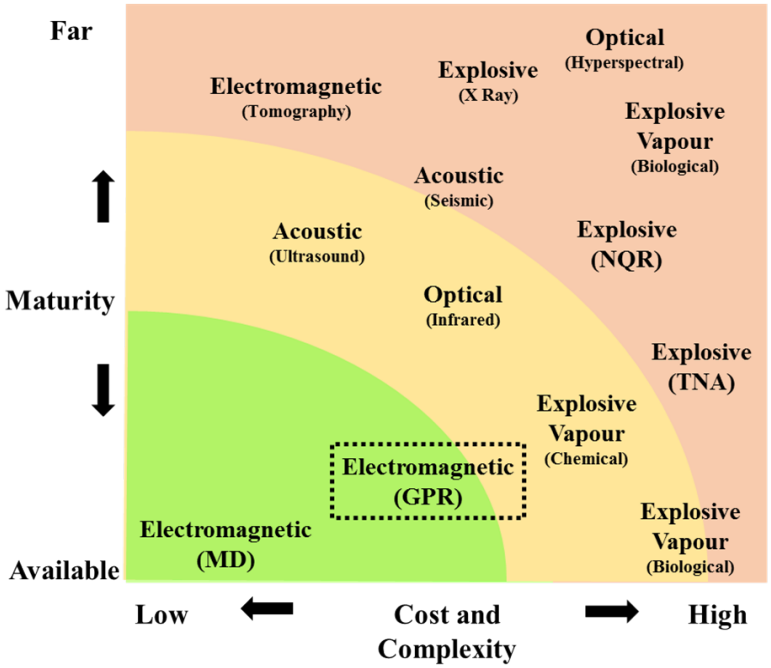

Figure 2.26: Inferences about the maturity of mine detection technologies.

A promising solution that can further limit the current landmine detection shortcomings is to merge the information obtained by the different sensors through the use of dedicated signal processing techniques, commonly known as sensor fusion schemes.

The mutual processing of data acquired through different sensors can be computed at three different levels: (1) data-level fusion, (2) feature-level fusion, and (3) decision-level fusion. In the majority of multi-sensor platforms developed so far, data acquired by different sensors are fused at a decision level.

Even if a decision level fusion can represent a sub-optimal approach, as a missing detection would impact the performance of the strategy, fusion at lower levels requires more computational power and a deep physical and operational understanding of the performance of each sensor, as well as individual access to the sensor raw data. Sensor fusion at feature level, while being significantly complex to realise, on the contrary, is expected to provide meaningful performance improvements, in therms of both object detection and clutter rejection. Operationally, features are firstly retrieved from each sensors and associated to a specific target of interest, thus providing a list of potential object candidates. Such lists are then reciprocally reconciliated, i.e. features from different sensors are combined to determine what is commonly named an associated object, and the final decision on these candidates will be typically made at a statistical

level by combining the confidence levels computed from each individual sensor and the ones obtained by the joint ensemble. The most complex task within this sensor fusion scheme is to determine the optimum number of selected features, as the selected features ensemble must first of all reliably characterise the target, at the same time it should be taken into acocunt the compuitational weight of the required exhaustive search over all feature combinations.

This work will focus on Ground Penetrating Radar (*GPR*) technology, a highly regarded candidate to improve mine detection efficiency and considered one of the few that can provide meaningful operational capabilities.

GPR is beginning to be deployed for landmine detection, as a result of its performance against minimum metal mine, often exceeding the ordinary metal detector sensor. Reports on the successful field deployment of GPR can be found in [112, 113, 114, 115]. While some works have been done to integrate a GPR sensor with the Nuclear Quadrupole Resonance techniques, as a way to additionally detect the explosive content, or with microwave and millimetre wave radiometers [116, 117], the the complexity and cost of these systems has made the solution not feasible. Therefore, considering also their almost complementary operating principles, a field deployable solution has been found in a dual sensor, MD/GPR combined platform.

In terms of technology readiness level, there are three systems currently in use: the US Army AN/PSS-14 (also known as HSTAMIDS, Fig. 2.27a) hand-held detector [118], the Anglo-German Vallon - Cobham VMR3 Minehound (previously known as MINETECT, Fig. 2.27b) humanitarian detector [119, 120], and the ALIS platform, developed by Tohoku University Sedai, Japan [121] (Fig. 2.27c).

The AN/PSS-14 system combines a metal detector manufactured by MineLab International of Australia with a stepped frequency continuous wave (SFCW) GPR system manufactured by CyTerra Corp. (now L-3 Communications, US). The VMR3 Dual-Sensor platform includes a metal detector produced by the german Vallon GmbH and a custom designed 1 GHz impulse GPR system developed by ERA Technology (now Cobham Ltd, UK). ALIS is a combination of a metal detector produced by CEIA (IT) and two alternative GPR systems, a stepped frequency radar and an impulse one.

Operationally, the signal from the metal detector, representing the prime search capability, is used to trigger the GPR, methodology which constitutes the simplest form

(a) AN/PSS-14. **(b)** VMR3. **(c)** ALIS

Figure 2.27: GPR-based demining equipment in actions. *Courtesy of gichd.org*

of data fusion. Each sensor returns a unique audio signal and can be heard by operators individually or in combination with the other. Following the MD alert, the GPR unit checks the area around the metal reading to verify whether the response of can be associated to a landmine like material. Joint occurrence of these two events confirms the presence of landmine. The ALIS platform additionally provides positioning information through a camera-based tracking system, permitting therefore a 3D reconstruction of the investigated subsurface and consequently an image-based object recognition. In all handheld systems, classification of detected objects is left to the operator.

Reports from the field trials of these equipment have demonstrated the potential of GPR technology in improving the performance of the landmine detection process. In particular, the AN/PSS-14 has shown improvements of a factor between 7 to 17, with respect to a single metal detector unit, while test of the VMR3 exhibited a reduction of the false alarms rate from 5 to 7, subjected to the environmental conditions. Closely similar performance have been reported for the ALIS platform.

Reports on field evaluation trials for the described equipments can be found on the *gichd.org* repository.

2.6 Ground Penetrating Radar

Historically, the development of Ground Penetrating Radar methodology has followed the invention of radar, and only six years after Hülsmeyer obtained the first patent for

his naval anti-collision system, Leimbach and Löwy applied for a patent to implement such technology to locate buried objects (Fig. 2.28) [122]. The approach consisted of inserting a pair of transmitter and a receiver in an array of vertical boreholes and correlating the recorded signal magnitude with the value obtained when successive pairs were used. In addition, they also described a technique using surface laid antennas for determining possible reflections from ground water interfaces.

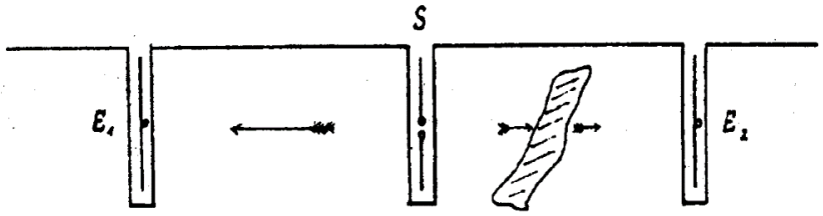

Figure 2.28: Original sketch of the first GPR system comprising an array of borehole antennas. *Taken from [122]*

Except for some early experiments aimed at measuring the depth of glaciers in 1929 [123], the technology largely overlooked until late 1950s, when a U.S. Air Force plane attempting to land in Greenland crashed because the onboard radar systems were actually seeing through ice and therefore provided the pilots an erroneous altitude measurement [124]. Such accident is considered the spark of the wide understanding of the potential of the radar methodology in exploring the subsurface, not only for ice sounding purposes but also for subsurface properties determination. An additional boost was given by the lunar soil investigations within the Apollo programme [125, 126]. Initially, GPR technique was mainly researched for military applications, including the mapping of underground tunnels constructed by the Viet Cong during the Vietnam War and within the demilitarised zone separating North and South Korea [127, 128]. From then on, industrial players, such as public utility and construction companies, got interested in such subsurface investigation tool, regarded as a fast and effective mean for utilities mapping under city streets [129]. GPR became a publicly recognised instrument also in supporting forensic investigations [130] after the well-known ”Fred West murders” case (United Kingdom, 1994), where it was able to accurately locate the remains of a number of victims buried under a concrete basement [131, 132]. Nowadays, Ground Penetrating Radar is a widely employed near surface geophysical technique for subsurface sensing in a variety of domains, from geology, archaeology and utility

detection to civil and geotechnical engineering (refer to [15] and [133] for a comprehensive overview). Within the field of landmine detection, GPR technology aims at improving the detection of non-metallic mines and reducing the typically experienced high false alarm rate [134, 135].

Compared with other subsurface sensing technologies, the potential benefits of GPR can be summarised as follows:

- False alarm reduction by target identification based on measured target responses.
- Ability to detect both metal and non metal cased landmines, and generally every dielectric discontinuities occurring in the subsurface.
- Ability to detect both surface laid and buried landmines, theoretically without the need of being in contact with the surface.
- High resolution 3D imaging capability.
- Unmanned operations and sensor combination suitability.

GPR is a non-destructive technique that can provide a 3-D image of the subsurface [136], with the additional information brought by the colour dimension (scaled to signal amplitude), thus providing an accurate depth estimate for a wide range of subsurface objects [137], as well as precise details on their nature, under favourable conditions.

GPR is an electromagnetic method similar in principle to the seismic reflection technique, except that it is based on the propagation and reflection of electromagnetic waves rather than acoustic ones. Essentially, a transmitter antenna radiates an electromagnetic wave that propagates into a material, with a velocity primarily determined by the permittivity of the material, until it encounters a contrast in the electromagnetic impedance. At this interface, part of the wave is scattered back, depending on the contrast magnitude, as well as the physical and geometrical features of the object, and its reflection is recorded by the receiving equipment. The other portion of the wave might instead be transmitted and therefore it will continue to propagate.

It is therefore clear that the electrical properties of both the target and the surrounding soil are fundamental variables [138], as they directly influence the experienced propagation and scattering phenomena.

2.6.1 Operational principles and survey techniques

At a first instance, GPR equipment can be fundamentally categorised depending on the domain characterising the generated waveform, and therefore:

- **Time Domain Radar**: the transmitter emits a short pulse of electromagnetic energy, while the received signal is built by combining the collected echoes over a certain time period. The specific application dictates the type of the antennas and consequently the shape of the pulse.
- **Frequency Domain Radar** [139]: the transmitter generates a sweep of discrete set of frequencies (similar in principle to the seismic vibroseis technique), and the received signal is the result of the convolution of such sweep with the recorded one.

Most frequently, impulsed GPR systems are adopted, as a consequence of their easiness of usage and manufacturing, even if it is well known the improved flexibility and level of information that can be achieved through a stepped frequency equipment. For both system architectures, the subsurface response is obtained by combining the responses generated by the subsurface reflectors and it can be inverted using several imaging algorithms [140].

Concerning the configurations of the antennas, a GPR system is configured as:

- **Monostatic**: a unique antenna operates as both transmitter and receiver.
- **Bistatic** or **Multistatic**: transmitter and receiver are separated and independently managed.

Typically, GPR systems consist of separate transmitter and recevier antennas, even if they are housed in a single case with no means of varying the antenna geometry, commonly referred to quasi-monostatic configuration.

Further on, an additional distinction is commonly made between **ground coupled** (Fig. 2.29a) and **air launched** (Fig. 2.29b and Fig. 2.29c) systems, defining whether the equipment is working in contact with the surface or above it.

The selection of deployment approach represents a trade-off between both operational simplicity and data quality or interpretability. It should be noted that the height at which antennas need to be placed for the configuration to be considered air-launched is poorly defined, as well as how close is close enough to be considered ground coupled.

Figure 2.30 presents a simulated example of the effects originated by elevating the

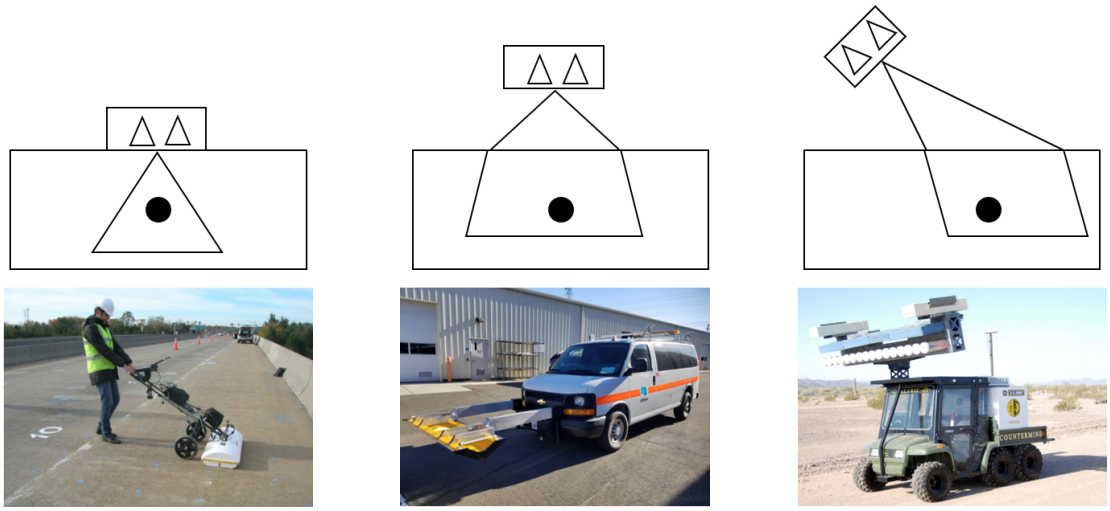

(a) Ground coupled. *courtesy of idsgeoradar.com*

(b) Air launched. VMR3. *Courtesy of 3d-radar.com*

(c) Forward looking. *Courtesy of arl.army.mil/ [141]*

Figure 2.29: Examples of principal GPR survey strategy.

antennas from the ground.

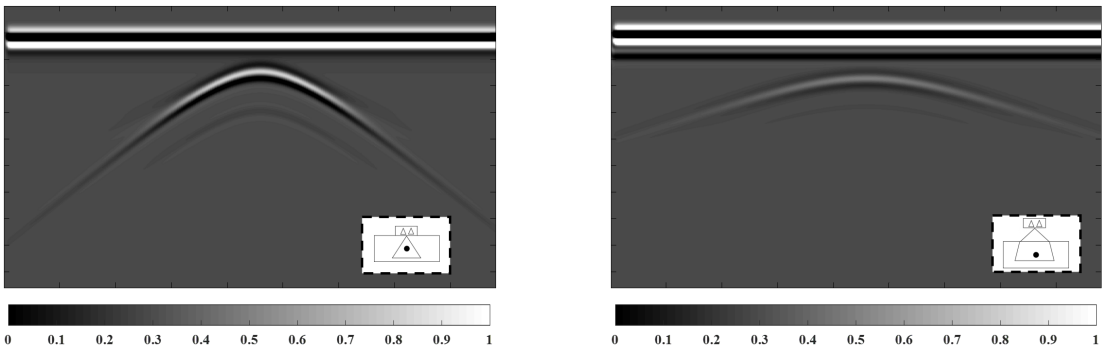

(a) Ground coupled data.

(b) Elevated antennas (5 cm).

Figure 2.30: Comparison of GPR imaging performance of a dielectric target buried at 13cm in low loss soil.

Generally, the probability of detection by close-in sensors such as GPR degrades rapidly as the sensor is lifted from the ground due to reductions in both the ground coupling and reduced sensitivity caused by the spreading loss resulting from the increased distance to the mines [142, 143].

Ground coupled GPR measurements are generally more effective, since raising the antennas off the ground surface degrades lateral spatial resolution. In addition, despite being intuitively an optimal choice, the efficacy of airborne GPR systems is affected by the roughness of the ground surface and from a degraded coupling efficiency, since complex angles of refraction might occur, potentially leading to severe losses in case of

incident angles larger than the Brewster angle. A rough surface would randomly scatter the incident GPR wave, making the received data difficult to analyse, as well as complicating the prediction of the the effective propagating waveform [144, 145]. In addition to the problem of coupling energy into the ground, one should take into account that the scattering amplitude of all landmines decreases when they are buried. However, working at a stand-off distance has its straightforward advantages, especially considering that it can be operated at high speed and is more adaptable to vehicle mountings [146].

On the contrary, signal penetration and data resolution are highly enhanced through the use of a ground coupled platform [147], as the subsurface propagating waveform is almost unaffected by the previously mentioned phenomena and, in principle, closely resemble the emitted one, hence it can be more intuitively predict and interpreted [148]. Ground coupled systems survey an area at slower speeds and cannot be operated on every surface topography, but are less prone to external noise, surface clutter (as it is incorporated into the first echo), and take advantage of a theoretically perfect coupling between the antennas and the soil interface [149].

Considering the system architecture, GPR surveys are commonly carried out in common offset (CO) or alternatively single-fold (SF) configuration. Such acquisition scheme consist of a single transmitter and receiver pair moving together over the surface maintaining the same distance (offset). In particular, with a monostatic system, this configuration is denominated zero-offset geometry. This architecture is the most commonly adopted approach, as this allow a relatively fast and operationally straightforward data acquisition (Fig. 2.31).

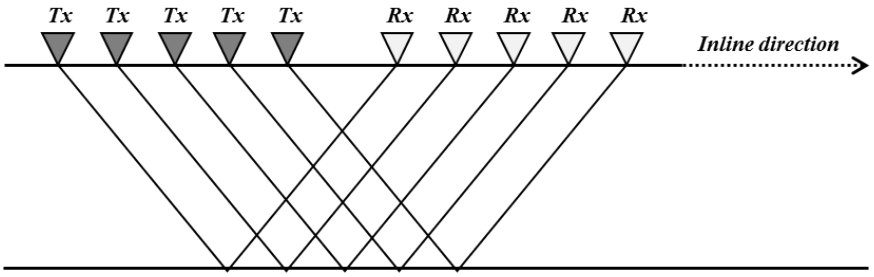

Figure 2.31: Common offset GPR survey. Tx and Rx represents respectively the transmitter and the receiver.

To be able to maximise the information that can be extracted from a GPR survey,

it is in principle essential to have some preliminary knowledge on the target characteristics and properties. For an efficient energy coupling process, the transmitter and the receiver should be separated by a distance ensuring the correspondence between the pattern focusing peak and the target depth of interest, hence it might be varied. However, the need for operations flexibility, this value is typically fixed and set to a minimum.

Concerning the acquisition approach, the survey is commonly carried out along profiles which are perpendicular to the expected directional pattern of the object, due to the increased easiness in interpreting the data from the generated diffraction hyperbola.

Until about 20 years ago, surface GPR studies were based on sparse 2D profiles. Unfortunately, interpretation is often not sufficient for complex scenarios or extended targets and thus recognition and identification remains a challenge. This challenge could be mitigated if a properly sampled 3D dataset is available, allowing the extraction of physical and geometrical information of the buried target, as well as eliminating ambiguities due to soil effects and other spatially-extended noise artefacts.

3D GPR is able to provide a deeper insight of the subsurface features, as well as to visualise their spatial extent. Although the significant advantages of three dimensional surveying strategies are well documented [150, 151, 152], they generally require much greater acquisition expenditure and effort than traditional sparse bidimensional acquisitions. Three dimensional imaging with GPR has been tested in most domains of shallow subsurface disciplines [153, 154, 155]. The price to pay is a very high accuracy in trace positioning and acquisition regularity [156, 157, 158].

As the final scope of a GPR survey is to retrieve information about the subsurface characteristics and geometries, the wavefield must be properly sampled and recorded, in both time and space. Therefore, survey design must adhere to fundamental sampling principles [159, 160]. From the sampling theorem [161], in order to reconstruct the buried features as accurately as possible, trace spacing should be dense enough for the unaliased recording of all diffraction hyperbolae:

$$\Delta x \geq \frac{v}{4 \cdot f \cdot sin\theta} \tag{2.1}$$

where v is the wave velocity, f is the working frequency and θ is the dip angle along

a diffraction hyperbola. For large angles, the *sin* function could be approximated as unity, thus leading to the common adopted sampling parameter of $\lambda/4$.

This means that to satisfy the Nyquist criterion, the collected GPR samples must be at most distanced by quarter of the wavelength corresponding to the highest frequency present in the spectrum, and this value should be applied in all survey directions, given the rotational symmetry of diffraction hyperbola. In principle, the technology for performing 3D GPR acquisitions is readily available, but in practice the density specifications that are implicit in all 3D surveys can be a demanding requirement [156, 157, 162, 163], as summarised in Table 2.4.

Table 2.4: GPR spatial sampling criterion for different frequencies and soil velocities.

Frequency	**Velocity** 8 [cm/ns]	**Velocity** 12 [cm/ns]	**Velocity** 18 [cm/ns]
200 MHz	10 cm	15 cm	22.5 cm
600 MHz	3.3 cm	5 cm	7.5 cm
1 GHz	2 cm	3 cm	4.5 cm
3 GHz	0.66 cm	1 cm	1.5 cm

It is always possible to acquire a 3D grid with slightly larger sample distance, however such approach should be considered only in certain circumstances, e.g. when acquisition speed and computational constraints have to prevail over the integrity of the collected data. The principal consequence is that the data will not be able to properly delineates geometrically complex structures, including steeply dipping layers. At the same time, data over-sampling, i.e. acquiring a grid with a sample distance which is smaller than the required one, does not provide significant benefits. As previously mentioned, the choice of the survey line offset depends on the characteristics of the target of interest and the subsurface features, such as target orientation or inclination, as well as from the purpose of the survey, and therefore it is possible that a single profile might be sufficient to fulfil the task. On the contrary, when not enough information are available, as in many cases, or there relevant heterogeneities are expected, the design of the acquisition grid must comply with the Nyquist sampling interval.

Despite the majority of experimental trials have been performed with a fixed antenna separation, a bistatic geometry in which the transmitter and the receiver are independently managed may offer several key benefits, especially for low-observable targets or low Signal to Noise Ratio (*SNR*) scenarios [133, 164]. Common offset ap-

proach suffers from a limited imaging capabilities, as the retrieved information derives from a single look of the subsurface from a fixed geometry. Conversely, a multi-offset survey is based on the recording of the signals arriving along different reflection angles, thus involving multiple looks for each surveyed location [165]. A separate receiving antenna allows to record the character of the transmitted signal as it appears entering the ground. An incident wave over a target exhibiting irregular shape or relevant roughness, with respect to the wavelength, can be reflected along a particular direction, which might be not aligned with the monostatic system radiation pattern, thus varying the antenna spacing, and consequently the incidence angle of the wave, could facilitate the extraction of discriminant features of the target and therefore its recognition and identification [166].

Multi-offset data acquisition presents several imaging advantages over a common offset approach, including increased SNR, resulting in an increased penetration performance, better reflector contouring and dip delineation [167, 168]. In addition, benefits in the capability of resolving lateral velocity variations scenarios have been demonstrated [169]. Further on, it will be useful for remotely surveying the area by setting a transmitter at a fixed position and only the receiver scanning the ground surface. Obviously an accurate relative antenna position knowledge is required. These systems provide more information as pairs of antennas provide different views of the target.

Finally, GPR propagation is along raypaths defined by Snell's law, hence wave propagation and target scattering characteristics are equally affected by directional dependencies, and they have a significant impact on the final image. Polarisation is one of the fundamental feature of radar, as the way in which a target scatters signal of different polarisations provides important additional information [170]. In addition, even the subsurface, under certain conditions, is capable of depolarising the EM wave ([171, 172]) as a result of combination of multiple reflection phenomena [173, 174, 175]. The same considerations apply for a change in the angle of incident of the wave, i.e., a variation of the antenna separation [176]. For example, targets designed to minimise backscatter might be easily detected by a bistatic configuration. Separating the transmitter and the receiver will allow the ground wave to detach from the surface reflection, providing a finer estimate of the dielectric characteristics of the propagating soil, and surface clutter effect can be reduced through a bistatic acquisition.

All the described acquisition procedures, however, are operationally limited by several factors related to both the physics of the EM wave propagation and to the instrumentation. First of all, the minimum achievable antenna offset is limited by the physical dimension of the antennas, which are inversely proportional to the central frequency, hence for low frequency survey, this might represent a notable shortcoming. In addition, shielded antennas are typically bigger than unshieled one. Concerning the physical constraints, accurate subsurface characterisation is typically performed in the far field region, i.e. Fraunhofer or radiating region, and hence attention should be put when operating in the proximity of the antennas, where the complexity of wave propagation behaviour and ground coupling processes is high. At the same time, a large offset capable of fulfilling such far field condition might not be feasible as a result of abosrption and attenuation phenomena, particularly if highly conductive materials are involved. As a general rule, it is agreed that the maximum antenna separation generally does not exceed two times the depth of the target [164].

In addition, the progressive transmitter-receiver separation for the acquisition of a bistatic profile should not exceed the Nyquist sampling interval defined above. Therefore, for each successive reading, the transmitter-receiver separation should increase by Δx (referring to Eq. 2.1), meaning that the transmitter and receiver should be moved a distance $\Delta x/2$.

2.6.2 Performance factors

Easy understandable, the major design control in a GPR system is the frequency of the emitted wave, and thus its wavelength and bandwidth. Image quality improves according to a decrease in the wavelength, although at high frequencies a limited soil penetration can be expected. It is clear therefore that a compromise should be found when evaluating the suitability of a GPR equipment for a specific application.

Two major factors determine the performance of a radar system, specifically the radar resolution, either vertical or lateral, and the maximum detectable depth. The maximum detectable range is defined as the maximum distance at which the target reflected signal amplitude exceeds the receiver threshold, while the radar resolution is derived from the resolvable limit threshold set by the Rayleigh criterion, determining the limit of certainty, in both time and space, in distinguishing between two close targets, before

their individual identity vanishes (Fig. 2.32) [1].

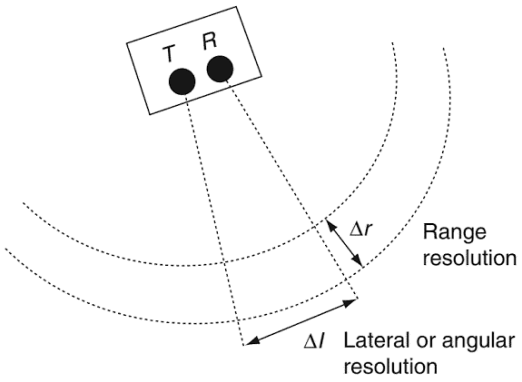

Figure 2.32: Resolution concept for GPR. *Derived from [15].*

The vertical (also range or depth) resolution provides information about the possibility of differentiating in time two closely occurring reflections as individual events. The vertical resolution for unmodulated transmissions primarily depends on the effective duration of the radar pulse, corresponding to the width of the signal envelope. Considering that GPR systems are typically designed with a 100% fractional bandwidth, i.e. the central frequency being equal to the total frequency span, these two parameters are often interchangeable.

This suggests that the shorter the pulse duration (i.e. the wider the bandwidth), the better its resolution, and that the slower the propagation in the medium the higher the discrimination performance, as the effective pulse duration depends on the wave propagation velocity in the medium.

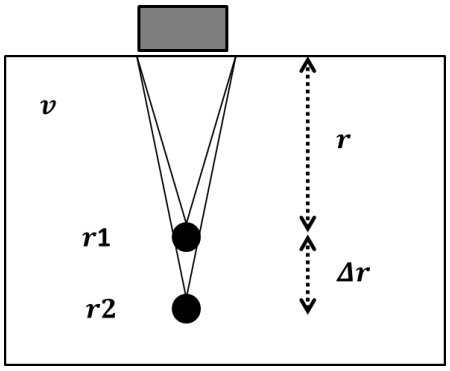

Figure 2.33: GPR vertical resolution concept.

Theoretically, taking into account Fig. 2.33, Δt can be defined as:

$$\Delta t = t_2 - t_1 = \frac{2\Delta r}{v} \tag{2.2}$$

where t_1 and t_2 are the travel times for reflections r_1 and r_2 and v is the wave velocity. As a general rule, it is possible to differentiate two targets when the time difference between their reflections is at least half the effective pulse duration, defined as the pulse half width or alternatively the -3 dB envelope width. Therefore, the theoretically achievable vertical resolution can be derived considering such pulse duration (τ_p) and the wave propagation velocity in the medium:

$$\Delta r \geq \frac{\tau_p v}{4} = \frac{v}{4B} = \frac{\lambda}{4} \tag{2.3}$$

in which is clear that the pulse width and the velocity in the material determine the range resolution.

Practically, two pulses, one reflected from the top and the other from the bottom of the target are distinguishable from each other when offset by a quarter of the wavelength of the GPR signal (for a 100% fractional bandwidth system).

Table 2.5 lists achievable values for vertical resolution for different materials and typical bandwidth.

Table 2.5: Vertical resolution of GPR systems.

Soil type	**Soil velocity** [cm/ns]	**Bandwidth** [GHz]	**Resolution** [cm]
Dry Sand	15	0.6 3	6.3 1.3
Limestone	12	0.6 3	5 1
Clay	6	0.6 3	2.5 0.5
Silt	8	0.6 3	3.3 0.7
Ice	16	0.6 3	6.6 1.4
Air	30	0.6 3	12.5 2.5

These values are in principle independent of the distance from the source, as they only depend on the emitted pulse width, but in practice the propagating wave experiences the so-called dispersion effect, causing an increase of the attenuation of the signal

with frequency. Essentially, the material behaves as a low-pass filter, hence increasing the duration of the pulse, as its high frequency content is muted, and consequently degrading the resolution performance.

Clearly, a large bandwidth signal is needed to have to possibility of distinguishing between closely spaced targets and to be capable of reconstructing the internal structure of a buried target.

Horizontal (also lateral or angular) resolution defines the minimum spatial distance that must exist between two targets located at the same depth so that the radar detects them as adjacent events. It mainly depends on the radiation pattern of the antenna and the depth of investigation, resulting therefore in a degradation of the resolution performance for targets that are farther from the source, as a consequence of the larger wavefield footprint.

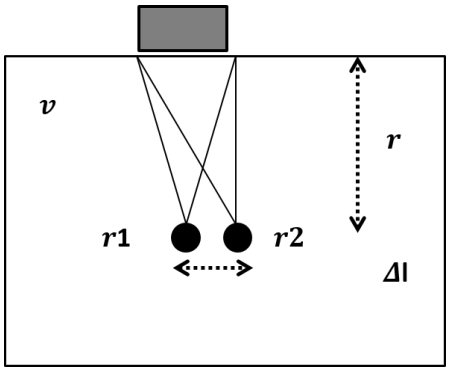

Figure 2.34: GPR horizontal resolution concept.

It is evident that the concept stems from the the Fresnel zone one, defining the area including a second target that however cannot be uniquely resolved. Hence, horizontal resolution can be essentially identified with the footprint size, commonly identified with the diameter of the first Fresnel Zone. As before, the time difference between the two events is expressed as:

$$\Delta t = t_2 - t_1 = \frac{2(\sqrt{r^2 + \Delta l^2} - r)}{v} \tag{2.4}$$

Employing the approximation of considering the target sufficiently distant from the antennas, the time difference becomes:

$$\Delta t = t_2 - t_1 = \frac{\Delta l^2}{vr} \tag{2.5}$$

and therefore the horizontal resolution must be:

$$\Delta l = \sqrt{\frac{\lambda}{2} r} \tag{2.6}$$

which corresponds to the Fresnel zone radius for monochromatic signals of that particular frequency. Note also that the horizontal resolution defines an area of resolution since all targets encompassed by a radius of $\Delta l/2$, perpendicular to r cannot be resolved. Finally, at best it is equal to the distance between transmitting and receiving antenna.

Table 2.6 lists achievable values for horizontal resolution for different materials and typical bandwidth, considering a target buried at 10 cm.

Table 2.6: Horizontal resolution of GPR systems for a 10 cm buried target.

Soil type	**Soil velocity** [cm/ns]	**Bandwidth** [GHz]	**Resolution** [cm]
Dry Sand	15	0.6 3	11 5
Limestone	12	0.6 3	10 4.4
Clay	6	0.6 3	7 3
Silt	8	0.6 3	8 3.7
Ice	16	0.6 3	11.5 5.3
Air	30	0.6 3	15.8 7

In general, to obtain an acceptable lateral resolution, a sharp beam is needed. However, small antennas with significant gain typically exhibit a high carrier frequency, which might suffer from a limited depth penetration. The footprint dimensions are related to the propagating material, hence plan resolution together with attenuation, provided that the collected signal content is enough to discriminate it with the clutter conditions [143]. In addition, it is dependent on the survey design, which will determine the lateral variations able to be imaged.

Figure 2.35 shows the effect of resolution for targets discrimination using a system

with a central frequency of 1.5 GHz.

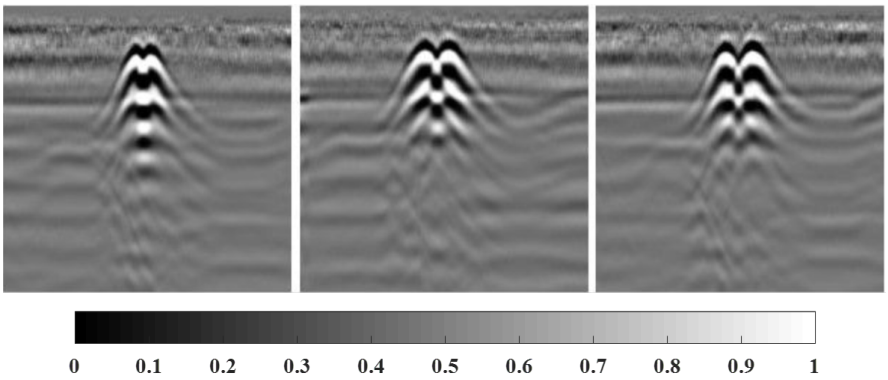

(a) Horizontal resolution. Objects separation is respectively 100 mm, 200 mm and 250 mm.

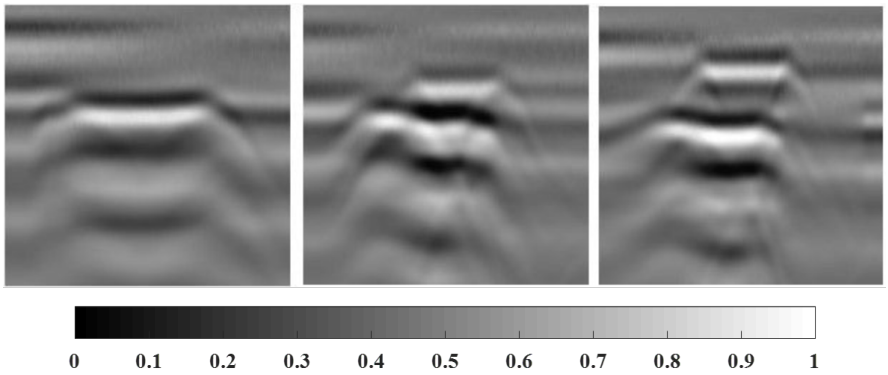

(b) Vertical resolution. Objects separation is respectively 0 mm, 50 mm and 100 mm.

Figure 2.35: Examples of GPR resolution concept. *Courtesy of geoscanners.com*.

Finally, while typical radar range performance, defined with respect to the receiver minimum detectable signal level, can be reliably estimated by solving a radar equation, GPR penetration performance cannot be defined in an absolute manner, as it strongly depends on the electromagnetic properties of the encountered subsurface materials, which are commonly unknown beforehand.

The definition and quality of a GPR images is highly affected by the propagation characteristics of the surrounding soil, and therefore, considering that the ratio of the wavelength with respect to the physical dimensions of the target is generally close to unity, it is clear that a GPR image will not correspond to its actual geometrical representation, conversely to what occur with optic, in which such ratio is considerably larger than unity.

2.6.3 Radar cross section and clutter

One of the primary factors determining the system detection performance is the target Radar Cross Section (*RCS*), which describes the magnitude of a scattered field observed in the far-field. Strictly theoretically, it is defined as "*the area intercepting that amount of power which, when scattered equally in all directions, produces an echo at the radar equal to that from the target*" [173, 177], and mathematically expressed in Eq.2.7.

$$\sigma_{RCS} = \lim_{r \to \infty} 4\pi r^2 \left| \frac{E_s}{E_i} \right|^2 \tag{2.7}$$

where E_s and E_i are the far field scattered and incident electric field intensities, respectively, and r is the target distance. It depends mainly on target dimensions (compared with the wavelength), shape, materials, polarisation and aspect angle [177]. In particular, it has been demonstrated that targets showing some directional features have a significant polarisation dependent scattering [178]. This is particularly true for elongated objects, as pipes and cables [179], but even complex targets could show a polarimetric behaviour [180].

In practice, it describes the spatial distribution of the reflected energy throughout the surrounding medium. This property can be interpreted as a consequence of constructive and destructive interference of the field reflected from a collection of coherently illuminated point scatterers.

Examples of RCS diagram for different targets are provided in Fig. 2.36.

When the scattering object is small its RCS is proportional to its physical size, thus the complexity of detecting landmines. Given this, the knowledge of the physical design of landmines is essential, as it significantly influences the corresponding RCS [182, 183].

The majority of landmines are composite objects moulded almost completely from plastic materials, with a very low metallic content. Given this design, a landmine may be in principle considered as the superimposition of a number of dielectric cylinders, each with its own specific angular scattering pattern and whose mutual interference is expected to produce a specific impact on the overall target signature and RCS in the form of multiple reflections. For example, such scattering events might originate from the presence of air layers and pockets, as well as other components and assemblies

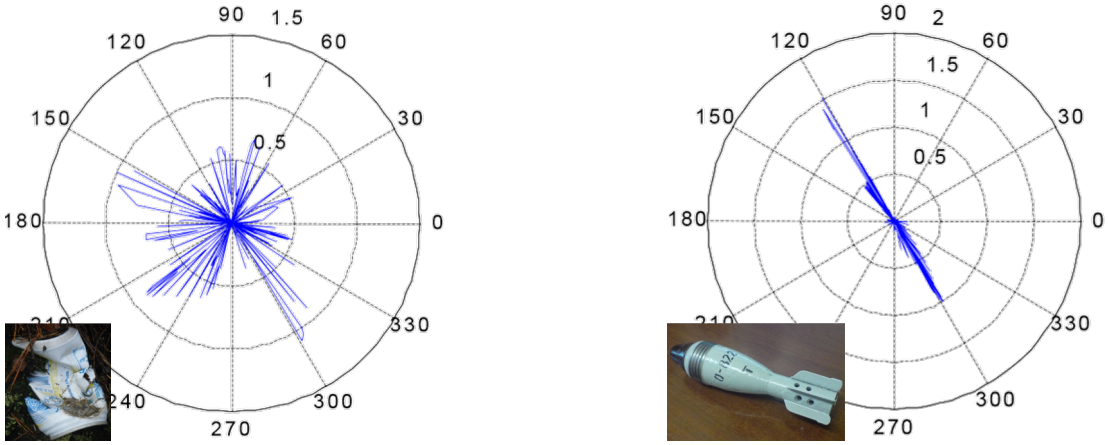

(a) RCS pattern for a randomly-shaped target.

(b) RCS pattern for an elongated target.

Figure 2.36: Examples of typical Radar Cross Section diagram for geometrically different objects. *Derived from [181].*

enabling the pressure action to be transferred from the pressure plate. Additional scattering anomalies can be attributed to other phenomena, mostly related to the rounded shape of the target, including specular reflection, diffraction scattering, creeping waves reflection and the equivalent waveguide effects, as well as the contribution generated by resonant scatterers, i.e. the interference of multiple discontinuities. Although the individual magnitude of these scattering contributions might be too limited to be identified, the ensemble of these events is likely to enhance the RCS, thus being beneficial for target detection.

Both target and clutter RCS are a function of the look angle and hence multiple looks at a target from different antenna spacings could facilitate the discrimination between targets of interest and clutter, as landmines could have some geometrical features and symmetry that are not present in clutter signature [184].

lutter in radar technology is commonly defined as deterministic reflections generated by events which are separate from the target scattering contributions but appear in the received signal within the same time frame with similar spectral features. Being stable in time, this interference cannot be removed via traditional clutter filtering algorithms and might provoke a decrease of the system detection threshold. It is clear that within the subsurface imaging domain, the term clutter might represents a significantly large number of sources [185, 186].

Soil heterogeneity, in terms of high fluctuations of the dielectric permittivity and

conductive texture of soil, causes the electromagnetic wave to be reflected and results in very high level of ground clutter which could mask weak target signatures. Small stones and gravel, as well as tree roots, animal burrows, metal fragments and other debris included in the soil are causes of undesired reflections [187, 188]. These conditions are often found in minefields, as exemplified in Fig. 2.37, thus underlining their operational relevance [189].

(a) Clearance operation in dense and thick vegetation, Colombia.

(b) Waterlogged minefield in the Falkland Islands.

(c) Barely visible AT mines within a rocky beach in the Falkland Islands.

Figure 2.37: Examples of minefield scenarios. *Courtesy of fenix-insight.com.*

Seeming unusual, these disadvantages brings equally significant benefits: imaging all discontinuities in the subsurface brings a large amount of data yielding a significant amount of information. Features can then be extracted and behaviour outlined, making the methodology suitable for classification and identification processing.

In summary, the detection performance of a GPR system employed as a landmine detector mainly depend on the mine RCS, thus including both physical and geometrical

properties, its burial depth and the electromagnetic characteristics of the above and surrounding soil.

2.6.4 GPR Data presentation

GPR data are generally presented and interpreted through a one-, two-, or three-dimensional display, commonly addressed as A-, B- and C- scans respectively:

- **A-scan**, Fig. 2.38a, displays the amount of received energy as a function of time. The energy is plotted along the vertical axis and the elapsed time is displayed along the horizontal one. In the A-scan presentation, changes in the impedance of the different materials can be estimated by comparing the obtained signal amplitude to that from a reference reflector. Reflector depth can be determined by the position of the signal on the horizontal sweep.
- **B-scan**, Fig. 2.38b, is a two dimensional plot representing an ensemble of A-scan acquired moving the equipment on a straight line. The horizontal axis typically describes the number of inline traces or scan length, whereas the vertical axis represents the time scale.
- **C-scan**, Fig. 2.38c, is a three dimensional display of GPR data resulting from a side by side arrangement of several B-scans. It can be seen also as a collection of horizontal slices, where each slice corresponds to a particular depth.

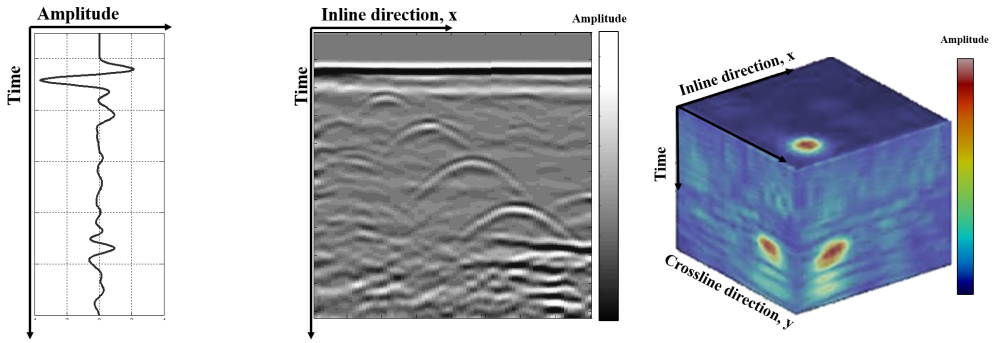

(a) A-scan. **(b)** B-scan. **(c)** C-scan.

Figure 2.38: GPR results visualisation techniques.

It is obvious that the three display modes are in ascending order according to the acquisition effort, but also by increasing level of information that can be gathered.

Depending on the objective and complexity of the survey, each visualisation method might better accomplish the required task. A single A-scan are commonly

used for retrieving the exact target position and for detection tests, but does not allow for extracting geometrical and physical properties of the object. A 3D survey represents the most challenging and demanding strategy, but the yielded information content greatly exceeds the one provided by other approaches. 2D profile analysis is a middle ground, as it limits the computational requirements at the same time highlighting valuable target properties. For the analysis of the hyperbolic pattern, it is important to note that its shape changes with depth, as hyperbolas become flatter at greater depth.

As for the other mentioned GPR features, the choice of a specific presentation mode, which clearly provides different ways of looking at the investigated target, mostly depends on the requirements of the survey and its objectives.

2.7 Summary

Landmines are a persistent and complex problem. Although numbers have declined significantly in the last two decades, landmines still affect almost 30 per cent of countries, and have caused an average of more than 5,000 casualties per year in the last 5 years, with sharp rise in the last two. Landmines still pose a serious and global problem despite the work of engineers, NGOs, and policymakers, who have made real headway in the last 20 years, reducing both the number of landmines deployed, and their use. Moreover, landmines pose a problem that is complex, seen in different terms by different players, and therefore defies a clear solution.

Conventional antipersonnel mine detection equipment and procedures have not significantly evolved, as detection and clearance approaches developed during the Second World War still represent the most widely adopted technique for detecting and removing landmines: metal detectors for object identification, and a manual and careful analysis of the affected zone.

Difficulties in detecting limited amounts of metal in a minimum metal landmine through a metal detector sensor, have led to the surfacing of Ground Penetrating Radar as a promising technology. GPR is a widely adopted near surface geophysical technique within the civil engineering, environmental and soil investigations, as well as geology and geotechnical engineering, mainly as a consequence of its high resolution imaging and non-destructive approach. Considering also that it can detect both metallic and non-metallic objects, it is intuitive that detection of buried landmines has proved to be

a successful application of GPR technique.

Compared to alternative detection and sensing solutions, GPR exhibits several operational advantages, the first being the fact that it senses electromagnetic variations in the ground, hence its detection capability is not bounded by the presence of a specific material or substance. Consequently, it can locate mines with a wide variety of casing and internal composition, including minimum metal landmines. Under this perspective, GPR can be considered a complementary technology to conventional metal detectors. In addition, it can generate an image of the subsurface anomaly, on which basis the detected object can be confidently identified and classified. Finally, the scanning rate might be comparable to that of an EMI system. However, being sensitive to any electromagnetic heterogeneities occurring in the subsurface implies that all the related sources might be in principle considered as potential objects, which should be discriminated with advanced data processing schemes, hence the high false alarm rate to which GPR is subjected. Finally, it should be mention that system performance are highly variable and difficult to forecast, as the possibility of detecting a landmine depends not only on the equipment properties, but also on soil texture, moisture and stratigraphy, surface characteristics, and landmine location. On account of these elements, in the near future GPR might hardly represent a standalone detection solution, but it can play a decisive role within a multi-sensor platform.

While considerable research into target recognition techniques has been carried out, the variability of the soil and target parameters has challenged the development and implementation of robust and reliable signal processing methods, meaning that there are still considerable opportunities for improvements in detection performance as well as reduction of false alarms.

Chapter 3

Research Context

The saddest aspect of life right now is that science gathers knowledge faster than society gathers wisdom.

Isaac Asimov [190]

Ground Penetrating Radar surveying is aimed at retrieving unknown physical properties of the internal status of the structure under investigation by making use of limited measurements of scattered electric fields. Traditional radar approaches allow the extraction of qualitative information from the collected radar signals, whilst in several applications, including forensic investigations, a quantitative characterisation of the detected target might be advantageous. This requires to cope with an electromagnetic inverse scattering problem that is non-linear and ill-posed [22]. Inverse scattering theory demonstrated that ideal noise-free data for orthogonal polarisation and all aspect angle can uniquely determine a target. In reality, due to measurements uncertainties and errors, the inversion is strongly ill posed, thus only approximate solution can be retrieved [191].

The application of Ground Penetrating Radar for landmine clearance is by no means an undiscovered topic in scientific literature.

However, an effective deployment for the purpose is not so straightforward, mainly as a consequence of both operational and physical weaknesses. First of all, it should be considered that the majority of antipersonnel landmines are dielectric objects, with minimised metal content and a physical dimension not exceeding 15 cm. Properly reconstruct an object with these features necessitates a the system with a very high resolution, which might be challenging to achieve in both lossy soils, which act as a

frequency low-pass filter, and in low-loss soils, situation in which the dielectric contrast between the target and the surrounding soil might be low.

Although technologically advanced, GPR systems still suffer from severe limitations concerning clutter reduction and image resolution. The effects of surrounding soil, landmine characteristics (both geometrical and physical), equipment design and acquisition strategies are only a few of the major aspects affecting the quality of the outcomes [192].

The next challenge is therefore to move from qualitative interpretation, which depends heavily on the human visual interaction with the data, towards the extraction of quantitative target parameters and identify target attributes quickly and (possibly) automatically.

To cover the research in these areas, contributions from several research communities have been evaluated and the main contributions have been reviewed.

3.1 Scattering from composite targets - landmines perspective

When exploiting the signature generated by a plastic cased landmine, a feature rarely considered is the presence of the internal structure, i.e. the ensemble of components that allow the device to properly work. Although each type of landmine has its characteristic internal mechanics, a common ground can be defined.

Considering a blast antipersonnel landmine, the most common among mine categories, the internal design might be outlined as composed of: (1) the external mine casing, including the pressure plate, (2) the main explosive charge and the detonator one, (3) the fuze, and (4) the trigger mechanism. Since plastic materials have permittivity similar to those of explosives (Table 3.1), it is a common approach to consider the casing and the explosives as one.

In plastic landmines, the fuze typically represents the only metal component, even if such content might be circumscribed to the presence of small firing pins and springs, for only about few grams [193]. What is to be highlighted is the existence of air gaps, essential components for the triggering movement, which are expected to amplify the scattering response of the landmine, and consequently to facilitate its detection. Fur-

Table 3.1: Relative dielectric constant of landmine constituents.

Material	**Relative dielectric constant ε_r**
Neoprene rubber	6-9
Bakelite	3-5
Polycarbonate	2.9-3.5
Polyethylene	2-2.5
Epoxy resin	3-4
TNT	2.7
PETN	2.72
Comp B (RDX TNT)	2.9
Tetryl	2.9
Semtex (RDX PETN)	3
Comp C-4 (RDX)	3.14
Nytroglycerine	19

thermore, due to their unique design, the potential of imaging these components (location and spatial extension) could be beneficial for target classification and identification.

Figure 3.1 shows two examples of disassembled landmines, picturing the typical included internal components.

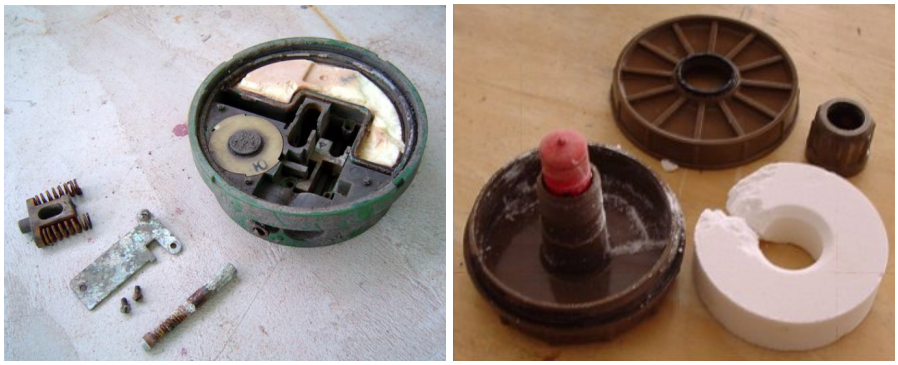

(a) Soviet PMN-2. *Courtesy of or-data.info*

(b) South African R2M2. *Courtesy of nolandmines.org*

Figure 3.1: Examples of anti-personnel landmines internal design.

Simplifying the situations, the target can be modelled as a three layer objects, inlcuding (1) the activator plate, (2) an air-filled layer, and (3) the main body, as sketched in Fig. 3.2.

Very few works have addressed the task of detecting the reflections generated by the internal components of buried landmines and determining their effects, as most trials have been performed employing devices and surrogates which accurately replicate the external design of real landmines and are moulded from a material, typically a resin,

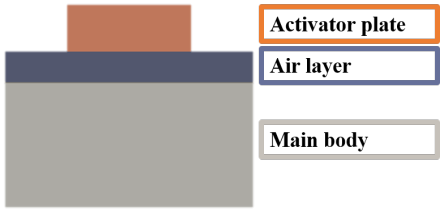

Figure 3.2: Simplified model of anti-personnel landmines.

exhibiting a dielectric constant similar to the values of the most common explosive substances.

As a starting point, a signal having a large bandwidth is required to be able to distinguish between the different target scattering contribution and to delineate the internal structure of the landmine. Therefore, in this context the effective spectral content, and in particular the high frequency components, becomes a fundamental aspect [194, 195, 196].

In [197], it has been found that the internal structures of penetrable objects can perturb the phase property of radar waves, therefore a distinction of objects with different internal structure can be made exploiting the phase variations induced by rough surface scattering. Unfortunately, the method allows this distinction for target located in the same homogeneous layer of soil, and buried under a flat surface. Similarly, the Authors of [198] explicitly employ the impedance discontinuity profile of a landmine in a syntactic, rather than statistical, pattern recognition scheme to discriminate landmines from clutter, underlining that these patterns are unique in the presence of clutter since they are based on the internal structure of the landmine. However, the impact is limited by the evaluation of anti-tank landmines only. Work in [199], even if with a completely different aim, gives an experimental evidence of the resonance effect of the GPR waves entering the mine and reflecting internally inside the mine.

In addition, research reported in [200, 201] both indicate that the signature resulting from minimum metal landmines is affected by the internal structure, providing modelling and approximation in order to take into account this effect in the scattering theory. Another evidence of the internal scattering is given in [202], in which a cross-polar contribution in the radar signature, quite unexpected considering cylindrical objects, is to be attributed to the presence of the detonator and other internal mine structure. What can be inferred is that identifying landmines by looking for targets with

negligible cross-polar response is not to be recommended.

3.2 System design

For the purpose of enriching the information received from the target, a strategy is to employ GPR configurations with multiple components and a particular emphasis will be put on the exploitation of angular diversity. This diversity can be obtained varying the relative geometry between the system and the target, hence separately managing the transmitter and the receiver.

3.2.1 Multistatic GPR

Most of the contribution to GPR development has been directed at monostatic systems or bistatic systems with closely spaced antennas, as for the case of the previously described GPR systems. Although most of the current GPR cover wide frequency bandwidths and some of the advanced ones utilise polarimetric antennas, the quality of the acquired information and processing can still be enhanced.

The expected advantages brought by the adoption of a multistatic system is the possibility of enhancing the information that can be retrieved from the resulting data through the exploitation of the angular domain [203, 204]. Principal drawbacks are the physical limitations that could not allow a hand-held implementation. The increased complexity of these configurations is expected to pay back in an enhanced image resolution or clutter suppression [205, 206].

During the last years, one of the major GPR advancements is represented by the implementation of multi-channel systems. In particular, GPR arrays have gained a relevant importance for their vehicle mounting potential and forward-looking imaging capability, enabling for operationally advantageous stand-off distances and rapid survey of wide areas [207]. A multi-channel GPR system can exploit the angle-dependent scattering information, i.e. the bistatic scattering behaviour, and thus it is expected to improve the capability to discriminate landmines from clutter [208]. Generally, it is understood that these acquisition schemes allow to obtain enhanced subsurface imaging.

First of all, multistatic GPR, intended here as a system in which the transmitter and the receiver are separated and independently managed, has three surveying modes (Fig. 3.3) depending on how the transmitter and receiver antenna moves:

- **Multi-offset** (Fig. 3.3a): both antennas move together in the direction of survey with a fixed offset, changed for each profile.
- **Common source/receiver** (Fig. 3.3b): the transmitter (receiver) is fixed, however, the receiver (transmitter) moves along the survey direction.
- **Common depth** or **common mid point** (Fig. 3.3c): both, the transmitter and receiver antenna, move away from a common point in opposite direction.

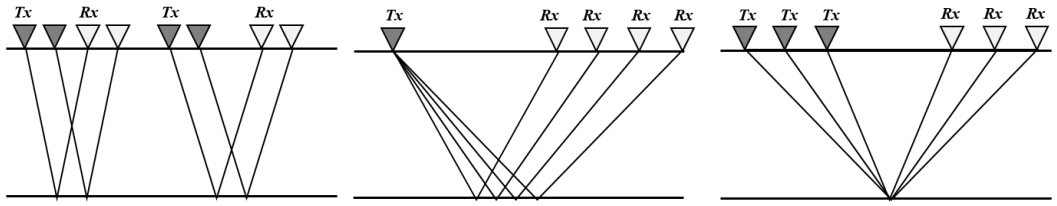

(a) Multi-offset. **(b)** Common source. **(c)** Common mid point.

Figure 3.3: Multi-offset GPR survey. Tx and Rx represents respectively the transmitter and the receiver.

The expected potential of these strategies is to yield lighter weight, lower cost systems and improved performance, in terms of detection, identification and coverage, and system flexibility, as they can operate in several modes.

From an operational perspective, the most efficient acquisition scheme is the multi-offset one (Fig. 3.3a), as it only requires a single channel equipment, followed by the common source or common receiver approach, where only a single element is shifted, while a CMP acquisition procedure (Fig. 3.3c) represents the most demanding one. Conversely, in terms of results accuracy, it is clear that the situation is the reverse, as it might be difficult to ensure the multi-offset profiles correspondence.

Considering the aim of the work, the advantages of the first scheme are limited by several reasons. Landmines are small objects, and their internal components are even smaller, and if one considers the width of the radiation pattern it is hard to imagine that sharp, preferential scattering directions exist, as it could be for highly reflective large planar targets. What has been found is that a change in the antennas separation could highlight internal reflections and that there could be evidence of asymmetry in the target design, but it is not possible to determine an optimum offset under which there are unique features to mark. For such a family of targets, the information gathered from a multi-offset scheme converts to the content of a single offset one. Reflections generated by the internal structure are a result of multiple reflections/transmissions events,

therefore these returning waves will have a limited amplitude, bounding the effective antennas spacing. Practically, this means that from these bistatic profiles it is not possible to extract clear indications on the presence of internal scattering components, and consequently that multiple profiles are needed, with all the drawbacks that have been previously highlighted.

To provide a conceptual explanation, Fig. 3.4 describes the expected impact of an offset variation applied to the characterisation of the internal structure of a buried target, comparing the two cases of a solid dielectric object (Fig. 3.4a to Fig. 3.4c) and a target including an internal assembly (Fig. 3.4d to Fig. 3.4f).

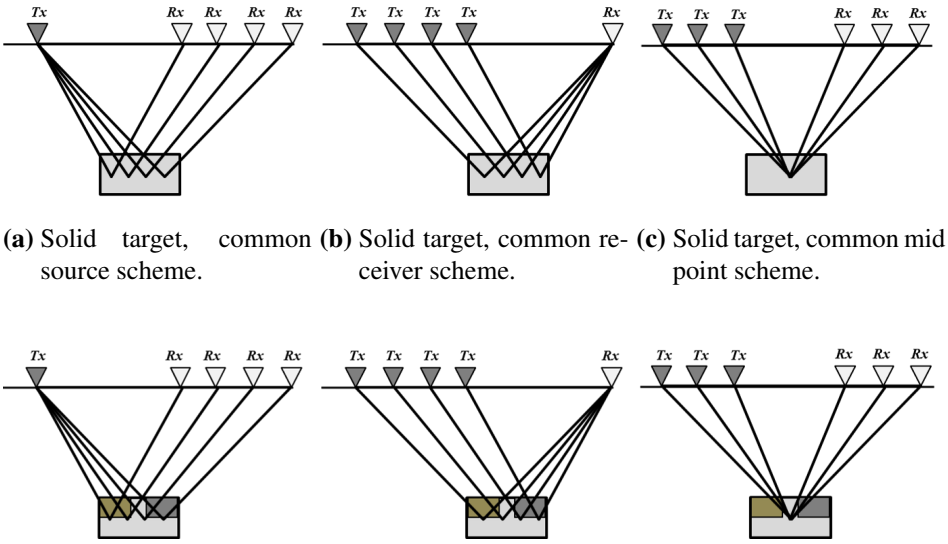

(a) Solid target, common source scheme. **(b)** Solid target, common receiver scheme. **(c)** Solid target, common mid point scheme.

(d) Composite target, common source scheme. **(e)** Composite target, common receiver scheme. **(f)** Composite target, common mid point scheme.

Figure 3.4: Effect of antenna separation for solid and composite targets.

As the wave propagation is defined by the ray path, a signature collected at particular incident angle will be characterised by a number of propagation phenomena which may be different for complex and composite targets. This is not supposed for a solid dielectric target, for which a change in the angle of arrival of the wave should not produce noticeable changes. Hence, these changes are highly dependent on the internal design of the target, as previously described. Regarding the terminology, the term multi-offset comprehensively includes all the geometries involving a change between the transmitter and receiver separation.

Figure 3.5 provides a schematic example of a bistatic radar image and the information that can be extracted.

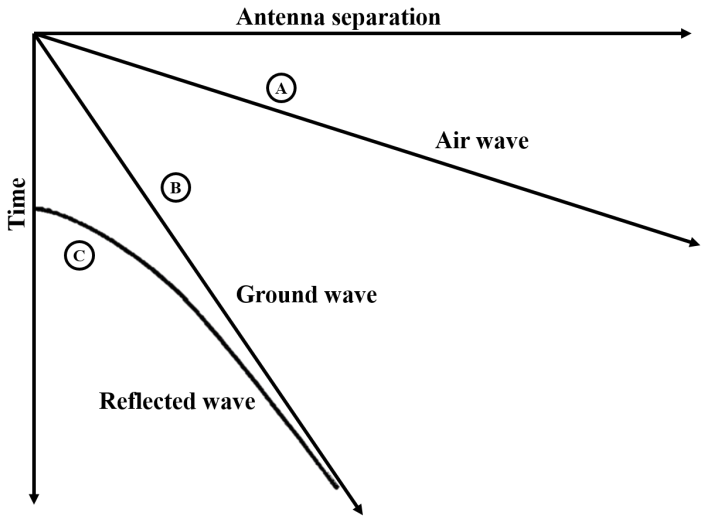

Figure 3.5: Event recognition on a multi-offset GPR image.

From a bistatic or multi-offset image, three fundamental events can be determined: (1) the air wave (event marked A in Fig. 3.5), representing the direct wave travelling from the transmitter towards the receiver, (2) the ground wave (event marked B in Fig. 3.5), which is the wave following the previous path but propagating over the surface, and (3) the reflected wave (event marked C in Fig. 3.5), generated by the target scattering. Considering that the gradient of each wave is inversely proportional to its velocity, it is clear that the air wave will always have the same slope, while the inclination of the ground wave will be governed by the dielectric characteristics of the very first layer of the subsurface. The hyperbolic pattern of the reflected wave will asymptotically tend to the ground wave only when homogeneous materials are involved, otherwise these waves will diverge or cross each other as a consequence of subsequent reflection or refraction. Finally, the bistatic angle, which is the angle seen by the target including both the transmitter and the receiver, can be obtained solving the trigonometric function considering the antenna separation and the depth of the target.

These multi-offset strategies have been extensively employed for the characterisation of the medium velocity, as they could provide a more accurate and precise estimate, compared to the hyperbola fitting approach, and to enhance the SNR values by reducing random and non-coherent disturbances, even through a directional and selective removal. In addition, they allow for constructive data stacking, thus improving the quality of the obtained images, and can better reconstruct vertical and lateral velocity distributions.

However, the adoption of these configurations has been merely considered as a way to improve the scanning rate and augment the surveyed areas, leaving aside the exploitation of the additional scattering information yielded by such system architecture, as well as the potential for deploying multi-channel GPR platforms with frequency, orientation and offset diversity features.

Under this hypothesis, a number of works have exploited the advantages of having multiple looks at a target from a variety of antenna spacings.

Work in [209] employed numerical scattering models to compute the monostatic and bistatic image of two metallic targets (ogive and missile-like shape) to provide an imaging comparison. With different acquisition geometry and bistatic angle, it demonstrated that bistatic images could lead to a better description of the higher order scattering effects, thus depicting different target features. Similar comparison has been made in [210], where it is shown that angular diversity allows for highly resolved images from single frequency data.

In [211] a multistatic GPR array is used on a number of targets in both free space and in soil, evaluating as well the effect of surface clutter. Results show that for shallow targets a close proximity yields *SNR* ratio, while a large spacing is unsuitable for their detection. Obviously, the concept is reversed for deeper targets. In addition, a coherent sum of the collected bistatic pairs demonstrated some potential for enhancing the quality of the obtained images. The same concept is demonstrated in [212], where a target to clutter ratio can be improved combining images from different bistatic configurations and elevations. Authors in [213] used a similar same approach for testing an inversion algorithm, underlining the strong interference generated by the surface clutters.

In [214], an approach based on the combination of monostatic and bistatic systems is presented in order to lower the effect of multipath scattering. Starting from the assumption that false targets detected by the monostatic case are located at different positions from the bistatic one, a simulation with three point scatterers illustrates the benefits that can be obtained by cancelling the multipath effect using information contained in the bistatic data.

The authors of [215] presented a feature extraction scheme to obtain bistatic scattering information from a vehicle mounted GPR system with multistatic capabilities. The resulting images effectively demonstrate the symmetrical behaviour of landmines,

as opposed to some clutter objects. The applied processing is based on the extraction of the seven moment invariants from a space-wavenumber processed image, which contains frequency and aspect-angle information, in order to obtain invariant properties. The assumption is that a landmine is a perfect body of revolution.

Studies in [216, 217] exploited the angular diversity for increasing the informative content of a GPR 2D image, providing at the same time a practical hardware and signal processing implementation of the proposed solution. Examples of what can be gained from multiple illumination are provided through experimental and simulated data.

Work in [218] provided a demonstration of the improved resolution that could be achieved using a multistatic array processing, in particular overcoming the influence of target radar cross sections and antenna radiation directions of monostatic 2D GPR data.

A multistatic geometry can be beneficial also for features extraction scheme, as evaluated in [219] in which an array of receivers increased the robustness of a resonance-based feature classification technique, recovering many characteristic target resonance signature. Authors in [220] applied a non-linearised image formation scheme relying on single frequency angular diversity data, hence requiring a multistatic radar system. The same factorisation method has been used in [221] to combine information gathered from a mulstistatic geometry, realised in the form of multiple fixed offset. Similarly, work in [222] shows that measurements using bistatic observations can be valuable for evaluating target symmetry, but also underlines that a large and diverse collection of measures formed from different bistatic geometries are needed for a proper classification.

Independently managing the transmitter and the receiver means that interferences from the ground reflection can be properly mitigated estimating the Brewster angle and set up the system accordingly, as shown in [223, 224].

3.2.2 Polarimetric GPR

The polarisation information contained in the reflected wave is highly influenced to the geometrical structure and orientation of the given target, as well as to its physical properties [225]. Polarisation refers to the locus of the electric field vector in the plane perpendicular to the direction of propagation, hence geometrically it describes the pattern outlined by the vector, whose length and rotation rate are respectively de-

termined by the amplitude and frequency of the wave, representing the the magnitude and direction of the electromagnetic field as a function of time and space.

Three main polarisation states can be defined:

- **Linear** polarisation: the vector is confined to a plane that is parallel to the direction of propagation. It can be further divided in horizontal and vertical.
- **Elliptical** polarisation: the rotating E field follows a path that traces an elliptical pattern with time.
- **Circular** polarisation: A special case of elliptical polarisation. It can be further divided in right and left.

For linearly polarised waves, the only way to change the orientation of the E field is to rotate the transmitting or receiving antenna. This is why in most cases, polarisation and antenna orientation terminology are alternatively employed. Hence, antenna orientation is critical for antennas that generate linearly polarised signals, but it is not as critical for antennas that generate elliptical or circular polarised signals. Finally, any linearly polarised wave can be obtained as a superposition of a left circularly polarised and a right circularly polarised wave, whose amplitude is identical. Most commercial GPR antennas are dipole or bow-tie antennas that radiate linearly polarised energy with the majority of the radiated electric field oriented along the long axis of the dipole or bow-tie.

Circular polarisation, which is commonly achieved through spiral antennas, has some advantages over linear polarisation. In particular, when the target exhibits significant polarisation attributes, the strength of the reflected wave will be affected by the relative geometry between the object and the antenna, if linearly polarised. In addition, in case of a pronounced polarisation mismatch, for example when adopting a cross-polarisation configuration for reducing antennas mutual coupling, the reflected wave might be hard to detect. Another advantages of circular polarisation is that, as a result of the permittivity ratio between soil and air being larger than one, at oblique incidence the polarisation sense of the wave reflected by the surface will reverse, making the system in principle insensitive to surface scattering. Unfortunately, these advantages are compensated by a reduced efficiency in converting the input power into radiated one.

Wave polarisation can be represented in a number of ways, usually in terms of the polarisation ellipse [226], which defines the polarisation state through the parameters of

ellipticity angle, which is the ratio between the two ellipse axes, the orientation angle, corresponding to the rotation of the major axis and the horizontal one, and the polarisation sense, given by the rotation sense of the field vector. In the Poincaré sphere representation [227], the polarisation state is represented by a point in a polar coordinates system. Every point on the sphere uniquely defines a polarization state. A descriptive sketch is provided in Fig. 3.6.

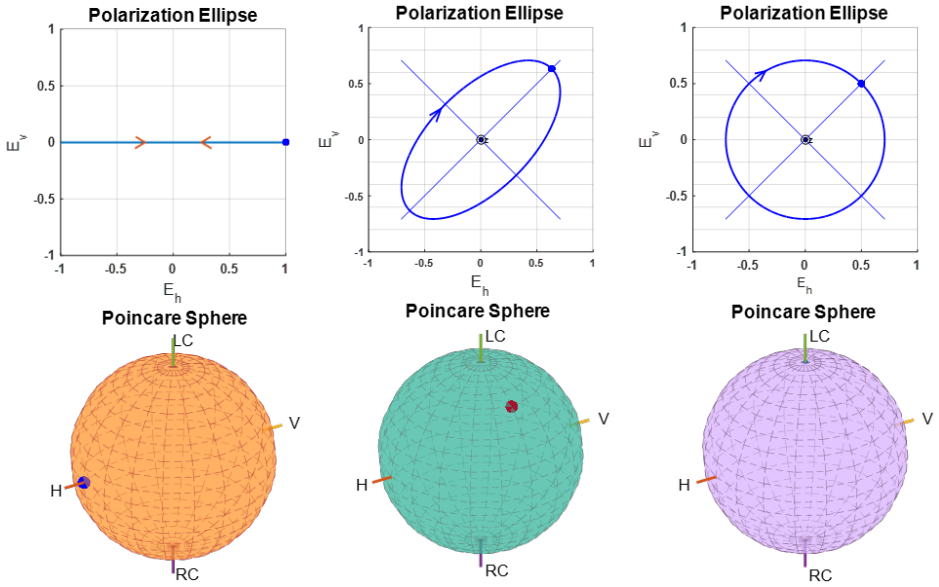

(a) Linear horizontal polarisation. **(b)** Elliptical polarisation. **(c)** Circular polarisation.

Figure 3.6: Representation of different wave polarisation state.

Another useful representation is the polarisation chart, obtained by an orthogonal projection of the Poincaré sphere on its equatorial plane. Lastly, the polarisation state of waves can also be described by the Stokes vector [228].

As per the reciprocity theorem, the polarisation vector of the backscattered wave can be expressed as a function of the monostatic scattering matrix of the target [229, 230, 231] ([232, 233] for the bistatic equivalence), which represents a set of parameters for describing the symmetry, structure, torsion and helicity of a target.

Polarisation affects how a radar system perceives the objects in the scene. Therefore, collecting images using different polarisation combinations may provide different and complementary information [234, 235].

In particular, through reception diversity, i.e. a dual-polarisation receiver, it is possible to retain the information included in the target backcsattered wave, while if

diversity is adopted also in transmission, the target scattering behaviour can be completely determined. The price is an increased system complexity.

Within the GPR domain, the benefits of considering polarisation properties can be summarised as follows:

- Discrimination: two waves arriving at the same time might be difficult to distinguish basing the analysis on frequency, amplitude or phase only, but they can be differentiated in polarisation.
- Optimisation: considering that the shape of some specific targets can be better estimated using a polarisation configuration other than the conventional linear one, the adoption of a certain type of input polarisation might better fulfil a given task.
- Identification: since the polarisation property of the reflected wave is affected by both the geometry of the scatterer and the propagating material, it might be possible to pick out such information by analysing the polarimetric characteristics.

When discussing wave polarisation of GPR signals, three concepts are to be mentioned: (1) polarisation due to antenna design, (2) polarisation due to antenna orientation, and (3) depolarisation (or changes in polarisation) due to target orientation.

The target geometrical properties influence the polarisation of the scattered wave, as well as the incident angle of the wave and the electromagnetic impedance contrast of the involved materials. This means that polarisation characteristics can be either maintained or the scattered wave can be polarised differently from the incident one, in which case it is said to be depolarised. Various targets of GPR investigations, including not only pipes and cables, but also fractures, exhibit pronounced polarisation-dependent scattering characteristics, implying that their detection is subjected to a favourable combination of antenna configuration and relative orientation. As a consequence, certain subsurface objects might not be properly reconstructed using a single polarisation configuration.

For linearly polarised equipment, the antenna orientation concept defines the relative orientation between the transmitter(s) and the receiver(s), as well as the antenna orientation with respect to the survey direction. Following this convention, antennas arranged in parallel orientation (i.e. transmitter and receiver parallel to each other, the most commonly adopted solution) can be further classified depending on whether they

are in broadside (i.e. parallel to the survey direction) or end fire (i.e. perpendicular to the survey direction). Conversely, when the transmitting antenna is orthogonal to the receiving one, they are said to be cross-polarised [170]. These configurations are sketched in Fig.3.7.

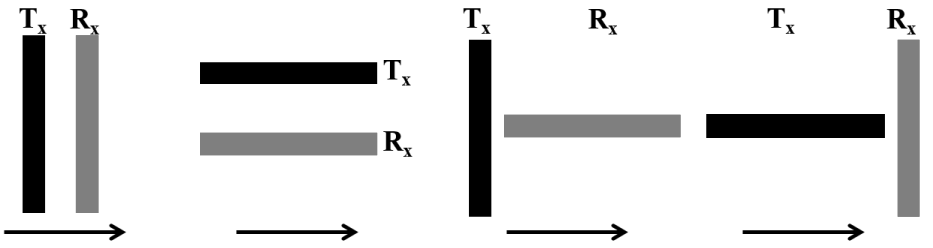

(a) Co-pole, end fire. **(b)** Co-pole, broadside. **(c)** Cross-pole, end fire transmitter. **(d)** Cross-pole, broadside transmitter.

Figure 3.7: Representation of different antenna configuration for multicomponent data acquisition. The black arrow represents the survey line direction.

For a monostatic system, which utilises the same or at least co-located antennas for both transmit and receive functions, the two cross-polar configurations coincide, i.e. the scattering matrix is symmetrical and has only 3 independent elements.

The magnitude of a wave reflected from an isotropic target (such as rounded and spherical objects) is independent of the transmitter polarisation, while for target exhibiting some directional features (i.e. elongated objects) the reflected field exhibits a specific polarisation characteristics regardless the transmitting one. For a random target, the amplitude and polarisation of the reflected field are influenced by the transmitter polarisation [236]. Extended targets, and consequently their relative scattered wavefield pattern are usually 3-D, hence transmitter and receiver polarisation diversity will generate different polarimetric images, which can be used or combined for target identification purposes.

It is clear, then, that polarisation plays a fundamental role in applications such as pipes and utilities detection, but also for the correct imaging of extended targets. It is also clear that the way in which the target respond to an impinging polarisation is critical in the light of wave depolarisation.

Polarisation is implicit in the definition of a target radar cross section, and it is commonly assumed a polarimetric match between the transmitted and received fields. But in principle the radar cross section can be , or must be, specified for arbitrary

polarisation combinations.

The RCS for circular polarisation is supposed to be equal to the RCS for linear polarisation if the angle between the E-field and the wire is 45 degrees, i.e., half of the RCS for parallel orientation, hence elongated targets with arbitrary orientation can be detected by GPR using either a circularly polarised antenna or two perpendicularly oriented antennas with linear polarisation.

Several detailed works on the effects of polarisation for common GPR targets have been produced. Polarisation is understood to have a significant impact for the identification of elongated objects and asymmetrical subsurface features [237, 238], and it is widely exploited as an additional instrument that could provide further features of the buried objects [239, 240, 241, 242]. However, few GPR sensors use more than one polarisation.

In [243], a Finite-Difference Time-Domain (FDTD) modelling solution and analytical measures were developed to simulate the polarimetric response of both symmetric and asymmetric targets, providing a demonstration that such symmetry features can be used to adequately separate between those target categories. The advantage is that the methodology is independent of target shape, size, material, or depth, hence it does not require beforehand knowledge or information about the target.

Authors in [244] described a polarimetric GPR which is invariant to rotations (demonstrated in [245]) to acquire quantities related to the shape and dimension of the target from the target scattering matrix. Target used was a disk brake rotor, hence the formation of the scattering matrix is facilitated.

In [246] the author offers an insight from what can be gained from polarimetric analysis of GPR backscatter signal. Assuming the target being metallic, elongated and buried at a shallow depth, simulations provide interesting results in terms of (1) length, (2) orientation and (3) radius inference. Graphs show a clear implications of the angular patterns: backscattered magnitude drop down when there is a misalignment between the antenna and the target, following the well-known trends of linear target.

Work in [247] has a similar aim, to show the influence of geometry on the fingerprints of different landmines. In particular, a comparison of landmine signature for different observation points, both vertically and laterally shifted and tilting objects is discussed. The analysed target is a M14 mine, characterized by a low metal content

and a reduced dimension (40 mm height and 56 mm diameter) with a cylindrical shape. Results show a variation in the magnitude of the backscattered electric field as receiver position and orientation changes. Results illustrated that the shape of the fingerprint within the bandwidth always remains nearly the same. Differences are visible with the highest part of the spectrum, in which of course the spatial resolution is higher. It can be noticed that a tilting of the landmine significantly changes the energy trend.

Results in [248] demonstrated that the backscattered fields from a body of revolution (BOR) target illuminated through either an horizontally or vertically polarised plane wave exhibit a negligible cross-polarisation contribution. This characteristic has been highlighted through an experimental campaign carried out with a metallic landmine surrogate, and is proven to be valid while the BOR conditions are satisfied.

3.3 Summary

In this Chapter literature considered relevant to the research problem has been presented and discussed. This analysis has confirmed that rather few works have addressed the task of discriminating landmines on the basis of their internal scattering contributions, and that there is a lack in understanding of the significance of these signature components and how they can improve GPR performance. Even if the presence of such reflections has been pointed out, the feature has not been exploited and researched. Moreover, there are few experimental results available characterising the landmine GPR response, and in particular plastic-cased ones, mainly as a consequence of the difficulty in accurately extracting the target signature and isolating it from the surrounding environment, as well as considering that in a typical landmine detection scenario, the target is located in the near field of the antennas, complicating its scattering characterisation.

Up to now, the exploration of angular diversity in the sense of monostatic and bistatic look angles at the target has only rarely been taken into account. The majority of works on bistatic GPR configurations have focused on the evaluation of geometrical features, showing some potential but highlighting also limiting hypothesis, both concerning target modelling and acquisition scheme. Similarly, publications on polarimetric GPR largely focus on the challenge of distinguishing targets with a predominant geometry from objects showing a symmetrical structure. Theoretically, multicomponent analysis may produce a useful discrimination, however, it is currently not

clear whether polarimetric information can as well be exploited for very small targets like anti-personnel landmines, and whether it could cope with inclined targets, for which the symmetrical feature will vanish.

From this review of recently published work, it can be stated that the research questions formulated in Section 1.7 and the scientific innovation summarised in Section 1.8 have not previously been addressed in the literature.

Chapter 4

GPR Design and Modelling

In theory, there is no difference between theory and practice. But, in practice, there is

Jan L. A. van de Snepscheut [249]

The objective of this Chapter is to establish a theoretical justification of the addressed problem and to provide an analytical basis for the subsequent experimental section. This Chapter covers the fundamental principles governing the GPR methodology, emphasising the differences not only between GPR and conventional radar, but also between GPR as a landmine detector and for other GPR applications.

Firstly, a succinct overview of the key concepts influencing electromagnetic wave propagation and reflection is provided and the physical issues evaluated in order to give a sense of the role played in the process. Through the radar range equation, the analysis continues considering the primary factors influencing the design and achievable detection performance of a GPR system to illustrate their dependencies and repercussions. To examine the impact that a dynamic separation between the transmitter and the receiver has on the involved parameters, bistatic developments of the previous formulations are given as well.

As the aim of the work is to characterise a landmine in light of its internal structure, particular attention is put on the constraints in place for a landmine detection equipment, discussing the principal challenges concerning the identification of the internal scattering contributions.

In the latter part of the Chapter, a number of numerical simulations based on FDTD

modelling involving the key variables affecting the imaging performance is developed and assessed in the light of the research objectives previously described.

4.1 Electromagnetic principles of GPR

The foundations of GPR lie in electromagnetic theory, of which Maxwell's equations and the electrical properties of materials are the basis, and the aim of this section is to provide the primary elements required to quantitatively exploit GPR phenomenology.

4.1.1 Physics of propagation

4.1.1.1 Energy transfer

In the case of an electrically small linear antenna with a uniform current distribution,shown in Fig. 4.1, the electric and magnetic field components in free space are described in Equations 4.1, directly derived from Maxwell's equations.

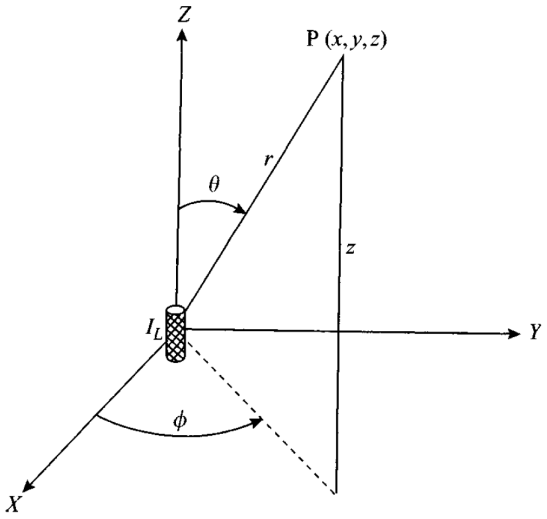

Figure 4.1: Electrically small antenna.

$$E_r = \frac{\eta_0 Idl}{4\pi} e^{-jkr} \left[\frac{2}{r^2} + \frac{2}{jkr^3} \right] \cos\theta \tag{4.1a}$$

$$E_\theta = \frac{\eta_0 Idl}{4\pi} e^{-jkr} \left[\frac{jk}{r} + \frac{1}{jkr^3} + \frac{1}{r^2} \right] \sin\theta \tag{4.1b}$$

$$H_\phi = \frac{Idl}{4\pi} e^{-jkr} \left[\frac{jk}{r} + \frac{1}{r^2} \right] \sin\theta \tag{4.1c}$$

in which

dl is the length of the element.

I is the current in the element..

η_0 is the free space impedance.

θ is the zenith angle to the radial distance r.

ϕ is the azimuth angle to the radial distance r projection.

r is the distance from the element to the observation point.

k is the wavenumber.

Three field components can be identified:

- **Inverse cube term**: electrostatic field term, resulting from the presence of charges at the boundaries of the element.
- **Inverse square term**: induction term, representing the alternate re-radiations between the field and the element. Fields do not display a spherical wavefront, thus the pattern varies with distance.
- **Inverse term**: radiation term, describing the contour of the energy radiating away from the conducting element. The E and H fields support and regenerate one another as their strength decreases as the inverse square of the distance.

These three components further determine the existence of different propagation region, principally known as near field, further classified as reactive and radiating, and far field. The reactive region is the area immediately surrounding the transmitting aperture and where the fields contributions are primarily reactive ones, i.e. the electric and magnetic fields are out of phase, while in the radiating region, also known as Fresnel zone, radiating field behaviour emerges, even if the exhibited angular pattern is influenced by the distance from the transmitting antenna. Finally, the far field region, or alternatively the Fraunhofer zone, defines the propagation region where such dependency vanishes [173].

Solving the equations, it can be seen that at a distance of $r = \lambda/2\pi$, all the previously identified and described contributions exhibits the same magnitude (Fig. 4.2), and this range is commonly defined the transition between the near and the far field. The initial boundaries of the three regions are commonly defined as in Table 4.1.

Table 4.1: Boundaries for field region definition.

Reactive NF	Radiating NF	Radiating FF
$r = 0$	$r = \lambda/2\pi$	$r = 2D^2/\lambda$

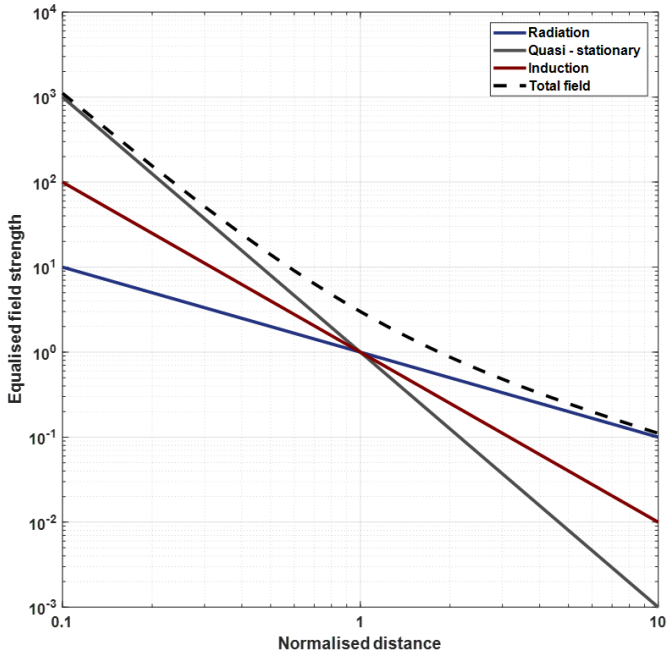

Figure 4.2: Signal level versus distance for EM field components. Distance is normalised to $r = \lambda/2\pi$

in which D is the maximum dimension of the antenna. The last formula corresponds to a phase error, due to the curvature of the actual spherical wavefront, of no more than 22.5 degrees ($\pi/8$) across the aperture. Such formulation is generally considered not strictly accurate for the reactive components since the boundary conditions are undefined. Therefore, the analysis of a received signal should necessarily consider such propagation regions [250].

The principal differences between the near field and the far field propagation behaviour can be summarised as follows:

- **Near field:**
  - E and H fields are out of phase by 90 degrees.
  - Plane wave assumption does not hold.
  - Energy decays very rapidly with distance.
  - The average energy density remains constant regardless the distance from the antenna (localised energy fluctuations).
  - The shape of the radiation pattern may vary appreciably with distance
- **Far field:**
  - E and H fields are orthogonal to each other.
  - Plane wave assumption holds.

- The energy angular distribution is independent from the source distance.
- The power decay adheres to the inverse square law with distance.
- Radiation in a given direction from separate parts of an antenna are approximately parallel.
- Radiation pattern does not vary with distance.

With reference to Fig. 2.29, the scattering response collected from GPR platform deployed in air launched and forward looking configuration completely satisfies the far field assumptions, and hence potentially predictable, while a ground coupled GPR equipment typically operates in the near field region, characterised by an increased complexity of the electromagnetic radiation and a higher sensitivity to the electrical properties of the soil, which however might produce better performance due to the coupling between induction and quasi-stationary fields. In both cases, the antenna firstly radiates in air then through the dielectric subsurface material. Conversely, borehole radars actually radiates within the dielectric, hence the antenna radiation pattern will be significantly affected, both spatially and temporally. All these features need to be exploited when designing a dedicated GPR equipment for a specific application [251].

4.1.1.2 Wave nature of EM fields

The electromagnetic field behaviour over time is commonly categorised as either a dispersive and diffused field, i.e. the characteristics are frequency-dependent, or exhibiting a wave-like response, meaning that attenuation and velocity of the wave properties are not subjected to frequency-dependent variations. Operationally, this means that reflected signals generated by an impedance contrast will be in principle highly correlated with the emitted one. The effectiveness of GPR is traditionally acknowledged within the non-dispersive domain, where the energy loss, connected to the material conductivity, is small compared to the energy storage characteristics, associated with the material permittivity [15].

The field behaviour characterises the 1 MHz to 1 GHz frequency range, commonly denominated the GPR plateau. At lower frequencies, all the wave properties, including attenuation, velocity and EM impedance, are frequency-dependent, determining a variations of the pulse shape, as a result of the slightly different velocity of propagation of the different frequency components.

At higher frequencies, instead, these properties become frequency-independent, and all the frequency components of a waveform experience the same attenuation and exhibit the same velocity. Hence, the shape of the pulse will not be modified, but its high frequency contents will limit the achievable depth as a result of the increased absorption.

For successful GPR measurements a plateau exists where these properties become frequency independent, as shown in Fig. 4.3. The obvious success of the GPR method indicates that many applications are not subject to severe dispersion, however in some high loss materials, the plateau may not be present.

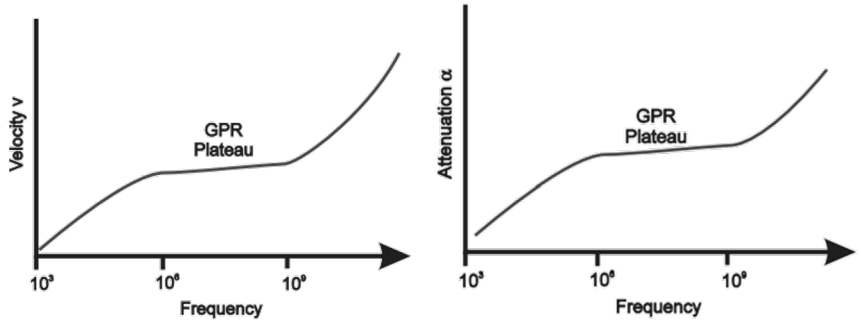

(a) Wave velocity versus frequency. **(b)** Wave attenuation versus frequency.

Figure 4.3: Wave velocity and attenuation versus frequency. *Derived from [15].*

The transition frequency between diffusion and propagation behaviour is defined as follows (Eq. 4.2):

$$f_t = \frac{\sigma}{2\pi\varepsilon} \tag{4.2}$$

It can be seen that the plateau still presents a minor frequency-dependent pattern, as both attenuation and velocity slightly increases with frequency, as a result of (1) the higher absorption properties of water, and (2) the impact of the frequency-dependent scattering losses. These factors should be taken into account as they both influence the efficacy of a GPR survey.

The simplest solution of Maxwell's equations is the transverse electromagnetic (TEM) plane wave. The wavefronts are planar, the direction of propagation is the same everywhere, and the electric and magnetic fields are orthogonal to one another and to the direction of propagation. A wave propagating in the positive z-direction in a perfect

dielectric can be described by equation 4.3

$$E_z = E_0 e^{-jkr} \tag{4.3}$$

and the velocity of propagation (Eq. 4.4) is:

$$v = \frac{1}{\sqrt{\varepsilon\mu}} = \frac{c}{\sqrt{\varepsilon_r}} \tag{4.4}$$

In this case, no propagation losses are experienced and therefore attenuation phenomenon is neglected, conversely to what happens in real dielectric. The phase constant is defined as $k = \omega/v = \omega\sqrt{\mu\varepsilon}$ (referred also to as the propagation factor), and the ratio of the electric and magnetic fields is equal to the characteristic impedance of the medium (Eq. 4.5)

$$Z = \sqrt{\frac{\mu}{\varepsilon}} \tag{4.5}$$

For nonmagnetic media, $\mu = \mu_0$, and $Z = \sqrt{\mu_0/\varepsilon}$ may be written in terms of the impedance of free space ($Z_0 = 377\Omega$) as in Eq. 4.6:

$$Z = \sqrt{\frac{\mu_0}{\varepsilon}} = \frac{Z_0}{\sqrt{\varepsilon_r}} \tag{4.6}$$

As a reference, materials exhibiting constant and frequency independent magnetic susceptibility and electric permittivity, as happens in free space, are defined not dispersive.

4.1.1.3 GPR source near an interface

GPR antennas are commonly deployed in proximity to the ground surface, and therefore the radiated field can locally be considered as a planar wave hitting the ground interface at a specific incidence angle [252]. At this location, the signal is reflected, transmitted and refracted according to Snell's law and the Fresnel coefficients.

Analysing the behaviour of the wavefront propagating into the subsurface, as shown in Fig. 4.4, the effect of the previous consideration are visible considering that its pattern does not exhibit a spherical outline anymore, as a result of the different degrees of bending occurring. Such behaviour represents the most common situation, as commonly the antennas are located very close to the surface.

As a reference, it can be considered the case in which the source is located right at

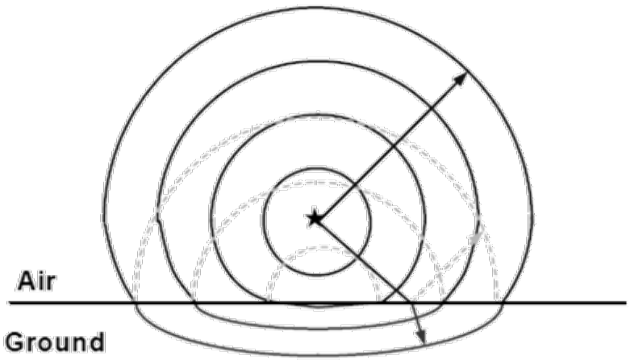

Figure 4.4: Wavefronts from a localised source located above the ground. *Derived from [15].*

the interface of the two mediums, i.e. air and lossy dielectric, shown in Fig. 4.5.

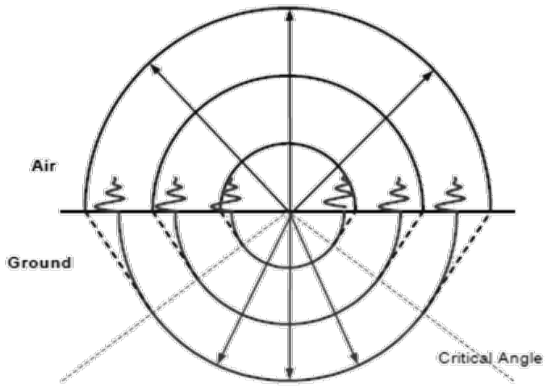

Figure 4.5: Wavefronts from a source located on the ground interface. *Derived from [15].*

When the source is in contact with the ground surface, two main phenomena can be highlighted. In air, the incident and reflected waves merge into an upward travelling spherical wave, while the wave propagating into the ground splits into a spherical wave and a planar wavefront, connecting the correspondent air and ground spherical waves [15]. Close to the surface, such spherical wave propagates in air as an evanescent field, as a result of the energy coupling process [253]. Finally, at a sufficient distance from the source, with respect to the wavelength, these components become separate in time and space. It is therefore clear that varying the distance between the source and the surface might significantly affect the characteristics of the resulting radiation pattern, in particular concerning the reactive field contributions.

When considering a bistatic system, which in principle represents almost the entire GPR design approaches, it should be additionally taken into account the effect of the changes in geometrical distance between the antennas, whose consequences are vi-

sualised in Fig. 4.6 depicting the wavefront pattern for a dipole antenna, one of the most common equipment employed in GPR design.

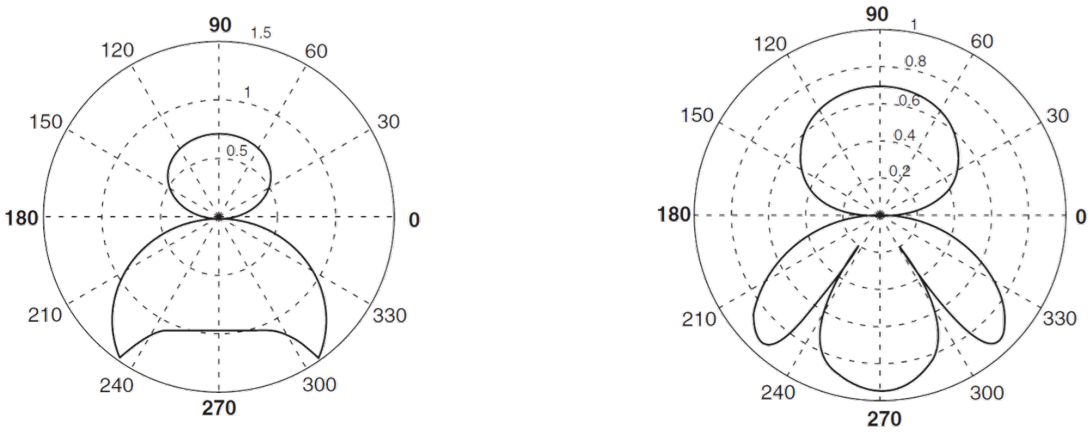

(a) E-field. **(b)** H-field.

Figure 4.6: Wavefronts from a dipole antenna located on the ground interface. *Derived from [82].*

There can be several possible paths from a transmitter to the receiver, sketched for a simple two layers model in Fig. 4.7 and characterised as follows:

1 **Direct air signal**: travelling through the air in a direct line from the transmitter to the receiver. As a result, the direct air wave is always the first signal measured by the receiver.

2 **Direct ground signal**: travelling along the surface interface at velocity v_1.

3 **Direct reflected signal**: travelling through medium 1 at a velocity v_1 and back after reflection at the interface.

4 **Critically refracted signal**: because $v_1 < v_0$ reflected waves are critically refracted at the surface. While this wave propagates along the surface interface, it will have velocity a velocity roughly the speed of light.

The weight of each of the described paths is determined by the target depth, the antenna offset and the distance from the surface. Moreover, the refracted path (4) includes the refraction/reflection path and its specular reflected/refracted one, even if they can't be distinguished.

In most GPR cases, the transmitter receiver separation is small and the predominant paths are (1), (2) and (3), even if for proximal operations the direct air and ground arrival can hardly be separated from the background reflection. The signal following

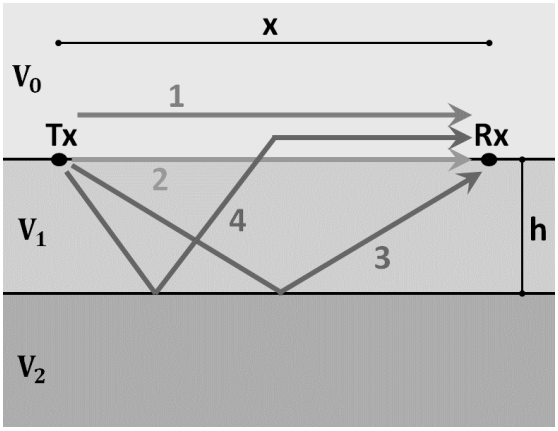

Figure 4.7: Signal paths between a transmitter and a receiver on the surface. *Derived from [15].*

path (4) might become relevant if the target is at a considerable distance from both the transmitter and the receiver.

4.1.1.4 Reflection, refraction and transmission at interfaces

To characterise the wavefield behaviour and quantify its amplitude across the interface between two materials, a planar boundaries for Snell's law and the Fresnel reflection coefficients are typically exploited.

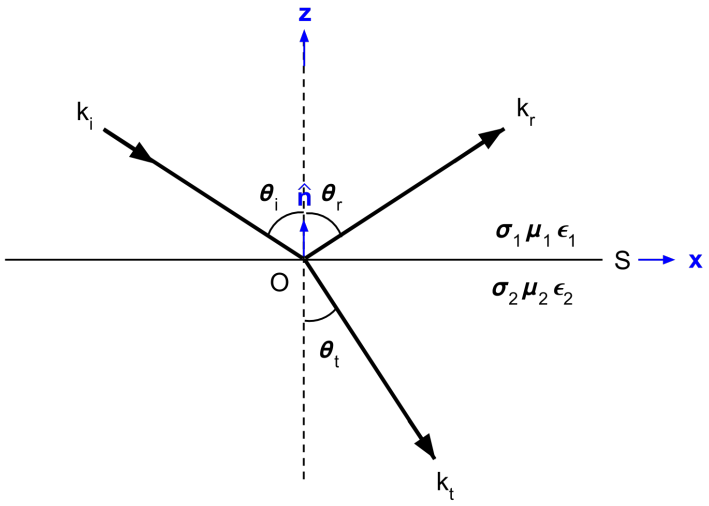

Figure 4.8: Geometry for Snell's law.

Snell's law defines the experienced change of direction of a wavefront as it propagates through materials exhibiting a velocity variation. The concept is sketched in Fig. 4.8, showing a wave incident (k_i) on the boundary between two adjacent materials with different electromagnetic properties (σ, μ, ε).

First of all, Snell's relations mathematically impose a continuity between the horizontal component of the propagation vector in each material, and hence:

$$k_1 \cdot \sin\theta_1 = k_2 \cdot \sin\theta_2 \tag{4.7}$$

When the material are low loss (i.e. wave regime approximation), Snell's law can be simplified to (Eq. 4.8):

$$\frac{\sin\theta_1}{v_1} = \frac{\sin\theta_2}{v_2} \tag{4.8}$$

In this case, the angle of incidence and refraction are directly related to the propagation velocity of EM waves within each media. In case of an increasing velocity gradient, i.e. $v1 > v2$, the second medium exhibits a critical angle, and hence the energy does not propagate.

As initially mentioned, the Fresnel coefficients describes the amplitude variations of the wavefield when propagating across an interface between two materials. At this location, as shown in Fig. 4.9, the field separates into two independent components, referred to as the TE (transverse electric field) and TM (transverse magnetic field) component, which are defined by field orientation with respect to the material boundary.

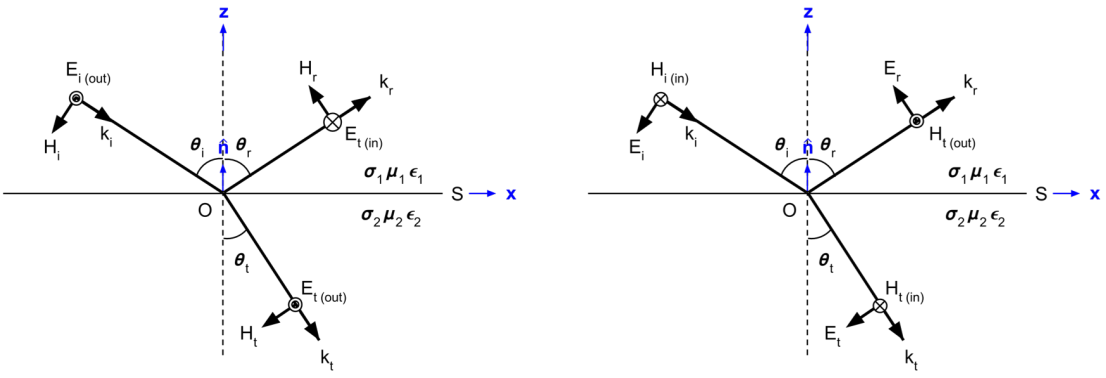

(a) TE mode. **(b)** TM mode.

Figure 4.9: Incident wave at planar boundaries. *Taken from em.geosci.xyz/index.html*

The incident, reflected, and transmitted field strengths are related by the following equations (4.9):

$$I_{TE} + R_{TE} \cdot I_{TE} = T_{TE} \cdot I_{TE} \tag{4.9a}$$

$$I_{TM} + R_{TM} \cdot I_{TM} = T_{TM} \cdot I_{TM} \tag{4.9b}$$

R and I coefficients are primarily determined by the satisfaction of the Snell's law , the continuity of the electric and magnetic fields, and the equality between the crossing electric current and magnetic flux density.

The result is described by equations 4.10 and 4.11:

$$R_{TE} = \frac{Y_1 \cos\theta_1 - Y_2 \cos\theta_2}{Y_1 \cos\theta_1 + Y_2 \cos\theta_2} \tag{4.10a}$$

$$R_{TM} = \frac{Z_1 \cos\theta_1 - Z_2 \cos\theta_2}{Z_1 \cos\theta_1 - Z_2 \cos\theta_2} \tag{4.10b}$$

$$T_{TE} = 1 + R_{TE} \tag{4.11a}$$

$$T_{TM} = 1 + R_{TM} \tag{4.11b}$$

where Z_i and Y_i are the impedances and admittances of the $i-th$ material. These expressions highlight the fact that an EM impedance contrast must exist for generating a response.

For normal incidence only, i.e. $\theta_1 = \theta_2 = 0$, the coefficients for the TE and TM modes become identical.In a non-conducting medium (and considering only a single frequency), the expressions in Eq. 4.11 may be rewritten as Eq. 4.12:

$$R = \frac{\sqrt{\varepsilon_{r2}} - \sqrt{\varepsilon_{r1}}}{\sqrt{\varepsilon_{r2}} + \sqrt{\varepsilon_{r1}}} \tag{4.12a}$$

$$T = \frac{2\sqrt{\varepsilon_{r2}}}{\sqrt{\varepsilon_{r2}} + \sqrt{\varepsilon_{r1}}} \tag{4.12b}$$

where ε_r is the relative permittivity of the medium.

From these results, the following considerations should be pointed out:

- For low impedance contrast, most of the incident wave is transmitted through the interface, and viceversa.
- The reflection magnitude increases as the angles increase.
- The TM reflection coefficient might reduce to a minimum when the incident angle approaches the Brewster angle, where maximum transmission occurs.
- For Brewster angle to exist at the interface, TE and TM waves must exhibit a decreasing admittance and impedance, respectively.

- When the waves are subjected to an increasing velocity gradient, angles greater than the critical one determine the magnitude of the reflection coefficients to approach unity, meaning that the wave is completely reflected. Across the interface, field components exist in the form of evanescent signals, exponentially decaying with the distance from the interface.
- The reflection coefficients might be either positive or negative, and governs the eventual polarity reversal phenomenon. Consequently, such feature can be used to determine whether the impedance of the first layer is greater than or less than the below one.

The normal incidence reflection coefficients for some air-dielectric interfaces are provided in Fig. 4.10.

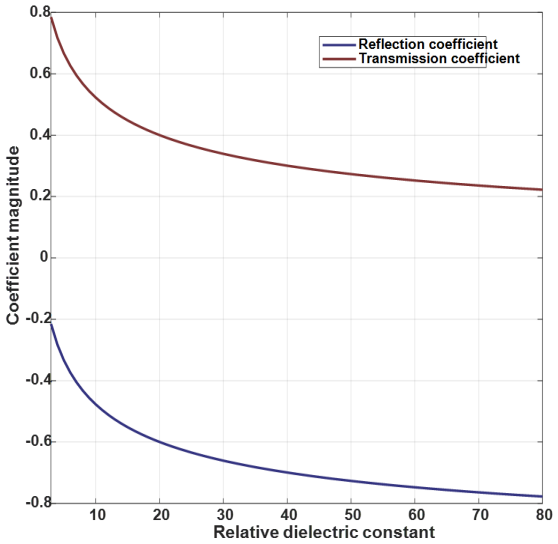

Figure 4.10: Reflection and Transmission coefficients for normal incidence as a function of material dielectric.

4.1.2 Propagation in a dielectric

The signal pulse consists of an electromagnetic wave which oscillates at a particular frequency, and as it propagates through the subsurface, it is distorted due to the distribution of subsurface electromagnetic properties $(\sigma, \mu, \varepsilon)$.

Electromagnetic waves propagating through materials are subjected to different types of losses, affecting both the electric (E) and magnetic (H) fields [82], mainly causing the attenuation of the original radiated wave. For the majority of such materials, however, the variation imposed on the magnetic component is limited, and conse-

quently this variable can be considered a real quantity, contrary to the permittivity and conductivity that must be addressed as complex elements.

The propagation of a plane wave along the z-direction, perpendicular to the surface, in a homogeneous medium is governed by the wave equation (Eq. 4.13):

$$\frac{\partial^2 E}{\partial^2 z^2} = -\omega^2 \mu \varepsilon E \tag{4.13}$$

where

$E = \Re\left\{E_0 e^{j\omega t}\right\}$ is the sinusoidal time varying electric field vector (V/m), with E_0 the amplitude of the electric field vector (V/m).

ω is the angular frequency (rad/s).

z is the distance along the propagation direction (m).

μ is the magnetic permeability.

$\varepsilon = \varepsilon' - j\varepsilon''$ is the complex permittivity (F/m).

$\sigma = \sigma' - j\sigma''$ is the complex conductivity (Ω/m).

The electrical conductivity σ characterises the capability of an electric field to generate an electric current, considering that the resistance to the charge flow causes an energy dissipation. On the other side, dielectric permittivity ε, characterises the energy storage capacity of a material, as a result of the constrained charges displacement as a result of the presence of an electric field [1]. The real component, ε', represents the energy stored through electrical polarisation (relative permittivity), and the imaginary component, ε'' represents a measure of energy loss associated with both conductivity and frequency.

The solution of Maxwell's equations for a wave propagating within a homogeneous medium describes an EM field which is affected by an amplitude decay dependent on distance (Eq. 4.14):

$$E = E_0 e^{-jkz} \tag{4.14}$$

with propagation constant (Eq. 4.15):

$$k = \omega\sqrt{\mu\varepsilon(1 - j\tan\delta)} \tag{4.15}$$

in which the loss tangent $\tan\delta = \frac{\sigma' + \omega\varepsilon''}{\omega\varepsilon' - \sigma''}$, sometimes expressed as a dimensionless

factor $\frac{\varepsilon''}{\varepsilon'}$, can be interpreted as the ratio between the conduction current density to the displacement current one. In the case of a relatively lossless material, it may be reasonable to consider a constant loss tangent value over the GPR frequency range. However, such approximation doe snot hold for materials that are wet and lossy.

If the real and the imaginary parts of jk are separated, the attenuation parameter α and the phase parameter β are described by Eq. 4.16:

$$\alpha = \omega\sqrt{\left[\frac{\mu\varepsilon}{2}\right]\sqrt{1+(\tan\delta)^2}-1} \tag{4.16a}$$

$$\beta = \omega\sqrt{\left[\frac{\mu\varepsilon}{2}\right]\sqrt{1+(\tan\delta)^2}+1} \tag{4.16b}$$

Therefore, Eq. 4.14 can be rewritten as:

$$E(z) = E_0 e^{-\alpha z} e^{-j\beta z} \tag{4.17}$$

The amplitude of the GPR pulse decreases as it propagates in the material medium, and the pulse shape is distorted because of the nonlinear phase term βz.

The exponential term $e^{-\alpha z}$ defines the plane wave attenuation when propagating within a lossy medium, with a decay rate specified by the parameter α, also known as the attenuation constant. The second exponential term $e^{-j\beta z}$, instead, expresses the wave propagation mechanism, which is governed by the phase term β. It can be calculated that a distance equal to $z = 1/\alpha$, denominated the skin depth, brings an attenuation value of $1/e$, commonly considered an indication of the achievable penetration depth of the GPR system, although highly theoretical.

Attenuation defines the continuous loss of amplitude a wave experiences as it propagates through a particular medium. A few constrictions can be assumed when considering typical GPR scenario and the related frequency range. First of all, the relative magnetic permeability of commonly encountered materials is equal to one and can be consequently neglected in the calculations, and secondly, the real part of the electrical conductivity can be considered to be frequency independent and equal to the DC conductivity, while its imaginary part can be ignored.

From the above expressions, it can be noticed that to a first order the material attenuation constant (expressed in dB/m) is linearly dependent to the frequency (Fig.

4.11), and secondarily to the square root of the material permittivity.

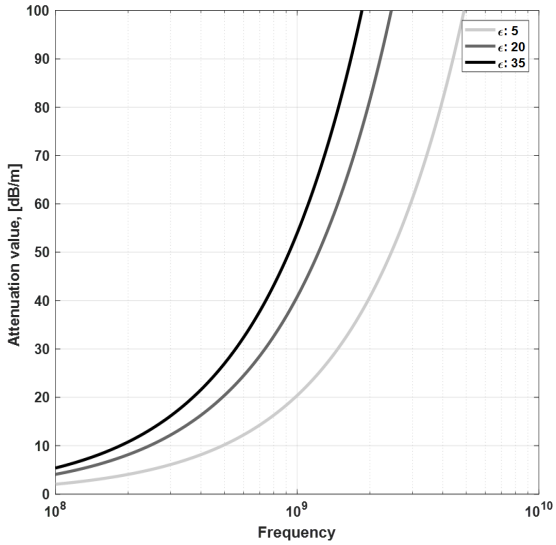

Figure 4.11: Material attenuation as a function of frequency and relative dielectric constant.

Applying the wave regime approximation, the expression for the material attenuation in Eq. 4.16 becomes:

$$\alpha = \frac{\sigma}{2}\sqrt{\frac{\mu}{\varepsilon}} \tag{4.18}$$

This essentially underlines that the higher the conductivity of the material, the faster the wave will dissipate into the ground.

The relationships and the mutual influence among soil permittivity, electrical conductivity and volumetric water content over the propagation properties of a specific material have been demonstrated and determined through a number of empirical equations, such as Topp's relationship [254] and variations of Archie's law [255, 256]. It is clear that a material exhibiting a high electrical conductivity might limit the achievable penetration depth, as a consequence of the high rates of signal attenuation, and that such parameter is directly related to the water content, the presence of soluble salts and organic materials, and clay contents. As a figure of merit, the permittivity of a material with almost zero water content lies in the range $3-4$ and its conductivity is usually very small. Increasing the water content leads to a sharp rise of these values, reaching their maximum when the porosity of the material reaches a complete saturation.

The velocity of electromagnetic wave propagation in a medium with electrical parameters as described in Eq. 4.13, and considering nonmagnetic material ($\mu_r = 1$), is

expressed as:

$$v = c\left\{\frac{\varepsilon' - \frac{\sigma''}{\omega}}{2\varepsilon_0}\left[\sqrt{1+\left(\frac{\varepsilon'' + \frac{\sigma}{\omega}}{\varepsilon' - \frac{\sigma}{\omega}}\right)^2}+1\right]\right\}^{-\frac{1}{2}} \tag{4.19}$$

Considering ω large compared to σ' and σ'', the expression becomes:

$$v = c\left\{\frac{\varepsilon'}{2\varepsilon_0}\left[\sqrt{1+(\tan\delta)^2}+1\right]\right\}^{-\frac{1}{2}} \tag{4.20}$$

It can be seen that the velocity value decreases as a consequence of a rise of the loss tangent variable and the relative dielectric constant, even though $\tan\delta$ should be considerably greater than unity for appreciably influence the velocity. The effect is shown in Fig. 4.12a.

Under this approximation (ε'' is small compared to ε'), Eq. 4.20 can be approximated as:

$$v = \frac{c}{\sqrt{\frac{\varepsilon'}{\varepsilon_0}}} = \frac{c}{\sqrt{\varepsilon_r}} \tag{4.21}$$

The propagation velocity decreases with increasing relative permittivity (Fig. 4.12b), and consequently the wavelengths will decrease as well.

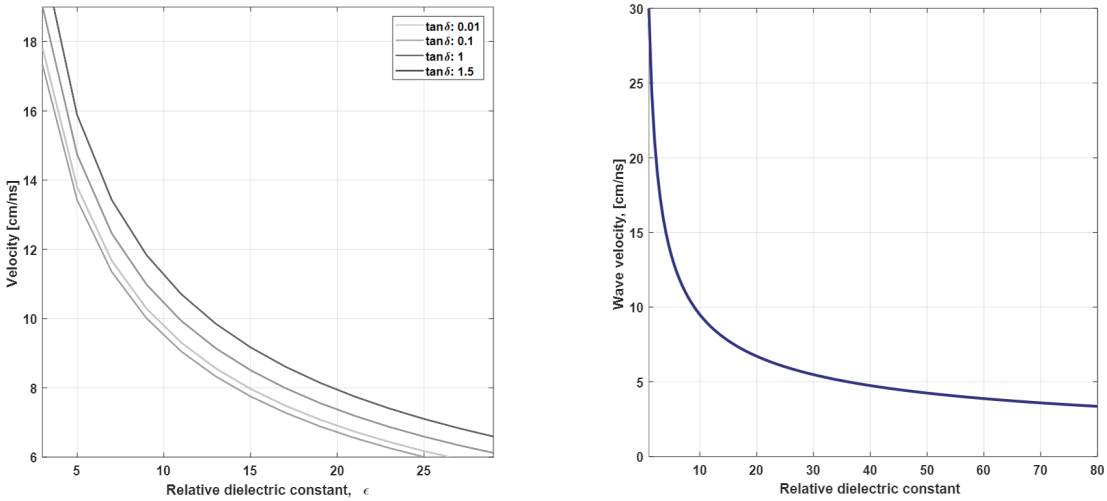

(a) Loss tangent

(b) Relative dielectric constant.

Figure 4.12: Effects on wave velocity of loss tangent and relative dielectric constant.

From the general equation for propagation velocity, we see that as $\sigma \to \infty$, the propagation velocity goes to zero, meaning that the wave cannot propagate through extremely conductive objects. Because of this, when a wave reaches the interface between the

Earth and a highly conductive object, the wave is completely reflected regardless of the incident angle.

4.1.2.1 Properties of lossy dielectric materials

As previously mentioned, the characterisation of the dielectric properties of the subsurface can't be deterministically calculated, and hence the definition of both permittivity and conductivity properties is still largely based on an experimental approach, as a consequence of the inner complexity of the involved materials and the differences in their formation process, even within the same family. However, some general considerations can be pointed out. Most materials contain moisture, and since the relative permittivity of water is approximately 80, it can be stated that its influence on the dielectric properties of the material is significant, as even a small amount might cause a significant increase of its relative permittivity of the material.

Table 4.2 lists the values for the dielectric constant and electrical conductivity exhibited by typically encountered materials.

Table 4.2: Typical electromagnetic properties for common geological materials at 100 MHz [1].

Material	Dielectric constant	Electrical conductivity (mS/m)
Air	1	0
Sea water	80	30000
Fresh water	80	0.5
Distilled water	80	0.01
Ice	3-4	0.01
Limestone	4-8	0.5-2
Sand, dry	3-5	0.01
Sand, wet	20-30	0.1-1
Silts	5-30	1-100
Clay	5-40	2-1000

In addition to what has been stated in the previous parapgraph, Table 4.2 also highlights that water has both the highest and lowest conductivity, and hence attenuation rate, depending on the salinity measure. This again demonstrates that the presence and composition of water is the single most relevant contributor to the dielectric properties of the material, and consequently to the experienced GPR performance. As well, clay content represents another important player, as even a limited amount of clay might drastically reduce the GPR penetration performance.

Among the methods of classifying soils, the clearest way is probably the textural triangle, shown in Fig. 4.13, which represents all possible combinations of soil separately.

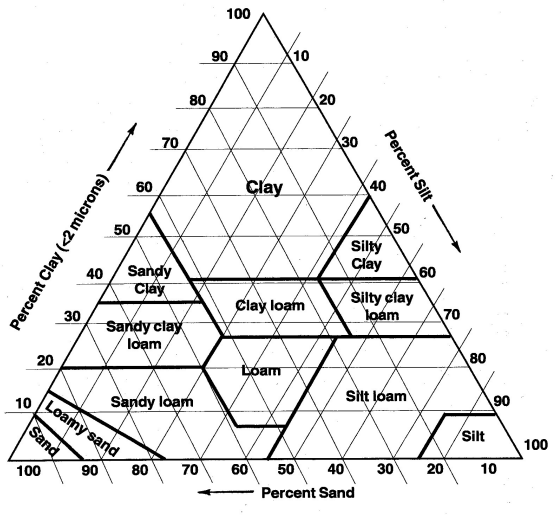

Figure 4.13: Soil textural triangle, as defined by the USDA.

Following this classification, some useful soil mixture can be described (Table 4.3), from which it is once again evident that the permittivity of a material can significantly change, particularly in presence of water.

Table 4.3: Typical electromagnetic properties for common soil mixtures at 100 MHz [1].

Material	Dielectric constant	Electrical conductivity (mS/m)
Sandy, dry	4-6	0.1-100
Sandy, wet	15-30	10-100
Loamy, dry	4-6	0.1-1
Loamy, wet	10-20	10-100
Clayey, dry	4-6	0.1-100
Clayey, wet	10-15	100-1000

Finally, recalling Table 3.1 describe the dielectric properties of landmine constituents, from which it is easily understandable why detection of zero metal landmines is a very challenging task [257].

It can be inferred that the limited scattering from buried landmines is caused by the reduced impedance contrast between the object and the surrounding soil, meaning that a wet soil might in principle represent a favourable condition for detecting a minimum metal mine, though limiting the penetration performance [258, 259]. Examples

Table 4.4: Relative dielectric constant of landmine constituents.

Material	Relative dielectric constant ε_r
Neoprene rubber	6-9
Bakelite	3-5
Polycarbonate	2.9-3.5
Polyethylene	2-2.5
Epoxy resin	3-4
TNT	2.7
PETN	2.72
Comp B (RDX TNT)	2.9
Tetryl	2.9
Semtex (RDX PETN)	3
Comp C-4 (RDX)	3.14
Nytroglycerine	19

of detection performance depending on soil characteristics and environmental factors can be found in [260, 261]. As an electromagnetic subsurface imaging technique, GPR is highly sensitive to soil heterogeneity and anisotropy, thus soil texture should be considered as well [262, 263].

4.2 System design

Conceptually, GPR system design relevantly diverges from general purpose radar mainly as a consequence of the limited range of the targets, which is of the orders of metres, and the lossy propagation media experienced by the EM waves, for which the attenuation and the inhomogeneous nature of the earth become a dominant factor.

In addition, the target dimensions sought with GPR are of a different order of magnitude than the ones which are usually detected with atmospheric radar, and they are in all case stationary.

4.2.1 GPR range equation

In principle, GPR system performance is well described by the standard radar range equation, even if a number of additional losses have to be considered, given the fact that the wave is radiated into the subsurface rather than in air, and that the majority of GPR targets of interest are dielectric objects, and not metallic. As a consequence, transmission and propagation losses, as well as spreading and coupling phenomena mus be included within the formulation.

The modified GPR equation can be written as:

$$P_{rx} = \frac{P_{tx}\varepsilon_{tx}G_{tx}A_{rx}G_{rx}\varepsilon_{rx}\sigma_{RCS}}{(4\pi z^2)^2} \cdot \left(Z_{tx} \cdot e^{-2\alpha z} \cdot e^{-2\alpha z} \cdot Z_{rx}\right) \tag{4.22}$$

in which:

P_{tx} is the transmitted power.

$\varepsilon_{tx}, \varepsilon_{rx}$ are the transmitter and receiver antenna efficiency.

G_{tx}, G_{rx} are the transmitter and receiver antenna gain.

A_{rx} is the receiver antenna effective area.

σ_{RCS} is the target cross section.

z is the distance of target from transmitter (assumed equal to the one from the receiver).

Z_{tx}, Z_{rx} are the coupling losses.

α is the attenuation coefficient of the material.

A schematic diagram of the different variables of the radar equation is provided in Fig. 4.14.

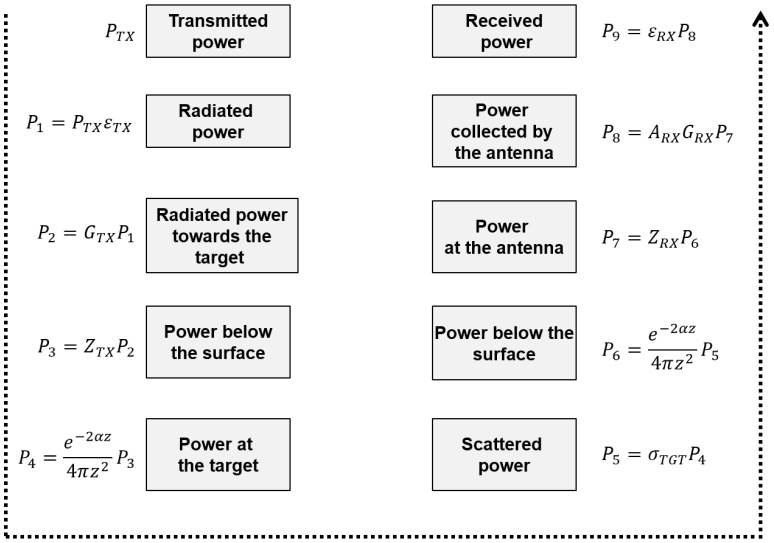

Figure 4.14: Block diagram of the GPR range equation.

The strength of the received signal depends on the radar cross section of the target and the losses experienced by the signal as it couples into the ground, propagates from the transmitter, reflects from the target and returns to the receiver. The processes producing losses are sketched in Fig. 4.15.

All the parameters are detailed in the following sections.

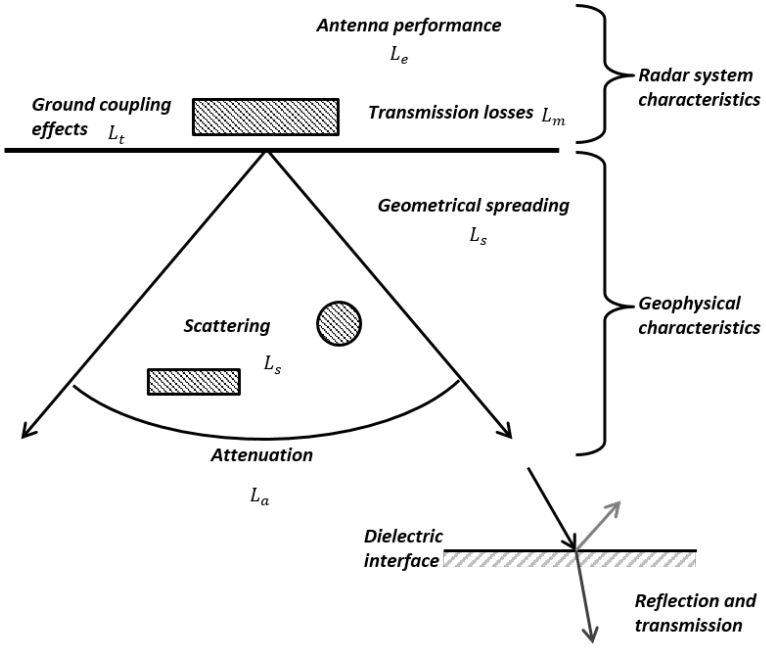

Figure 4.15: Processes that lead to reduction in signal strength.

4.2.1.1 Antenna efficiency and mismatch

Antenna efficiency represents the power available for radiation, i.e. the effective power, with respect to the power applied to the antenna, whle the antenna mismatch loss is a quality measure of the match with the transmitter. Both of these quantities reflect the fact that all physical antennas suffer from losses, regardless the design or configuration.

4.2.1.2 Coupling losses

Recalling what has been previously defined, at any material interface a portion of the radiated energy will be reflected back to the receiver, while the remainder will continue its propagation, the magnitude of which depends on the Fresnel equations, defined for each frequency component of the emitted wave. It should be also noted that the calculation of the coefficients in principle supposes a flat boundary and a distance sufficiently large to consider the interface in the far field of the antennas.

The ground has a frequency dependent characteristics impedance which lies in the range of 50 to 200 Ω, whereas most antennas are designed to radiate into free space (impedance of 377 Ω). Such variability of the ground impedance is a primary source of loading and mismatch, hence a cause of efficiency reduction. Even if the efficiency of the coupling process is typically high when in proximal operation, as a consequence of the limited thickness of that air layer, for standoff radar systems the situation might

be more complicated, considering that complex angles of refraction may occur during propagation.

4.2.1.3 Spreading losses

Spreading losses are related to the decay of energy due to the distribution of the energy on the front, as the energy of the wavefront is spread over an increasingly larger area.

In traditional radar equipment, the target is typically located in the far field region and hence the spreading loss is proportional to the inverse fourth power of distance, given a point source scatterer. These assumptions are commonly respected. Conversely, the majority of GPR surveys deal with targets located in the near field and Fresnel zone, and such relationship does not hold anymore.

Therefore, the physical nature of the target should be considered as well, as it influences the magnitude of the received signal characteristics. As inferable, at a given depth and with comparable dielectric properties, a planar reflector will produce a higher backscattered energy contribution compared to the one that can be expected from an object exhibiting a different shape. Therefore, the following adjustments should be considered when evaluating the parameter:

- Point scatterer: inverse fourth power.
- Line reflector: inverse cube.
- Planar reflecting surface: inverse square

4.2.1.4 Scattering losses

Scattering is a phenomenon associated with variations in the electrical and magnetic features, and hence always encountered at any change in material properties. The result of these heterogeneities, at both macro and micro scale, is that some propagating energy is randomly scattered in all directions. It is a function of the dielectric contrast, its spatial pattern, as well as of the angle of the propagating wave with respect to the boundary, its polarisation, and its spectral characteristics. Essentially, it is equivalent to having another antenna located at the interface and radiating upward.

Many of the targets which are the subject of GPR investigations are non-metallic, so their scattering cross section, determining the characteristics and magnitude of the reflected field, is influenced by the properties of the surrounding soil. As well, as detailed in the previous Chapter, the geometrical shape of the target might affect polar-

isation of the backscattered wave, hence it can be considered as a way for preferential detection. Finally, the target RCS also depends on the system design, and in case of a bistatic architecture, the formulation of the RCS must account for this diversity.

Scattering losses due to subsurface heterogeneities are critical for GPR because they reduce the amplitudes of signals of interest while increasing extraneous noise, especially in cluttered environments. Several sources of scattering, on different scales, are:

- Irregular surface shape of extended buried objects.
- Presence of rock fragments, soil minerals and water.
- Gas or air pockets and voids within a material.
- Scattering from small and distributed buried objects.

In this last case, i.e. the presence of a large number of scatterers with a physical size smaller with respect to the wavelength, the incident waves are randomly reflected following deviated trajectories, similar to the situation of scattering from rough surfaces.

4.2.1.5 Attenuation losses

Signal attenuation can be considered the principal factor that must be taken into account when assessing the feasibility of a GPR investigation. Attenuation is exponential with distance, hence there is always a finite depth of exploration, and it primarily depends on the physical and electromagnetic properties of the ground, such as soil type, its constituents and the moisture level [1]. In addition, given the potential subsurface heterogeneities, the path loss is not always a linear function of depth. Achievable depth can be increased by lowering the operating frequency, but such shift will reduce the available bandwidth, directly related to the resolution performance of the GPR system. An intuitive way to visualise these losses is to consider the ground as a low-pass filter, with parameters depending on the soil characteristics. Essentially, ground attenuation has the effect of placing a window across the aperture [82].

A typical range of loss for various materials at 100 MHz and 1 GHz is shown in Table 4.5:

In the table the linear dependency that exists between attenuation and frequency is evident.

Table 4.5: Attenuation properties of common materials at 100 MHz and 1 GHz.

Material	100 MHz Attenuation dB/m	1 GHz Attenuation dB/m
Sea water	100	1000
Fresh water	0.1	1
Ice	0.1-5	1-50
Loamy, wet	1-60	10-600
Sandy, dry	0.01-2	0.1-20
Clayey, wet	5-300	50-3000

4.2.2 Bistatic GPR corrections

Separating the transmitter and the receiver means that in what has been described above, an additional variable needs to be included and its effect on Eq. 4.22 evaluated.

In particular, the principal variations moving from a rigid platform to a bistatic one are related to (1) the experienced attenuation due to the different path travelled by the wave, and (2) the target scattering modelling, as in this case the angle of incidence differs from the direction of the receiver.

4.2.2.1 Attenuation

The difference in the geometry of the problem is clearly inferable comparing the distance from the target corresponding to the shortest travel time, i.e. when the receiver is directly located above the target. For a monostatic system, its equal to twice the target depth, as the transmitter and the receiver are collocated. Employing a bistatic system, instead, means that only the receiver is located in the optimum location, and therefore the distance calculation needs to count also for the target-transmitter distance. The wider the transmitter and receiver separation, the longer will be the path travelled by the reflections, and therefore the attenuation might reduce the amplitude of the wave below the sensitivity threshold of the receiver. In the presence of a high loss ground, the signal might vanishes before the maximum separation is reached.

Considering a target at 10 cm below the surface, Fig. 4.16 compares the experienced attenuation by a monostatic and a bistatic configuration for different material properties. It is evident that due to the increased path length the suffered attenuation is notably higher for the bistatic case, thus limiting the maximum allowable separation. Essentially, this means that the dynamic range of the signals to be handled is reduced,

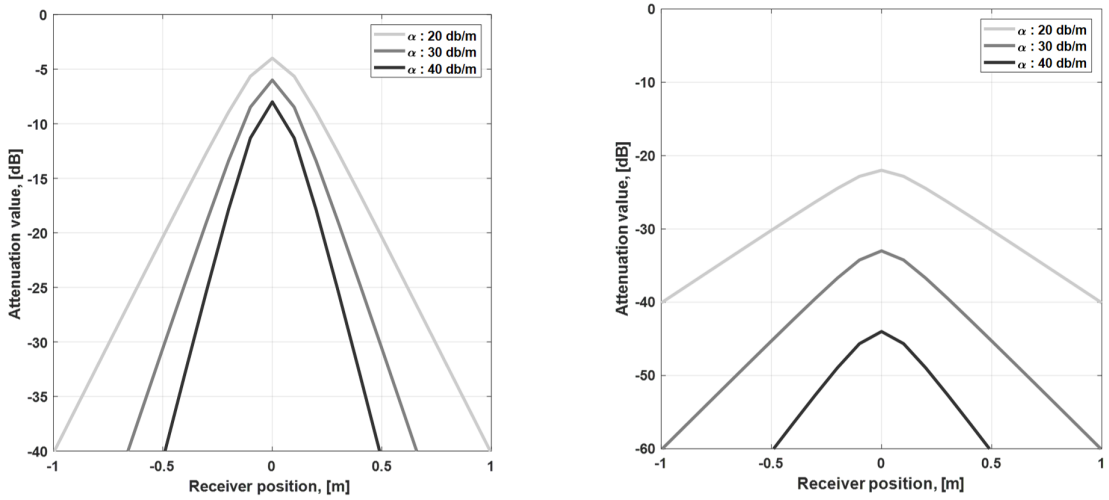

(a) Monostatic system configuration.

(b) Bistatic system configuration.

Figure 4.16: Modelled attenuation for monostatic and bistatic system under different soil attenuation conditions.

because of the defined minimum range from the radar equation. As for the depth performance, the soil variability does not allow an accurate estimate of the maximum separation or of the optimum antenna separation for a unique target characterisation.

4.2.2.2 Target scattering

Bistatic scattering is subject to a greater variability than the monostatic case, because more variables are involved with such geometry, primarily the dependency from the antenna separation. Although numerous mathematical formulations have been developed for retrieving the bistatic RCS from its monostatic equivalent, mostly based on the equivalence theorem, such methods have a number of assumptions that for GPR applications can't be met, especially for complex targets and for objects whose dimension is close to the wavelength.

Moreover, when the antenna separation is large compared to the target depth, the so-called small spread approximation (SSA) does not hold anymore, and the reflection traveltimes cannot be approximated by simple hyperbolas [160].

These considerations apply obviously to every source of scattering, including clutter sources and scattering generated by anisotropic and heterogeneous soils. In addition, for air launched systems, the terrain roughness may represent another aspect to be considered.

4.3 GPR design for landmine internal structure detection

Three main conceptual differences can be identified between the design of a conventional GPR system and a platform specifically designed for landmine detection tasks. First of all, the required resolution for detecting buried landmines and to properly separate their scattering component from the ground surface reflection (for shallowly buried targets) must not exceed few centimetres. The same necessity exist for distinguishing between the top and the bottom of a landmine, vital information for target classification step. Secondly, it is mandatory to avoid triggering of surface-laid landmines, hence it might be desirable to carry out operations at standoff distance. For example, the sensor head of a hand-held equipment is typically raised up of few centimetres, while for vehicle-mounted GPR, though rarely deployed, the elevation can increase up to several decimetres. Finally, target classification through GPR requires a considerably higher signal stability and reconstruction accuracy than that typically achievable through conventional systems.

Regarding the operation settings, minefields rarely consist of ordered rows of landmines in flat deserts or grassy fields, but they might be located within the remnants of collapsed buildings and post-conflict environments. The complexity of the framework brings several issues when evaluating the parameter of a GPR system for landmine detection.

To begin with, frequency selection is mainly governed and influenced by three parameters:

- Necessary resolution.
- Clutter characteristics.
- Required penetration.

There is a trade-off between spatial resolution, depth of penetration and system portability. High resolution is generally a desirable parameter, but a high resolution, in addition of requiring a high operating frequency, means a high clutter level and high scattering losses, as previously described. Hence this trade-off is one of the major challenges. In addition, antenna size increases as the frequency decreases. For most of the currently employed GPR system, the solution has been found by choosing a central

frequency in the range 500 MHz-3 GHz.

GPR, as well as many other EM techniques, is commonly operated very close to the surface, therefore it is possible that the far field assumptions may not hold. The propagation regions, which depend on the covered distance in wavelength, need now to be calculated considering the effective frequency that is propagating.

Fig. 4.17 presents the near field boundary for a number of frequencies and with varying dielectric properties of the subsurface.

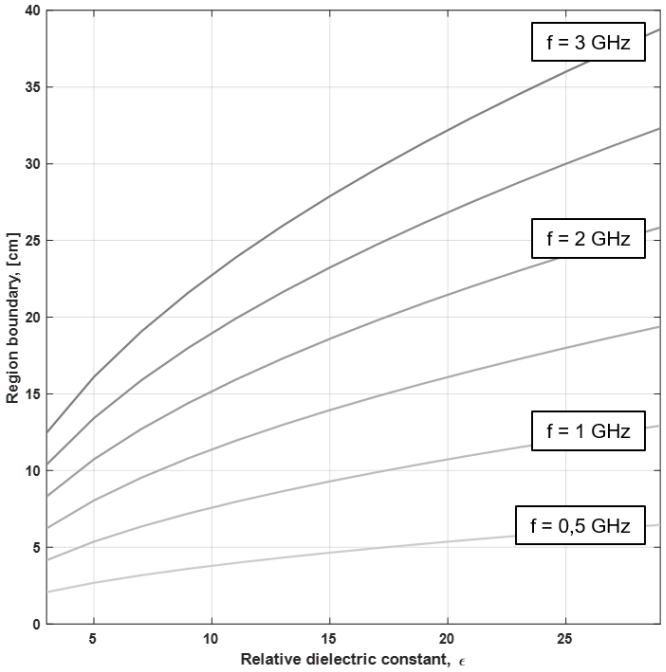

Figure 4.17: Near field boundaries for varying frequencies and dielectric.

It can be seen that for an average soil dielectric of 9 and a frequency range of 0.5 GHz to 2 GHz, the near field condition is dominant up to a distance of approximately 15 cm, from which it is evident that the target may very often be situated in this region, rather than in the far field one. Therefore, the analysis of the recorded signal should consider the proximity of the antenna and target.

First of all, propagation losses decrease at lower rates depending on the landmine dimensions for near field boundary conditions, and hence targets closer than that distance will have increased field contributions, resulting in greater signal levels from targets very close to the antenna (when in proximal operations). When the antenna is moved further away, the signal levels return to those of the induction fields. These considerations suggest that antennas for GPR applications should be designed to operate

within the near field distance to optimise the received signal levels. In addition, the boundary between the two regions is actually hard to predict and define, because of the small scale variability of the soil electrical properties.

Considering the target scattering perspective, the RCS of a target is usually defined in the far field, where it is an intrinsic characteristic of the object under test, totally independent of the antenna orientation and of the distance of the radar from the target. These properties can be considered valid as long as the transmitted wave appears locally planar at the object surface and the scattered waves appear locally planar at the receiver. For the near field condition of typical GPR operations, instead, the object ehibits a significant angular extension as seen from the antenna, hence the definition of a reliable RCS might be challenging and ambiguous.

Several works have addressed the issue of converting a far field RCS to a near field one, but still the unpredictable electrical properties of the subsurface may frustrate the attempts.

4.3.1 Detection of the landmine internal structure

Detecting the internal structure of a landmine means detecting a signal that is repeatedly reflected and transmitted as shown in Fig. 4.18a.

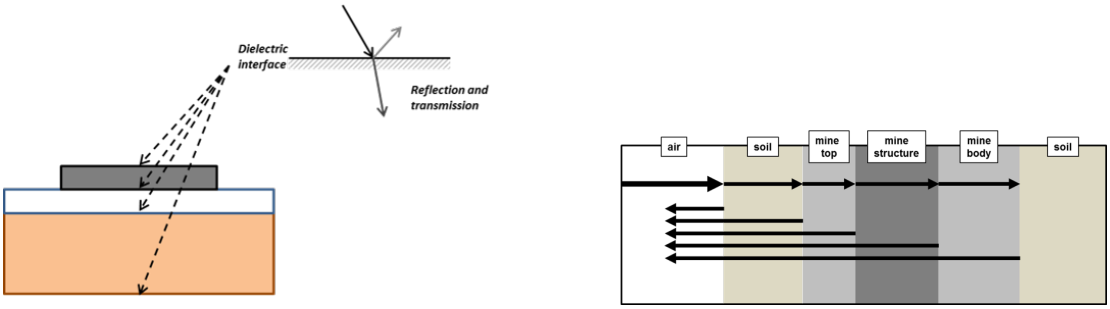

(a) Schematic diagram. **(b)** Simplified transmission line scheme.

Figure 4.18: Sketch of the addressed scenario. Dimensions are deliberately exaggerated.

Moreover, it should be taken into account that the scattering event generated by the internal structure should reach the receiver antenna with enough strength to be detected (Fig. 4.18b). It is inherent that a suitable resolution is needed for a reliable detection and identification, otherwise some of the components might be missed. This will be evaluated later in this Chapter.

From Fig. 4.18b it is also possible to visualise why a bistatic approach could lead

to a better signature characterisation. Each interface that is depicted has its own scattering characteristic, in terms of transmission and reflection angles, therefore a system capable of exploiting the angular diversity can offer significant advantages.

4.4 System modelling

Numerical modelling can be undoubtedly considered one of the principal and most topical GPR research field, mainly as a consequence of the increase computing resources and physical understanding of the problem. It is widely agreed that the possibility of simulating arbitrarily complex scenarios could provide an efficient way to achieve an in-depth understanding of the physical concepts, as well as to assist and facilitate the interpretation and comprehension of complex scenarios. In addition, a numerical model might help in optimising the acquisition approach, and to quantify the buried target or structure response, therefore defining the performance requirements of the GPR system to be employed and predicting the actual system quality figures.

Essentially, modelling facilitates the translation of geophysical observations into ready and usable information, the extraction of which is typically a complex process mainly because the operating principles of the methodology are complex and highly variable. As a result, numerical modelling has become a widely adopted approach within the GPR domain.

4.4.1 Computational methods comparison

GPR geometry can be exploited in different ways, from the evaluation of the path losses experienced by a single frequency signal, to a full 3D description of the whole ensemble of GPR component and the surrounding environment [264]. As a first step, given the high frequency regime and low conductivity condition, one can adopt a ray-based approximation of the EM wave propagation within the subsurface, meaning that it can be defined along ray paths defined by Snell's law. Under these hypotheses, the problem can be addressed by geometrical ray theory [265].

Mathematically, the electric and magmetic fields components can be defined starting from the Maxwell's equation, which can be expressed in either differential or integral form, leading to the so-called differential equation methods (DE) or integral equation methods (IE) respectively, as well as formulated in the time or frequency domain,

in which case the methods are denominated as either time domain methods (TD) or frequency domain methods (FD) [266] [267]. The choice of the best approach is obviously dependent on the specific problem to be solved.
To provide a brief comparison, a FD approach in principle provides the numerical solution for a single frequency input, and therefore it requires the simulation to be repeated for all the frequencies involved. Conversely, a time domain method produces a single time sequence, thus directly generating the solution for the entire spectrum of frequencies. Considering that the majority of GPR equipment are impulse-based, ultra wideband systems (UWB) systems, it is clear that a TD implementation represents the optimal modelling choice, as it additionally does not need the application of the Inverse FFT operator to retrieve the time domain representation [268].

The main difference between an integral equation approach and a differential one is commonly acknowledged to be the better capability of the latter one in addressing heterogeneous problems, as well as in providing computationally more efficient solutions [269].

The most intuitive model is represented by the Transmission Line Matrix method (TLM), a circuit-equivalent approach in which each layer is vertically cascaded and modelled as an equivalent impedance. Transmission and reflection coefficients are calculated for each interface and the analytical reflection, represented as a Dirac function, is finally convolved with the input driving function to determine the obtained composite waveform [270] [271]. This conceptually essential scheme includes the fundamental propagation parameters, but it clearly ignores several additional propagation parameters, as for example the spreading losses, layer inhomogeneities and multipath effects.

The Method of Moments (MoM) [272] is a frequency domain method which discretises the surface of the source to solve current density or charge density. The procedure is based on the derivation of the most suitable integral equation and its discretisation into a matrix equation through a weighted residual technique, which will then be solved to obtain the parameters of interest. Once calculated, the radiated and scattered fields can be computed through the regular radiation integrals. MoM technique can be adopted for both closed and open problems, such as radiation and scattering phenomena, but it is mainly limited by the fact that it requires the scattering source to be electrically large, as a consequence of the otherwise required computational resources

for inverting the matrix.

The Finite Difference Time Domain (FDTD) approach [266] is a numerical method resolving the time-dependent Maxwell's equations in differential forms by discretising the partial derivatives adopting a central differencing approximation. The resulting equations are then propagated through an iterative procedure to calculate the required solution. The main strength of the FDTD schemes is the possibility of addressing EM problems involving a wide range of frequencies in a highly efficient way [273].

4.4.1.1 Assumptions and approximations of models

According to George E.P. Box, FSR [274]:

> "Is the model true?". If "truth" is to be the "whole truth" the answer must be "No". The only question of interest is "Is the model illuminating and useful?"

Although designed with individual specific modelling approach, numerical solutions aim at simulating the actual propagation of EM waves from radiation to their interaction with the subsurface materials. Therefore, the ability of a model to realistically replicate the true 3D geometry of the involved components is a critical aspect.

Analytical modelling can be applied under simplified hypotheses on the nature of the problem, resulting in problem specific solution. For example, the aforementioned radar equation enables an estimate of the received signal level and related detection performance, but it has significant weaknesses concerning the near-field condition in which most GPR systems operates, whereas such signal modelling intrinsically assumes a far field one.

On the other side, more sophisticated numerical modelling can deal with the complex geometry and its boundary conditions, but they often suffer from low computational efficiency leading to difficulty in real time implementation.

Obviously, the development of a GPR model requires some assumptions to be made, considering also the necessity of limiting the computational resources so that features of interest can be properly exploited without excessively complicating the solution, keeping in mind that for a model to be reliable, it should also be able to tackle even highly complicated situations. This trade-off between sophistication and usefulness is strongly bounded to the problem to be solved.

4.4.2 Finite Difference Time Domain scheme

The FDTD technique has emerged as one of the most adopted modelling methods particularly due to the increase in accessible computational resources. There are different FDTD formulations, but there are a number of key common elements [273].

Firstly, the FDTD approach for numerically solving Maxwell's equations is based on the discretisation of both space and time domains. Therefore, the choice of such discretisation cell size ($\Delta x, \Delta y, \Delta z$) is critical when employing the FDTD technique, as it must be small enough to ensure accuracy and stability even at the highest frequency of interest, at the same time be large enough to limit the resource requirements. For instance, a domain including materials with high permittivity will require the design of a highly dense mesh, as a consequence of the reduced wavelength involved.

To understand why the cell must be smaller than one wavelength, the Nyquist sampling theorem must be considered. At any particular time step, the grid represents a discrete spatial sample of the field distribution, and the theory requires this spatial period, i.e. a wavelength, to be sampled by at least two samples for a proper spatial information retrieval. Because a preliminary definition of the smallest wavelength might not be possible, the consequence is that more than two samples per wavelength are required. In addition, another important factor is the error associated with numerically induced dispersion, inherent in the discretisation process and related to the fact that waves characterised by different frequencies will propagate at slightly different velocities through the grid, in a sense violating the non-dispersive nature of a material. Another aspect to be account for is related to the need for an accurate geometrical modelling of the problem geometry [275].

The building block of a FDTD model, as originally defined by [276], is the Yee lattice, i.e. a grid of predetermined cells that stagger electric field components, magnetic field components, and material properties on the grids in time and space. The original drawing is illustrated in Fig. 4.19. Arbitrary shaped targets and materials can be included by defining and allocating the appropriate constitutive parameters. However, it should be always considered the such staircase approximation might introduce relevant error when modelling curved objects.

The analysis is performed by computing the electric field at a specific time instant and space location, while the its magnetic counterpart is computed within the same spatial

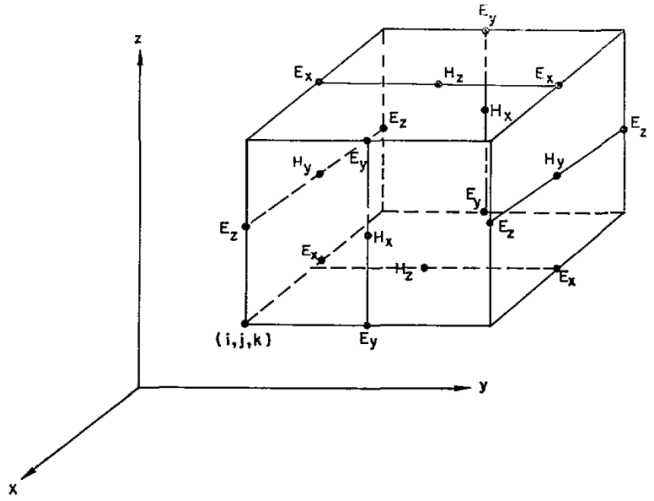

Figure 4.19: The Yee lattice structure. *Taken from [276].*

volume but at the subsequent time step. The process is then iteratively advanced by approximating the derivatives using a differential approach until an assigned simulation time Δt has elapsed [277] [276]. As a consequence of the imposed stability condition, known as the Courant condition [278], the maximum size of the time step depends on the volumetric cell size $(\Delta x, \Delta y, \Delta z)$, obeying to the following relationship (Eq. 4.23):

$$\Delta t \leq \frac{1}{c\sqrt{\frac{1}{\Delta x^2} + \frac{1}{\Delta y^2} + \frac{1}{\Delta x^z}}} \tag{4.23}$$

where c is the speed of light in the medium. The stability condition for the 2D case is easily obtained by letting $\Delta z \to \infty$. Smaller steps do not generally result in computational accuracy improvements, while larger ones result in instability. In fact, when the equality holds, the discretised wave most closely approximates the actual wave propagation, and grid dispersion errors are minimised. However, exceptions to this occur. Even if the stability step is set by the speed of light in free space, and hence by the maximum velocity of propagation in any medium, for conducting materials stable calculations may require time steps smaller than the Courant limit, as well as for nonlinear materials.

Another critical feature when solving forward scattering problem is that they are usually defined as open problems, i.e. the domain in which the field has to be computed is unbounded. This means that the solution can be obtained only after the propagating field reaches zero value, obviously an unrealistic approach [279, 280]. As a conse-

quence, the computational mesh must be truncated to limit the effective computational domain, always considering that such step must be carefully addressed as (1) truncation might corrupt the data, (2) the target must be completely included in the resulting domain, and (3) the artificial boundaries must still accurately approximate the infinite surrounding space.

A solution to this has been found by explicitly defining a condition known as Absorbing Boundaries Condition (ABC, [281]), to prevent reflection of the signal at the boundary of the computational space from propagating back into the domain. The actual effects of the absorbing contours on a propagating wavefield is illustrated in Fig. 4.20.

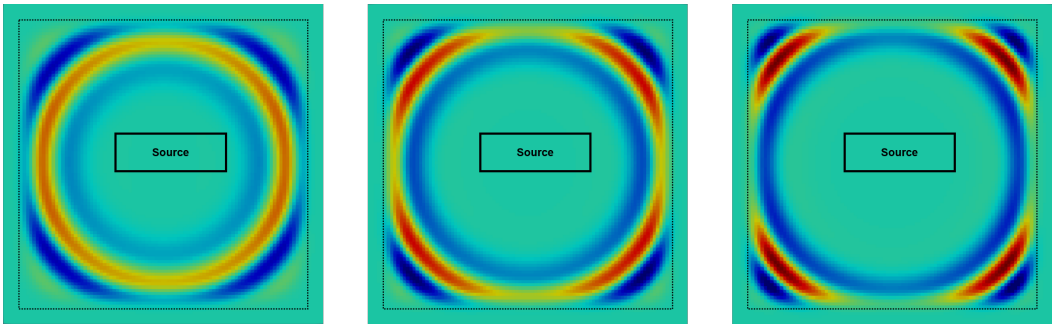

Figure 4.20: Effects of the ABC contours on the FDTD solution.

Essentially, at these boundaries, the EM field is completely absorbed either by imposing an energy decay [282] or by specifically modifying the wave equation definition across the boundary [283], therefore what is to be ideally achieved is either a zero reflection or a full transmission, at the same time minimising the residual error. The main difference between the approaches is the need for additional computational resources for developing the revised wave formulation or the additional space allocation required to include the absorbing boundaries [284]. A conceptual sketch is provided in Fig. 4.21.

The FDTD method has several inherent advantages over alternative electromagnetic modelling technique in hat :

- The solution is produced through a time stepping procedure, hence advantageous for computer implementation.
- The method is robust and relatively intuitive to implement, and exhibits a good scalability of computing resources with respect to the domain size.

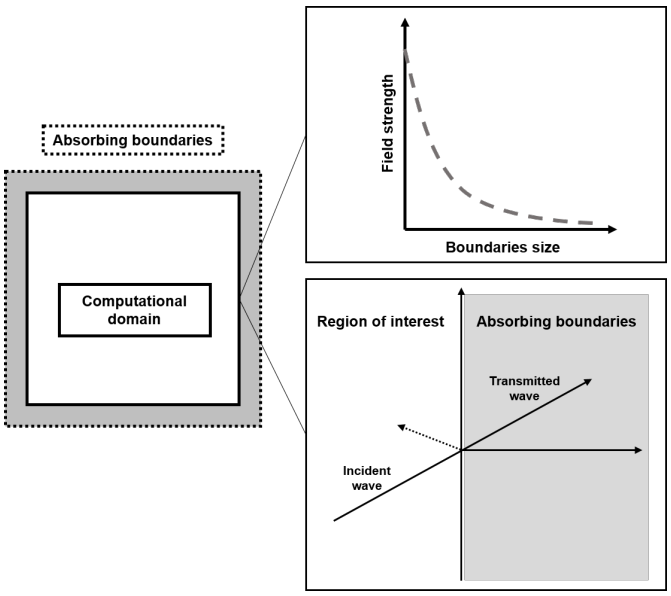

Figure 4.21: Schematic diagram of the FDTD computational space and ABC behaviour.

- The time domain formulation increases its computational efficiency, as retrieving frequency domain data from time domain data is easier than the converse.
- Arbitrary 3D model geometries, as well as complex dielectric and magnetic materials can be flexibly included.

In summary, the strength of the FDTD method can be considered its flexibility to handle arbitrary materials, waveforms, antenna configurations, and objects, as well as its suitability for parallel computing, a highly attractive potential. The main weaknesses are related to the staircase approximation, hence the potential inaccuracy when modelling sharp edges and curved shapes, and the fact that the entire computational domain must be discretised, empty spaces included. This last aspect is particularly critical when high permittivity materials, which requires a fine grid, are included.

4.4.2.1 Software description

The FDTD solver used in this section is gprMax, an open-source software simulating electromagnetic wave propagation available at http://www.gprmax.com. The software was firstly introduced in 1996 [275] and intended to provide a numerical modelling platform for a wide range of typical GPR applications. Architecturally, it includes a parallelised CPU-based solver and a NVIDIA CUDA programming model based GPU-based. gprMax employs a text-based input file in which pre-defined commands specifies all the simulation parameters, including mesh size, time steps and domain features,

and simulation elements, from radiation source to materials and geometries, are specified through pre-defined commands [285] [286].

Compared to some widespread commercial software, such as the computer-aided design (CAD) tool CST Microwave Studio Computer Simulation Technology (CST, http://www.cst.com), gprMax exhibits similar numerical performance and sufficient flexibility for handling typical GPR simulation environments. In addition, although a CAD-based GUI might represent a valuable aid in designing geometrically complex scenarios, it suffers from being quite inefficient when systematic and methodological analysis are required, as well as when the domain includes significant heterogeneities. For instance, gprMax allows anisotropic objects, dispersive materials and specific soil topography to be easily modelled, advantages hardly replicable through a CAD environment. Another feature to be considered, given the application domain, is the fact that in CST the near field response can be obtained only through the inclusion of a realistic antenna model, which may become overly expensive.

4.4.3 Forward modelling

A number of simulations have been carried out to get a preliminary insight of the effects that the presence of a components within the target has on the radar signature, at the same time to provide a basis for the following experimental campaigns.

First of all, running a 2D simulation means solving the transverse-magnetic mode (TMz) with respect to z direction, thus the computational domain should be designed in agreement with this requirement (a single cell dimension in the direction representing the infinite one). In this case a theoretical Hertzian dipole source fed with a Ricker waveform with amplitude equalling 1 V is used to simulate the GPR antenna. The resulting radiation pattern, independent from the radial distance, is described by a circular section toroid, symmetrical about the dipole axis, while the frequency-bandwidth relationships are determined from [287].

The simulation parameters are detailed in Table 4.6:
In this scenario, a landmine-like target is modelled including both the activator or pressure plate and the internal structure, commonly sketched as a thin air layer located between the activator and the main body of the mine. The target is 8 cm wide and 6 cm height. The relative dielectric for the activator is 7, while the explosive is considered to

Table 4.6: Model set-up

Parameter	Value
Spatial discretisation ($\Delta x, \Delta y, \Delta z$)	0.1 - 0.05 - 0.1 cm
Domain size	50 x 80 cm
Number of cells	8e5
Antenna separation	6 cm
Time window	12 ns
Time step (Δt)	0.0015 ns
Number of iterations	8045

have a dielectric of 3. The soil is simulated as a homogeneous material.

The configuration is pictured in Fig. 4.22. The two points above the soil are the transmitter and receiver antenna that are polarised orthogonal to the plane of the page (z polarity)

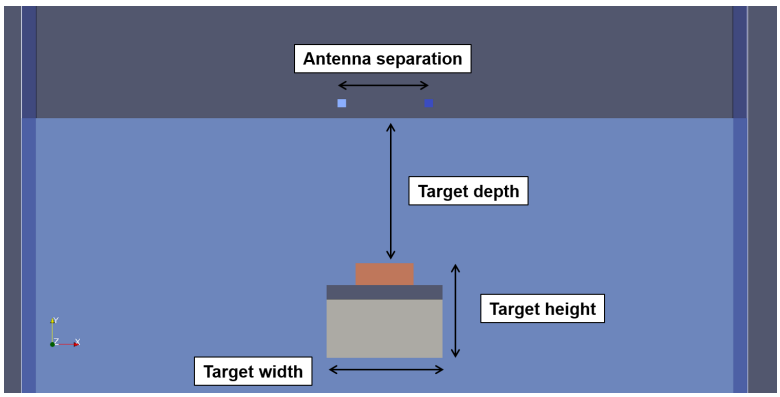

Figure 4.22: Geometry of the gprMax model.

This section will consider the effects of a range of key parameters to show their impact on the detection performance. These variables include the bandwidth of the excitation source, its height above the ground, the physical design of the object and the soil attenuation. The range of variables is listed in Table 4.7.

Table 4.7: Simulation variables

Parameter	Value
Source bandwidth	0.5 - 1 - 1.5 - 2 - 2.5 - 3 GHz
Source height	1 - 6 - 11 - 16 - 21 cm
Internal air layer	0 - 1 - 2 - 3 cm
Pressure pad	1.5 - 2.5 cm
Target depth	5 - 15 - 25 cm
Soil texture	low loss - high loss

The aim of such a process is to give evidence of the impact that the characteristics of the excitation, environment and target have on the resulting signature.

4.4.3.1 Bandwidth evaluation

As previously anticipated, a proper signature characterisation is only possible when the achievable resolution is high enough to separate each component of the modelled landmine-like target. Therefore, the first set of simulations involves the assessment of the bandwidth boundary for being able to detect the internal components of a mine. In the section the fractional bandwidth is considered to be 1, therefore the terms ”central frequency” and ”bandwidth” are interchangeable.

The same scenario which has been previously described is employed, and the source frequency is varied according to Table 4.7. Modelled soil is a sand-like material with a relative dielectric of 4.5, while the target is located 10 cm below the surface. With such a configuration, the velocity dispersion error is less than 1% and the wavelength is sampled by 12 cells, obeying the rule of thumb of a tenth of the wavelength.

The computed time domain signatures of a landmine-like target with varying bandwidth are shown in Fig. 4.23.

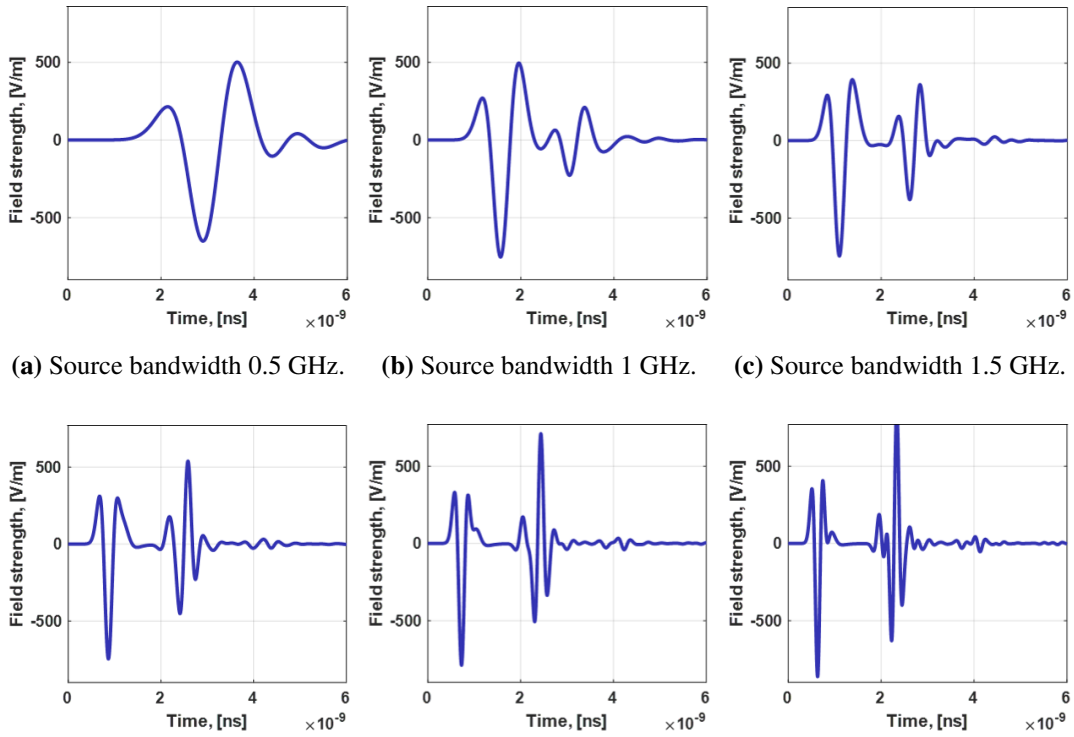

(a) Source bandwidth 0.5 GHz. **(b)** Source bandwidth 1 GHz. **(c)** Source bandwidth 1.5 GHz.

(d) Source bandwidth 2 GHz. **(e)** Source bandwidth 2.5 GHz. **(f)** Source bandwidth 3 GHz.

Figure 4.23: Time domain signature of a buried landmine with varying source bandwidth.

First of all, it can be noted that a low frequency source does not allow the separation of the mine reflection from the background one, impeding the detection of very shallow targets. This effect is also a consequence of the soil texture, as the ground reflection pattern depends on the dielectric properties of the subsurface. Instead, a wider bandwidth is capable of discriminating even thinner layers.

The late signal perturbation visible in the radar signatures can be associated with multiple reflection events generated by the ground ringing, as they appear as highly attenuated and delayed replica of the target response.

These considerations are evident after a background subtraction, shown in Fig. 4.24.

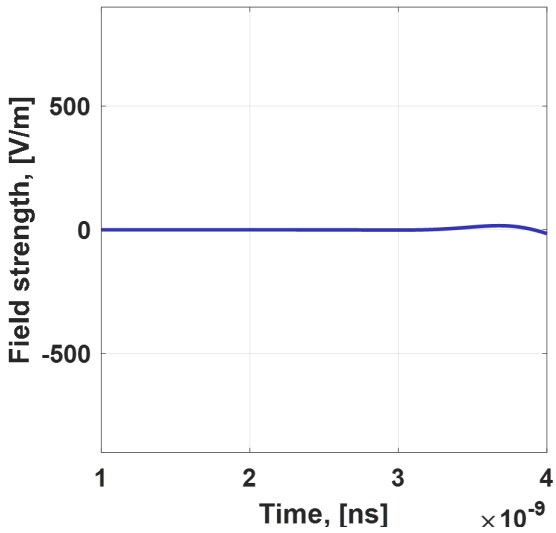

Figure 4.24: Simulated response from a 500 MHz bandwidth source after background subtraction.

As long as the bandwidth does not reach 2 GHz, the target is detected as a single reflection, due to an insufficient resolution of the different landmine components. At this boundary, highlighted in Fig. 4.25, three separate events can be identified: the upper part of the landmine (marked A in Fig. 4.25), a sharp reflection after it (marked B in Fig. 4.25) and a weak response indicating the bottom of the target (marked C in Fig. 4.25).

The reflection belonging to the bottom of the target appears as a very weak reflection due to (1) the limited impedance contrast between the explosive ($\varepsilon_r = 3$) and the sandy soil ($\varepsilon_r = 4.5$), and (2) the reduced signal amplitude caused by the strong earlier neoprene/air interface reflection.

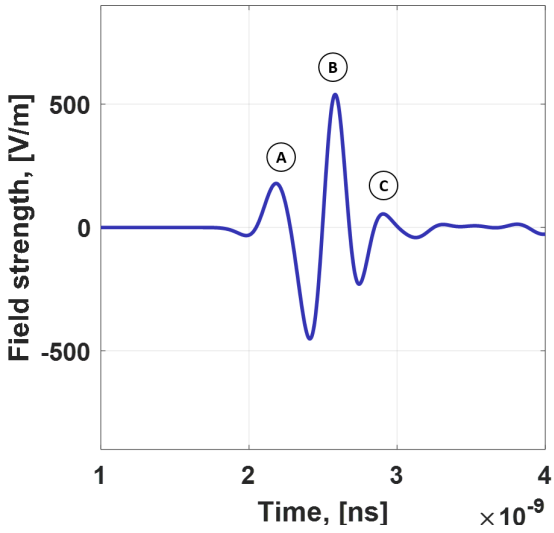

Figure 4.25: Simulated response from a 2 GHz bandwidth source after background subtraction.

A wider bandwidth is not only able to describe the complexity of the target, but is also capable of fully resolving the upper activator pad, due to the improved resolution of the wave. In this case the resulting radar signature includes the reflections generated by both the top and the bottom of the layer (shaded region in Fig. 4.26).

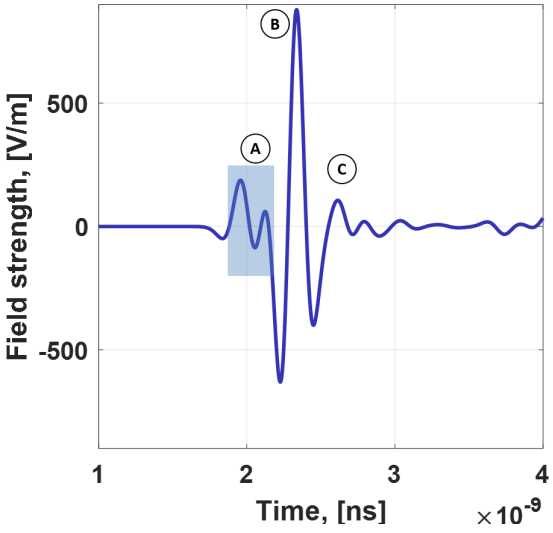

Figure 4.26: Simulated response from a 3 GHz bandwidth source after background subtraction.

Moreover, the signature confirms the considerations made on the characteristics of the bottom reflection, as it can be seen that the resulting reflections shown appear closely similar. Due to its high velocity characteristic, a correct geometrical reconstruction of the air layer would be hardly achievable, as its thickness would probably be consistently larger than the resolution performance.

A useful way to visualise what has been described and for a better understanding of the physical reasons beyond the results is the representation of the propagating wavefield, shown in Fig. 4.27. for different bandwidth. Each snapshot has been numerically computed at the same time instant.

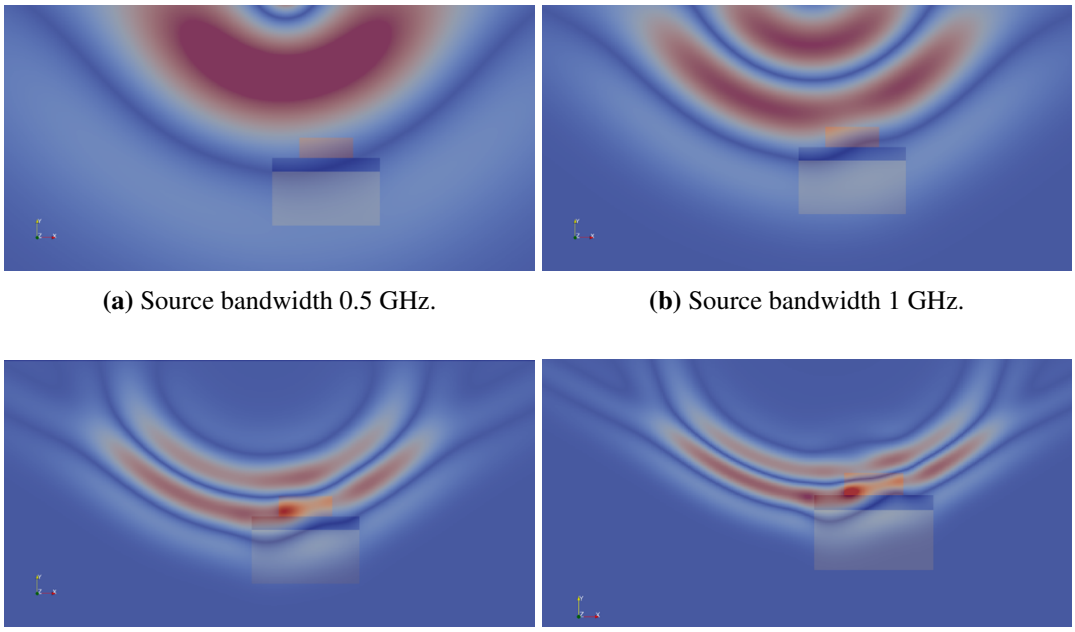

(a) Source bandwidth 0.5 GHz. **(b)** Source bandwidth 1 GHz.

(c) Source bandwidth 2 GHz. **(d)** Source bandwidth 3 GHz.

Figure 4.27: Snapshots of the E field with varying bandwidth.

The wider the bandwidth, the shorter the wavelength and hence the shorter the distance between two subsequent wavefronts. The consequence is what has been described before, the inability of narrow bandwidth of discriminating between closely spaced features. This is evident if one looks at the modification of the pattern of the wavefront produced by the target.

4.4.3.2 Antenna height

As previously discussed, the antenna height above the ground is a critical factor, both concerning the design of the GPR platform and the quality of the collected data. Recalling the described concept, it is clear that a stand-off radar system might represent a reasonable choice when surveying a minefield, but the impact of elevating the antennas on the reflected signal strength must be evaluated.

Considering a central frequency of 2 GHz, the source has been progressively elevated from the ground according to Table 4.7, in order to assess the influence of the parameters on the target radar signature. As before, a fixed scenario has been main-

tained, in therm of soil properties and target depth.

The resulting signatures, plotted in the A-scan mode and normalised by the maximum value of the closest situation (height of 1 cm) are presented in Fig. 4.28.

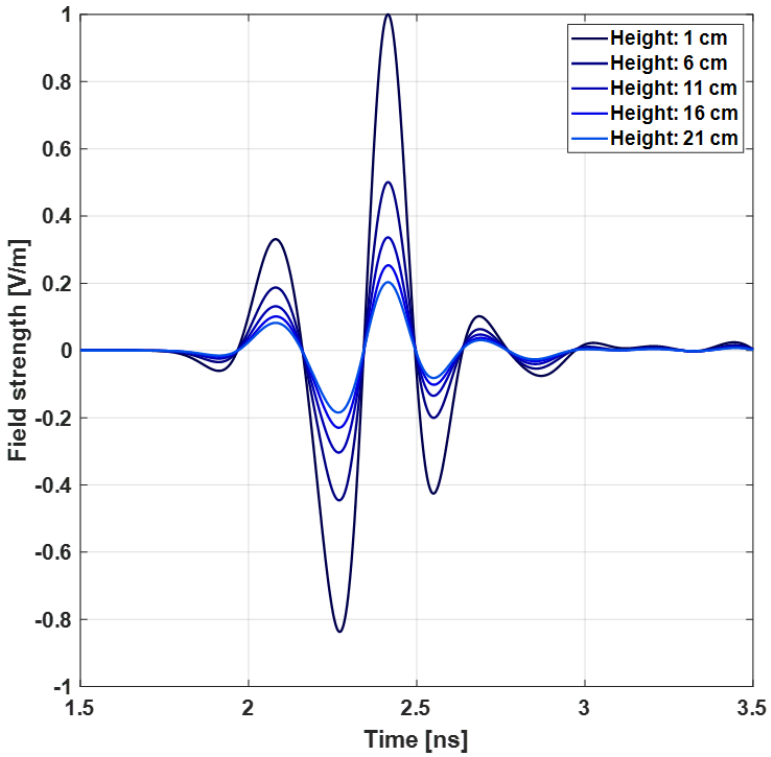

Figure 4.28: Time domain signature of a buried landmine with varying source height above the ground.

All the graphs show that the target response reduces as the height of the antenna is increased, with the most significant losses occurring in the first steps, i.e. just detaching the antenna from the ground. In this region, approximately, half of the amplitude is lost, as described in Fig. 4.29.

Obviously, the reflection generated by the bottom of the landmine, which is the weakest contribution, is marginally affected by the loss of strength as it occurs after the air interface, boundary causing a marked signal reflection, thus even in favourable conditions the amount of energy reaching the bottom of the target is limited. Then, the signal strength suffers a less pronounced reduction, but still the limited amplitude may lead to a signal below the sensitivity of the system.

It is clear that for high loss propagation environment these patterns and signal reductions will be emphasised, as well as when increasing the depth of the mine as the path attenuation will become higher.

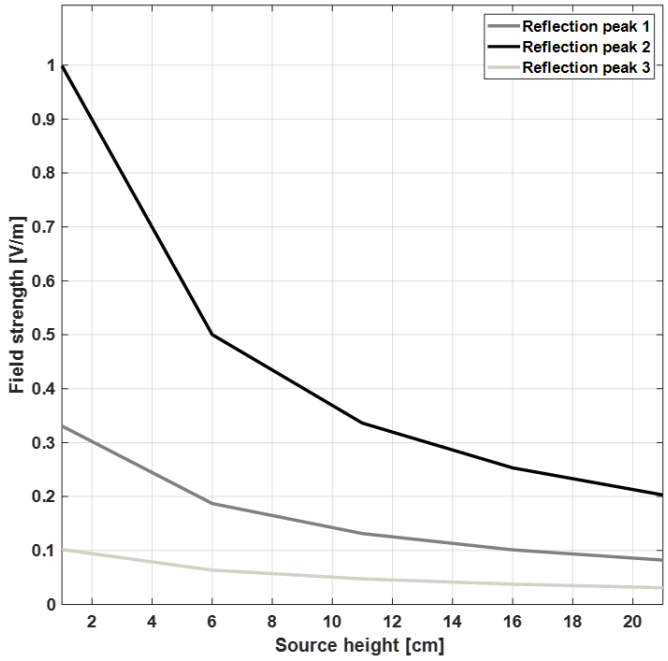

Figure 4.29: Comparison between reflection peaks magnitude and source height

However, the internal scattering contribution remains a clearly detectable event, even if its prominence vanishes with the antenna elevation, as it can be noticed that the spread among the reflection peaks is visibly reduced. This concept is described in Fig. 4.30.

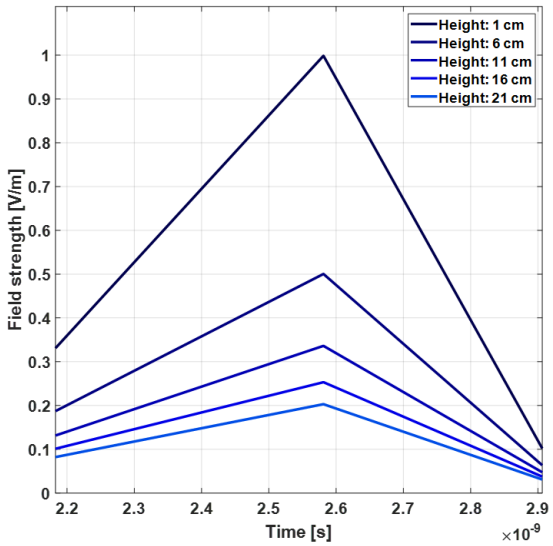

Figure 4.30: Comparison between reflection peaks spread.

Consequently, the information is that the nearer to the ground the source is, the stronger the reflected signal will be.

4.4.3.3 Target parameters evaluation

From the previous analysis, it can be assumed that a close proximity with the ground and a minimum bandwidth of 2 GHz are requisite to ensure a proper internal structure detection. The logical step ahead is to evaluate the target physical parameters that may modify the signature of the target and weight their impact on its pattern. Nominal values are listed in Table 4.8.

Table 4.8: Target design: model set up

Parameter	Value
Source bandwidth	2 GHz
Source height	1 cm
Soil relative dielectric	4.5
Target depth	10 cm

For a proper assessment of the results when altering the target design, its total vertical size has been maintained.

Air layer effect The first step is an investigation of the weight of the effect of the internal air layer on the target signature. The principal reason is to prove the importance of employing objects closely resembling the real devices, and not simpler surrogates.

The analysis compares a solid, homogeneous mine-like target and one with a progressively thicker air layer (Fig. 4.31).

From the graph it is possible to make the following considerations:

- A solid dielectric target shows the top and bottom reflection only, without any variations in the signature. The low signal level is due to the small contrast between the target and the surrounding soil.
- The presence of the internal air gap produces a significant modification of the pattern of the signature.
- Increasing the thickness of the air layer does not alter the shape, but contributes to the magnitude of the internal reflection peak.

When the thickness of the air layer becomes relevant, a variation in the temporal extension of the target can be noted, due to the propagation in a faster medium. However, as the velocity of propagation in the air layer is high, even a 3 cm layer is not completely resolvable, due an insufficient vertical resolution.

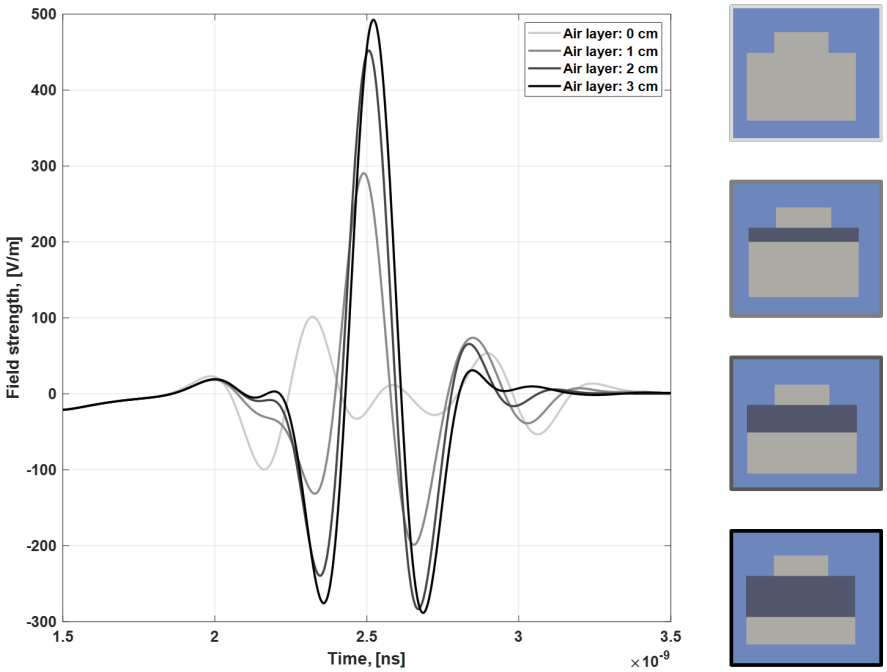

Figure 4.31: Comparison between internal air layer thickness.

These considerations confirm that the presence of the air layer is beneficial for the detection of minimum metal landmines with GPR, as the reflection generated by this layer are clearly stronger than the other components of the target signature.

Activator plate effect The second aspect that has been analysed is the effect produced by the upper activator plate. What is expected is (1) a stronger reflection due to a higher impedance contrast, and (2) a different signature shape, probably resembling the one previously obtained, as the lower boundary of the activator plate coincides with the upper boundary of the air gap.

The comparison between a solid target and the described one is provided in Fig. 4.32.

The graph confirms what was expected, in particular regarding the variation in the signature shape. Moreover, in this case the target response is longer in time, due to the fact that the wave travels through a slower material. Finally, it is worth noting that in this case the reflected wave experiences a reverse in polarity compared to the correspondent homogeneous target, as a consequence of the change in the sign of the reflection coefficients. It can be also noticed

As the vertical resolution is related to the size of the feature compared to the wavelength, a wider activator enables the wave to generate a reflection for both the top

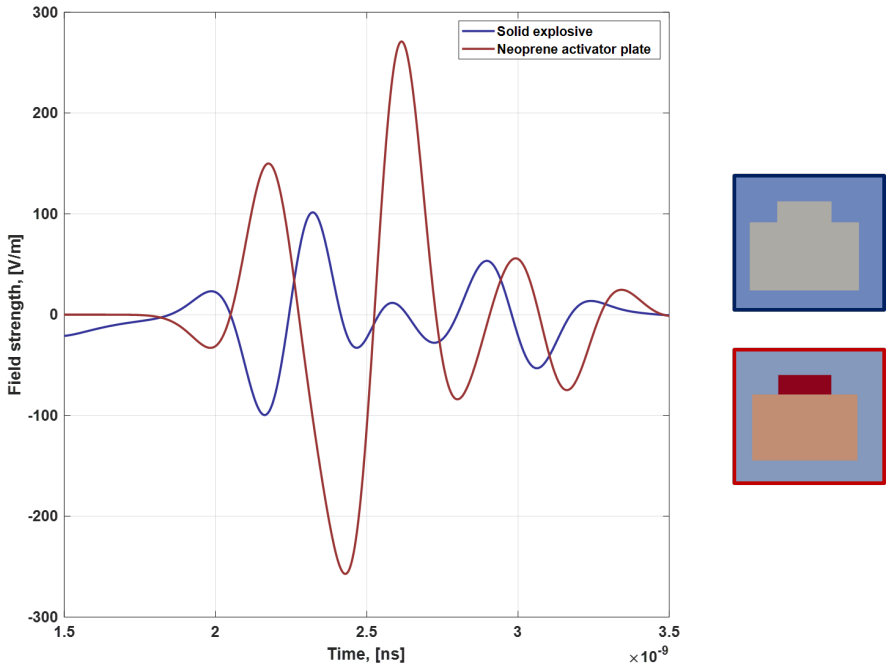

Figure 4.32: Comparison between presence and absence of the activator plate.

and the bottom of the layer, as shown in Fig.4.33.

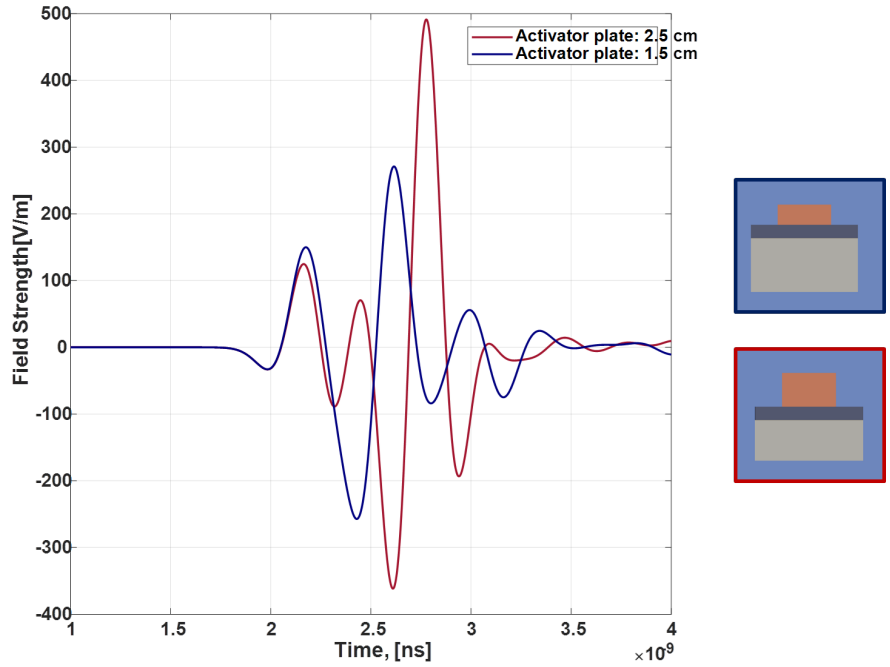

Figure 4.33: Comparison between activator plate thickness.

Except for this, no additional modifications are produced by a thicker activator plate.

Combined effect The last results may cast some doubts on whether the additional reflection visible in Fig. 4.33 is generated by the air layer or by the activator plate. To remove any uncertainties, the combined effect of these parameters has been evaluated.

In particular, the activator plate size is kept constant, while the air layer is progressively increased to verify the responsible of the internal peak. Results are shown in Fig. 4.34.

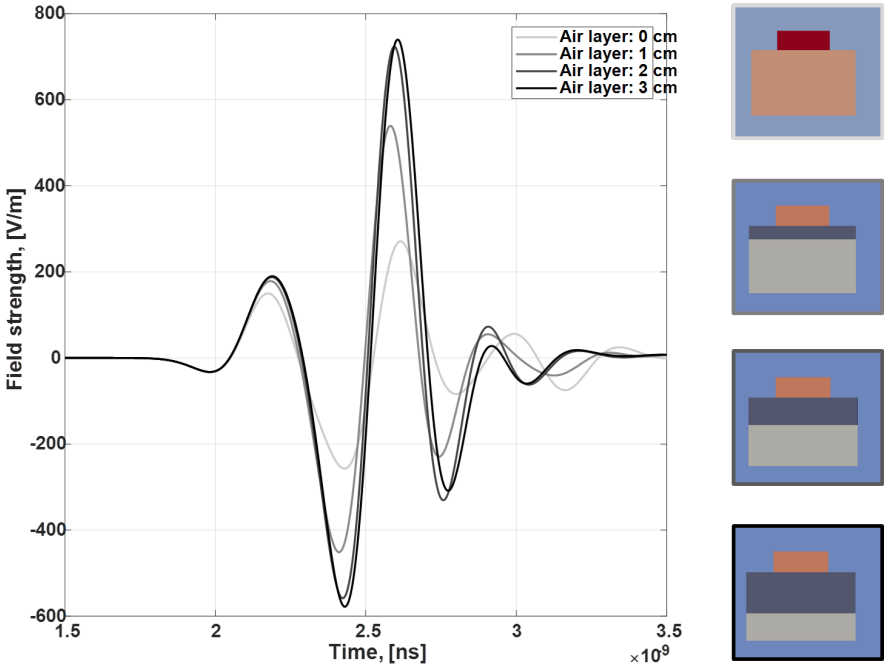

Figure 4.34: Comparison between internal air layer and activator plate.

The resulting signatures show that the two effects are indeed almost coincident, but a significant difference in the magnitude of the reflection exists. Whichever way one considers the result, it is evident the need for a precise and accurate target design.

As before, the representation of the propagating field for the full landmine model and for a solid object is provided in Fig. 4.35a and Fig. 4.35b respectively, in which a set of 0.1 ns snapshots has been extracted starting from 1 ns to 3 ns.

Two main aspects can be highlighted: (1) the strongest reflection is generated by the air layer, and (2) the effects on the shape of the wavefront. In particular, the modifications are a function of the layer permittivity and size, therefore a complex shape variation can be noted. Conversely, the propagation through a homogeneous dielectric target does not affect the spherical pattern in the same complicated way, as can be seen in the right-column frames.

4.4.3.4 Target depth and soil impact evaluation

Having demonstrated the impact that the target design has on its signature, the last section is dedicated to a brief assessment of the extensibility of the approach, investigating

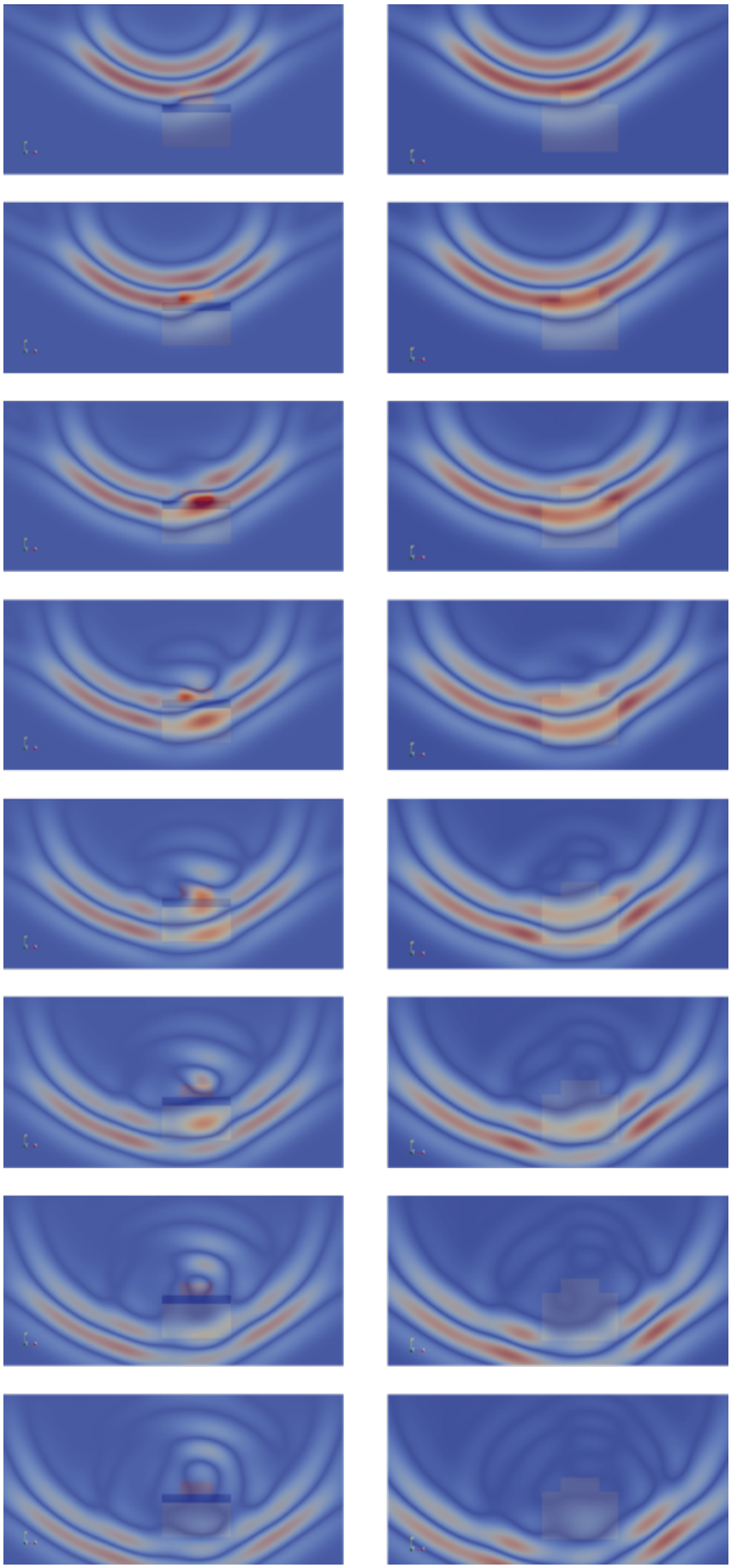

(a) Landmine-like object. **(b)** Solid object.

Figure 4.35: Comparison between field propagation a landmine-like target and a solid object.

the effect of the target depth and soil attenuation characteristics.

To verify the reliability of the strategy two different scenarios have been simulated. The first one describes a highly beneficial situation in which a landmine is covered by a sandy material with an attenuation of approximately 10 dB/m, while the unfavourable case is described by a high attenuation soil, represented by a material with a higher moisture level and a higher clay content, with attenuation coefficient of 30 dB/m. The two situations represent two representative environments in the landmine contamination framework. Details of the soil properties are given in Table 4.9.

Table 4.9: Target design: model set up

Parameter	Value
Soil dielectric (ε)	Low loss: 4.5 High loss: 20
Soil conductivity (σ)	Low loss: 0.01 S/m High loss: 0.05 S/m

There were three guiding principles behind this design decision. Firstly, the choice of the geophysical parameters determining the heterogeneity of the target may be hard to define. Secondly, modelling a heterogeneous/nonlinear/dispersive material would bring additional variables at that point would need a deeper exploitation. Lastly, a complex environment makes the interpretation of the resulting signatures difficult, as it will be hard to clearly separate and characterise the effects of soil attenuation and scattering losses.

The soil effect is essentially of placing a window across the aperture, trimming the spectrum and deteriorating the maximum resolution, which is dependent on the maximum propagating frequency. Therefore, as the strategy is to determine the nature of a buried object whether or not there are scattering contributions from the internal structure, it is more useful and noteworthy to test if the internal reflections previously characterised appear also for a more hostile environment.

Three depths have been investigated covering the typical range of antipersonnel landmine location. In particular, a shallower situation in which the target is buried at 5 cm, a depth close to the UN standard requirement (15 cm) and a third one in which a deeply buried mine has been considered (25 cm). Fig. 4.36 shows the geometry of the model.

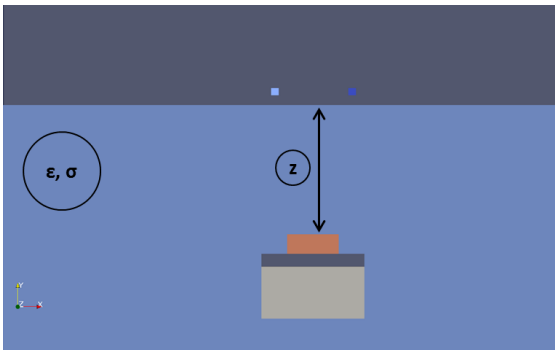

Figure 4.36: Geometry of the gprMax model.

Results from the low loss scenario, characterised by an attenuation factor of approximately 10 dB/m, are provided in Fig. 4.37.

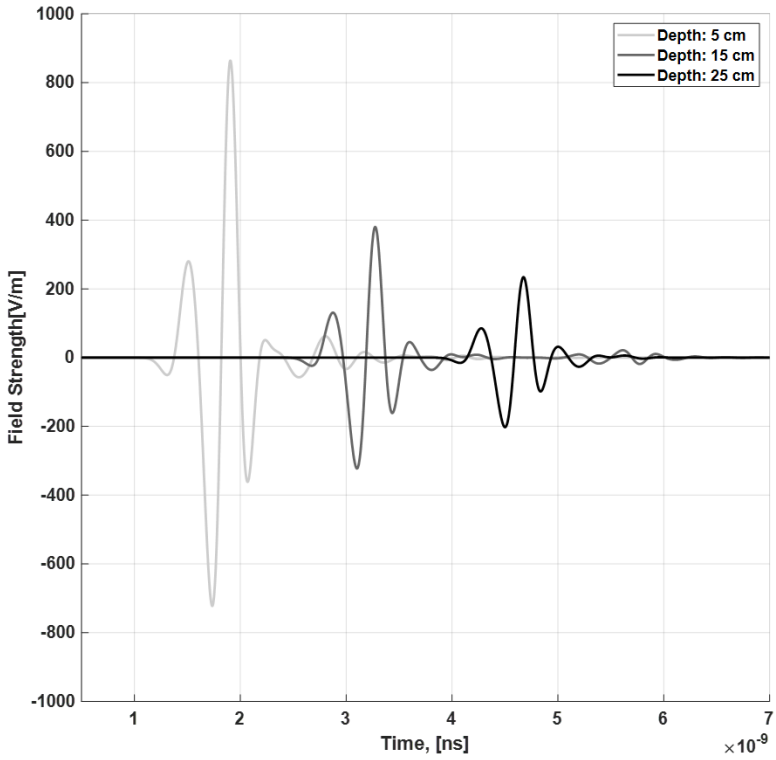

Figure 4.37: Comparison between landmine depths for a low loss scenario (α = 10 dB/m).

As expected, all the simulated signatures show the internal air layer reflection, regardless the burial depth, and their correlation is very high, as no significant modification of the shape are visible. The trends of the signal are in agreement with the well-known exponential decay related to the attenuation coefficient.

Results from the simulation of a soil with a higher attenuation coefficient (approximately 40 dB/m) are illustrated in Fig. 4.38.

In this case, the following considerations can be pointed out:

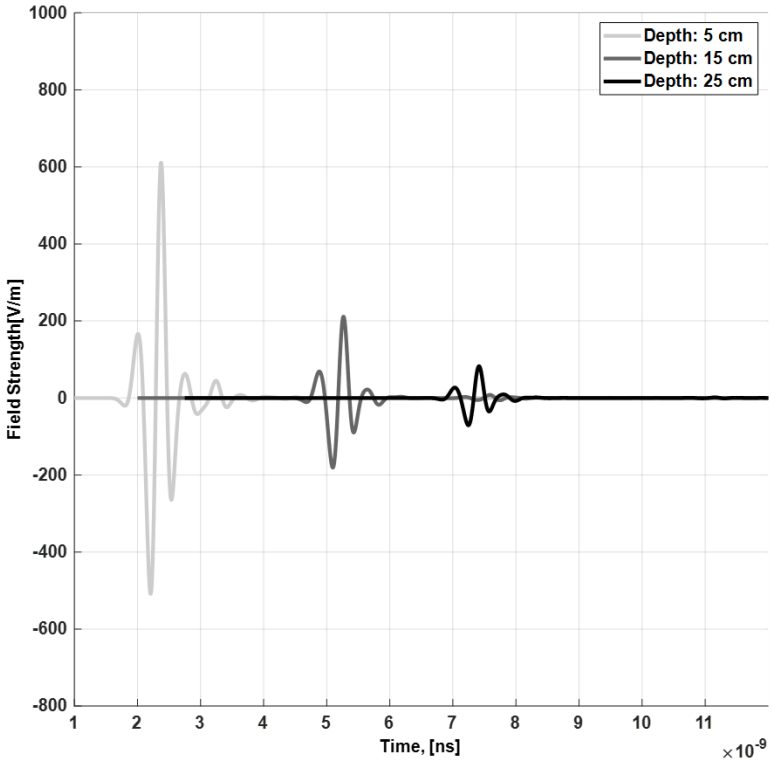

Figure 4.38: Comparison between landmine depths for a high loss scenario (α = 40 dB/m).

- The amplitude of the signatures is significantly lower and the decrease rate is sharper than the previous case, in agreement with the ratio between the attenuation value. In addition, the homogeneous texture of the modelled soil produces a signature qualitatively similar to the one computed in Fig. Fig. 4.37.
- The internal air layer reflection appears to be the only visible contribution, due to the loss of resolution produced by the soil texture. Theoretically, the scattering from the layer is consistently visible regardless the target depth, and particularly the deeper mine almost shows the air layer contribution only, demonstrating once again that it plays a fundamental role for the detection.

The critical condition is that the limiting factor of detectability is the dynamic range of the receiver. Therefore, it has been proved true that the internal air layer emerges also in high loss soil situation and for deeply buried mine, but it is also true that the detection of this contribution depends on exceeding the noise figure threshold of the GPR system.

4.5 Summary

In this Chapter, the fundamental EM relations which are the governing equations of the GPR forward problem have been presented, as well as a basilar assessment of the parameters affecting the range performance of a GPR system. The dependencies within the main variables have been exploited in detail.

A comparison between a monostatic system and a bistatic one has been included to appraise the advantages that the inclusion of an additional variable (the antenna separation) may have or not on the system performance. In particular, the principal modifications are related to the target scattering and the experienced attenuation. Following the same concept, a brief section has discussed the issues that a GPR system should face when employed for demining operations, both in terms of system design and operational context.

From the examination of simple modelling scenarios, the effects of the GPR parameters, target design and soil properties on the GPR responses have been examined. Apart from the assumption involved in considering an infinitesimal source, there are no other simplifications in the modelling procedure. Therefore, all the EM phenomena are taken into account by the model.

In particular, given a suitable bandwidth (at least 2 GHz) and a close proximity to the ground, the reflections generated by the internal components of the landmine can be clearly identified, and the favourable conditions are consistent with the range of frequencies typically employed. Further, results from numerical experiments have revealed that the target design (external and internal) significantly alters the target radar signature, both in terms of magnitude and pattern, highlighting the importance of this aspect. Finally, results from the soil effects suggest that the detection of the internal structure is possible even for a deep target in high loss environment, provided that there is enough dynamic range for the system to record the reflection.

Chapter 5

Methodology and Results

Landmines do not distinguish the foot of a combatant from that of a playing child. Land mines do not recognize ceasefires or peace agreements.

G. Strada, 1996, [9]

This Chapter presents the results of the field campaign carried out for the purpose of the study. As described in depth in the research scope, the internal components of a landmine are expected to act as multiple scattering elements with a certain radiation pattern, therefore their effect should be evident and may be highlighted exploiting the angular domain of the problem.

The adopted strategy moves progressively from a preliminary evaluation of the magnitude of these contributions in a single mono-dimensional radar signature and in a 2D GPR profile, towards a full 3D imaging methodology, capable of overcoming unfavourable geometries and asymmetric target design, the two main issues that arose from the initial measurements.

Defining the productiveness of a GPR survey as trade-off between the level of information gathered from the data and the acquisition effort, whether survey time or deployment, it is clear that ideally a survey should collect as much information as possible, as quickly (or easily) as possible. Under this perspective, the Chapter ends presenting the radar results obtained from two different bistatic geometries, each of them with advantages and limitations, but both having the capacity of providing an equivalent level of information at the same time lowering the acquisition effort.

A detailed description of the employed targets and the experimental settings for

each campaign are provided, together with a summary of major findings for each section.

5.1 Target description

The radar signature of a landmine is highly dependent on the materials used to make the external and internal components as well as the chemical properties of the explosive content. Landmines are objects which are difficult to obtain and replicate to carry out a measurement campaign and therefore it was the first priority to obtain properly constructed inert landmines to ensure the collection of landmine signatures as close as possible to those of a real live device.

Three representative landmines, provided by the Defence Academy of the UK, were used: a Soviet PFM-1, an Italian SB-33 and an Italian VS-50. These were complete with all their external and internal components and were filled with a high explosive simulant commonly used to train UK Ammunition Technical Officers. As the purpose of the research is to evaluate the effects of the internal structure on the radar signature, the correspondent VS-50 simulant mine provided by *Fenix Insight* was also tested. The surrogate is moulded from the actual mines in a resilient epoxy resin, accurately resembling in appearance the real target but without the internal assemblies. Dimensions and characteristics are provided in Table 5.1.

Table 5.1: Experimental targets description.

Target	Shape	Dimensions [*cm*]	Outer material	Metal content
VS-50 (Fig. 5.1a)	Cylindrical	9 x 4.5	Plastic	Low
SB-33 (Fig. 5.1b)	Cylindrical	8.5 x 3	Polycarbonate	Low
PFM-1 (Fig. 5.1c)	Maple seed	120 x 60 x 20	Polythene	Medium

A photograph of the three landmines and the surrogate is displayed in Fig. 5.1.

The VS-50 (Fig. 5.1a) is an anti-personnel mine which consists of a circular plastic body with vertical ribs moulded into the circumference. The VS-50 landmine consists mainly of three sections: a main body containing the explosive charge, a section comprising the fuze and the arming mechanism, covered with a plastic cap, and the upper par including the neoprene pressure pad. It is a minimal metal mine, with a ribbed, waterproof and blast resistant plastic case. The mine incorporates an anti-shock feature which will reduce the effectiveness of landmine countermeasure techniques such

(a) Inert Italian VS-50. **(b)** Inert Italian SB-33.

(c) Inert Soviet PFM-1. **(d)** Italian VS-50 surrogate.

Figure 5.1: Photographs of the employed devices.

as fuel air explosives and explosive line charges. A downward force of approximately 10 kg for a minimum of tenth of seconds is needed for the landmine activation. The middle section includes the air pressure delay mechanism, composed of an anti-shock bladder to block the detonation if the force on the pressure pad is of insufficient duration. The assembly has the additional consequence of allowing the mine to be scattered by a ground vehicle or by helicopter-carried dispensers. It can therefore be regarded as a blast resistant mine. A picture of the internal components of the landmine is provided in Fig. 5.2. The original model have been replicated under different names in Iran, Egypt and Singapore.

The SB-33 landmine (Fig. 5.1b) consists of a glass reinforced plastic case, with a covering neoprene flexible pressure cap, to ensure minimal deterioration of the mine casing and it exhibits a unique irregular shape to aid concealment and impede visual detection. Its asymmetric internal structure includes a cylindrical stab-fuze assembly in the middle of the target, just below the pressure note, and a void section on a side, covering only a portion of the main body. This sector allows a locking collar to rotate until the striker charge is released into the detonator container. As for the VS-50, a sudden pressure, such as that generated by mine clearance machines, causes only a

Figure 5.2: VS-50 landmine, component details. *Taken from ordata.info*.

partial activation, as the rotating collar is locked in position for the duration of the pressure, thus preventing the mine from detonating.

The disassembled landmine is shown in Fig. 5.3, in which one can clearly see that the metal content is minimum. Variants of this mine have been produced by Argentina, Greece, Portugal and Spain.

Figure 5.3: SB-33 landmine, component details. *Taken from ordata.info*.

The structure of the PFM-1 (Fig. 5.1c, also known as *Green Parrot* from its NATO reporting name, or also butterfly mine) is such that the landmine cannot be easily opened and hence it was not possible to take a picture of its internal components.

The device is a reverse-engineered copy of the US BLU-43, a scatterable air-dropped anti-personnel landmine designed during the Vietnam War. The mine is essentially a plastic bag containing a liquid explosive substance attached to a cylindrical detonator, activating when a deformation of the soft plastic case, even caused by a limited pressure (it is understood that a single pressure of 5 kg would be sufficient), drives the arming plunger to set-off the detonator. This mine is designed to float to the ground on plastic wings, usually air delivered, hence its nickname.

The surrogate (Fig. 5.1d) is fundamentally a solid explosive with a representative metallic content (mild steel pin). The four devices have been selected to investigate targets with different complexity, both internal and external.

To prove the electromagnetic consistency of the filling material, its dielectric properties were characterised by a coaxial probe measurement [288]. The same technique was used for characterising the epoxy resin employed for the landmine surrogate.

Results of the dielectric measurements are provided in Fig. 5.4. On average, the dielectric constant of the explosive simulant was around 2.95, while a value of 3.0 was found for the resin.

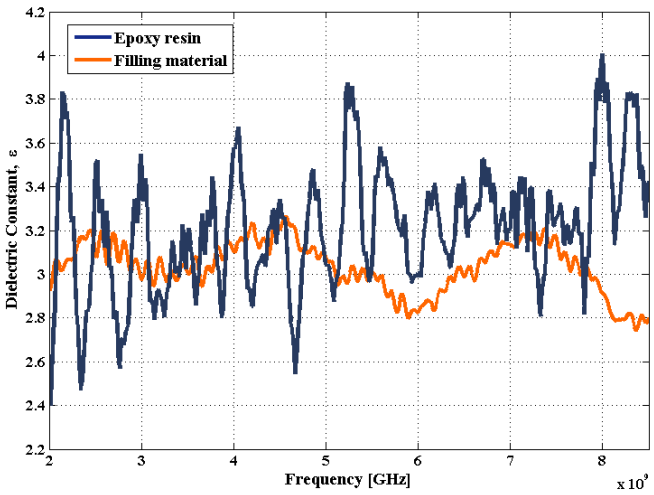

Figure 5.4: Materials dielectric characterisation.

The high variability of the results is a consequence of the uneven surface (and hence possible presence of air gaps) of the sample and its limited size. Considering the values of the commonly used explosive listed in Table 3.1, both the materials are sufficiently accurate for a reliable investigation.

5.2 Evidence of the internal structure: radar signature

First of all, it is necessary to understand the characteristics of mines, in terms of their shapes, case material and explosives, and their relative radar signature.The following section describes the preliminary analysis carried out to validate the research question and to provide an initial evaluation of the radar capabilities of detecting the internal reflections of the target.

5.2.1 Off the ground measurements

A set of free space radar signatures have been acquired in controlled conditions at the Defence Academy of the UK. Effects of polarisation and target inclination angle have been evaluated for off the ground landmines to exploit the landmine signature variations with acquisition geometries in the most favourable conditions.

Data were collected using a MS46322A Anritsu VNA transmitting a stepped frequency waveform with a bandwidth of 3.5 GHz from 5 to 8.5 GHz, with a frequency step of 0.4375 MHz. The dynamic range of the system is 115 dB, while the transmitted power was set to -20 dBm. The correspondent time domain signal has been obtained computing an Inverse Fast Fourier Transform (IFFT) with a zero padding step, thus the presented data are the result from the convolution of the antenna impulse response and the target response.

To prevent potential resolution degradation, no windowing functions have been applied, and the final envelope has been computed through the Hilbert transform.

In addition, an experimental characterisation of the antenna effects (impulse response and transfer function) has been carried out to verify the linear phase frequency response and the constant amplitude over the operational bandwidth. This evaluation has been performed by analysing the reflection from a metal flat plate located a sufficient distance from the antennas plane.

Although the frequency band employed would allow very limited soil penetration for subsurface imaging, it was selected to obtain a typical value of the ratio between common propagating wavelengths in the ground and the size of the landmine. A central frequency of 6.5 GHz corresponds to a wavelength λ of 4.6 cm in free space, and this value of the wavelength can be used to compute a hypothetical downshifted system for typical soil characteristics.

In particular, a 4.6 cm wavelength corresponds to a system with a central frequency of 2.4-3.2 GHz in dry sandy or loamy soil (ε_r:4-7) and 1.5-2.4 GHz in wet soils (ε_r: 9-20). Considering that mostly GPR equipment employed in demining operations works in a frequency range from 1 to 3 GHz, the achieved equivalence corresponds to a realistic operational configuration.

Another consideration is that air is a less dense material with a very low absorption rate, compared with typical encountered soils. This will lead to a better characterisation of the signature features, as all the expected multiple reflections coming from the different assemblies of the target will likely be effectively recorded. The effects on polarisation are such that the soil will have an impact in the presence of several heterogeneities, but homogeneous soil will not alter the wave polarisation characteristics.

Two identical horn antennas in quasi monostatic configuration and parallel polarisation were mounted on a LinearX precision turntable to collect polarimetric range profiles with a 5-degree rotation step over 180 degrees. The turntable was mounted on the vertical face of a L-shaped metallic frame to ensure a perpendicular alignment with respect to the ground. The antennas were arranged to transmit and receive with the same polarisation and rotating the turntable allowed measurements of the targets with different polarisation angles (i.e different angles of the incident linear E-field with respect to the landmine). Fig. 5.5 shows the antenna geometry.

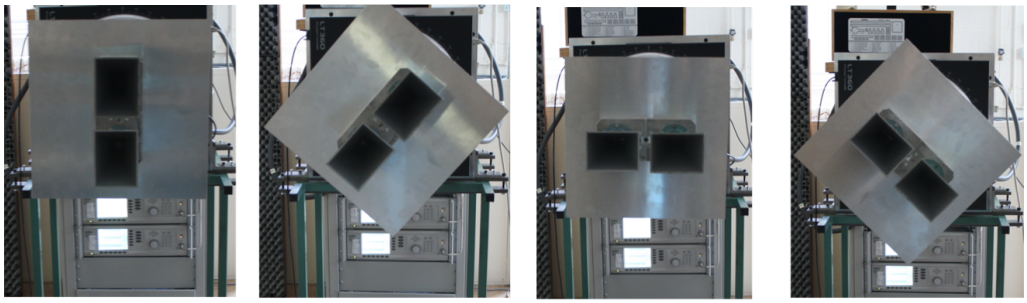

(a) Starting polarisation, HH. **(b)** 45 degrees orientation. **(c)** Orthogonal polarisation, VV. **(d)** 135 degrees orientation.

Figure 5.5: Off the ground measurements details.

A summary of the experimental activity is provided in Table 5.2.

The landmines under test were placed at a distance of approximately 170 cm from the antenna plane on a styrofoam cone (Fig. 5.6). The styrofoam material was used due to its low reflection properties to minimise the impact of the stand.

Table 5.2: Off the ground acquisition parameters and set up.

Parameter	Value
Frequency range [GHz]	5 - 8.5
Frequency step, Δf [MHz]	0.4375
Central wavelength [cm]	4.6
Angular range [deg]	0 - 180
Antenna dimension [cm]	9 x 12
Antenna offset [cm]	9
Antenna gain [dB]	16.5

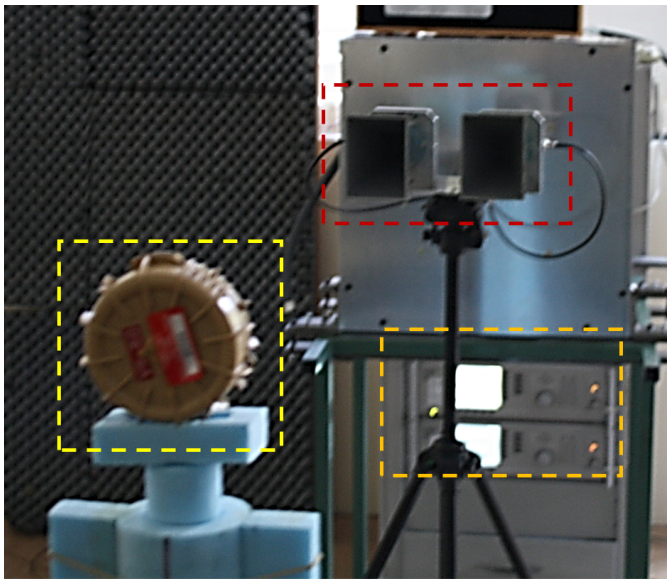

Figure 5.6: Experimental set up with the two horns connected to the VNA and facing the landmine under test on the stand.

Results for all targets are analysed in detail at two different aspect angles to further quantify the impact of target inclination on the signature. The geometry is shown in Fig. 5.7. The choice of evaluating the radar signature at different target angle is motivated by the fact that being a composite target with a number of internal scatterers, landmine response could provide different features and characteristics. In a large variety of environments, landmines may have been subject to alterations, such as landslips and flooding, which may have modified the geometry and orientation of the buried target.

To obtain the reflected signal from the object, a measurement of the background was taken to remove all stationary clutter from the target signature. Considering the non-optimal measurements environment, the placement of the target was accurately evaluated to ensure its spatial separability from room interference.

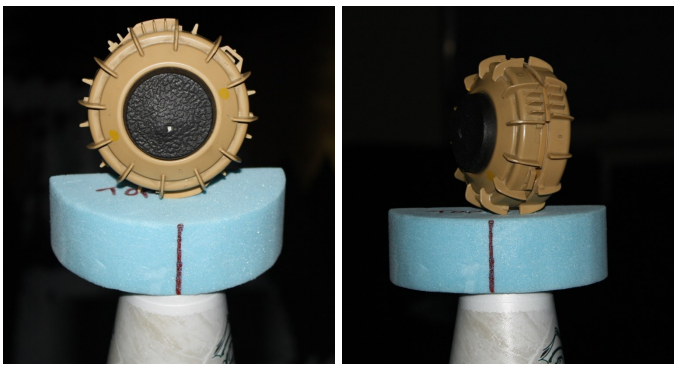

(a) 0 degrees orientation. **(b)** 45 degrees orientation.

Figure 5.7: Off the ground target aspect angles.

Analysis of the measurements environment is provided in Fig. 5.8, in which it can be seen that (1) interference generated from the room and multipath effects are very limited, in both range and magnitude, except for the strong reflections generated by the front wall (approximately 6 metres distant), and that (2) these events show an almost stationary and constant behaviour over the different antenna orientations, ensuring an accurate background whitening step.

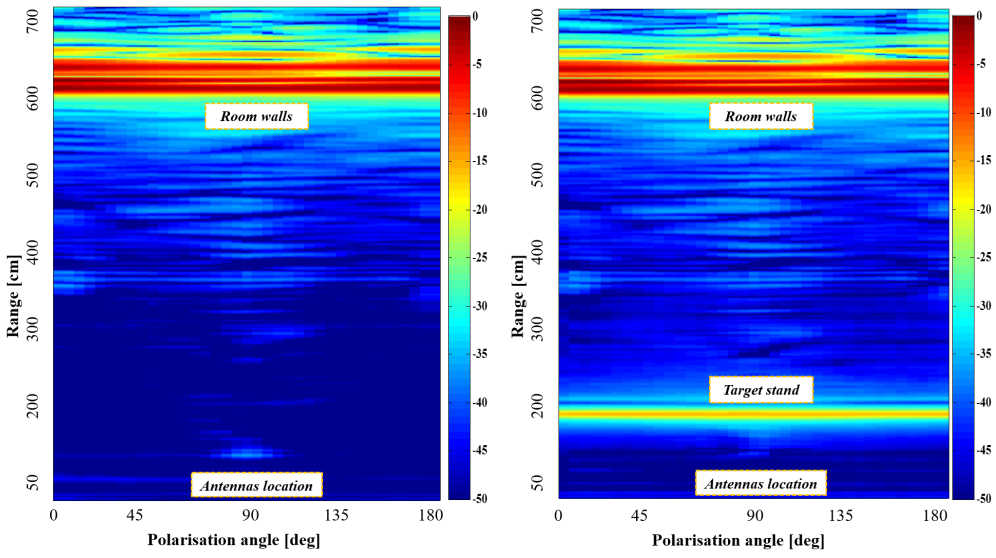

(a) Background only. **(b)** Target stand inclusion.

Figure 5.8: Background quality analysis.

Finally, as an additional figure of merit the acquisition set-up was tested against a metallic sphere with a radius of 3 cm, as shown in Fig. 5.9.

Resolving the canonical radar equation provided in Eq. 4.22 for the considered set-up and employed equipment, and assuming a target RCS of roughly -25 dB (given by a

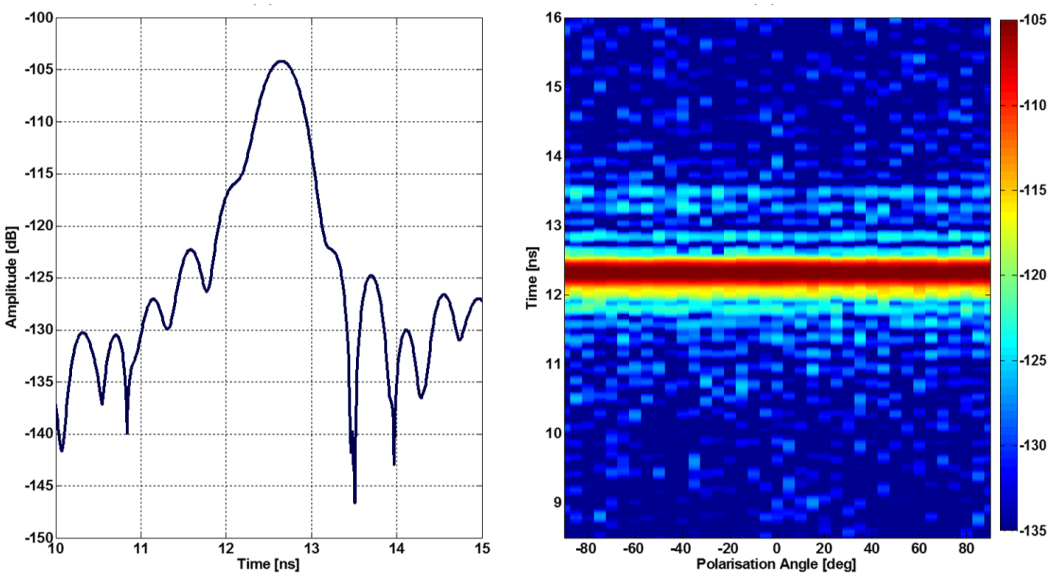

(a) Target 1D signature. **(b)** Target polarimetric profile.

Figure 5.9: Measurement set-up quality analysis.

radius of 3 cm), the received signal level would theoretically be around -102 dB, which is in close agreement with the amplitude of the main peak of Fig. 5.9a, nearly -104 dB. Further on, the polarimetric analysis, Fig. 5.9b, shows that no significant variations occur when changing the antenna orientation, as the amplitude values of both the main peak and the sidelobes are consistent throughout the whole angular space.

As the aim of this section is to provide a qualitative evaluation of the target response depending on its geometrical properties and orientation, the recorded time domain signatures of the inclined target (i.e. 45 degrees) have been normalised with respect to the maximum value of the aligned configuration (i.e. 0 degrees).

However, as a reduction of the signal level is expected when the target does not perfectly face the antennas plane as a consequence of the different projected RCS seen by the system, the magnitude of this amplitude difference is provided as well.

For the two described aspect angle, Fig. 5.10 presents the 1D time domain signature of the PFM-1 landmine.

Due to the simple design and absence of complex internal structure, the radar response of the PFM-1 landmine is mainly represented by a single reflection peak, regardless the relative geometry. Considering the physical design of the target, this contribution to its signature arises from the cylindrical detonator assembly, as the stabiliser wing is hardly contributing due to its limited size.

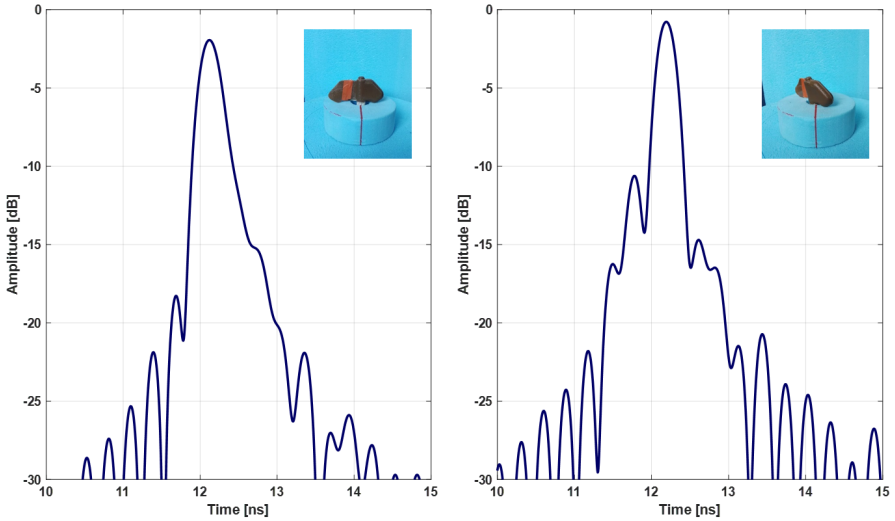

(a) 0 degrees. **(b)** 45 degrees.

Figure 5.10: PFM-1 landmine signature, 1D signature.

In Fig. 5.11 the radar response of the SB-33, as a function of the aspect angle is displayed.

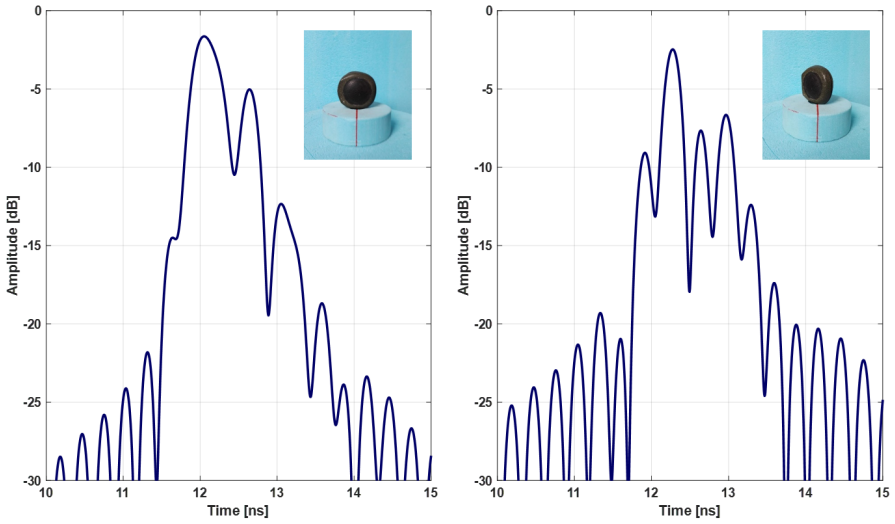

(a) 0 degrees. **(b)** 45 degrees.

Figure 5.11: SB-33 landmine signature, 1D signature.

When the target includes an internal design, the structure of the device significantly complicates its signature, in which several contributions can be highlighted. When the target is lying horizontally (Fig. 5.11a), the effects of the target complexity becomes evident, as an internal reflection is clearly visible, due to a combination of the reflections generated by the detonator and the void sector located aside of it. The presence of internal assemblies becomes even clearer when the target is inclined (Fig. 5.11b), as

several multiple reflections are identifiable.

The response of the real inert VS-50 is presented in Fig. 5.12.

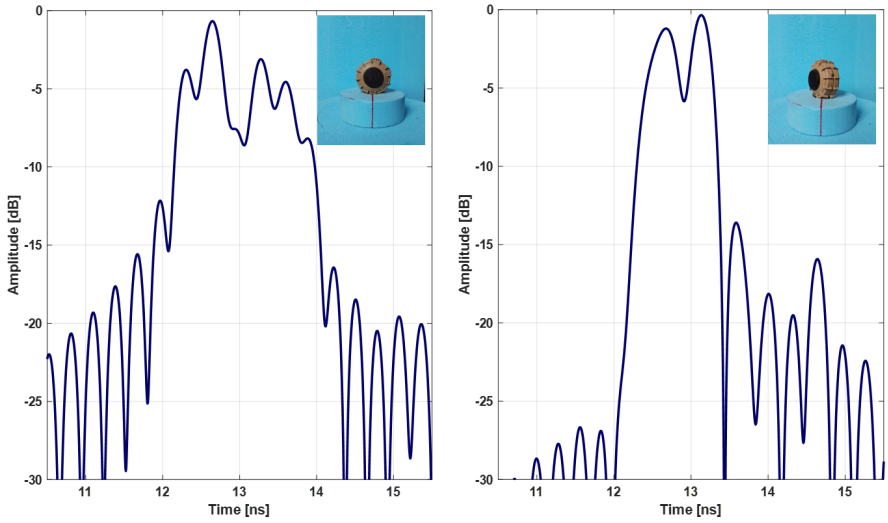

(a) 0 degrees. **(b)** 45 degrees.

Figure 5.12: VS-50 landmine signature, 1D signature.

Also in this case the internal structure of the landmine is clearly visible when the target is aligned with the antenna plane (Fig. 5.12a), as multiple reflections can be detected. Further on, it can be noted a close similarity with the numerical results obtained with a 3GHz bandwidth (Fig. 4.24) previously analysed.

While the first peaks could be identified with the activator plate response, fully resolved thanks to a suitable resolution, the second interface belongs to a scattering contribution generated by some internal assembly. Considering the landmine design, the responsible for this scattering contribution is the air gap layer behind the activator plate. The last peak is due to the bottom of the landmine. These considerations are no longer valid when the target is inclined: Fig. 5.12b shows only two reflections, belonging to the top and bottom of the landmine, generated by a combination of the air layer and the landmine main body. The increasing magnitude of the internal reflections are related to the parabolic effect of convex surface, which tends to focus the radar beam back to the antenna.

A final comment is related to the relevant amplitude of the range sidelobes which might be a results of small variations in the target stand position during the measurements, causing the background subtraction step not to completely cancel them out. The periodicity feature is then a result of the IFFT algorithm.

To give a quantitative evidence of the possible energy losses due to a target misalignment, Table 5.3 details the recorded amplitude strength of the three targets for both configuration.

Table 5.3: Reflections strength variability with inclination angle.

Target	Aligned configuration	Inclined configuration	Amplitude loss
PFM-1	-114.63 dB	-123.42	7.79 dB
SB-33	-117.91 dB	-121.37	3.46 dB
VS-50	-117.35 dB	-118.96	1.61 dB

The reduced scattering contribution recorded for the inclined PFM-1 landmine is a consequence of (1) a smaller projected RCS, limiting the target scattering, and (2) reduced target scattering directed towards the receiver. These considerations are supported by the fact that the recorded amplitude of the tilted PFM-1 is lower than the one observed for the other landmines. For the VS-50 model, instead, the regularity of the air layer limits the impact of a target rotation, as it still represents the more relevant contribution to the target signature. In this case, almost no differences can be observed and this hypothesis is . As presumable from the geometry of its internal structure geometry, a change in the aspect angle of the SB-33 landmine leads to a more pronounced amplitude gap, compared to the VS-50.

The effect of antenna polarisation on the PFM-1 mine as a function of aspect angle is presented in Fig. 5.13. Each signature has been normalised to its own maximum value to help the comparison process and displayed as range profiles in the time domain.

As expected, the polarimetric behaviour of the target is almost constant due to its relatively simple structure. There is a main scattering contribution in the range of the target which is overall regular also with aspect angle. When the target is inclined (Fig. 5.13b) the effects of antenna polarisation become slightly evident from some weak variations due to the different illumination of the target. However, on average the polarimetric analysis shows high levels of correlation.

The polarimetric profiles for the SB-33 mine are presented in Fig. 5.14.

Just from the first view, it is clear how the internal structure of the landmine impacts the polarimetric response. In all the frames the signatures decorrelate very fast

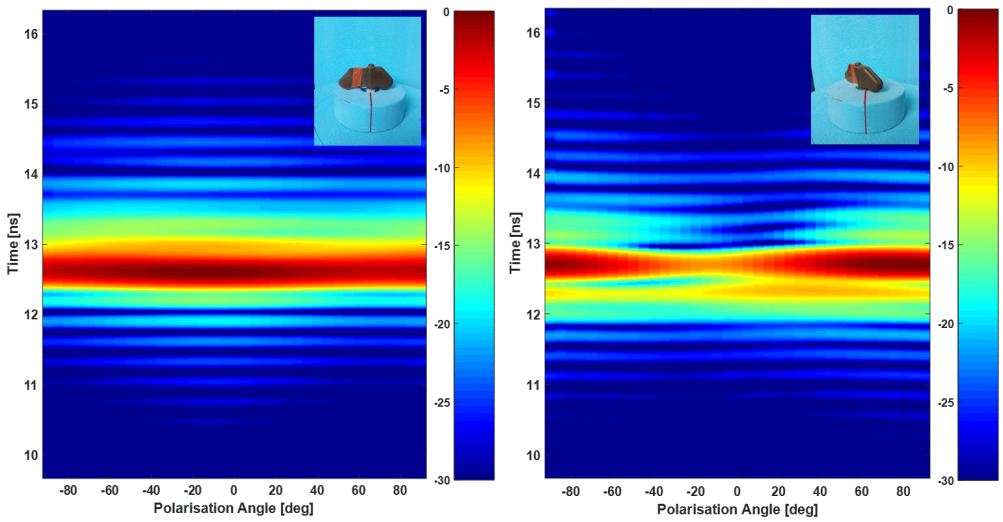

(a) 0 degrees. **(b)** 45 degrees.

Figure 5.13: PFM-1 polarimetric profiles.

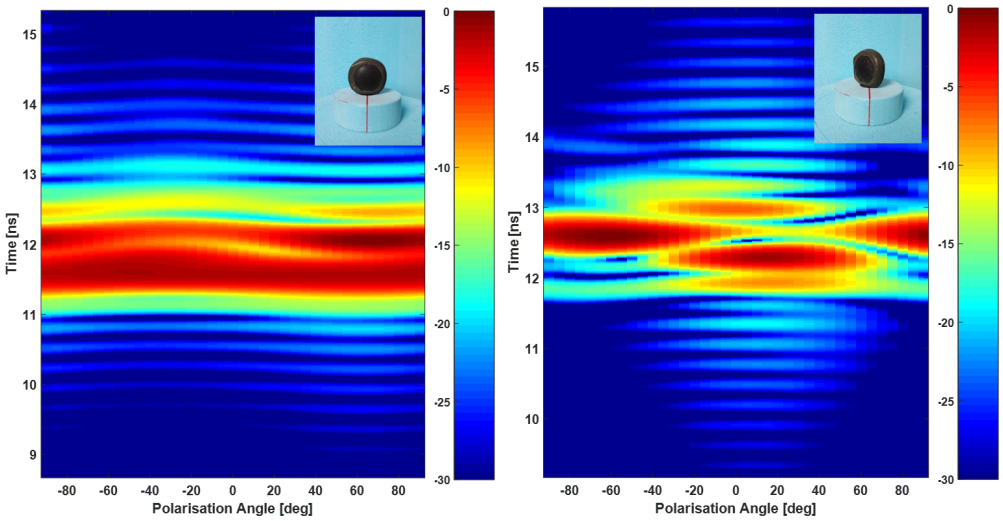

(a) 0 degrees. **(b)** 45 degrees.

Figure 5.14: SB-33 polarimetric profiles.

from angle to angle. The SB-33 has a larger physical dimension than the PFM-1, hence it is quite obvious that its response when the target is placed at no inclination angle (Fig. 5.14a) will be thicker in space, but what is to be noticed is that the main contributions is not constant, but some variations in the magnitude of the peaks occur. This feature is a suggestion of the presence of inner assemblies which gives rise to multiple reflections. The effect is even more evident when the target creates an angle towards the antenna plane (Fig. 5.14b) in which both reflection distribution and magnitude vary significantly with polarisation angle. This is a first demonstration that to gather reliable information regardless the relative geometry of the target, a set of signature is needed,

rather than a single trace. What is to be noticed is that at certain angles the contributions from the internal assemblies (the cylindrical detonator and the void sector) lose their singular identity and the resulting signature does not include a number of single reflections but a mixture of them. In practice, this means that even changing the orientation of the antennas, one can run the risk of wrongly determining the nature of the buried anomaly.

Figure 5.15 presents the acquired profiles for the VS-50 mine.

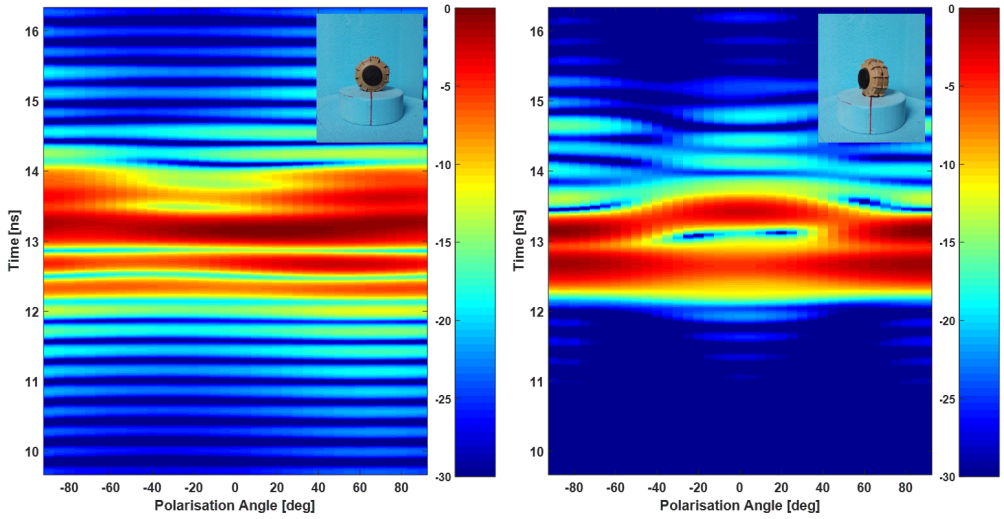

(a) 0 degrees. **(b)** 45 degrees.

Figure 5.15: VS-50 polarimetric profiles.

The same considerations made for the SB-33 mine hold here, as the internal structure affects the polarimetric trend in a clear and noticeable way. The profile in Fig. 5.15a is less heterogeneous compared to its SB-33 equivalent due to the presence, just below the activator plate, of a large number of air gaps, which modify the signature and balance out the illumination changes. When these gaps are not dominant over the signature, when the target is rotated, Fig. 5.15b, the profiles return to describe a more complex polarisation dependent behaviour.

5.2.2 Buried targets measurements

To validate the highlighted features in a more realistic setting, the same acquisitions were carried out burying the landmines in a sand pit. The test bed, located at the Defence Academy of the United Kingdom, Shrivenham, is a confined bay composed of several quadrants, Fig. 5.16a, and filled with a sharp sand material characterised by

a very low clay content and a gritty texture (Fig. 5.16b). The material is representative of several mine-affected regions of the world.

(a) Overview. **(b)** Highlight on the filling material.

Figure 5.16: Defence Academy test bay overview.

From a radar perspective, the conditions were favourable, as the material was relatively homogeneous and free of clutter, with an average particle size of less than half centimetre. A background-only profile is shown in Fig. 5.17a.

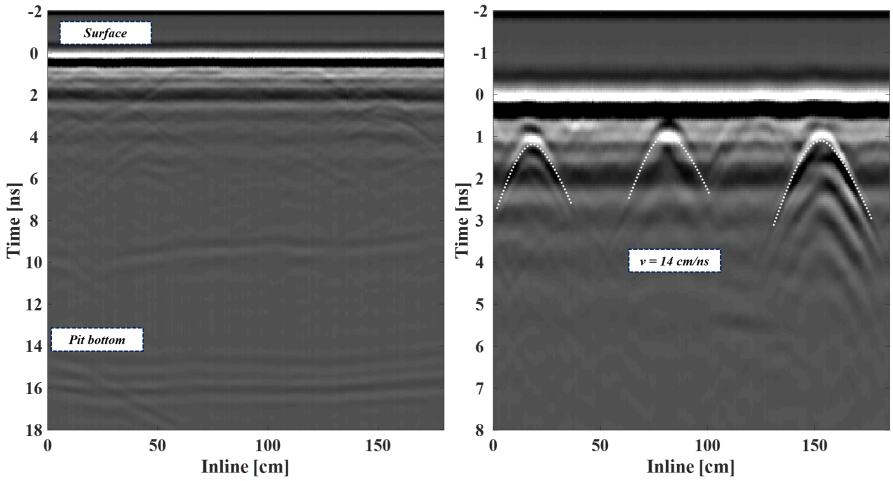

(a) Background profile. **(b)** Estimated wave velocity.

Figure 5.17: Defence Academy test bay soil properties.

Despite the environment humidity, the sand maintained a velocity, computed from hyperbola fitting in Fig. 5.17b, of 14 cm/ns and a consequential relative dielectric constant of 4.5. Soil attenuation properties are such that it is possible to detect the bottom of the pit, approximately at a depth of 120 cm, with an attenuation coefficient around 10 dB/m.

The equipment employed was an IDS Aladdin (IDS Georadar srl) georadar platform, a shielded ground coupled dipole antenna, spaced 6 cm, with a central frequency and bandwidth of 2 GHz. These parameters bring a minimum wavelength of 4.5

cm, therefore a consistency with the free space measurements has been successfully achieved, in terms of wavelength to target size ratio. Obviously, the existing difference between the two employed bandwidths exists and will affect the overall resolution capability.

The equipment is composed by two pairs of orthogonally polarised dipole antennas, as shown in Fig. 5.18a, located such that the reflection centre corresponds for both couples and coincides with the geometrical centre of the unit.

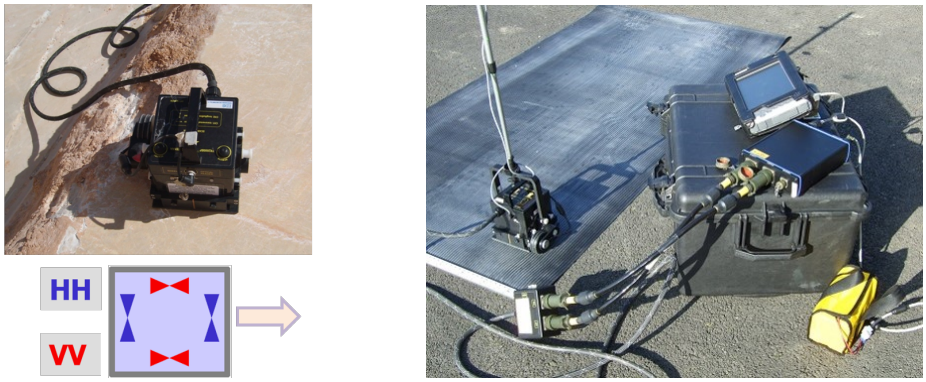

(a) GPR architecture scheme. **(b)** Complete platform.

Figure 5.18: Employed GPR equipment.

The radiation characteristics, i.e. the emitted waveform and the radiated spectrum are shown in Fig. 5.19a and 5.19b, respectively.

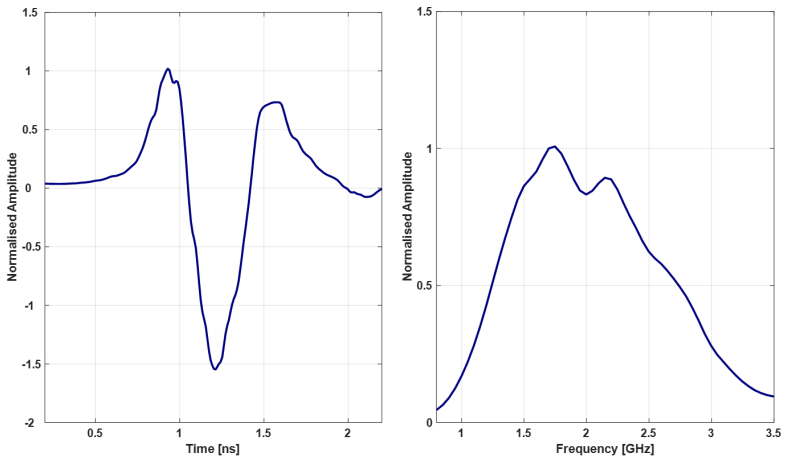

(a) Emitted waveform. **(b)** Emitted spectrum.

Figure 5.19: GPR equipment radiation characteristics.

The sensor head, which is essentially a passive component weighting approximately 2 kg and with a size of 12 by 12 cm, is connected to a central unit (Fig. 5.18b) responsible for the generation, transmission and reception of the signal.

To perform an accurate platform rotation a mechanical turntable was placed below the antenna Fig. 5.20.

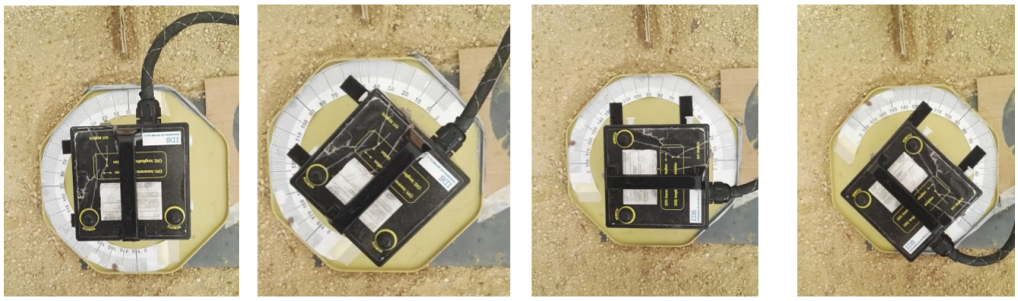

(a) Starting polarisation, HH. **(b)** 45 degrees orientation. **(c)** Orthogonal polarisation, VV. **(d)** 135 degrees orientation.

Figure 5.20: Off the ground measurements details.

The three targets were buried at a depth of approximately 13 cm, which represents the standardised clearance depth for humanitarian demining operations.

Data were collected with the reflection centre of the antenna right in the middle of the target and following the previous strategy: a 180 degrees rotation, with an angular sampling of 5 degrees, and targets buried at two different inclination angles (Fig. 5.22). The experimental setup is detailed in Table 5.4 and Fig. 5.21.

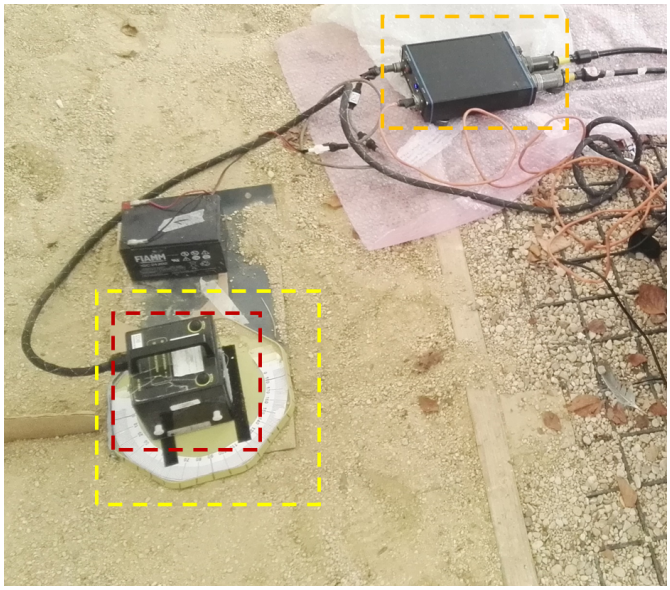

Figure 5.21: Experimental set up with the GPR equipment and the mechanical turntable below the platform.

The processing chain applied to the data consisted of a linear frequency filtering and a spherical exponential compensation gain function, matched to the soil characteristics, to recover the amplitude losses.

Table 5.4: Sand pit acquisition parameters and set up.

Parameter	Value
Frequency range [GHz]	1 - 3
Frequency sampling, $1/\Delta t$ [GHz]	17
Central/Minimum wavelength [cm]	7 / 4.5
Angular range [deg]	0 - 180
Time window, ΔT [ns]	20
Antenna offset [cm]	6

(a) 0 degrees orientation. **(b)** 45 degrees orientation.

Figure 5.22: Sand pit target aspect angles.

The A-scan signature of the PFM-1 landmine is provided in Fig. 5.23. Considering

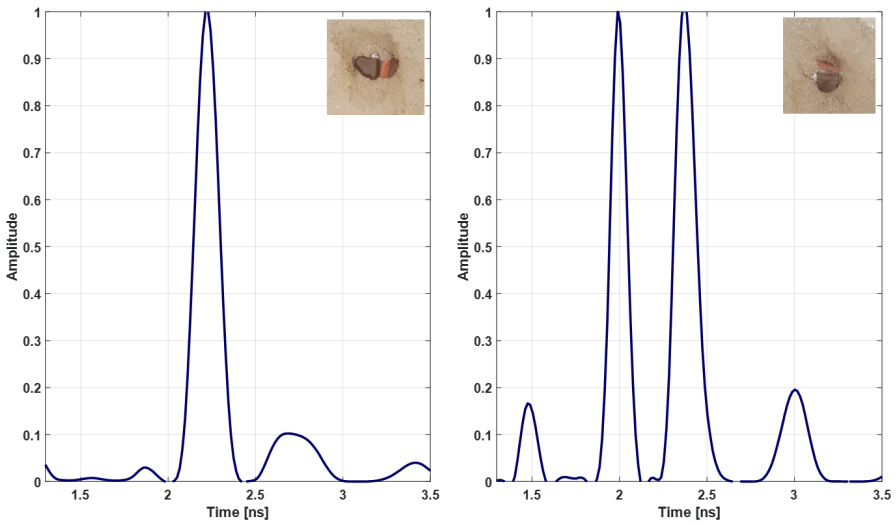

(a) 0 degrees. **(b)** 45 degrees.

Figure 5.23: PFM-1 landmine signature, 1D signature.

the design of the device, the radar signature is dominated by the scattering produced by the cylindrical fuze, represented by the narrow high amplitude peak. The same component is responsible for the reflection recorded when the target is inclined, even if more than a single contribution is visible. These multiple reflections are probably due

to a ringing effect generated by the metallic part of the landmine.

Figure 5.24 shows the collected signature of the SB-33 landmine. In this case, a

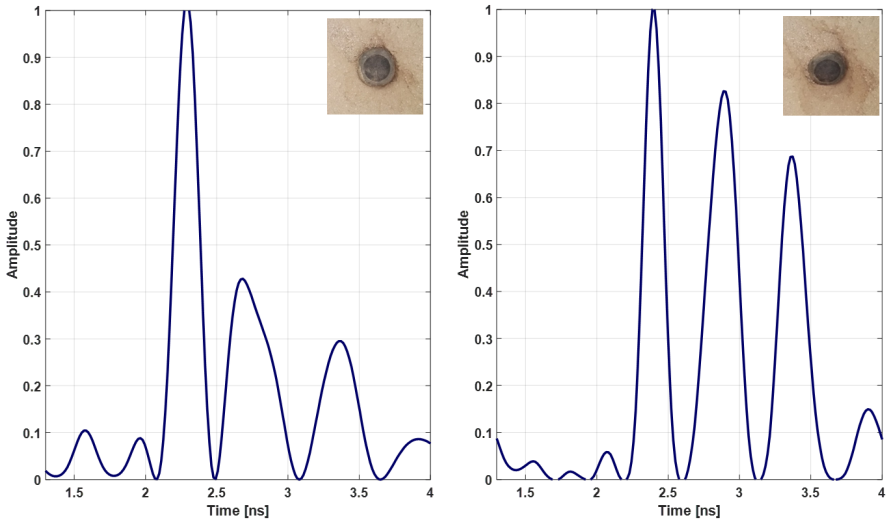

(a) 0 degrees. **(b)** 45 degrees.

Figure 5.24: SB-33 landmine signature, 1D signature.

very close correspondence with the free space results has been achieved, for both the inclination angles. Despite the propagation through a lossy material, the effects of the inner design of the target is recognisable as an additional reflection occurring after the first peak, though its relative amplitude is significantly lower (especially compared to the results in Fig. 5.11). The higher amplitude of the internal reflections of Fig. 5.24b is due to the higher contrast with the air gap inside the landmine.

Finally, results from the VS-50 investigation are shown in Fig. 5.25

A notable close correlation with the laboratory experiments can be highlighted, thanks to the regular design of the landmine, especially for the inclined configuration in which case, consistently with what has been individuated in Fig. 5.12b, the effect of the air layer vanishes.

As before, the validity of the feature has been addressed through a set of polarimetric measurements. The PFM-1 landmine results, depending on the antenna orientation and aspect angle are shown in Fig. 5.26.

As expected, due to the soil absorption the signature presents lower information content than the free space equivalent (Fig. 5.13), but the overall trend is consistent between the two experiments. A single reflection is detectable when the target is placed at an aspect angle of 0 degrees, and the same trend can be highlighted between the two

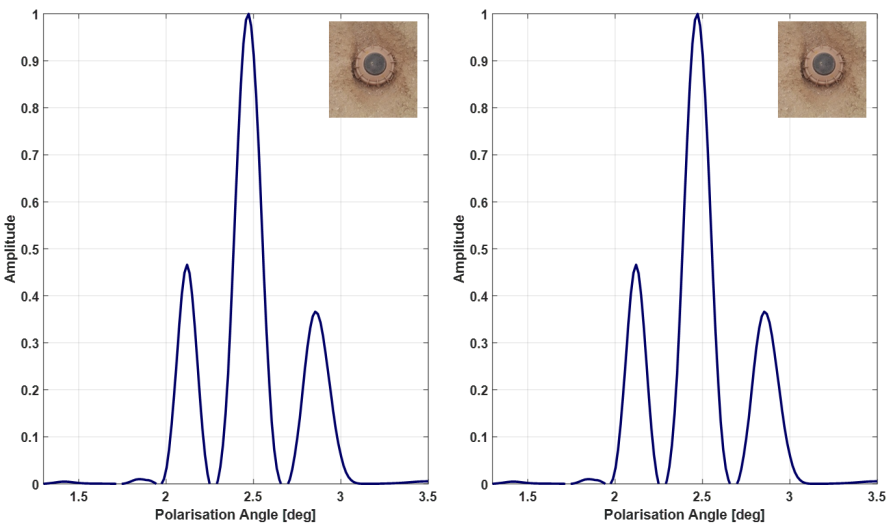

(a) 0 degrees. **(b)** 45 degrees.

Figure 5.25: VS-50 landmine signature, 1D signature.

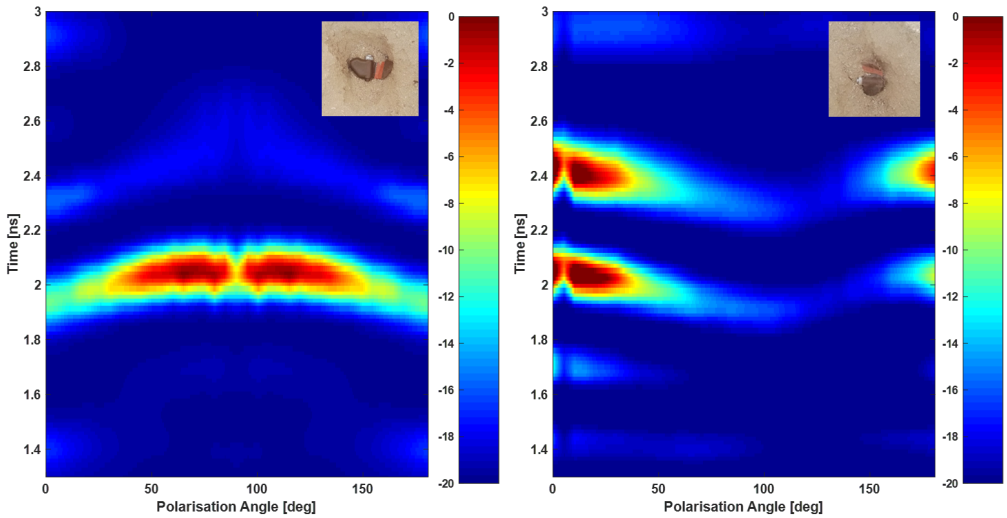

(a) 0 degrees. **(b)** 45 degrees.

Figure 5.26: PFM-1 polarimetric profiles.

trials. In particular, the response of the cylindrical fuze to a change in the antenna orientation follows the polarimetric behaviour of linear metallic targets. The difference from the free space measurements is likely be a consequence of the larger pattern of the dipole antennas, which is dominated by the presence of the metallic assembly. When the target is rotated, Fig. 5.26b, two events can be clearly identified, confirming the hint made from the mono-dimensional data on the ringing effect. This consideration is based on the fact that the two events follow almost exactly the same pattern, which would be unusual in case of two different scattering contributions. A consistent trend with the free space trial can be noticed, as the signature intensity decreases in the range

45 to 90 degrees.

Figure 5.27 describes the results from the analysis of the SB-33 device.

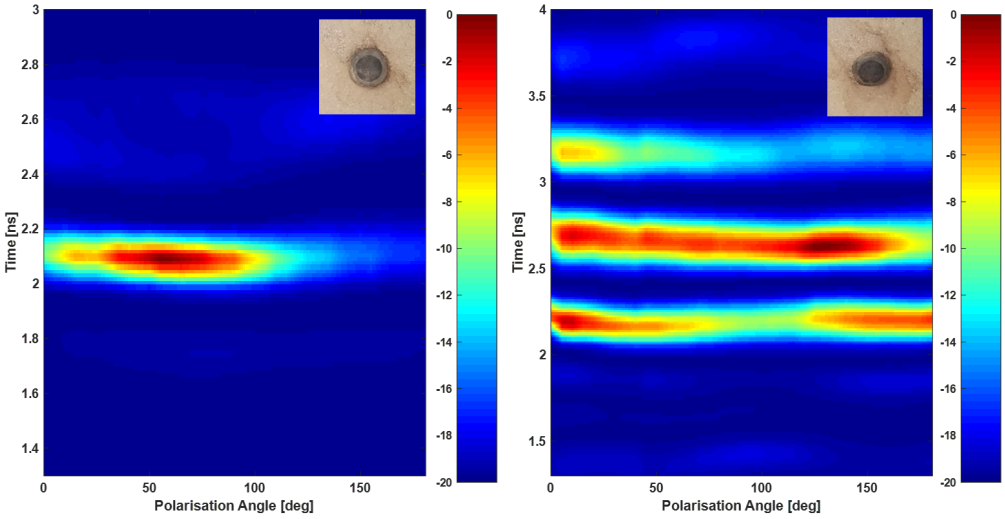

(a) 0 degrees. **(b)** 45 degrees.

Figure 5.27: SB-33 polarimetric profiles.

The same consideration can be outlined for the second device, characterised with a highly heterogeneous and composite design, with some exceptions. A single reflection is visible when the target is oriented at 0 degrees towards the antennas, with nothing related to the internal structure. As evident also in Fig. 5.14a, the bulk of the contribution is located in the 0 to 90 degrees range. A rotation of the target produces a richer response, as three well-defined events have been recorded. These belong to the upper surface, probably to the air gaps inside the landmine or the fuze assemblies (refer to Fig. 5.3 for the structure of the SB-33) and the bottom reflection, respectively. The latter reflection, obviously, has almost half of the magnitude of the other two, with the air interface being the higher and more stable one. These multiple scattering was visible when measuring the target in air (Fig. 5.14b), even if the presence of the internal reflections and a wider pattern complicated the identification of the three events.

Polarimetric profiles of the VS-50 are presented in Fig. 5.28.

The investigated device has an internal design (Fig. 5.2) characterised by the presence of a homogeneous layer of air gaps just below the activator plate: this is clearly identifiable when it is directly below the GPR platform with the stronger reflection in Fig. 5.28a. In an opposite way to the signature of the SB-33, in this case the number of detectable interfaces is higher for an aspect angle of 0 degrees than with for the in-

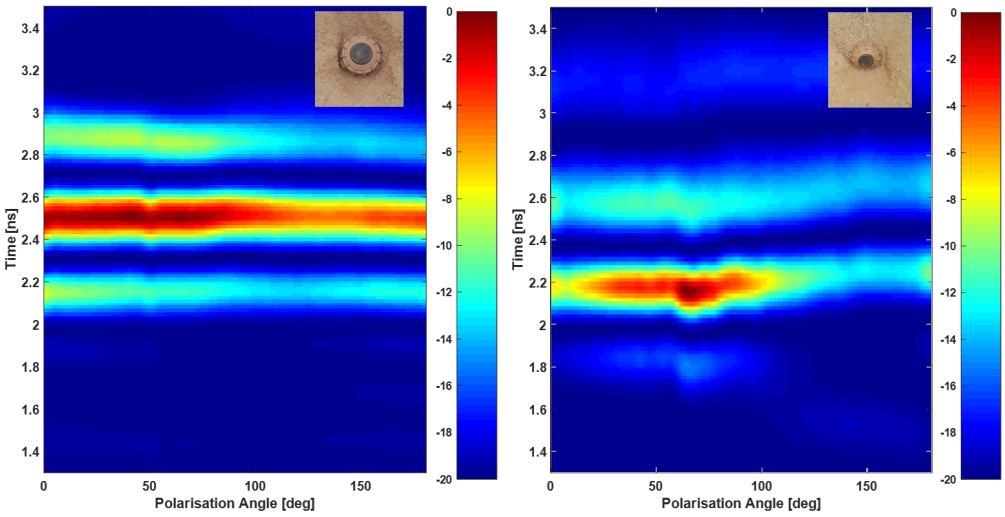

(a) 0 degrees. **(b)** 45 degrees.

Figure 5.28: VS-50 polarimetric profiles.

clined configuration (Fig. 5.28b). This is due to the fact that the air layer is located in the upper part of the target, thus becoming of secondary importance when the target is rotated. The SB-33, instead, has a bulk of air located beneath the target, hence still predominant even when the landmine is inclined.

5.2.3 Comments

The preliminary analysis carried out in this section has demonstrated two main points:

- Scattering phenomena generated by the internal assemblies of the target do have a noticeable effect on the target radar signature, thus demonstrating that the presence of such features can be properly recorded. There is also a consistent behaviour comparing the radar results and the actual design of the landmine.
- Internal components do not behave as the other parts of the mine, thus a change in the illumination pattern orientation is sufficient to highlight these phenomena, providing deeper information on the investigated object.

From a radar detection perspective, the presence of internal assemblies is beneficial as these mines, and zero metal mines in general, contain significant air gaps to allow movement behind the pressure plate. This affects to some degrees their strength and the features of their signature. For this reason, the possibility of detecting internal reflections or scattering from multiple assemblies could represent an important key point for target discrimination.

Effects of aspect angle on reflections distribution have been evaluated and proved

to be a further element to exploit. The results have shown that both the internal structure and the outer design give a varying contribution to the overall response, depending on the geometry relative to the antennas.

The VS-50 landmine, which includes a number of air gaps creating a thin, homogeneous layer in the upper part of the device, is a clear demonstration of the effects of target inclination: these voids are predominant when facing the antennas, while a rotation of the target will cause the layer to play a secondary role and vanishing.

The situation changes when investigating buried targets, as the absorption effects significantly alter the level of details and information gathered by the signature analysis.

A comparable trend was found, as the spatial distribution and location of the main reflections were consistent between the two trials. Differences have been noticed in the density of the reflections for the soil buried targets. While in free space the impact of internal assemblies and structures on the signature was clearly visible and easy to characterise, burying the target into a lossy ground allowed nothing but the strongest reflections to be successfully collected at the surface. Internal reflections are still detectable for the VS-50 and the SB-33, due to the presence of a relatively large air gap inside the structure but only in favourable geometrical conditions.

Finally, the comparison between the numerical simulations and the experimental results shows a close agreement, as shown in Fig. 5.29.

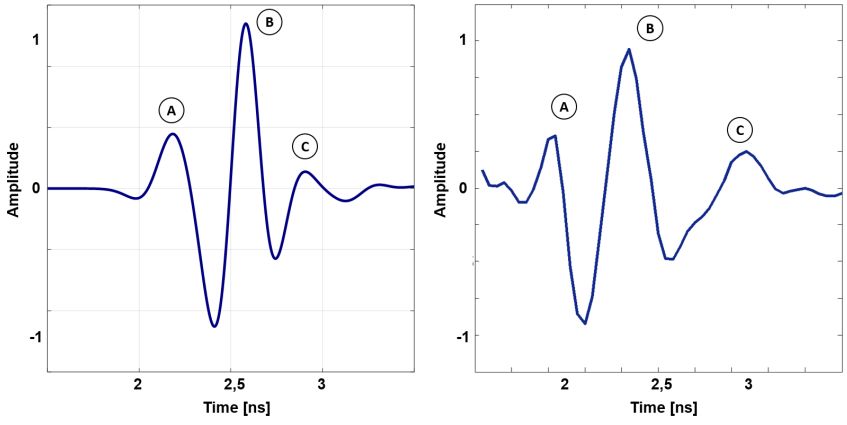

(a) 0 degrees. **(b)** 45 degrees.

Figure 5.29: Comparison of simulation and measurement.

From the two graphs the similarity between the two results is visible, as the temporal occurrence of the reflections and their pattern are highly correlated.

5.3 Evidence of the internal structure: radar profiles

The analysis of the mono-dimensional signatures have shown some deficiency in detecting the internal scattering contributions, in particular for targets presenting an irregular structure, as for the case of the SB-33. Consequently, even if results have proven to be reliable, confidence must be augmented, and the logical option for obtaining a higher information content is to increase the dimensionality of the problem, i.e. exploiting also the spatial dimension.

5.3.1 Trials description

A set of GPR profiles has been acquired in the test pit at the Defence Academy (Fig. 5.17) employing the same GPR equipment, with the three landmines buried at 13 cm and facing the surface and the GPR profile crossing the middle of the target (Fig. 5.30).

Figure 5.30: 2D GPR profiles, acquisition details. Profiles location is indicated with the dotted arrow.

In this case, to guarantee a precise profile collection, a soft pad, the PSG (Pad System for Georadar) was placed below the radar equipment, as shown in Fig. 5.31a. The surface of the pad is designed with parallel tracks that are a few millimetres high, so that the GPR antenna can slide over them ensuring a constant antenna orientation during the whole survey. The same pattern is attached to the bottom of the GPR platform so that it could be easily slotted in the tracks (Fig. 5.31c).

The acquisition is controlled by an odometric wheel directly connected to the sensor, Fig. 5.31b, equally constrained in the pad tracks.

The pad plays the additional role of compensating smooth surface topography in order to maintain the equipment always in contact with the surface. Table 5.5 lists the acquisition parameters.

A pictorial description of the survey is provided in Fig. 5.32.

(a) GPR platform and survey pad.

(b) Odometric wheel.

(c) GPR platform bottom.

Figure 5.31: 2D GPR profiles, acquisition configuration.

Table 5.5: 2D GPR acquisition parameters and set up.

Parameter	Value
Frequency range [GHz]	1 - 3
Frequency sampling, $1/\Delta t$ [GHz]	17
Inline sampling, Δx [cm]	0.4
Time window, ΔT [ns]	20
Profile length [cm]	50
Profile length [samples]	125

Considering the nature of the targets and what has been found characterising their signature, internal reflections are supposed to plainly appear only for the VS-50 landmine, while no evidence for the PFM-1. The SB-33 represents the principal ambiguity, as it has an asymmetric structure and its signature (Fig. 5.24a) does not presents any contribution from its internal design.

GPR profile obtained from the PFM-1 landmine is shown in Fig. 5.33.

As expected, the acquired scan of the target is characterised by a single hyperbola (marked A in Fig. 5.33), confirming what was previously highlighted. In addition, as the responsible of this reflection is the metallic detonator assembly, a ringing event is visible (marked B in Fig. 5.33) as a delayed version of the main contribution, closely resembling its pattern as has been pointed out in the previous section.

Figure 5.34 presents the B-scan results for the VS-50 device.

In this case there is a clear indication of the presence of the internal structure: after the reflection generated by the top of the landmine, marked A Fig. 5.34, the effect of the void ring covering the main body of the landmine is an additional hyperbola with a thicker shape and higher amplitude (marked B in Fig. 5.34). The last event, marked C in Fig. 5.34, is the bottom of the target. For such a design, a single profile is sufficient

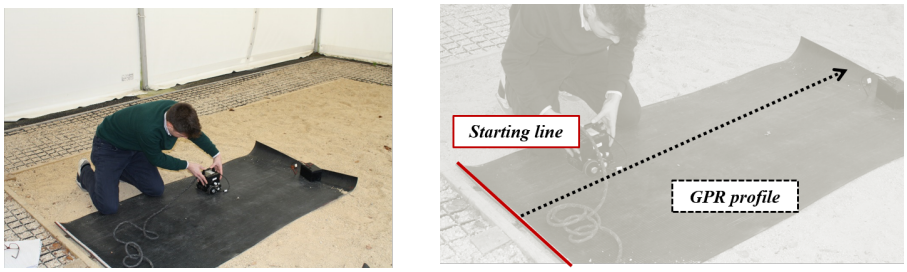

(a) Acquisition photograph. **(b)** Acquisition geometry.

Figure 5.32: 2D GPR profiles, acquisition photographs.

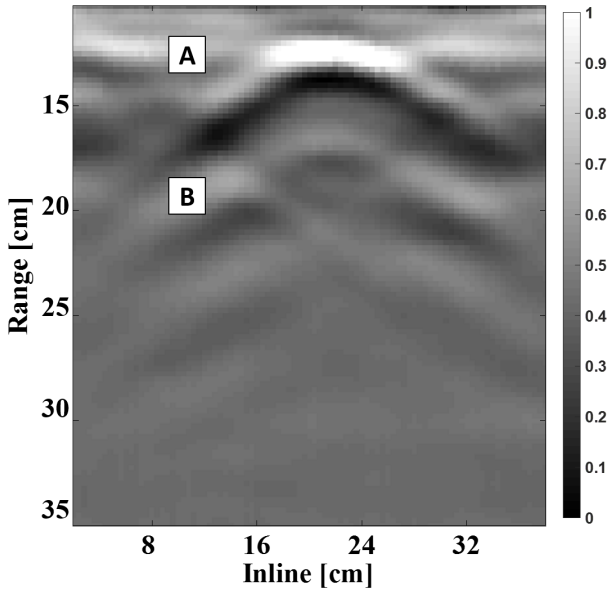

Figure 5.33: 2D GPR profiles, PFM-1 landmine.

for identifying the target and to recognise its internal design.

Finally, the profile acquired over the SB-33 is displayed in Fig. 5.35.

In this case a single reflection event is detectable (marked A in Fig. 5.35) and no hypothesis can be made on the presence of internal assemblies, in contrast to what is the actual design of the device. The non uniform internal design therefore produces a radar results which would provide a misleading basis for identifying the target, as no information on the internal structure is evident. Whilst the outcome validate the results obtained from the signature characterisation previously made, it can be concluded that a single profile is not able to provide reliable performance. Compared to the previous case, the diffraction curve which appears on the radar profile does not present a perfect hyperbolic pattern due to a more flattened shape of the SB-33 landmine.

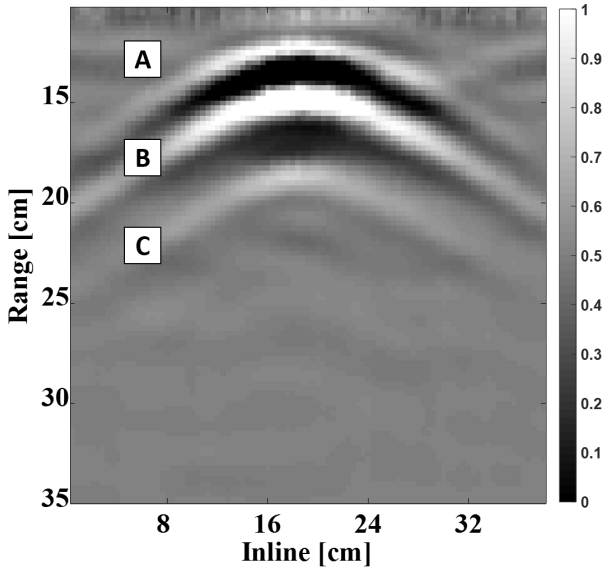

Figure 5.34: 2D GPR profiles, VS-50 landmine.

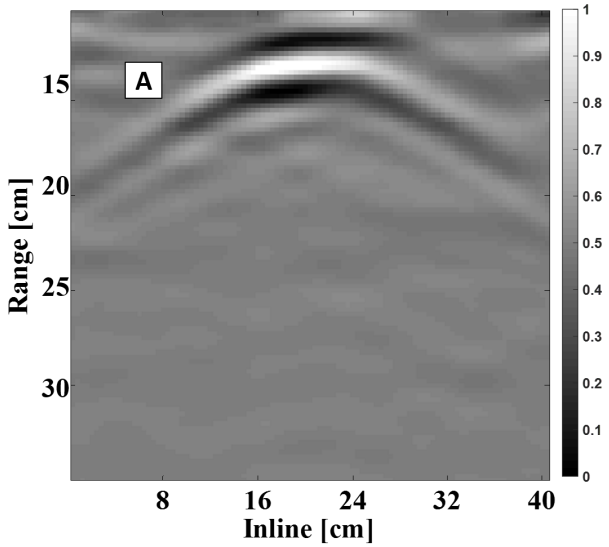

Figure 5.35: 2D GPR profiles, SB-33 landmine.

5.3.2 Validation of results

To confirm the highlighted features and to ensure that the detected additional reflections effectively represent the target internal structure, the VS-50 surrogate shown in Fig. 5.1d was also investigated. As described, the main difference between the two objects is that the surrogate does not include any internal assemblies, while the dielectric properties are closely correlated.

This essentially means that, being the survey scenario equal, any possible disagreements in the GPR results can be associated to a dissimilarity in the internal design

of the device, as the outcomes would otherwise be closely comparable.

The two GPR profiles are presented in Fig. 5.36. The profiles have been normalised by the joint maximum value.

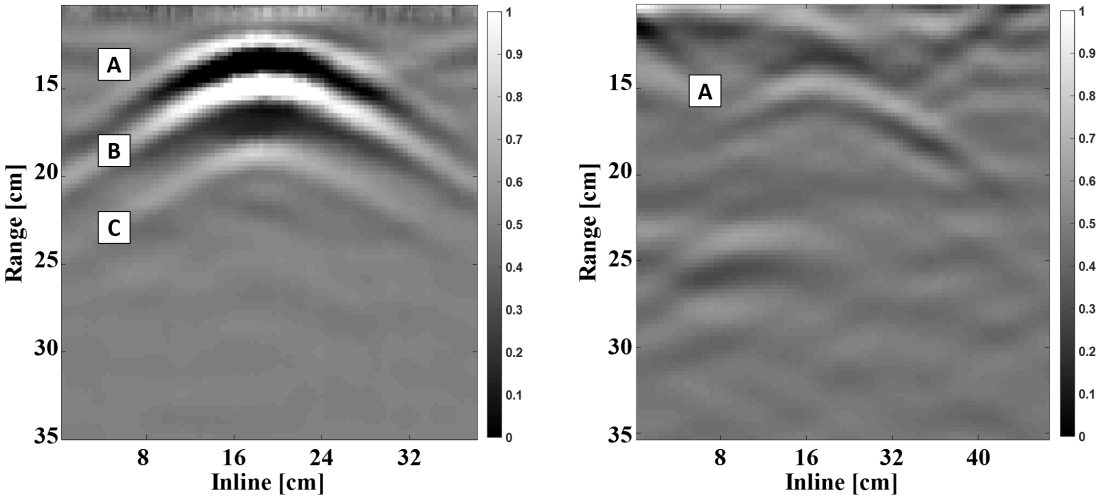

(a) Inert VS-50. **(b)** Surrogate VS-50.

Figure 5.36: 2D GPR profile, target comparison.

First of all, it can be noticed that the magnitude of the response of the inert VS-50 (Fig. 5.36a) is higher than its surrogate. This is due to the neoprene pressure pad which has a dielectric constant of approximately 9, while for the resin the value is roughly 3, producing a stronger impedance contrast. Secondly, and most important, the two results validate the suggested target characterisation, as it is evident the additional reflection generated by the internal air layer, feature which does not appear in the surrogate target (Fig. 5.36b, as expected).

In addition, as one of the critical limitation of the 1D signature is detecting the internal contribution when the target is not horizontally laying, a 2D profile has been acquired changing the inclination angle of the target to assess the robustness of the method. Resulting radargram is shown in Fig. 5.37

It can be seen that it is still possible to recognise the internal structure contribution, clearly with a different pattern and shape. Hence, this restriction can be overcome by increasing the dimensionality of the problem.

5.3.3 Comments

The analysis of the GPR profiles and the latter comparison with the target surrogate have first of all confirmed the hypothesis and suppositions made when characterising

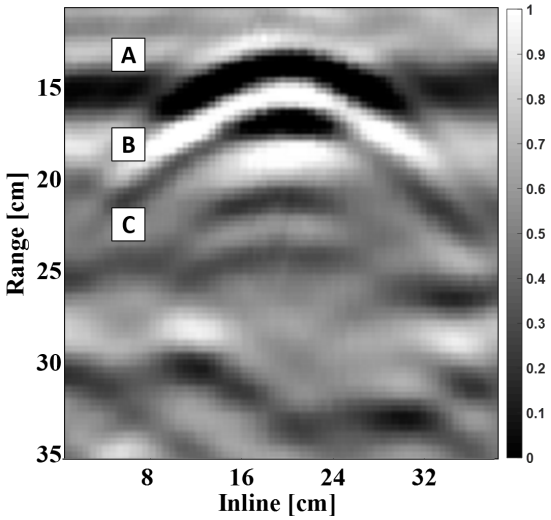

Figure 5.37: 2D GPR profile, inclined VS-50.

the multiple reflections visible in the A-scan signature response: these scattering components are induced by the presence of the air layer inside the target, providing a more readable proof of the suppositions.

Concerning the information content, it may be said that, compared to what can be extracted from the target signature, there is little benefit in acquiring a 2D profile as it still suffers from not producing consistent performance. The case of the SB-33 landmine is explicative: when the internal structure of the target has a non uniform shape, the single profile might not be able to clearly image its scattering contribution.

5.4 Evidence of the internal structure: radar images

Following the outcome of the previous campaign, to mitigate the recognition challenge a properly sampled 3-D dataset is needed, allowing the extraction of advanced physical and geometrical information of the buried target, as well as eliminating ambiguities due to challenging target properties. As a consequence, only the two inert landmines that include a structure, i.e. the SB-33 and the VS-50 have been evaluated, together with the VS-50 surrogate to further validate the results.

5.4.1 Trials descriptions

To ensure a proper data density and regularity, in order to obtain unaliased 3-D subsurface images, acquisitions were carried out once again employing the PSG. As a result of the acquisition set-up (Fig. 5.38a), the collected profiles (Fig. 5.38b) have been

linearly interpolated to create the subsurface volume.

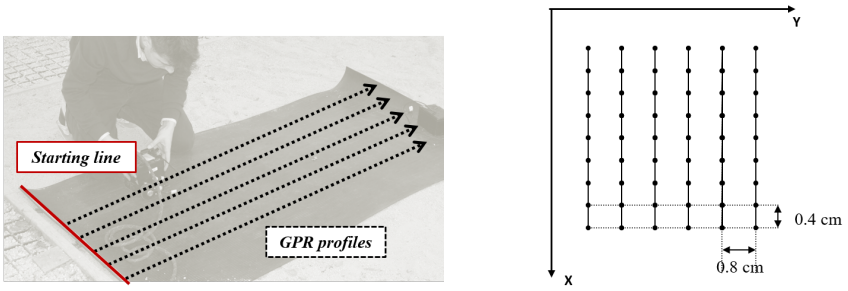

(a) Acquisition photograph. **(b)** Acquisition geometry.

Figure 5.38: 3D GPR, acquisition details.

The two inert landmines and the surrogate were acquired simultaneously, buried at approximately 13 cm and horizontally laying. Acquisition parameters and data details are listed in Table 5.6.

Table 5.6: 3D GPR acquisition parameters and set up.

Parameter	Value
Frequency range [GHz]	1 - 3
Frequency sampling, $1/\Delta t$ [GHz]	17
Inline sampling, Δx [cm]	0.4
Crossline sampling, Δy [cm]	0.8
Time window, ΔT [ns]	20
Acquired area [cm]	80 x 80
Acquired area [samples]	200 x 100

Results are shown in terms of a set of time slices, essentially a series of C-scans of the volume taken at a specified time instant (Fig. 5.39). This allows an easy investigation of the target reflections. Except for a time calibration to correct for jitter effects, a linear filtering operation to remove out-of-band noise and a spatial window, no other processing steps were applied to the data.

The time difference between subsequent slices is approximately 0.05 ns, given the frequency sampling of 17 GHz, which corresponds to a range difference of 0.65 cm. Obviously, this value can be computed only for a propagation in a homogeneous material, otherwise the relationship cannot be verified as the conversion becomes non linear. For this reason, the time indication provided on the presented time slices only represents their temporal occurrence.

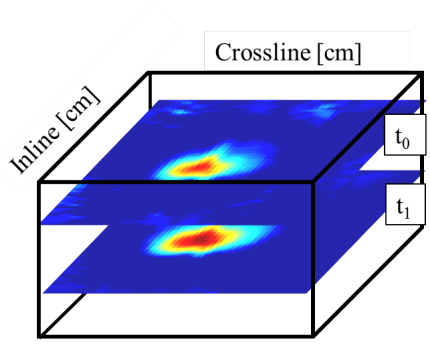

Figure 5.39: Radar time slice extraction.

Amplitude of the slices is displayed in a blue-yellow-red colourmap and normalised by the overall maximum value to the range [0-1].

GPR slices for the inert SB-33 landmine are provided in Fig. 5.40.

From a preliminary analysis, several considerations can be pointed out and, depending on the considered slices, it can be confirmed the capability of GPR of sensing the presence of internal reflections, as the collected frames exhibit different features which may be associated to distinct scattering events. What would have been expected from a solid objects would be a homogeneous pattern, net of absorption effects, and a close agreement between the thickness of the target and the number of slices including the target contributions.

Analysing the slices included within the target boundaries, represented by the first reflection generated by the pressure plate and the bottom of the landmine, Fig. 5.41 shows the selected sections.

If one analyses the two slices within the top (pressure plate contribution, Fig. 5.41a and the bottom (bottom cover contribution, Fig. 5.41d of the target, valuable information can be gathered.

The slice of Fig. 5.41b shows a uniform high reflectivity area centred on the middle of the target, indicating a regular scattering element smaller than the target and located in the centre of it. The hint on the contour of the feature arises from the fact that the maxima of the reflections are concentrated in a single location, with the amplitudes gradually decreasing following the typical hyperbolic behaviour.

Instead, the reflections distribution of Fig. 5.41c identifies a semi-circular shape, possibly generated by a number of scattering events near the outer border of the target. As before, the suggestion of an extended scattering element, rather than a single point

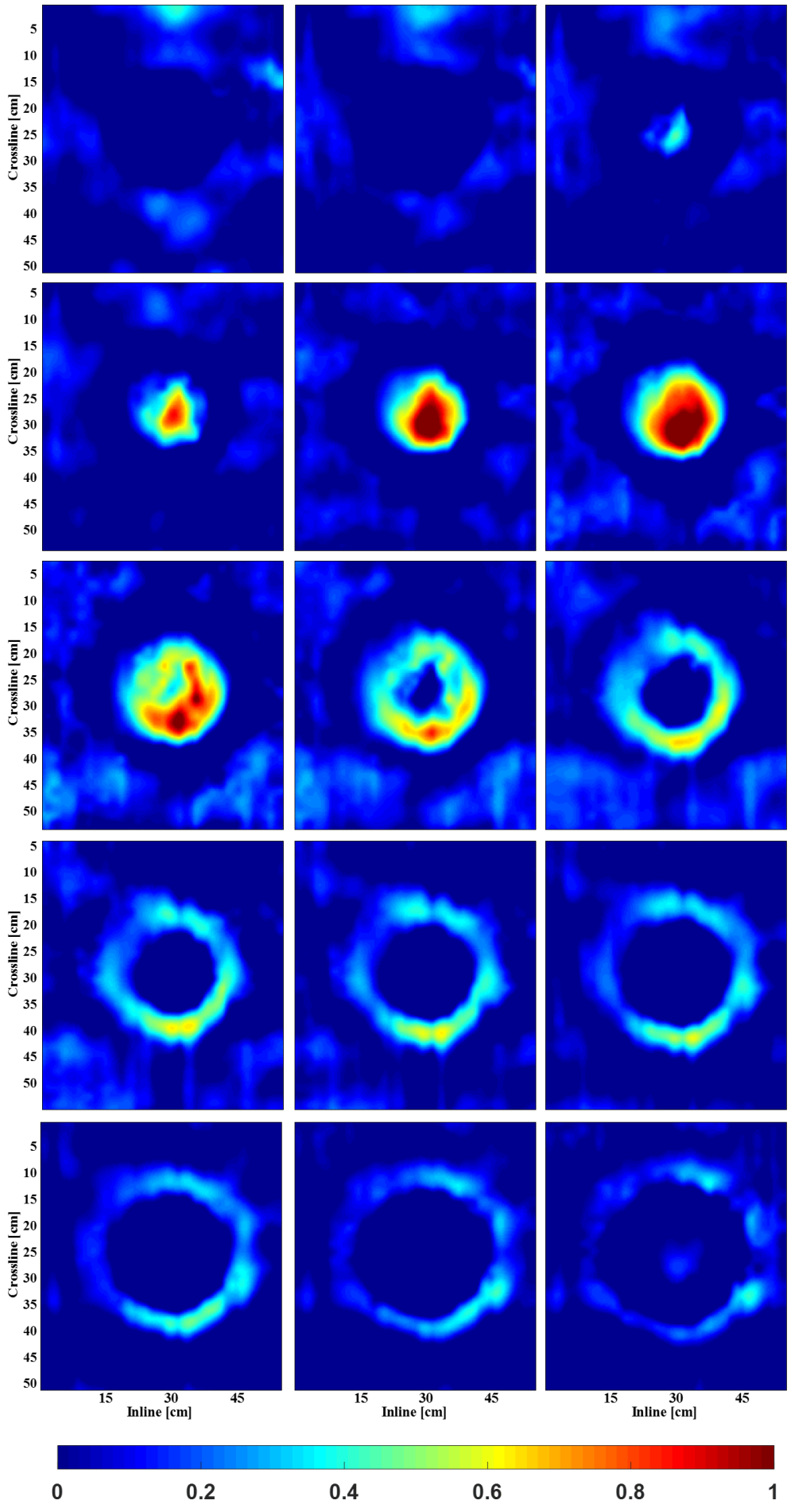

Figure 5.40: Inert SB-33 landmine time slices. Order from left to right, top to bottom.

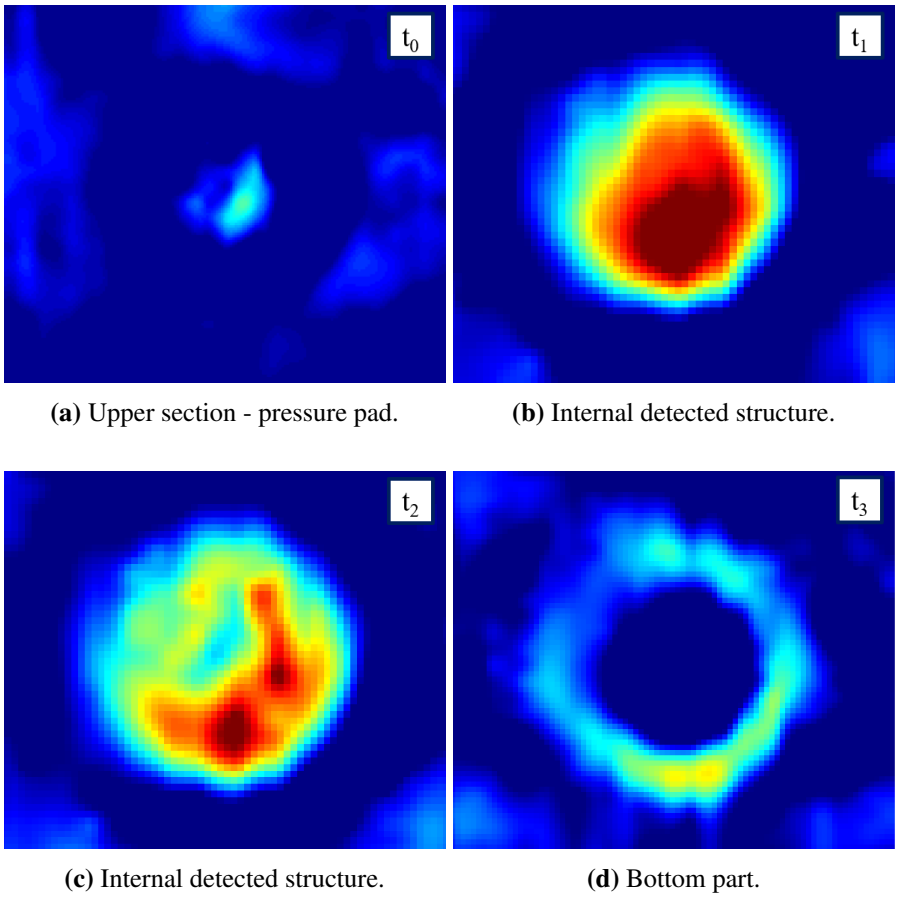

(a) Upper section - pressure pad. **(b)** Internal detected structure.

(c) Internal detected structure. **(d)** Bottom part.

Figure 5.41: Inert SB-33 landmine time slices, internal structure highlight.

scatterer, comes from the analysis of the amplitude pattern.

Essentially, the internal structure of the detected target, as hinted from the raw radar data, can be considered consisting of a central element, possibly regular, and a scattering region embracing it and covering a rounded sector of the landmine. This is consistent with the design of the SB-33 and, recalling the previous results, the fact that this feature is located in a certain area of the target makes the internal structure hard to detect in a single 2D radar profile.

To further validate these comments and to better identify the described features, an overlay of the radar slices and the optical picture of the landmine is shown in Fig. 5.42.

The central scattering feature highlighted in the radar slice is confirmed to be the fuze and striker assembly (Fig. 5.42b), which has a cylindrical shape and contains the entire metal content of the landmine, motivating also the high radar reflectivity. The radar anomaly of Fig. 5.41c fits particularly well with the void quarter of the landmine,

(a) Upper section - pressure pad.

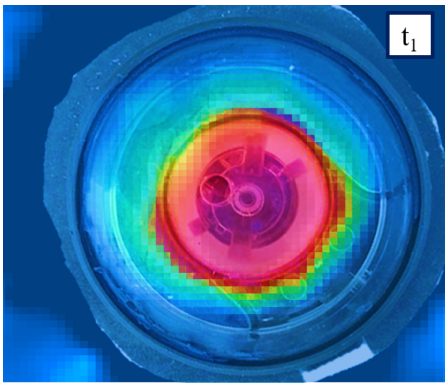

(b) Internal detected structure, fuze and striker.

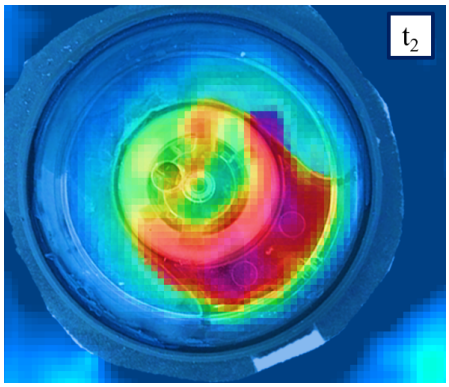

(c) Internal detected structure, void sector.

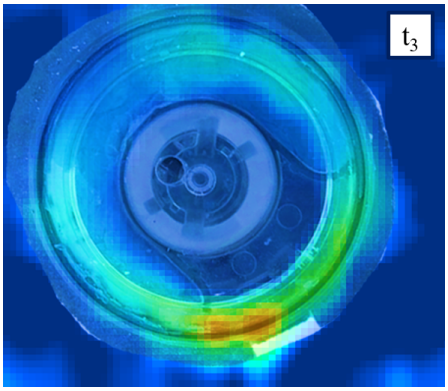

(d) Bottom part.

Figure 5.42: Optical overlay of the radar results, inert SB-33 landmine.

positioned aside of the fuze and encompassing it, both in terms of location and shape (Fig. 5.42c). Finally, the overlay provides also a further correspondence for the circular evidence of Fig. 5.41d, which was initially associated only to the bottom cover of the landmine. Superimposing the two images, one can note that the bolder part represents the detonator capsules, which is essentially a void cylinder (Fig. 5.42d).

Figure 5.43 presents the collected radar slices for the inert VS-50.

In this case, the overall pattern of the slices is different, as (1) the main target contributions are described by a higher number of slices, compared to the SB-33, and (2) the contribution seems to disappear for a couple of slices and then appears again before the end of the target, suggesting the presence of a highly reflective layer occurring after the top of the landmine. As before, Fig. 5.44 presents a highlight of the target slices.

The neoprene activator plate is clearly identifiable with the early reflections (Fig. 5.44a), as well as the bottom of the landmine (Fig. 5.44d) as the last collected reflec-

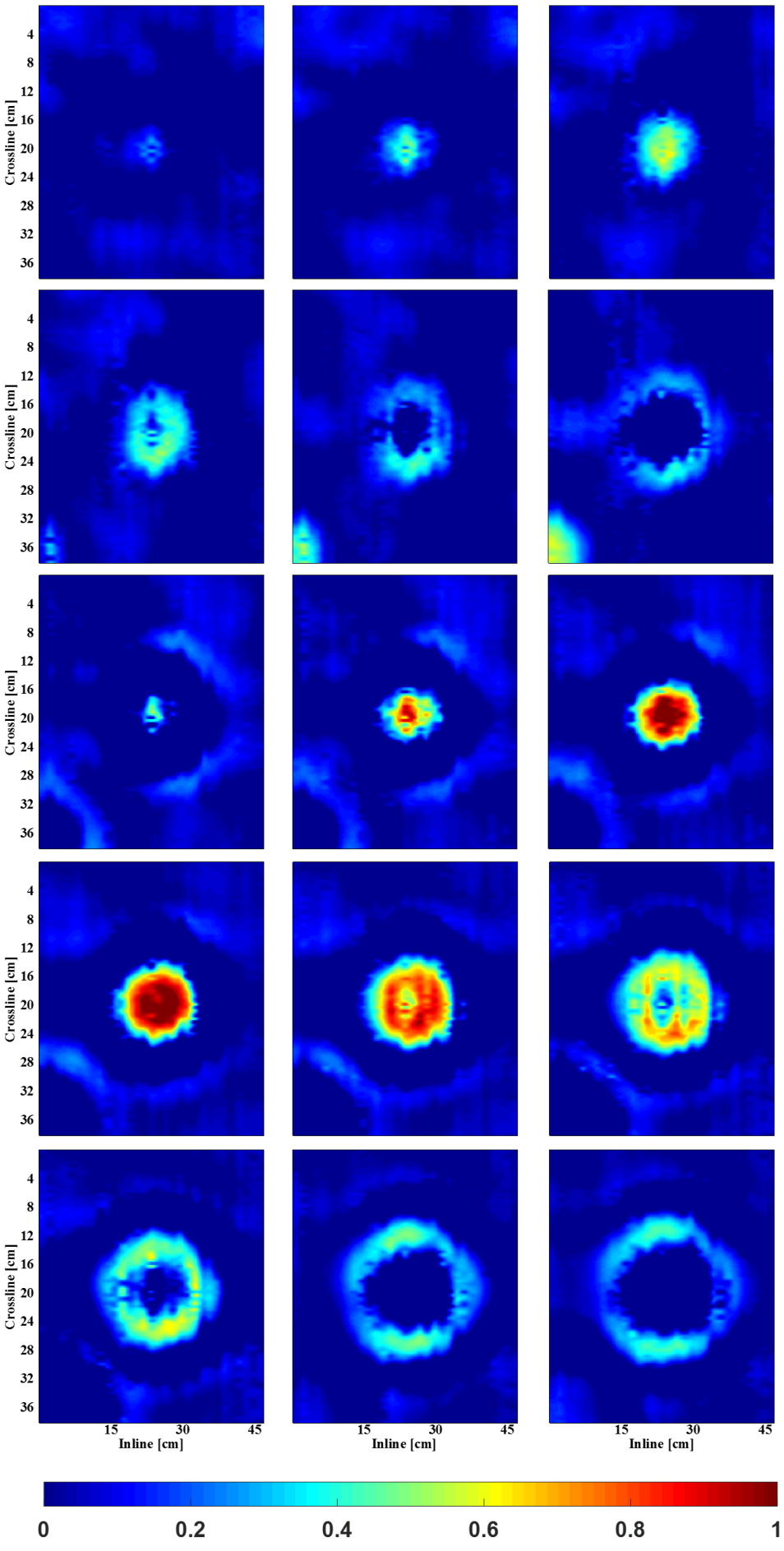

Figure 5.43: Inert VS-50 landmine time slices. Order from left to right, top to bottom.

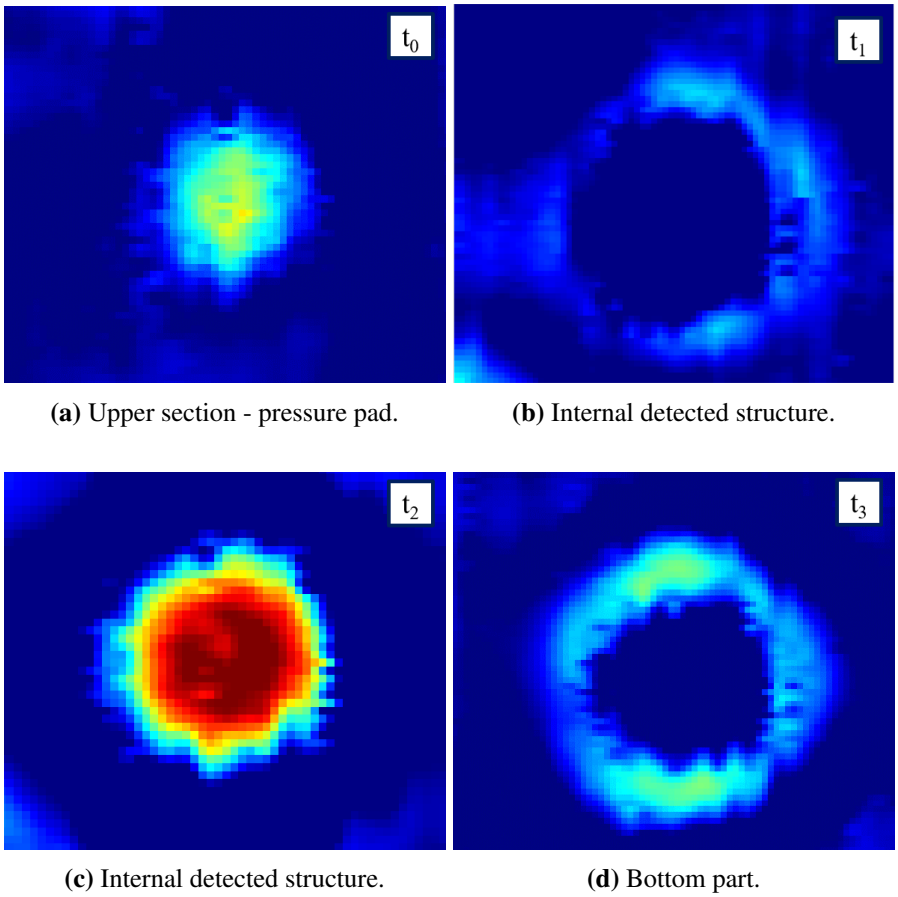

(a) Upper section - pressure pad. **(b)** Internal detected structure.

(c) Internal detected structure. **(d)** Bottom part.

Figure 5.44: Inert VS-50 landmine time slices, internal structure highlight.

tions. Regarding the pressure plate, it can be noticed a significant amplitude difference between Fig. 5.44a and Fig. 5.41a, despite being moulded from the same material: this is due to its higher density and thickness, which also justifies the fact that in this case it can be completely resolved (Fig. 5.44b).

What is worthy of note is the detection of a highly reflective area beneath these boundaries (Fig. 5.44c), with a slightly larger extension compared to the pressure pad contribution. As this layer lies within the target volume, and it has different characteristics (shape and amplitude) compared to the first frame, it can be considered as a contribution generated by the internal structure of the landmine, recalling also the landmine physical structure and what has been found analysing the 2D profile.

This conclusion arises from two main considerations: (1) the amplitude of the reflections is higher than the previous ensemble, suggesting a higher dielectric contrast, and (2) the spatial extension is relatively regular with an amplitudes distribution almost uniform. Both hints are consistent with the air layer below the activation plate,

representing the blast resistant assembly. Obviously, the dimension of each air hole is not sufficiently large for the equipment to be able to individually contour the single contributions.

The effects of the sectioned void ring can be recognised through a comparison with Fig. 5.41c. The two slices both described the effect of an air gap, but if for the SB-33 the pattern is more homogeneous, the slice extracted from the VS-50 shows a more milled pattern. This different appearance can be related to the fact that in the first case there is a single empty area while the latter scattering contribution is generated by a combination of multiple scattering.

The optical overlay is shown in Fig. 5.45.

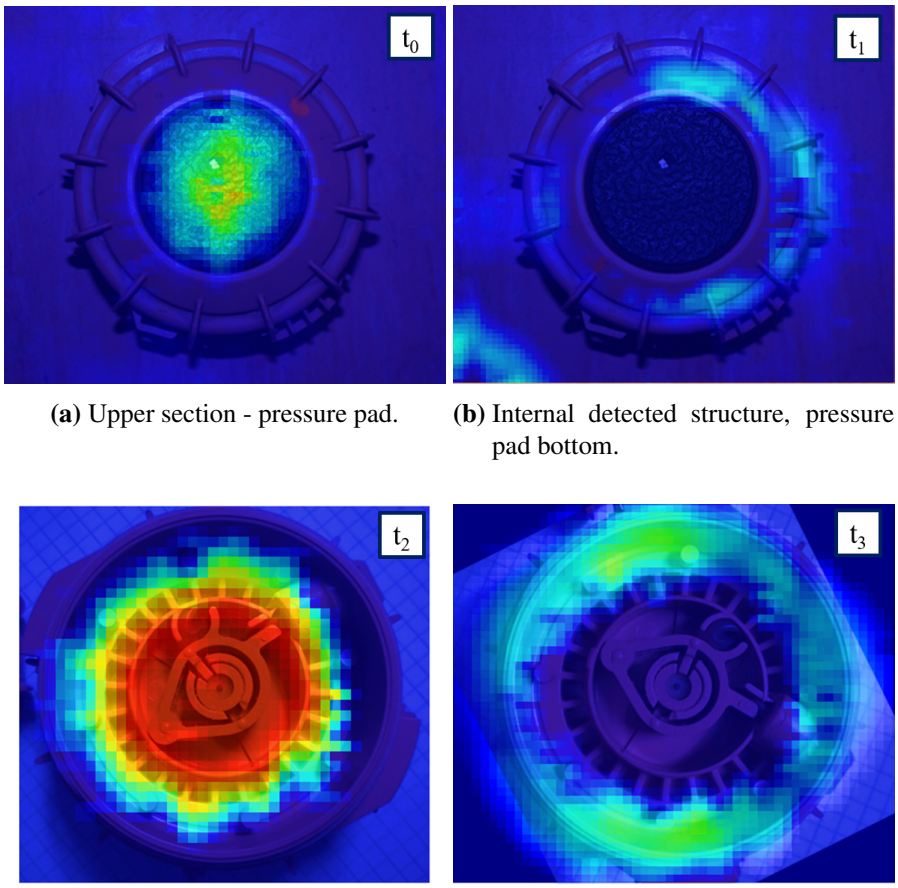

(a) Upper section - pressure pad.

(b) Internal detected structure, pressure pad bottom.

(c) Internal detected structure, void layer.

(d) Bottom part.

Figure 5.45: Optical overlay of the radar results, inert VS-50 landmine.

Thanks to a more regular design, in this case the overlay is clearly more readable and the previous considerations can be easily verified. What can be noted is the correlation between the last frame, Fig. 5.45d, with the outer part of the mine base. It should additionally be noted that there is a precise equivalence between the physical

dimensions of the landmine sections and the extension of the radar reflections.

5.4.2 Validation of results

Following a similar structure, the obtained results have been verified through the comparison with the VS-50 landmine surrogate, shown in Fig. 5.1d. What is expected from the surrogate is an ensemble of radar images in all respects consistent with the real inert objects and characterised by a homogeneous behaviour from slice to slice, with no multiple and/or internal reflections.

In addition, also the absence of the rubber activator plate in the target surrogate might have an impact on its radar response, as modelled in the previous Chapter and pointed out above.

The correspondent slices collected from the VS-50 surrogate are presented in Fig. 5.46.

Coherently with the previous considerations, the target exhibits a homogeneous behaviour throughout its volume, without any evidence of contributions from internal reflections. The comparison validates the hypothesis made on the nature of the reflections of Fig. 5.44c as the only differences between the two employed targets lies in the air layer below the activator plate.

As a figure of merit of the achieved resolution performance, and as a demonstration of the effect of the pressure pad, a correspondence between the inert VS-50 and its surrogate equivalent cannot be found considering the target extension, as the latter appears in a fewer number of slices. This is due to the neoprene pad which is a material with a velocity which is approximately 60% slower than the surrogate resin. Considering a relative dielectric constant of 3 for the epoxy resin of the surrogate, which produces a range difference between slices of approximately 1 cm, and six as the number of slices embracing the target volume, the estimated height is very close to the physical one (5 cm).

Figure 5.47 and Fig. 5.48 show the focus on the target depth slices and the optical overlay, respectively.

A valuable consideration that rises from the comparison between the two targets is that in comparison with an air gap, a small metal inclusion has a very weak effect on the target response. Therefore, the presence of an air gap notably facilitates the detection

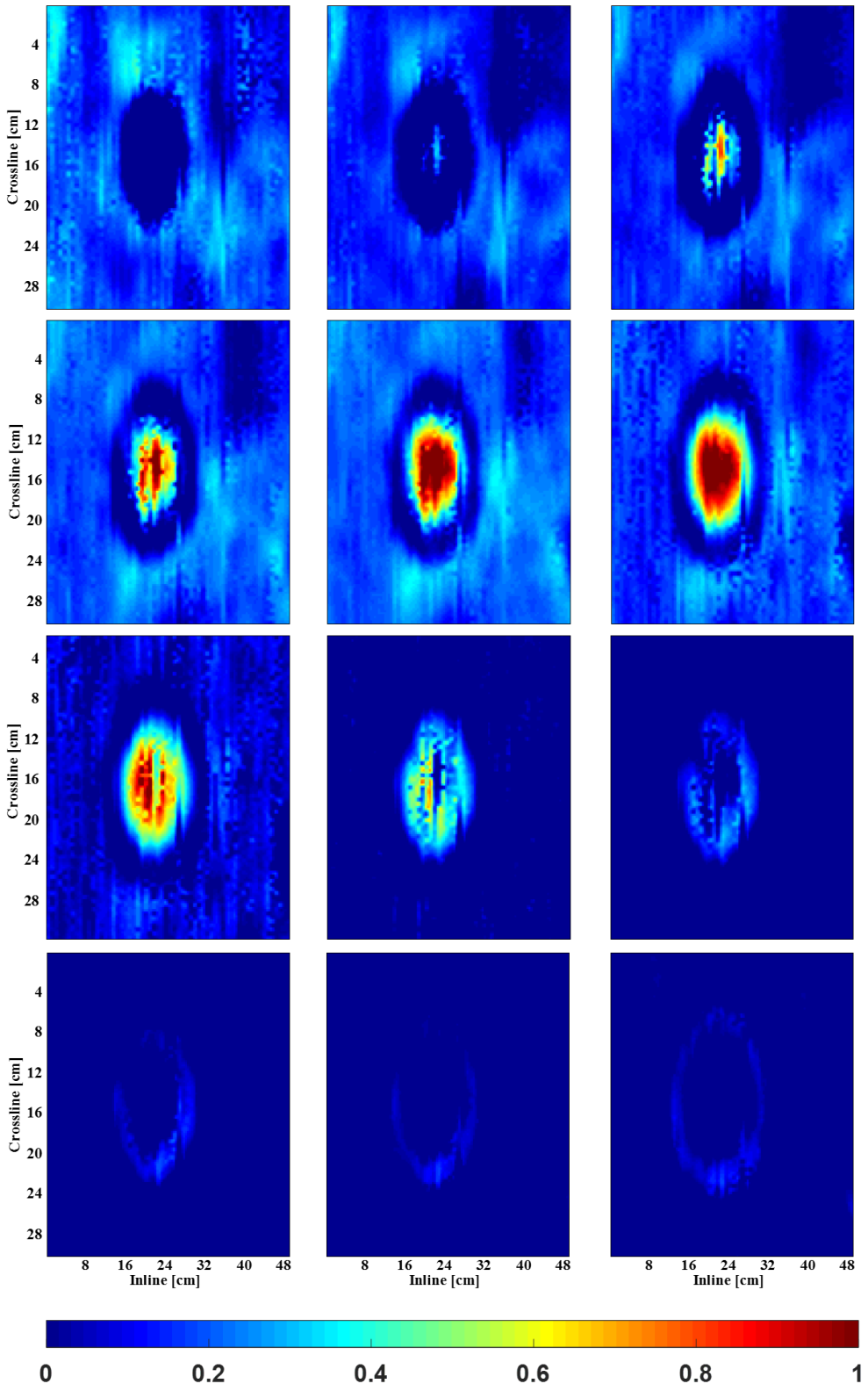

Figure 5.46: Surrogate VS-50 landmine time slices. Order from left to right, top to bottom.

of buried plastic cased landmines with GPR.

Finally, to provide a qualitative comparison among the investigated targets, the

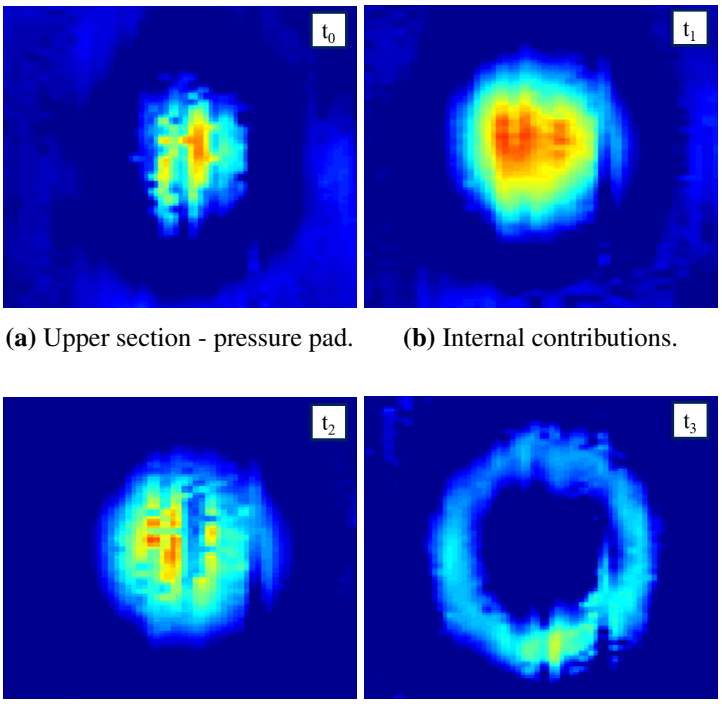

(a) Upper section - pressure pad. **(b)** Internal contributions.

(c) Internal contributions. **(d)** Bottom part.

Figure 5.47: Surrogate VS-50 landmine time slices, internal structure highlight.

ensemble of the characterised GPR depth slices have been arranged in a 3D volume visualisation, Fig. 5.49.

5.4.3 Constraints on GPR imaging

The quality of the produced images comes at the price of acquiring very dense and regular data. Even if it may be expected that the structure of the VS-50 could still be imaged also from degraded data, this will be definitely untrue for the SB-33.

The need for autonomous devices with higher mobility is a continuous research topic for GPR applied to landmine detection. However, to obtain a clear and readable image, a 3-D GPR acquisition should be carried out, meaning that precise and fine spatial samplings are needed. This logically affects the positioning devices, as it has to operate synchronously with the GPR and its accuracy should be definitely less than the GPR sample spacing.

Strictly theoretically, there is a bound beyond which the acquired data will be corrupted and aliased, making the acquisition ineffective. As described in the first Chapter, data gathered with an inline and crossline distance of $\lambda/4$ provide the maximum available information level. When the spacing of acquisition points is greater

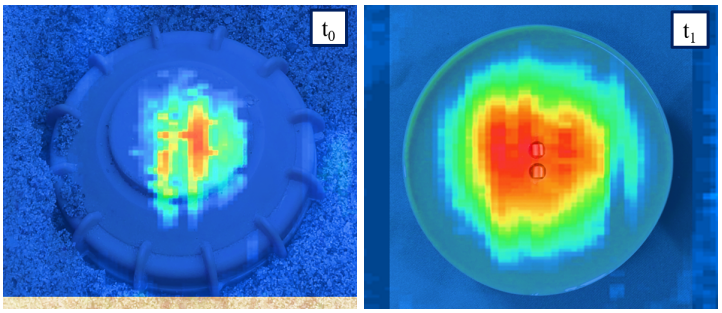

(a) Upper section - pressure pad. **(b)** Internal contributions.

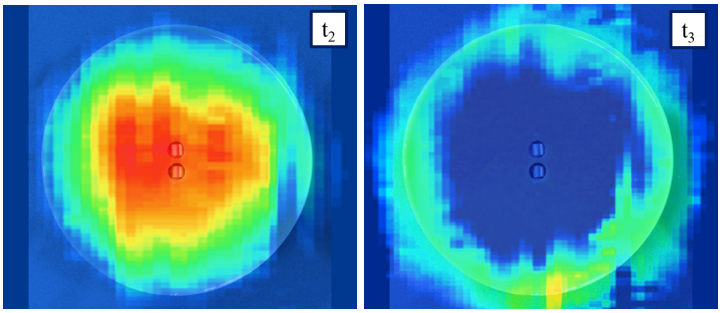

(c) Internal contributions. **(d)** Bottom part.

Figure 5.48: Optical overlay of the radar results, surrogate VS-50 landmine.

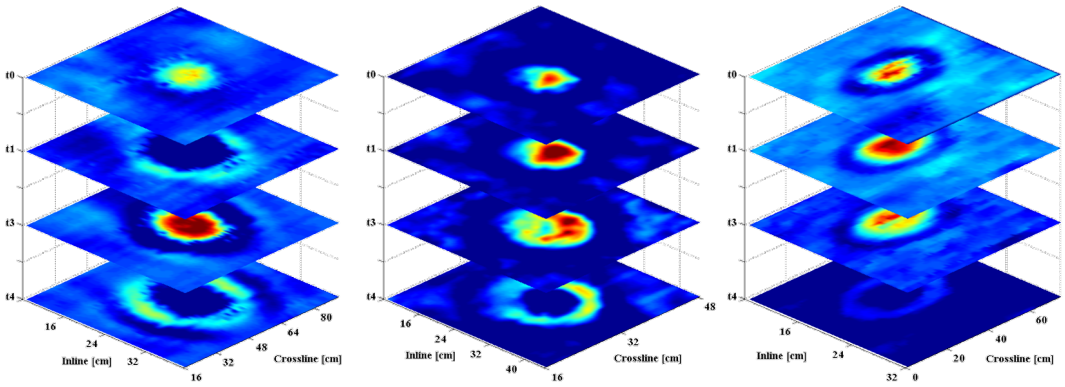

(a) Inert VS-50. **(b)** Inert SB-33. **(c)** Surrogate VS-50.

Figure 5.49: 3D visualisation of the radar depth slices.

than the Nyquist interval, one can expect a distortion of the quality and an increase in the number of artefacts in the final image. In particular, data will not adequately define diffraction tails or steeply inclined reflectors. If one includes also the fact that the volume should be acquired with a very high accuracy, it will be easy to understand why the 3D GPR technology is still far from being widespread.

The quarter-wavelength criterion represents the most restrictive requirement, corresponding to the most unfavourable situation when a very shallow target is struck laterally by a surface wave. In such a hypothesis, the signature of the target is repre-

sented by two steep lines departing from the location of the target, the inclination being inversely proportional to the medium velocity. Instead, when the object is buried it will appear as a diffraction hyperbola (Fig. 5.50).

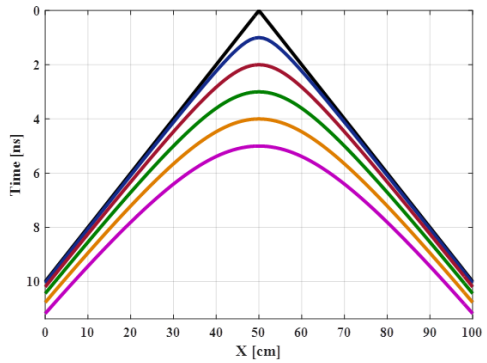

Figure 5.50: Diffraction curves expected on a radar profile.

The following experiments have been performed in order to quantify the level of data sparsity that allows a proper target reconstruction. The dataset employed was acquired at the former Multi-Sensor Mine-Signature (MsMs, Fig. 5.51a) test site, located at the European Commission's Joint Research Centre (JRC), Ispra, Italy. The main peculiarity of the site was that for each material plot, an ensemble of targets were buried at different depths. The investigated target was a large anti-personnel landmine (diameter of 11 cm) surrogate and the burial depth of the selected target was 5 cm and 15 cm. The target, visible in Fig. 5.51b, is designed to resemble mines in respect of their signatures and is moulded in silicone rubber. A low loss loamy material, with a relative dielectric $\varepsilon = 4$ and a resulting velocity of 15 cm/ns has been investigated.

(a) Test lane. **(b)** Investigated target, blue circled.

Figure 5.51: JRC test site details.

A 3D volume was collected using a shielded 1-GHz RAMAC/GPR equipment,

manufactured by Mala Geoscience, and employing the pad system previously described (Fig. 5.52a). The antenna consists of two bow-tie dipoles oriented perpendicular to the survey direction and separated 9 cm. Details on the acquired data and the acquisition parameters are provided in Table 5.7.

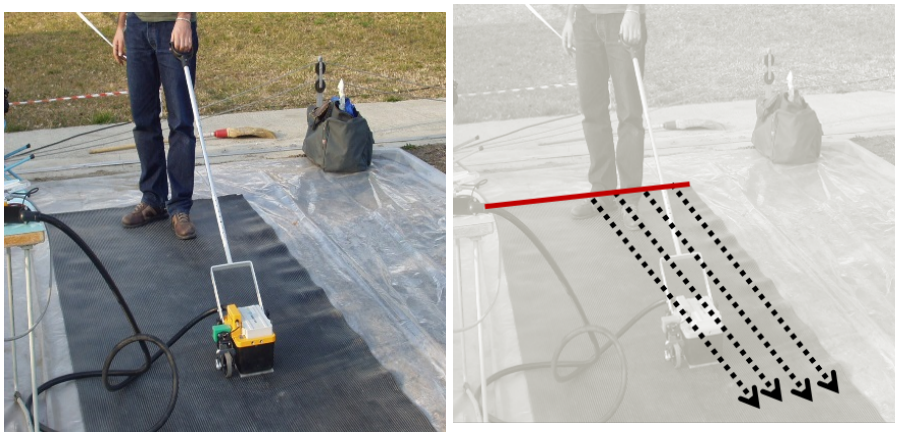

(a) Acquisition photograph. **(b)** Acquisition geometry.

Figure 5.52: JRC acquisition details.

Table 5.7: Data sparsity acquisition parameters and set up.

Parameter	Value
Frequency range [GHz]	0.5 - 1.5
Frequency sampling, $1/\Delta t$ [GHz]	11
Central wavelength [cm]	15
Inline sampling, Δx [cm]	0.8
Crossline sampling, Δy [cm]	0.8
Time window, ΔT [ns]	15
Antenna offset [cm]	9

Considering a maximum frequency of 1.5 GHz, the dielectric properties of the soil gives a quarter wavelength criterion equal to 2.5 cm.

Initially the data were collected with very dense spatial sampling, then they were progressively decimated by the same factor in the inline and crossline directions to obtain the minimum acceptable data density to preserve the features of the target. As the aim of the campaign was to investigate the maximum allowable sample distance to preserve a proper geometrical reconstruction, the processing chain included also a data migration step, performed via hyperbola focusing. A sketch of the methodology is provided in Fig. 5.53.

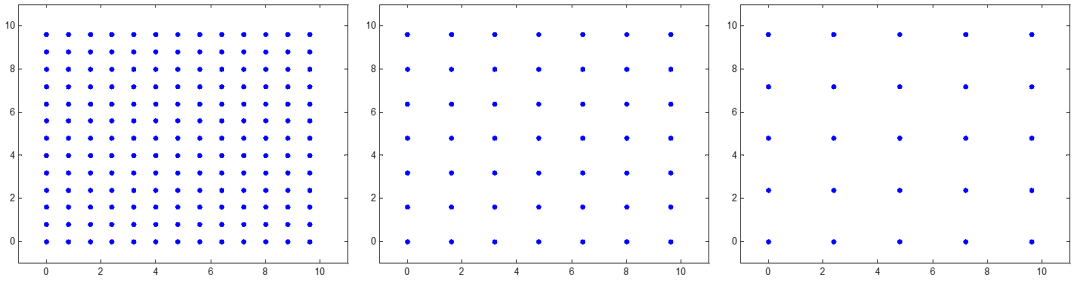

(a) Full grid. **(b)** Decimation factor 2. **(c)** Decimation factor 3.

Figure 5.53: Data sparsity analysis: grid decimation example.

Also in this case, results are shown through depth slices. Collected scans for the landmine buried at 5 cm are shown in Fig. 5.54.

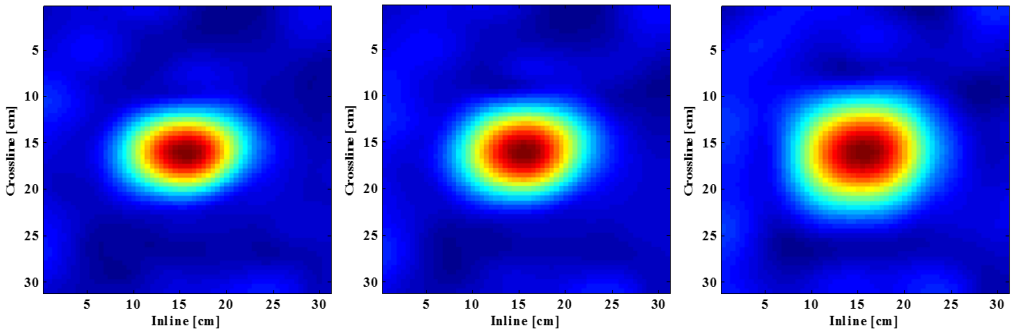

(a) Grid spacing: 1.6 cm. **(b)** Grid spacing: 3.2 cm. **(c)** Grid spacing: 4.8 cm.

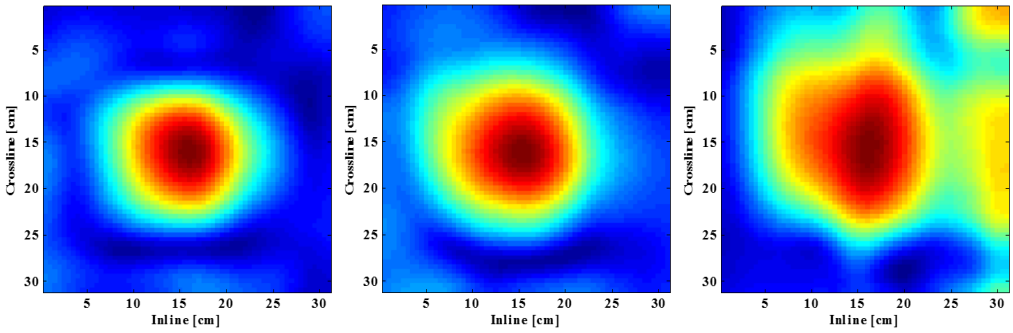

(d) Grid spacing: 6.4 cm. **(e)** Grid spacing: 8 cm. **(f)** Grid spacing: 12 cm.

Figure 5.54: Decimation results, landmines at 5 cm.

As expected, the necessary sampling rate to ensure a proper target reconstruction is sparser than the commonly adopted quarter wavelength. The distance between subsequent samples can be relaxed of an approximate percentage of 20%, Fig. 5.54b.

Due to frequency dispersion effects of the medium that cause a downshift of the central frequency, the target is still detectable even beyond the defined limit, but the degradation of the resolution is evident. In addition, one should consider also a further

quality decay produced by noise and soil effects, which in this case are both negligible. From Fig. 5.54c onward, a change in the geometrical reconstruction of the target shape can be noticed.

Applying the same methodology to a deeper target, buried at 15 cm, the difference between the Nyquist criterion and the actual grid spacing increases (Fig. 5.55).

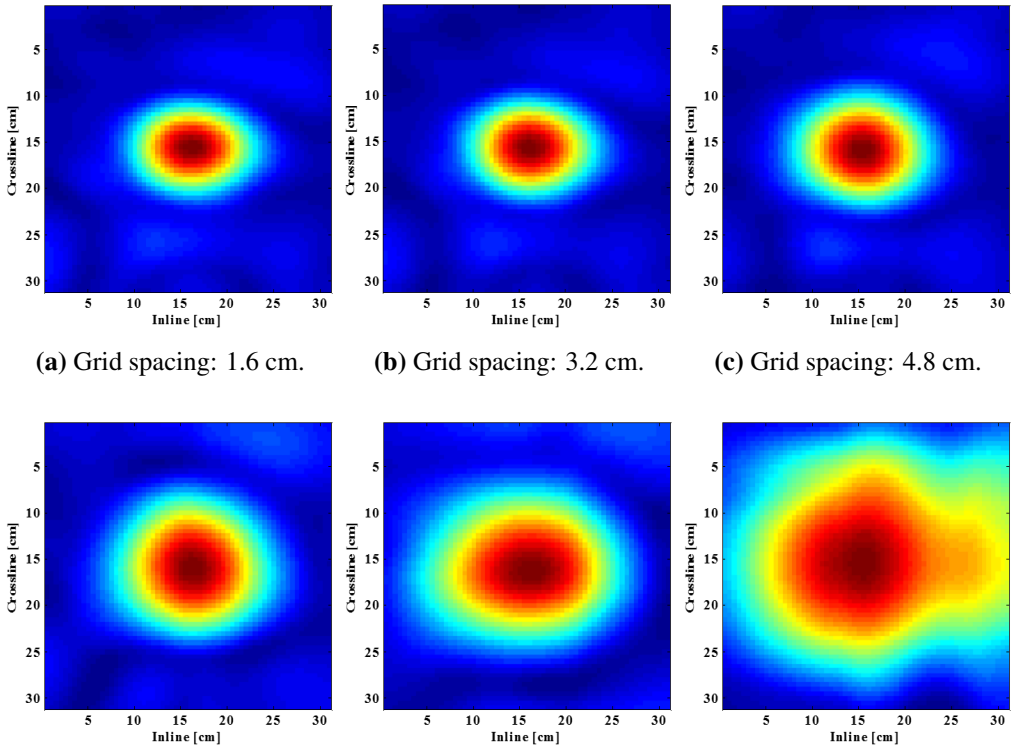

(a) Grid spacing: 1.6 cm. **(b)** Grid spacing: 3.2 cm. **(c)** Grid spacing: 4.8 cm.

(d) Grid spacing: 6.4 cm. **(e)** Grid spacing: 8 cm. **(f)** Grid spacing: 12 cm.

Figure 5.55: Decimation results, landmines at 5 cm.

In this case, the same information content can be obtained with a grid spacing which is almost two times the $\lambda/4$ criterion, Fig. 5.55c. As before, the geometrical focusing is still capable of retrieving the target properties even with a very sparse grid, but the shape is unacceptably corrupted.

Obviously, with no *a priori* information on the buried target, it is reasonable to consider the most restrictive case.

Addressing the second requirement of 3D GPR acquisition, a positioning error was introduced by substituting the acquired linear sample with a neighbouring trace according to a random criterion. As the purpose of the experimentation is to appraise the maximum affordable positioning error, the data were decimated following the outcomes of the density reduction step to obtain the maximum acceptable sample interval

and to create the worst possible scenario.

The synthetic positioning error, introduced on raw data (before the migration process) to effectively simulate a degraded acquisition, was computed by substituting the acquired sample (the nominal one) with an adjacent sample according to a definite but random criterion. The irregular grid has been created by randomly generating for each nominal sample a numeric flag indicating the axis and direction of the sample to replace the existing one. The chosen statistical distribution is a random uniform distribution, with a seed probability of 0.20 for each ill-positioned trace (4 in total) and 0.20 for the nominal sample (Fig. 5.56a). The histogram of the distribution sequence is shown in Fig. 5.56b.

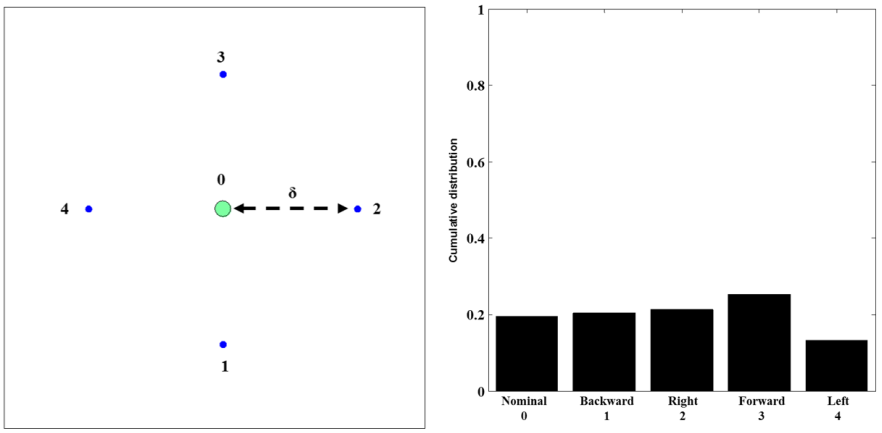

(a) Sample replacement scheme.

(b) Random distribution for traces substitution.

Figure 5.56: Regularity degradation.

It can be seen from the sample distribution that for each nominal sample, there is an equal probability of replacing it with the forward, backward, leftward, and rightward neighbour or maintain the correct one. Such a distribution was chosen to simulate the most unpredictable situation in which: (1) the accuracy degradation is not polarised along a preferential direction and (2) no prediction of the possible spatial distribution of the acquisition error can be made in advance.

The same error distribution was applied considering a different error radius (δ in Fig. 5.56a), which defines the distance with respect to the nominal position of the sample to be substituted, according to the mentioned geometry. Values for the radius are listed in Table 5.8.

A sketch of the resulting irregular grid is shown in Fig. 5.57.

Table 5.8: Data sparsity acquisition parameters and set up.

Target depth	Radius, δ	Distance from the nominal sample
5/15 cm	1	0.8 cm
	2	1.6 cm
	3	2.4 cm
	4	3.2 cm
	5	4 cm

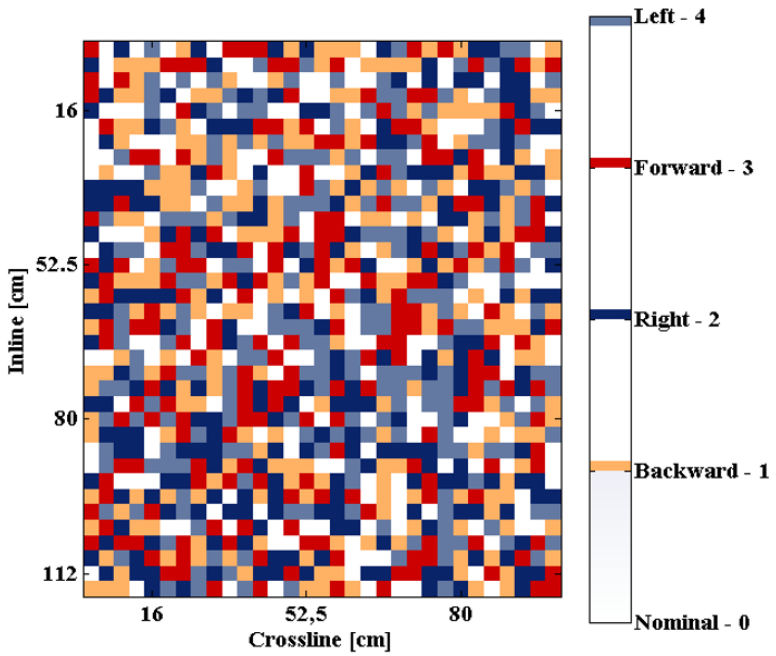

Figure 5.57: Synthetic acquired grid after irregularity superimposition

Processed slices for the landmine buried at 5 cm with varying error radius are presented in Fig. 5.58. Amplitude is displayed in a blue–yellow–red colour map and normalized in the range [0–1] with respect to each relative maximum value.

Considering that the first frame, Fig. 5.58a, is the original regular data, it can be seen that a pronounced degradation of the focusing performance arises from Fig. 5.58c onward, giving a maximum error radius of 1.6 cm. This value corresponds to half of the linear sample distance, suggesting that as long as the trace is included in the boundaries of the same information cell, no loss of information occurs and the reconstruction process is capable of correctly retrieving the spatial information.

Increasing the magnitude of inaccuracy causes processing artefacts faults which reduce the image quality. Obviously, the target is still detectable, thanks to the homogeneity of the host material, but the noise level could decrease the confidence in the

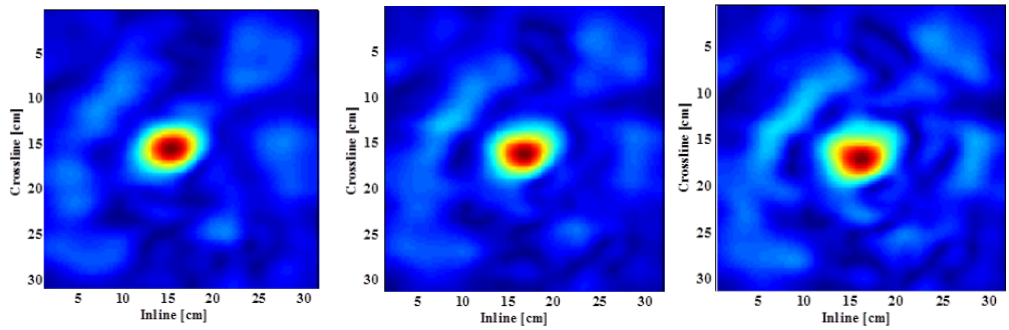

(a) Error radius δ: 0 cm. **(b)** Error radius δ: 0.8 cm. **(c)** Error radius δ: 1.6 cm.

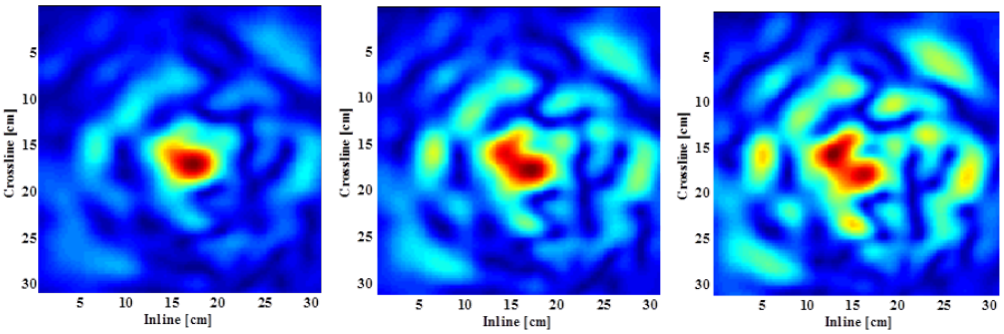

(d) Error radius δ: 2.4 cm. **(e)** Error radius δ: 3.2 cm. **(f)** Error radius δ: 4 cm.

Figure 5.58: Irregularity results, landmines at 5 cm.

recognition process.

Figure 5.59 presents the correspondent results for the deeper target.

In this case, given a maximum sampling distance of 4.8 cm, the radius beyond which the resolution starts to deteriorate is equal to 2.4 cm (Fig. 5.59c), confirming the outcomes found for the shallower target. Following the previous considerations, the target can be identified in each of the slices of Fig. 5.59, even without hints on the presence of a target, but a degradation in the shape of the reconstructed landmine and in the focusing performance is clearly noticeable.

To quantitatively assess the effect of the magnitude of the positioning error, the correlation between the regularly acquired slice and the irregular ones has been computed. The analysis of the images correlation for both the investigated targets is provided in Fig. 5.60.

For the deeper target, given a larger affordable spacing, the ultimate limit of the irregularity corresponds to a radius of 2.4 cm, consistent with the spacing of 4.8 cm of the regular data. This is identifiable as an increase of the inclination of curve after a radius of 3. The same applies to the shallower target, for which the limit is definitely

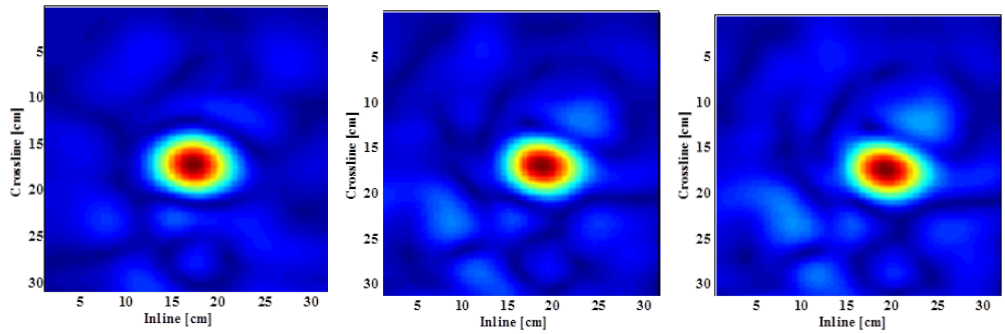

(a) Error radius δ: 0 cm. **(b)** Error radius δ: 1.6 cm. **(c)** Error radius δ: 2.4 cm.

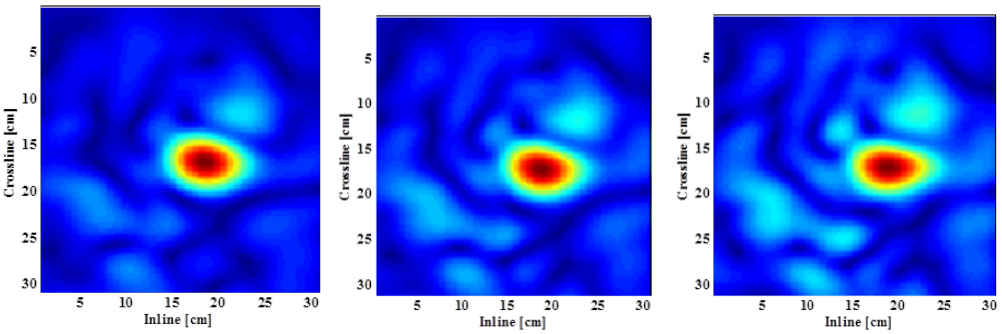

(d) Error radius δ: 3.2 cm. **(e)** Error radius δ: 4 cm. **(f)** Error radius δ: 8 cm.

Figure 5.59: Irregularity results, landmines at 15 cm.

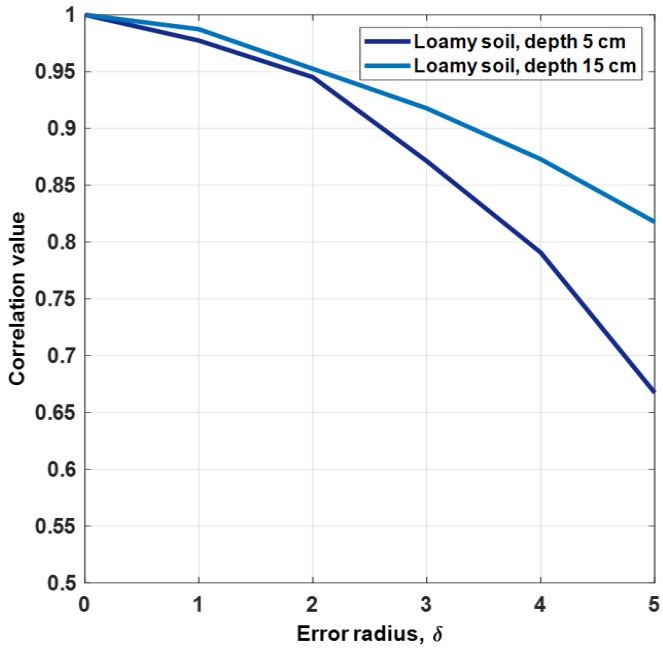

Figure 5.60: Irregularity results, image correlation analysis.

more evident. No significant losses of accuracy are evident elsewhere.

5.4.4 Comments

The set of extracted slices has allowed a precise and detailed definition of the internal composition of the targets, considering also the absence of data processing. Such a resolution means that the frequency content of the collected data, especially its higher portion, has been preserved, and this performance has been achieved mostly through the employment of a ground coupled GPR system, but also thanks to the low frequency absorption effects of the surrounding material. Obviously, the presence of inhomogeneities, multiple clutter scattering or soil texture variations, will dampen the collected energy and complicate a proper recording of these reflections.

The collected high resolution GPR slices showed that the internal design of the landmine can be properly imaged and characterised, confirming the applicability of the approach. The internal assemblies of the landmines under test were identified with a high degree of confidence, even from raw radar data. In addition, the superimposition of the radar slice to the picture of the unscrewed target provided a very close correspondence between the radar images and the actual structure, both in terms of anomalies location and spatial extension accuracy.

A notable conclusion is that the achieved precision can be a significant value for target recognition algorithm based on image matching. Furthermore, this capability may overcome the need for extensive data collection, as the level of accuracy is such that the correlation can be performed even with sketches and diagrams.

Another valuable consideration stems from the comparison between the inert VS-50 and its surrogate, and it is the evidence that for the detection an air gap has a predominant effect over a small metal inclusion.

However, this quality does not come without a price. Profiles spacing in the order of couple of centimetres maximum are usually adopted to ensure a proper target reconstruction and to avoid artefacts in the subsurface image. Considering that landmine detection and removal is a time-consuming business, and that the survey time is directly related to the data density, a decrease in the number of collected points will result in a shortening of the acquisition time. In addition, another challenging task given a high spatial sampling rate is a consequently high accuracy in linear samples positioning.

These two requirements may run the risk of not being fulfilled in particular situations, as for examples the presence of obstacles or obstructions and an uneven surface

topography.

The evaluation of the maximum affordable grid spacing and sample regularity, both intentionally altered creating a sparse acquisition grid, has shown that, even for small targets such landmines, there is space for reducing amount of data that need to be collected to maintain a suitable level of resolution. The experimental results taken together highlight that the same reconstruction performance that can be obtained with an uneven and coarser sampling grid, lowering the demanding and challenging requirements of samples precision.

5.5 Bistatic characterisation of landmine signature

The results generated by the 3D survey can comprehensibly justify the adoption of such strategy, as the produced images speak for themselves, but in the light of increasing the efficiency of GPR technology, a way to provide the same level of information but reducing the effort for data acquisition should be evaluated.

Easily understandable, the alternative methodology should go through a dimensionality reduction, as otherwise there will be no advantages, considering the clarity of the imaging results. At the same time, it should be as independent as possible to the geometrical variables, such as landmines inclination angle and internal design, as a deviation from a standard set-up could affect the detection performance.

As described in the research scope, a possible strategy that could gather the same level of information is the collection of a set of signatures changing the separation between the transmitter and the receiver, i.e. exploiting the angular domain of the problem.

The following section describes the related experimental campaign carried out to investigate the potential of a bistatic approach for buried target characterisation and identification.

5.5.1 Trials descriptions

A set of bistatic signatures from the three different inert landmines and the target surrogate has been acquired in the test sand pit located at the Defence Academy (Fig. 5.17) following the same arrangement of the previous experimental campaigns.

The GPR equipment employed for the measurements consisted of the IDS Aladdin

radar and an additional IDS THRHF radar, both provided by IDS Georadar srl. The two impulsed devices carry dipole antennas spaced at 6 cm with a central frequency and a bandwidth of 2 GHz and 3 GHz, respectively, pictured in Fig. 5.61. The two antennas were connected to the same central unit to allow a separate and synchronised configuration. The lower frequency equipment was chosen as a receiver to maintain uniformity with the previous campaigns and to take advantage of the finer sensitivity of the higher frequency equipment components.

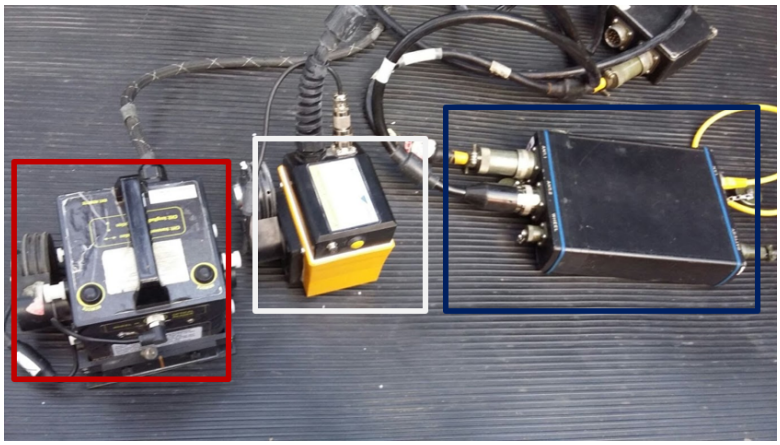

Figure 5.61: Bistatic characterisation, equipment details. From left to right: 2 GHz equipment, 3 GHz equipment and central unit.

To investigate the capability of a bistatic geometry to match the information content produced by a high resolution image, two different schemes have been evaluated, respectively the common receiver (CR) and the common mid point (CMP) scheme. The choice of a common receiver, rather than a common source method was made for convenience only, as the two acquisition strategies are reciprocal. Photographs of the acquisition are provided in Fig. 5.62.

A series of CR profiles were acquired each time moving the receiver toward the target, as sketched in Fig. 5.63b, so that also the CMP signature could be extracted from the data. This was made in order to avoid possible variations in the measurement set-up and consequential loss of consistency among all the results provided in the work. To guarantee precise profile matching and accurate acquisition, the soft pad was placed between the radar equipment and the soil.

Starting with both the equipment located at a distance of approximately 30 cm from the target location, the transmitter was moved at a 0.4 cm step, controlled by the odometric wheel attached to its side, until reaching a sufficient distance to consider

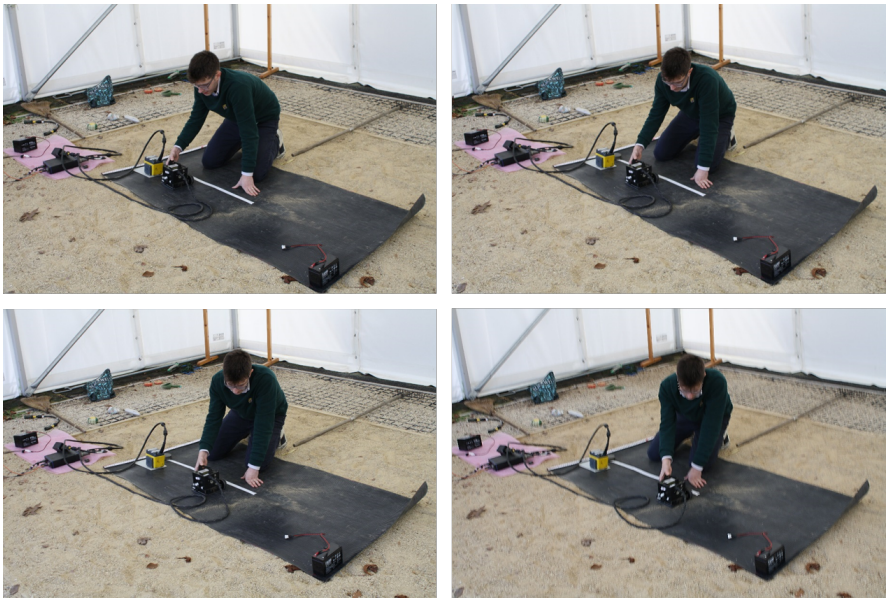

Figure 5.62: Bistatic characterisation, acquisition sequence.

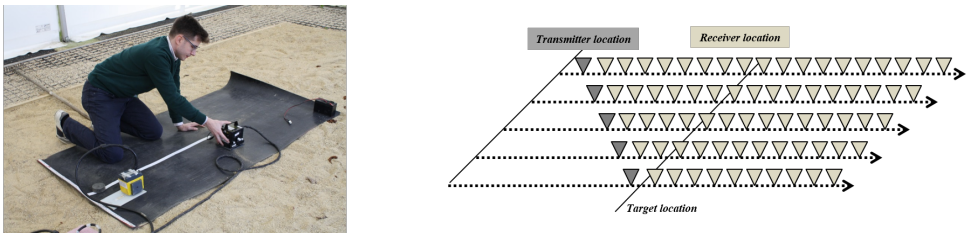

(a) Acquisition photograph. **(b)** Acquisition geometry.

Figure 5.63: Bistatic characterisation, common receiver acquisition scheme.

the target contribution vanished. Then, the receiver was advanced by 1 cm and the scheme was replicated. The last collected profile corresponds to the receiver located exactly over the target. Generally, no significant differences are expected between the two techniques in terms of gathered information, even if some logistical advantages and disadvantages are evident, as described in Chapter 1.

The process of arranging the CMP sounding from a set of CR profiles is illustrated in Fig. 5.64.

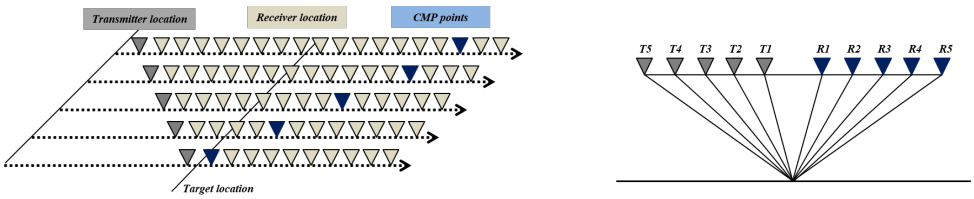

(a) CR acquisition geometry. **(b)** CMP geometry retrieval.

Figure 5.64: Common mid point signature extraction.

Acquisition parameters and data details are summarised in Table 5.9.

Table 5.9: Bistatic acquisition parameters and set up.

Parameter	Value
Frequency range [GHz]	Transmitter: 1-3, Receiver 1.5 - 4.5
Frequency sampling, $1/\Delta t$ [GHz]	17
CR inline sampling, Δx [cm]	0.4
CR profile length [cm]	50
CR profile number	30
CMP offset sampling, Δ_{off} [cm]	1
CMP offset range [cm]	6 - 33
Time window, ΔT [ns]	30

Bistatic signatures of landmines are presented in the commonly employed range versus offset format, which provides a very clear illustration of eventual amplitude variations with offset. In this case, to preserve integrity and to provide a proper comparison, the only processing step computed on the data consisted in the frequency filtering.

The results of the bistatic characterisation of the PFM-1 landmine is provided in Fig. 5.65, for both the described geometries.

The two results show similar content, though some differences, especially in the quality of the output are visible. A single reflection is visible (marked A in Fig. 5.65), with a spatial extension directly linked to the physical dimension of the target, and no further events are detectable. Considering the reflection pattern, the reflection can be attributed to the metallic detonator, confirming what has been found in the signature analysis and expected considering the design of the target. In addition, both results show the ghost replica of the target generated by the earlier strong reflection.

When the illuminated target includes internal assemblies, instead, the antenna separation might better highlight the additional internal scattering feature, as it essentially governs the incident angle of the wave and the vertical position of the reflection plane. The CR profile and the CMP profile of the VS-50 are shown in Fig. 5.66a and Fig. 5.66b, respectively.

In this case, three events are detectable, and these have almost the same spatial extension. While the upper and lower reflections are due to the top and the bottom of the landmine (marked A and C in Fig. 5.66, respectively), the middle one is generated from the internal scattering point. Its constant trend over the separation range means

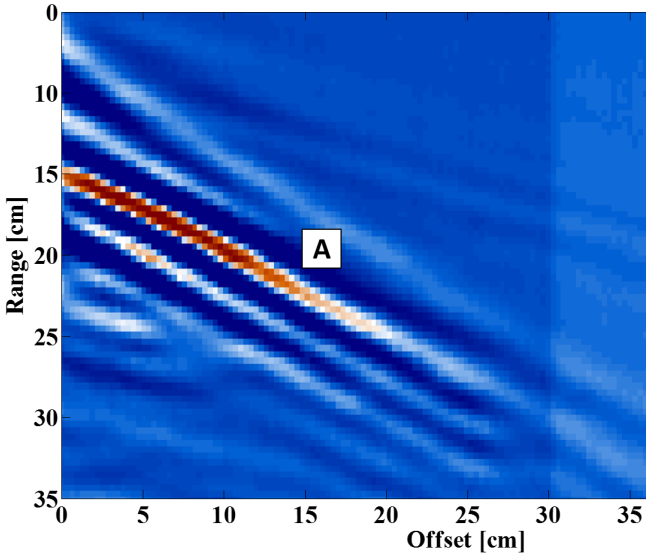

(a) CR profile.

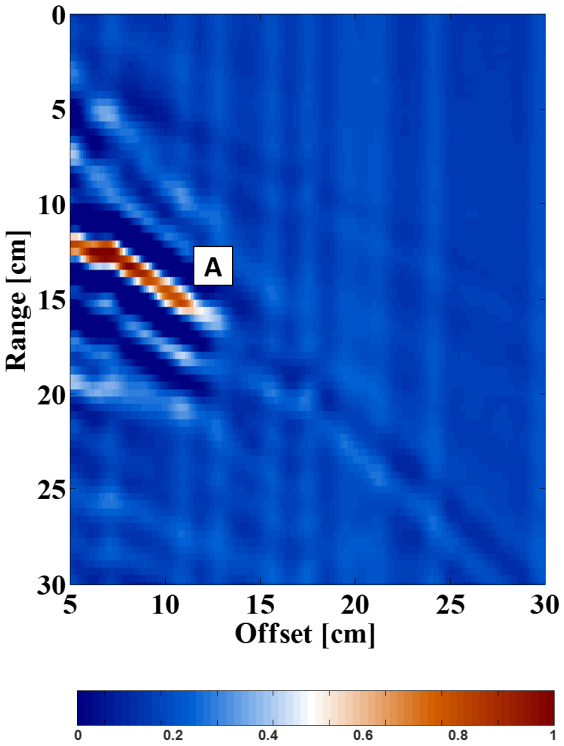

(b) CMP profile.

Figure 5.65: Inert PFM-1, bistatic characterisation.

that as long as the target is illuminated, this components will contribute to the radar signature. Considering the design of the target and the previous results on the target signature analysis, the detected reflections can be associated with the activation mechanism behind the pressure plate, which covers the whole landmine extension. This contribution is the same recognised from the 3D campaign as a homogeneous, high

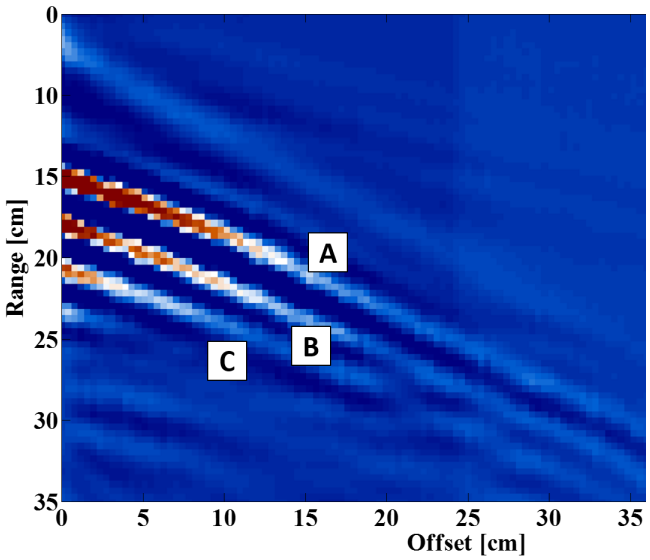

(a) CR profile.

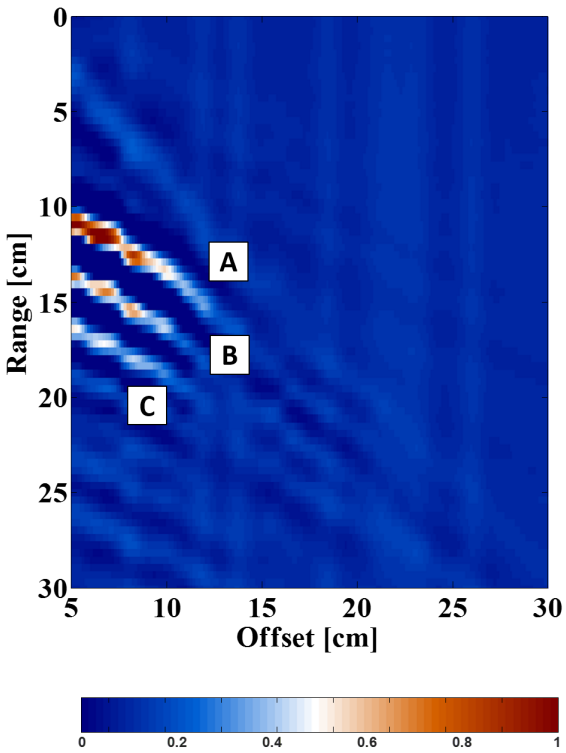

(b) CMP profile.

Figure 5.66: Inert VS-50, bistatic characterisation.

amplitude reflections occurring below the early recordings of the target.

Fig. 5.67 presents an interpretative diagram for a better identification of the feature.

The last investigated landmine is the SB-33, which presents an irregular internal design, including different components with different shapes. Its range versus offset

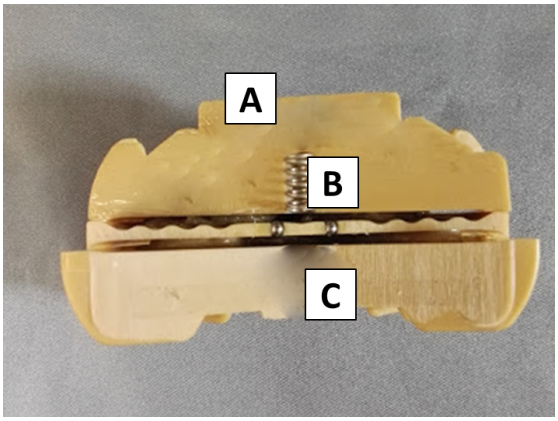

Figure 5.67: Inert VS-50, bistatic signature. Interpretative diagram.

results for both acquisition methodologies are provided in Fig. 5.68.

In a similar manner to the VS-50, more than one reflection is evident, therefore a preliminary indication of a target with a composite structure can be obtained. However, the middle reflection (marked B in Fig. 5.68) is spatially longer than the top (marked A in Fig. 5.68) and bottom one (marked D in Fig. 5.68), demonstrating that the scattering event is not homogeneous over the target space. This reflection is due to the void located aside the detonator (identifiable with reflection C of Fig. 5.68) which is located in a particular section of the target. In this case, the advantage of a bistatic approach is clearly visible, as this reflection is stronger under a particular angular range, differently from the other reflections.

If one considers the results presented in Fig. 5.11, this results represents a notable improvement. A descriptive cutaway is presented in Fig. 5.69

The last aspect is related to the target size. The diffraction hyperbola generated in a raw monostatic radar image depends mostly on the target size, orientation and depth, as well as the surrounding soil properties. Hence, a measure of the target actual extension is hard to guess from its hyperbolic representation. Progressively separating the transmitter and the receiver, instead, at some point will cause the target to leave the illumination region of the antennas. Substantially, the acquisition procedure reduces the hyperbola tails extension, as both the equipment are moving away from the target centre, and limits the collected target contributions. Taking as a reference the first or the last contribution from the target, i.e. the top or the bottom reflection, the target size can be easily inferred with a certain level of accuracy even from raw data.

Proof of this is provided in Fig. 5.70. Estimation accuracy can be evaluated by a

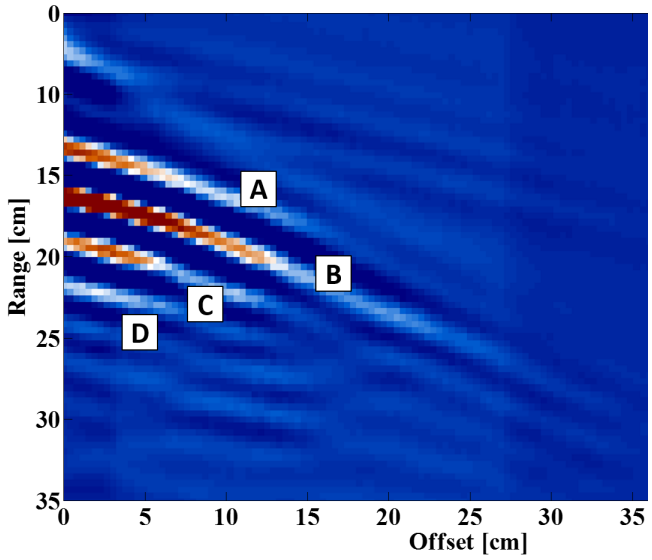

(a) CR profile.

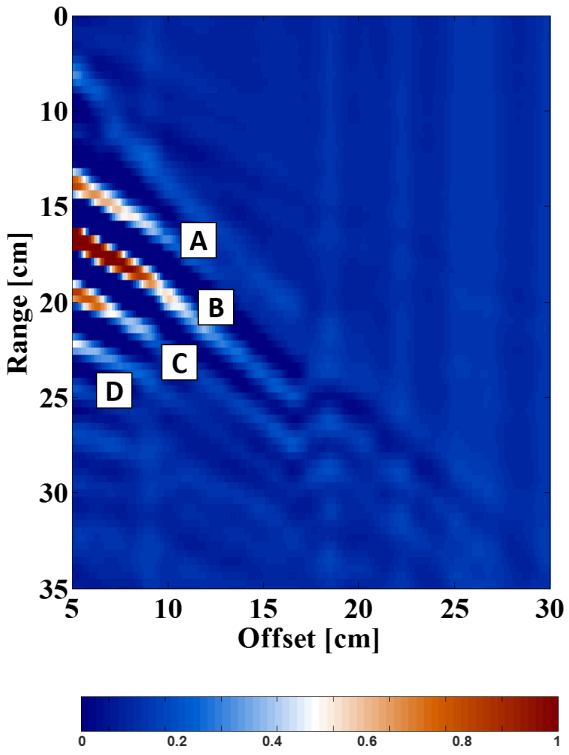

(b) CMP profile.

Figure 5.68: Inert SB-33, bistatic characterisation.

comparison with the actual dimensions (Table 5.1).

This feature represents probably the principal difference between the two bistatic methodologies, as it is evident the better accuracy achieved with a CMP scheme.

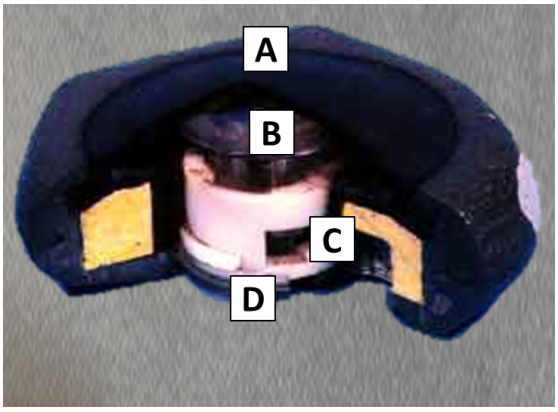

Figure 5.69: Inert SB-33, bistatic signature. Interpretative diagram.

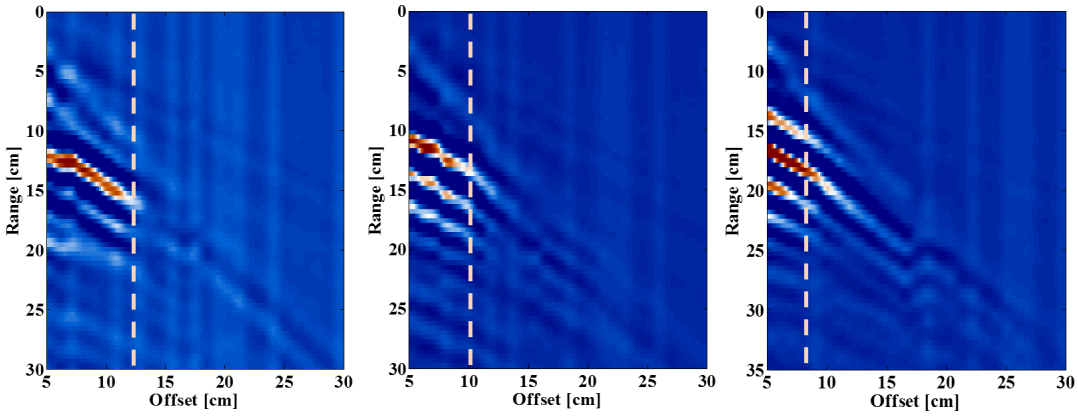

(a) Inert PFM-1. **(b)** Inert VS-50. **(c)** Inert SB-33.

Figure 5.70: Target size estimation.

5.5.2 Validation of results

As before, the surrogate VS-50 was investigated to prove the methodology. Recalling the previously made considerations, the bistatic signature of the surrogate should be almost constant regardless the bistatic angle, as (1) no internal structure is included, and (2) the metallic content does not provide a detectable contribution.

Due to the unavailability of the test site at the Defence Academy, the following acquisitions have been carried out in a conventional sand pit. Although a different texture and a higher level of humidity, the two materials have proved to show very similar propagation characteristics.

As no meaningful differences have been noticed between the two bistatic strategies, for validation purpose only the CMP signature of the landmine surrogate will be presented and commented. The collected signatures are described in Fig. 5.71.

As can be noticed, a single reflection (marked A in Fig. 5.71) appears, with a

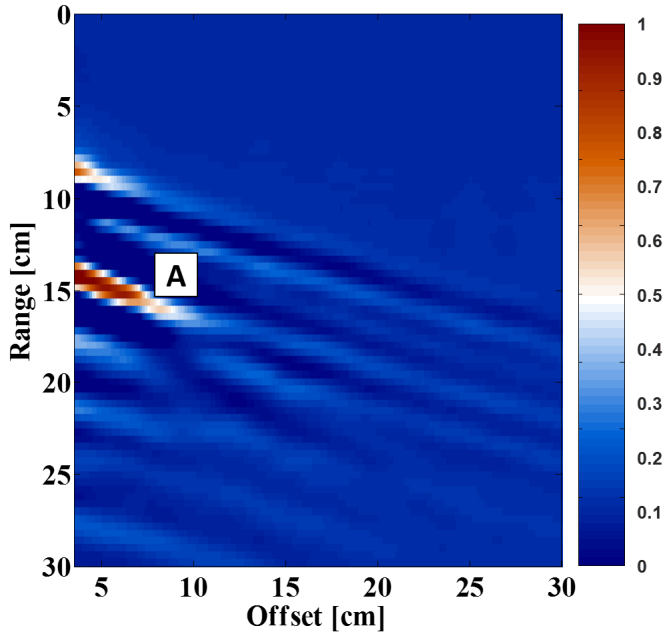

Figure 5.71: Surrogate VS-50, CMP signature.

spatial duration approximately equal to the target size and very close to its inert counterpart. Also in this case, the metal inclusion does not impact the signature.

Finally, recalling one of the limitations highlighted for the 1D signature analysis, to assess the reliability of the performance of a bistatic approach, an additional investigation has been performed changing the target inclination angle, variable that has a notable impact on the detection of the internal reflection.

Results from the inclined inert VS-50 and surrogate are shown in Fig. 5.72a and Fig. 5.72b respectively.

The collected CMP signatures demonstrate that the effect of the internal structure is robust to the target inclination, as all the three events previously detected (Fig. 5.66) are still identifiable, even though the reflections no longer appear constant, due to the change in the relative geometry. Compared to Fig. 5.12 and Fig. 5.25, it is evident the improved performance as in the mentioned situations, the internal scattering contribution was not detected. On the contrary, no significant variations are visible for the surrogate. In conclusion, no internal reflections are missed and no misleading reflections are produced.

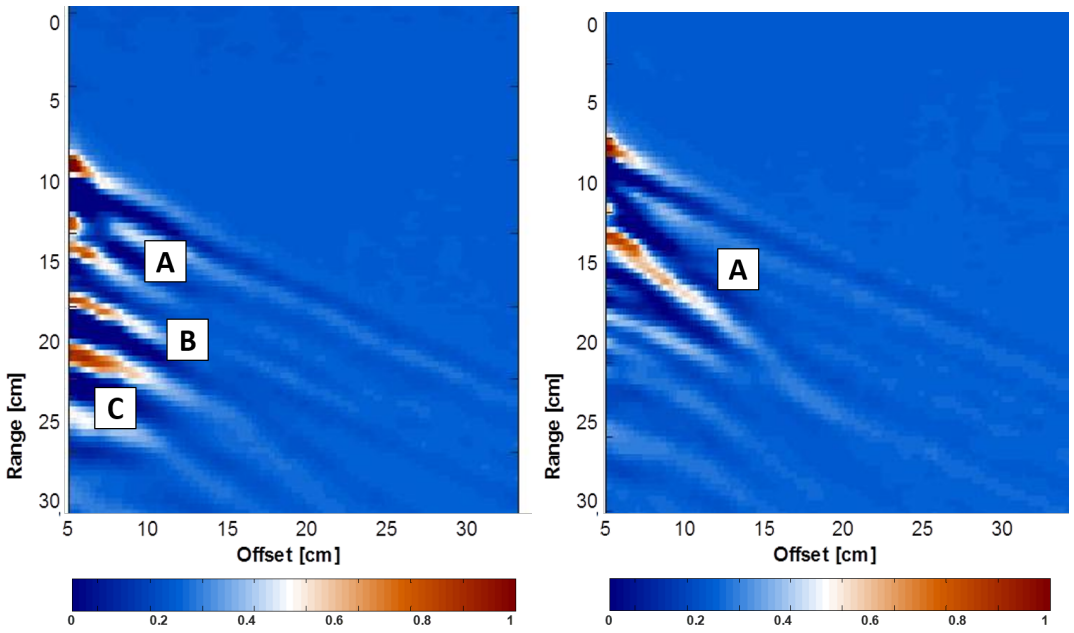

(a) Inert VS-50. **(b)** Surrogate VS-50.

Figure 5.72: Bistatic signature comparison, inclined targets.

5.5.3 Comments

From a target characterisation perspective, the outcomes have demonstrated that a bistatic acquisition methodology could yield as much information as a time consuming 3D GPR campaign, with the great advantage of being less expensive and demanding.

In particular, when the target does not include any internal assemblies, as for the PFM-1 landmine, no additional reflections are detectable, while when the object is characterised by a more complex design the contributions of these components are identifiable and a clear match to the actual design can be supposed.

Data have been acquired through two different bistatic geometries to provide a comprehensive evaluation of the technique. In particular, a common receiver (CR) and a common mid point (CMP) scheme were employed, using two different GPR equipment connected to the same central unit to ensure synchronisation.

The two proposed schemes were both able to properly characterise the investigated target, without significant differences between the acquisition geometries. This aspect is probably due to the width of the antenna pattern combined with the reduced dimension of the internal components of the landmine. The discriminant properties is related to the acquisition logistic only.

The results from the three devices under investigation have shown that, despite

a reduction in the dimensionality of the data, a close agreement between the physical structure of the internal assemblies and the radar imaging is maintained, especially considering the spatial extension of the reflections. In addition, what has been inferred from the bistatic results is consistent and analogous to what was previously suggested from the analysis of the 3D experimental campaign outcomes, demonstrating that the same information content was successfully achieved and that such details are sufficiently informative to ensure a correct target characterisation. Finally, a benefit of such an acquisition scheme was found to be a precise estimation of the buried target dimension. For all the three objects a close correspondence with the physical size was reached.

Even if the intelligibility of these results is lower than the immediate understanding gathered from the radar images, it should be take into account that in this case the identified features have been extracted from a single profile, therefore the performance and suitability of the methodology should be compared to the 2D results previously presented.

Following the same analysis scheme, the method was validated employing the VS-50 surrogate, for which the same considerations apply. In addition, the methodology has been tested also in the case of an inclined target, proved to be a critical variable and a source of missing detection. Also in this case, a bistatic approach shows reliable performance and robustness to variations in the geometry of the scenario.

5.6 Summary

The content of this Chapter can be strictly summarised through two main concepts:

- The GPR methodology is capable of recognising and extracting the internal scattering contribution from the target radar signature.
- Survey strategies significantly impact the robustness and interpretability of the results, as well as the detection performance.

In particular, a single 1D signature suffers from not being consistent when there is a change in the target inclination angle and when the internal design of the device is irregular, and even the inclusion of the polarimetric variables does not ensure reliable outcomes. Increasing the dimensionality of the problem, hence acquiring a 2D GPR profile of the object, can solve the issue of adverse geometries but it is not able to

properly characterise targets with complex internal structure.

If one expresses the efficacy of a GPR survey as a ratio between the amount of information that can be extracted from the data and the acquisition effort (time or resources as well), the two approaches that ensure an exhaustive detection, i.e. a 3D survey and a bistatic one, follow distinctive strategies and it is plainly inferable that a time consuming acquisition is justifiable only if the produced results bring a remarkable information content.

Even if this relation cannot be mathematically expressed, as it is not possible to define a unique connection among all the involved parameters, some considerations can be developed.

As previously stated, the choice of performing a 3D acquisition produces clear and straightforward information for the characterisation of the buried target, but the time required for the data collection cannot be neglected. As a general rule, a long acquisition time could be acceptable; however, a time consuming survey means that resources, from power consumption to equipment usage and human attention, are required. Data dimension, i.e. the volume in terms of number of inline and crossline profiles of the acquired data, means resources as well. If for traditional GPR applications these parameters could be easily reached and handled, in this framework they play an important role for determining the suitability of a surveying technology.

The information level brought by the results is closely related to the quality of the acquisition phase, as no processing step can solve the loss of information due to erroneous data collection. But in this case data processing and interpretation are activities that do not necessarily have to be performed during the acquisition process (i.e. there are no constraints on real time and on field data processing). For that reason, the key point is to be able to gather all the possible information in whatever form.

It is clear, therefore, that the GPR imaging approach tends to solve the ratio by maximising the interpretation ability while sidelining the acquisition phase. On the contrary, the bistatic characterisation strategy renounces to an evident readability in order to minimise the data collection expenses.

Chapter 6

Concept for a bistatic system

I believe it is possible for ordinary
people to achieve extraordinary things.

Jody Williams, 2006, [53]

Following the outcomes of the research, several considerations can be pointed out in the light of the development of a GPR system for landmine detection.

First of all, as described in the previous Chapter, a preliminary distinction should be made depending on the desired output. If the scope is to produce a high resolution image of the subsurface, the fulfilment of the spatial sampling requirements would be needed. Recalling the provided definition of system efficacy, conveniently defined as a ratio between the information content of the data and the survey effort, in this case the ratio is optimised by increasing the information content. However, the acquisition effort still represents an obstacle. Mechanical scanner with automated data acquisition can reduce the amount of labour required to collect the data, but the total acquisition time might be still negatively affected by the performance of the radar system and the time needed to reposition it. Even if the acquisition time is not as critical as the detection capability, this value becomes unacceptably high if one considers that this effort is required regardless the presence of not of a buried anomaly.

A bistatic survey strategy, instead, has proven to be able to overcome the problem of a time consuming survey, maintaining the same conceptual level of information of a 3D one. In particular, the strategy has demonstrated its valuable contributions providing information not only on the presence of internal reflections, which is a matter of resolution rather than acquisition geometry, but also showing a suitability for char-

acterising the design of the landmine structure. Moreover, all that can be extracted is evident in a single profile, therefore the acquisition effort can significantly benefit from the strategy. In this case, the time needed for the data recording depends on the desired data stacking only.

It is evident that following this strategy, the previously defined efficacy ratio is optimised by significantly reducing the survey time, accepting a less straightforward result, in terms of immediate understanding. It is furthermore clear that, to achieve an adequately time-saving performance, a certain amount of mechatronic and automation is needed. Finally, the system needs to be designed as much autonomous as possible, to improve the safety of personnel along with efficiency, productivity and flexibility.

This Chapter will firstly introduce motivations behind the development of landmine detection equipment, covering both technological and economical issues and then a conceptual idea for an efficient and affordable bistatic GPR for landmine detection, following the field trials experience and the obtained results. Clearly, the adoption of a dense bistatic acquisition scheme precludes the use of an hand held platform, as (1) such an equipment will hardly support the sensor head, (2) it will be hard to maintain the same set-up for all the survey, and finally (3) the weight of the equipment could negatively impact the performance of a human-based survey. Therefore, an automatic scanning platform may be the most reasonable choice.

However, the expected benefits of mounting a landmine detector equipment on a remotely controlled or automated vehicle must be judged against the consequential cost increase and possible efficiency reduction considering the overall field survey effort. In this case, an accurate and detailed cost analysis should be performed to determine whether such technological choice is sustainable and feasible for the application.

6.1 Motivations and platforms

While it can be in principle accepted to consider the manual procedure as an unsophisticated and retrograde approach, the actual truth is that the human eyes and experiences are the most powerful investigation tools. And consequently, it is commonly agreed that it will take a very long time before an artificial device or a machine, even if readily available, can match the operational performance of a human being.

The common belief is that the solution for increasing the efficiency of mine clear-

ance activities mainly lies in developing better sensors. It is obvious that if a sensor capable of achiving a 99% detection accuracy is mounted on a hand held device, the only remaining task to be accomplished is minimising the speed needed to determine whether a mine exists or not.

However, surveying using a hand held sensor still represents a dangerous operation for the deminer. As a figure of merit, 99 casualties among deminers per year have been recorded since 1999 [289]. In 2017, there were 60 casualties among deminers in 14 countries (18 deminers were killed and 42 injured), a decrease from 2016, when there were 102 casualties identified (Fig. 6.1a). Even if these numbers might seem limited, they are still unacceptably far from zero, and the statistics do not seem to indicate a decrease in the number of incidents.

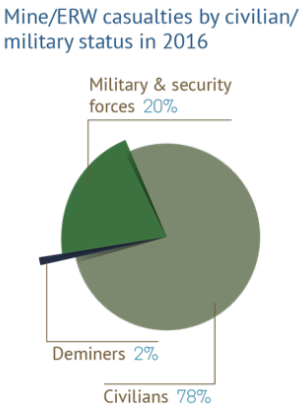

(a) Casualty demographics reported in 2017. *Taken from [11].*

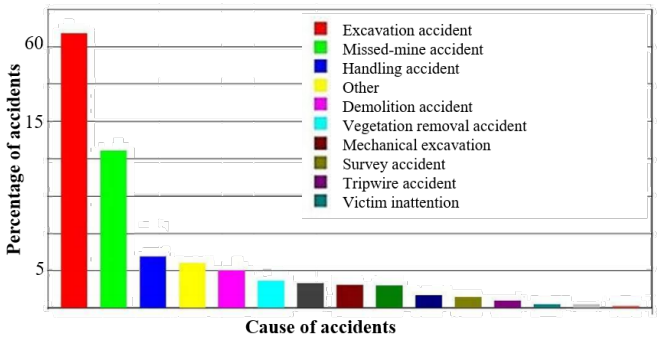

(b) Accidents classification (2000-2005). *Courtesy of noland-mines.com.*

Figure 6.1: Humanitarian operations casualties statistics.

From the reported classification of accident during demining operations, shown in Fig. 6.1b, it is possible to draw a global picture of the scenario. First of all, being the most common activity, excavation operations, either for investigating a detection alarm or to remove the ground surface, are at highest risk. Another significant cause of accident is represented by an accidental triggering of missed mines or pressure sensitive munitions, while a relatively limited number casualties arise from mine disposal procedures and handling accidents.

Even with training, mine disposal experts indicate that one person is killed and two severely injured for every 5,000 mines cleared [290]. Thus, it would be fair to say that having an autonomous platform to carry out the entire survey chain would be ideal for

this problem.

The dirty, dangerous and tiresome tasks found in landmine detection procedures, can be greatly benefit from remotely operated platform, as it is highly desirable to move the operator away from the proximity of the landmine, as such repetitive operations might lead to loss of attention and potential injury. The capability of automatically and consistently detecting mines over large areas surely represents a significant advance in humanitarian demining, as such potential could drastically reduce the determination of suspected mined areas, as well as improve the mine clearance process and assist during final quality assurance operations. Equally important is to identify landmine-free areas, as several field reports indicates that a considerable area out of the total mine suspected one is limitedly or even not at all contaminated.

Despite this airtightly considerations, the currently adopted methods are still based on handheld detectors and manual surveying, with very few variations due to the technological advances. Operationally, the detector is swept by the operator over the portion of area to be investigated, from side to side and with the operator progressively advancing to cover the designated sector (Fig. 6.2). A detection is typically confirmed by repeatedly sweeping the sensor over the candidate location, along different direction, with the detector head held at a sufficient height to avoid hitting the ground surface.

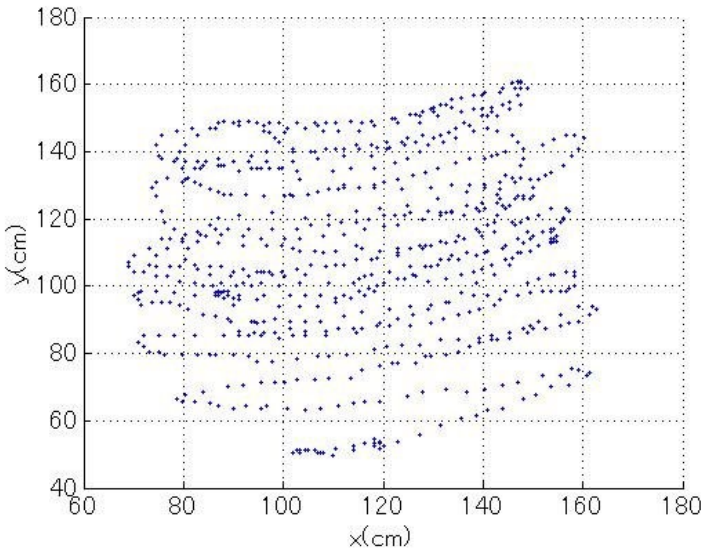

Figure 6.2: Example of manual area sweeping. *Taken from [115].*

The operator can vary the width of sweep to adapt to specific ground conditions, therefore operations are in principle not not limited by terrain. It is therefore evident

how this manual approach can be slow, hazardous, and stressful, features that prevent the operator to perform the task for a constant and continued period, consequently reducing the activity proficiency. In addition, the use of a hand held system makes it difficult to precisely replicate overpasses and multiple looks, unless additional instrumentations, potentially sensitive and heavy, are included within the scanning equipment.

The implementation of a GPR sensor in a handheld system is restricted by weight (typically in the range 2 to 5 kg) and size, considering that the area is manually surveyed. Generally, along with a metal detector coil, a handheld system includes a lightweight GPR sensor consisting in a single pair of antennas and the essential data processing capabilities.

The main alternative to the handheld devices are the vehicle-mounted ones, which can be mounted on various types of vehicles and may be used where the terrain allows them to move. Clearly, there is a logical tendency on developing stand-off systems which can spot the presence of a buried objects from safe distance, up to tens of metres. However, GPR performance suffers from not being in proximity of the surface and there are several constraints that need to be taken care before designing any vehicle-mounted system which makes the system expensive.

GPR of this type are divided into the two groups: downward-looking devices and forward-looking ones. The latter is obviously preferable as it does not necessitate the vehicle to have overpass capability. However, a theoretical limitation on the achievable system performance exists, as, while transmission losses at the ground interface are relatively small for incident angles smaller than the Brewster one, at larger angles such losses rapidly increase, thus impacting the system detection capability, in particular for buried targets. Conversely, this restriction does not in principle exist for the downward-looking architecture. Examples of vehicle mounted GPR equipment are shown in Fig. 6.3.

Arrays width lies between 1 and 4 metres, and they can reach an operational speed up to tens of km/h. In general, vehicle based GPR systems permit the acquisition of more reliable and informative data, as well as a higher processing capability with respect to the handheld systems. As the interpretation of the 2D GPR images is not trivial and strongly depends on the user ability, 3D processing and visualisation techniques is

(a) 3D-Radar DX.

(b) Niitek VISOR.

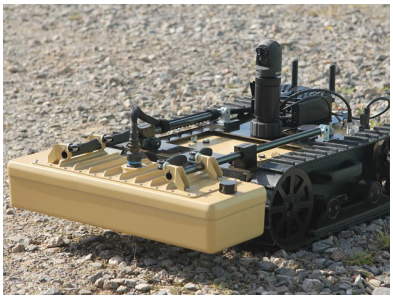

(c) Cobham AMULET.

(d) Ingegneria dei Sistemi MINERVA.

Figure 6.3: Examples of vehicle mounted GPR systems. *Courtesy of respective Owners*.

constantly growing, mainly thanks to the deployment of GPR arrays.

To date, vehicle-based systems mainly target anti-tank landmines because achieving an operationally suitable cross range resolution for detecting small, plastic buried anti-personnel landmines still represent a technological and economical challenge. This concept is strictly related to the antenna element spacing, which must be adequately designed to provide sufficient resolution performance, as the effect of spatial undersampling on the radar image degrades the image quality. Moreover, changes in ground topography negatively affect the path propagation and influence the collected signals, considering that array elements are generally fixed. As an example, the Wichmann/NIITEK GPR system currently employed by the US Army adopts a channel spacing of approximately 5 cm.

Several trials have been carried out to identify minefields from airborne platforms [291], employing both airships (as for the MINESEEKER, [292, 293]) and unmanned aerial vehicles (UAVs, see for example the TIRAMISU project [294]).

Improvements in UAV technology have supported the development of small and lightweight UAVs (less than 3 kg) for airborne Synthetic Aperture Radar (SAR) over small size areas, avoiding the need of large aircrafts. Within the domain of landmine

(a) A-60 airship equipped with camera and radar detector. *Courtesy of Mineseeker foundation.*

(b) Multicopter Microdrones equipped with camera and infrared detector. *Courtesy of TIRAMISU.*

Figure 6.4: Examples of airborne GPR systems.

detection, they exhibit notable advantages, including (1) higher scanning rate compared to ground-based robotic platforms, (2) capability of surveying otherwisely inaccessible and remote areas, and (3) increased safety during investigations.

These benefits, however, must be balanced against the limited cross-range resolution performance that can be achieved, as a consequence of the reduced positioning and georeferring accuracy [295]. Therefore, their effectiveness has been demonstrated in detecting buried targets larger than 25-30 cm, and hence mostly anti-tank mines, and/or exhibiting a significant impedance contrast with the medium [296]. In addition, as the aperture of any airborne sensor is not sufficient to detect anti-personnel mines, the resultant radar image, determined by the convolution of the antenna footprint with the target cross-section, might not be able to detect targets with small RCS.

Logically, these efficiency and performance limitations have strongly affected the usage of airborne GPR technology.

Drones are currently employed for their high resolution imagery, as they can efficiently assist the post-release development monitoring and demining operations planning. In addition, the capability of generating digital surface models can be useful in determining suitable access routes for demining machines. Hyperspectral imaging is another application employing aerial platforms, with the aim of detecting different temperature variations pattern in order to spot the presence of landmines. It is clear that both purposes are mostly related to surface or above ground object detection.

Detecting and removing landmines seem to be a perfect application for ground

robots. Having a mechanised and robotised solutions properly sized, with optimised structure and matching the specific minefield environmental conditions might notably improve operations efficiency and productiveness. In addition, such intelligent machines can speed the clearance process when used in combination with mine detection tools. Essentially, these systems emulate the downward-looking vehicle mounted GPR approach, substituting the vehicle with a small and agile scanning platform, and therefore representing the best survey condition from a GPR perspective, if technically feasible.

Robots have been repeatedly indicated as a candidate technology able to reduce the hazards to which demining operators are exposed, but there are still several factors hindering their effective deployment, the principal of which determined by a lack of problem awareness among developers, that has commonly led to the design of inappropriate or solutions that are far from the real needs. Most robotic equipment proposed so far have been overly expensive, from both the manufacturing perspective as well as considering their maintenance and deployment, mainly as a consequence of its inherent complexity. Finally, one should always consider the deminers understandable demand for complete safety and coverage, and at least a significant confidence in the technology on which their lives depend.

As can be inferred, the problem is mainly the delivery of technology, rather than the technology itself.

A comparable alternative might be a Remotely Operated Vehicle (ROV) landmine detection system, potentially capable of providing wider area coverage and limit the risks for human operator. Some examples of developed prototypes are shown in Fig. 6.5.

There have been important advances related to technology for mine detection and removal over the past decades, although none of the currently researched robotics platforms seems to have reached a wide scale production and deployment (except for military EOD/IEDD tasks).

6.2 Concerns regarding technology

There are several concerns and disputes when discussing the development and use of technology for humanitarian demining operations [297]. In particular, the principal can

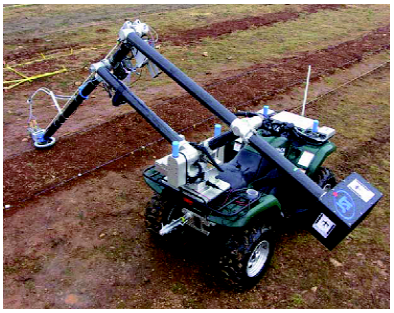

(a) Gryphon (Tokyo Institute of Technology).

(b) tEODor (Royal Military Academy of Belgium).

(c) ARES (University of Lisbon).

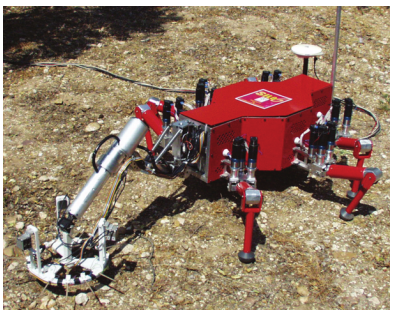

(d) SILO-6 (DYLEMA project).

Figure 6.5: Example of robotic platform for humanitarian demining. *Courtesy of respective Owners*.

be classified as follows:

- **Cost**: while it is widely acknowledged the produced benefits, especially related to survey impact and safety, it is a common impression as well that if all the research funds for developing new technologies were re-routed to already deployed methodd, then the figures about cleared landmines would have been significantly higher. What is to be further highlighted is that such ambivalence comes from NGOs directly involved in clearance processes, possibly as a result of the worries that an increase of the R&D funding might provoke a decrease in the amount available for operations [298].
- **Socio-economic impact**: a commonly adopted framework within mine action programmes requires the majority of demining operators to be locally recruited, as a way to engage local community and foster its development [299]. This means that demining activities represent a steady paying job, a stable source of income which can be highly desirable, especially in low-income countries. Therefore, even if it might be considered an odd motivation, in some places the potential introduction of new and more efficient demining technology is regarded

with diffidence [300].

A preliminary conclusion is that the first step should target the existing technology, rather than a radically new one. In this case, the assessment of the overall benefit expected from its technological and operational improvements should be based on the cost-benefit analysis of such incremental improvement, and its marginal impact on a number of key features, such as rate of demining, survey accuracy and operator safety [301].

This approach suggests that existing technology whose developments could demonstrate a readily capacity to positively impact on demining operations might have a better chance of being adopted, always subjected to the market.

To better contextualise this considerations, the average sales price of a conventional metal detector equipment does not exceed $5,000 (typically around $2,500 per unit), while their world annual market is estimated to be around $10 million [111]. Therefore, new detectors should not only align with this figures, but they also need to face the limited budget that NGOs assign to new technology purchasing [302]. Therefore, a basic comparison of these costs can be polarised by the fact that, being mostly carried out with locally employed people, the actual cost per day for demining operations is visibly lower than the cost needed for the development and deployment of new technologies. However, if one considers the total life time of the equipment, the costs directly and indirectly related to the manual operations might probably be higher [303].

6.3 Sensor fusion

As a general rule, a detector equipment must be capable of detecting every mine and recognising them from fragments of metal or other debris, so that they can be left in the ground without the need for the excavation and verification procedure. Considering the previously described concept of false alarms and clutter objects, it is clear that the most challenging task is to develop sensor architectures and algorithms that could allow for an efficient discrimination between landmines and non-mine targets. This capability becomes even more demanding is considering that, according to the GICHD [77], in many cases up to 98% of an area said to be mined is in fact mine-free. For example, during 6 years of humanitarian demining operations in Cambodia, only about the 0.3% of all the excavated objects (approximately 200 million items) were actually landmines

or explosive threats [304].

Sensor fusion methodologies represent a widely researched techniques for landmine detection in the last years, due to the agreed principle that combining different sensors exploiting different target features might improve the process. The majority of fusion methods includes MD and GPR, representing the most mature solution in terms of technology deployment, but there are examples which also comprise an IR or optical imaging sensor [305]. Despite the common belief, metal detector and GPR are not in principle orthogonal sensors, as the presence of a buried metallic element will equally produce the largest response. However, what can be additionally exploited with a GPR sensor is the evolution over time of the target signature, which might highlight internal reverberations or multiple reflection phenomena resulting from the presence of air gaps, significant permittivity contrasts or metallic components.

As an example, performance improvements of the VMR3 Minehound compared to single MD equipment are shown in Fig. 6.6.

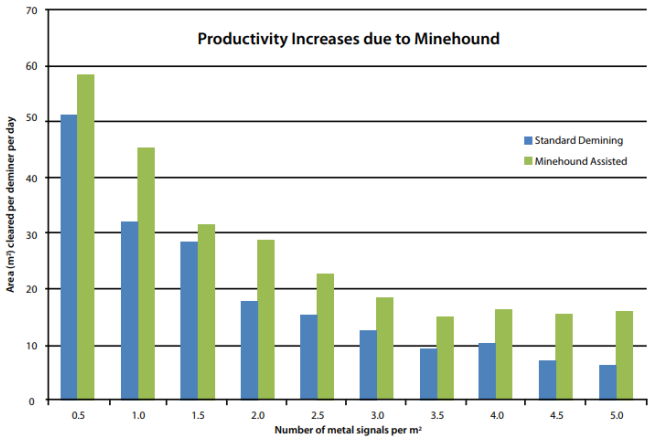

Figure 6.6: Productivity increases due to dual sensor equipment compared to MD only. *Taken from [306].*

As reported in several field verifications [77], the number of false alarms is drastically reduced when a dual sensor equipment, in which the metal detector represents the primary detector while the role of the GPR is confirmatory, is deployed. It is therefore clear that a compact and low-cost GPR, if economically feasible, could have an operationally critical impact. At a rough guess, the improvements in survey productivity and reduction in the predicted man-hours can cover initial cost, which of course must not be beyond the typical R&D budget of most organisations, within few years of widespread

implementation. In addition, over the following years this will produce a permanent reduction in the cost per cleared square metre.

6.4 Conceptual design

From what has been desribed in the previous Chapters, the logical implementation of a bistatic GPR takes the form of antenna arrays, in which each channel can be configured in order to acquire a bistatic signature of the detected target. Clearly, this means that the primary constraints are related to the physical system geometry:

- **Maximum offset**: how wide the array should be to ensure all contributions from the target are collected.
- **Maximum sampling**: how wide the spacing between channels should be to ensure all information from the target are collected.

The first item is basically a matter of soil attenuation (i.e. the maximum achievable bistatic range), and target dimension (i.e. the maximum spatial extension of the object radar contributions). Following the results of the field trials, one might consider the equipment size to be approximately 50 cm, allowing an effective recording of sufficiently extended and dense bistatic signatures. Moreover, these range of sizes can be suitable for unmanned platforms mounting.

The latter feature represents a more complex item to be addressed, as it is a compromise between the Nyquist sampling requirements and the effective physical (and electrical) dimension of the antenna elements, as in this case, the channel spacing corresponds to the offset sampling. A fixed array therefore would require a large number of elements, which themselves might be larger than the required spacing, causing the resulting equipment to be excessively under sampled. Even if interpolation can help, usually the minimum distance between the transmitter and the receiver corresponds to the largest dimension of the antennas, so that mutual interferences can be limited.

In particular, to take into account the reduction in the bistatic signature extension when the target is inclined (as shown in Fig. 5.72), the maximum tolerable spacing might be in the order of a centimetre. To date, minimum spacing of massive array systems is not less than 5 cm, reaching tens of cm for large scale applications.

To visually evaluate the effects of reducing the CMP profile density is shown in Fig. 6.7, in which the previously obtained results for the VS-50 landmine have been

decimated to synthetise a sparser sampling.

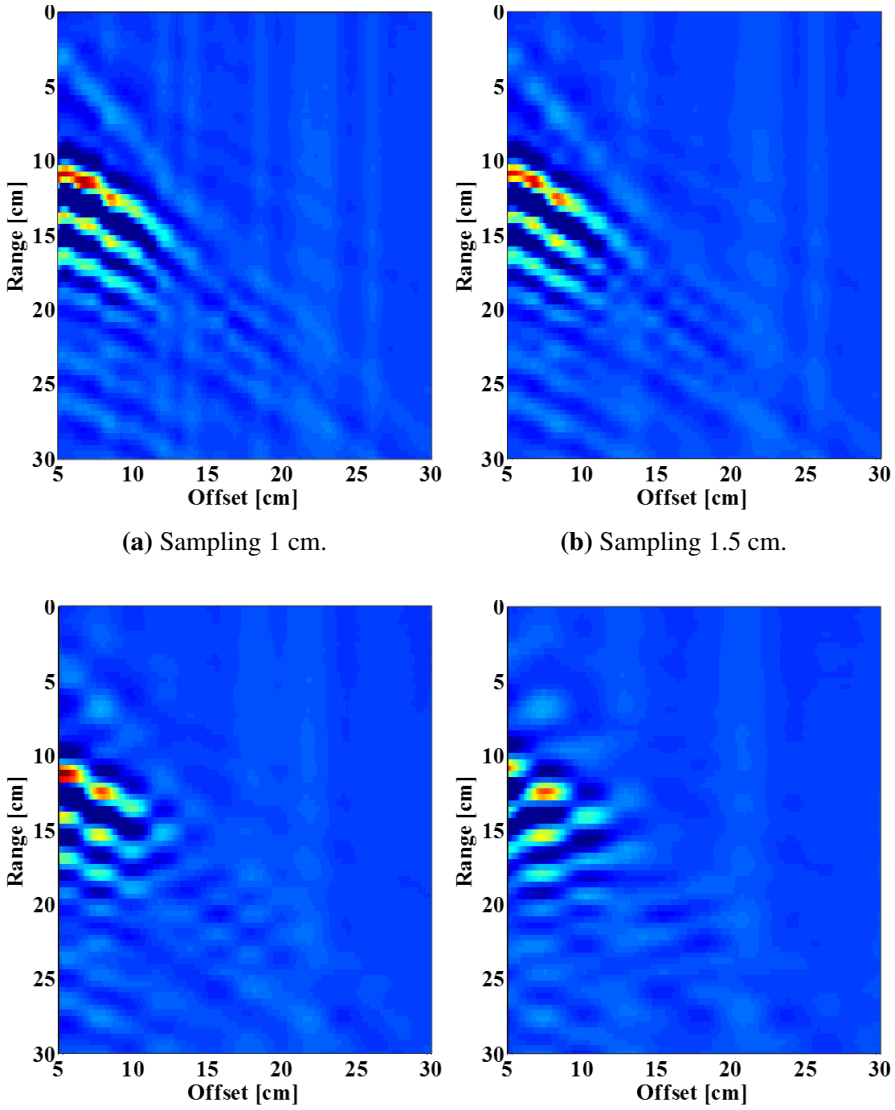

(a) Sampling 1 cm. **(b)** Sampling 1.5 cm.

(c) Sampling 2 cm. **(d)** Sampling 2.5 cm.

Figure 6.7: Effects of offset sampling on landmine bistatic signature.

It is evident the effects of reducing the number of collected bistatic signatures, as there is a severe loss of information when the spacing is higher than 2 cm. Practically, this means that there are limited possibilities in reducing the data density. In addition, it should be considered that the field experiments were carried out in favourable conditions, therefore the visible degradation may increase in case of more complex conditions.

A centimetric-spaced equipment can be ideally achieved by a reconfigurable system, in which a large number of very closely spaced elements can be dynamically activated and deactivated. However, even mitigated, the risk of having unwanted cross

talk and mutual interference still exists. In addition, accurate synchronisation might become harder to obtain.

The idea behind the conceptualisation a bistatic equipment can be found in the strategy adopted for the experimentation, i.e. having two different GPR equipment independently managed. It is clear that in this case, if the aim is to implement an autonomous platform, a key parameter is to maintain a reduced weight.

A raw diagram of the described equipment and concept is provided in Fig. 6.8.

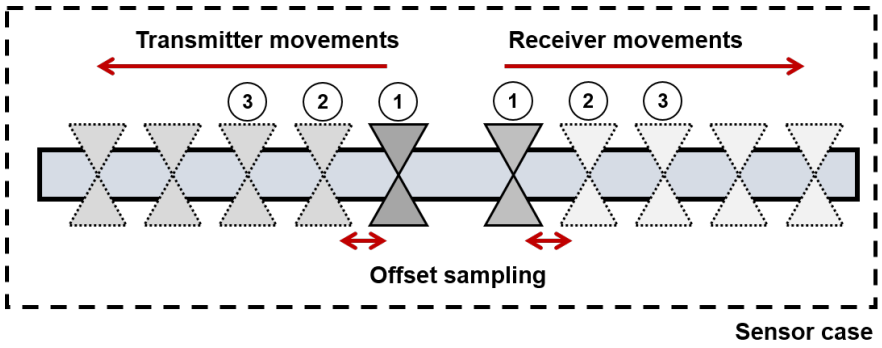

Figure 6.8: Raw diagram of automatic bistatic scanning GPR.

This essentially means that the bistatic data recording would require some sort of electro-mechanical components to systematically and precisely increase the distance between the transmitter and the receiver and to perform the series of periodic motion simultaneously. This mechanical effort is balanced by the fact that a single equipment has to be included in the sensor head, reducing the electronic and computational complexity of the system. The principal requirement is that the sensor head shall include only passive elements to keep a low weight and facilitate its mobility. In this way, the weight would not exceed the typical values for hand held equipment.

The employment of multiple and separated rows of elements to avoid the inclusion of automation will negatively impact the physical dimension of the equipment, as it would be wider and larger to accommodate the required number of channels.

Two assumptions are commonly accepted in landmine detection operations using GPR: (1) the need for a high frequency equipment, as a consequence of the high resolution requirements, and (2) the necessity of maintaining the antennas elevated from the surface to avoid accidental triggering. The first assumption is sustained by the potential GPR capability of classifying the targets depending on an accurate geometrical reconstruction, while the second considerations derives from safety reasons. However,

for a more efficient GPR operations, it is well known that the radar antennas must be as closest as possible to the ground, especially when high frequencies are involved, as a consequence of the increased field contributions from reactive coupling.

Following these considerations, one of the critical points is whether the platform should be in direct contact with the surface or whether it can be operated at a stand-off distance. In this case, the discriminant feature is the possibility of detecting the internal reflections of the target.

An experimental evaluation of the height effects on the detection performance of GPR has been performed, to verify also the numerical results shown in Fig. 4.27c in which it seemed that the reflections generated by the internal air layer appears in the radar signature for the first tens of centimetres.

In particular, a series of coincident 2D profiles have been acquired over the representative VS-50 landmine, each time inserting a styrofoam tiles between the radar and the soil surface to change the antenna height above the soil. Details are provided in Table 6.1.

Table 6.1: Antena height evaluation parameters and set up.

Parameter	Value
Frequency range [GHz]	1 - 3
Frequency sampling, $1/\Delta t$ [GHz]	17
Inline sampling Δx [cm]	0.4
Time window, ΔT [ns]	15
Antenna offset [cm]	6
Antenna height [cm]	5 - 10 - 15

The landmine was buried at a depth of 13 cm as previously made, horizontally laying. Photographs of the acquisition are shown in Fig. 6.9.

To highlight the target contribution, in this case a background removal step was applied to the data [307]. In particular, the subtraction has been applied through the application of SVD algorithm and eigenvalues/eigenvectors suppression, in order to selectively removes the flat horizontal reflections from the GPR profiles [308]. The resulting GPR profiles, normalised in the [0-1] amplitude range, are presented in Fig. 6.10.

Disregarding negligible topography variations and surface clutter, the landmine

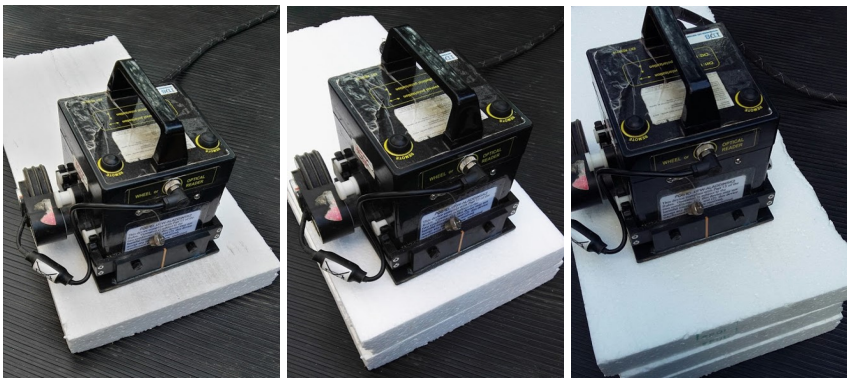

(a) Height 5 cm. **(b)** Height 10 cm. **(c)** Height 15 cm.

Figure 6.9: Antenna height evaluation, acquisition details.

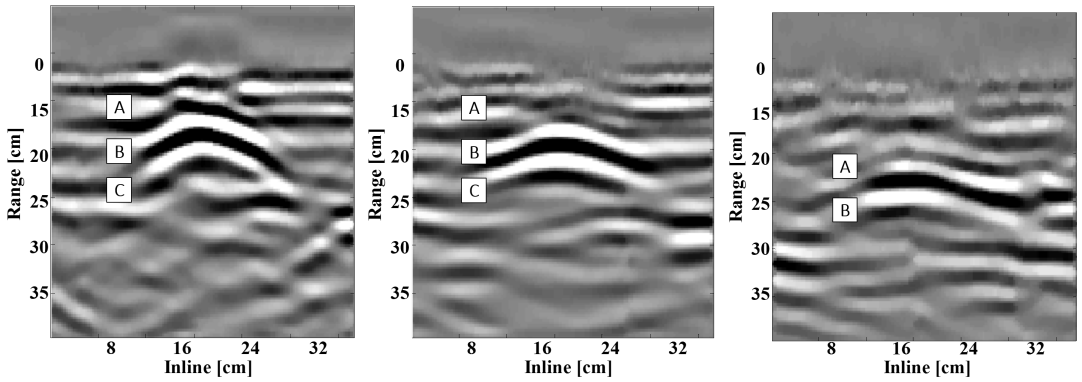

(a) Height 5 cm. **(b)** Height 10 cm. **(c)** Height 15 cm.

Figure 6.10: Antenna height evaluation, GPR results.

internal structure can be retrieved up to 10 cm, beyond which its scattering contribution becomes hard to recognise. In particular, Fig. 6.10c further demonstrates that the effects of air gaps located within the landmine is beneficial for its detection, as it can be noticed that the principal contribution detectable is the internal layer, rather than the top of the landmine. This is in agreement with the numerical results, showing the same pattern.

From a practical point of view, this represents a valuable advantage, as it means that the GPR equipment can achieve comparable performance even not in contact with the surface. For comparison purposes, the Proper Lane Sweep technique (PLS), requires the sensor head height not to exceed 5 cm. Moreover, possible interferences generated by closely located structures due to the wide pattern of the antennas are reduced due to the limited height of the platform.

However, these results might suggest that a ground based system is nearly the only feasible solution, as a UAV would need to fly at a very low altitude to allow a proper

radiation performance, feature closely bounded to the environmental factors and that may impact the scan accuracy and imaging performance. In addition, it should be taken into account the payload limitations of such platforms employed at low altitude.

A parallel advantage of this solution is that it would be also suitable for vehicle mounting integration

The last aspect to be considered is the acquisition step. Since landmine clearance personnel are concerned about not triggering the landmine, the scan pattern is often erratic, lowering the quality of the results and impeding a physical implementation of the described methodology in a hand-held system. Suitable performance of the currently employed platforms are obtained only when experienced operators are performing the survey, and it is well-known that operators skills decay with time, issue that vanishes when the task is carried out by a mechanical infrastructure. Mechanical infrastructure does not tire like humans, provided they have enough power, and their performance is not affected by psychological tension and trauma. In addition, the accidental triggering of landmines is minimised due to the mechanical capability of the system of adjusting the sensor head elevation to maintain a constant height above the ground. Finally, the operator can actually stand in a 100% safe position.

The data acquisition step represents the bottleneck of the problem, as described in detail in the previous sections, as target characterisation and potentially target identification both rely on very dense and accurate data.

The main question is therefore how to define a sufficiently sparse grid to ensure detection and maintain efficiency at the same time.

To increase the efficiency, the following considerations can be made: it has been demonstrated that detection of the diffraction hyperbola can be obtained also with a sparser acquisition grid, therefore the acquisition strategy can be configured so that most of the resources are concentrated when there is a precise need and evidence, i.e. when a target is detected and located, saving time and resources from non-contaminated areas (which represent the predominant situation). In addition, it should be take into account that the tougher barrier is the spacing between the parallel profiles, i.e. the crossline direction (Δy), while the inline one (Δx) could be easily managed, therefore the data sampling along this dimension does not significantly impact the acquisition effort.

The acquisition strategy can be analysed considering the antenna radiation pattern and the target size. In particular, most landmines may be classified with a size of approximately 10 cm, while the majority of GPR equipment, to maintain a practical size, employs wideband dipole antennas having a wide radiation pattern. As the radiation pattern can only be characterised taking into account the soil dielectric properties, which may be difficult to exploit, the optimum grid spacing can be estimated considering the the target size only and the need of having at least one profile located inside the target.

With a reliable estimation of the parameter and of the wave propagation characteristics, it would be possible in theory to dynamically adjust the grid spacing to the soil dielectric properties, further increasing the efficiency of the system.

From these considerations, it is clear that the maximum crossline spacing cannot exceed 10 cm, otherwise there is the risk of being inadequately sparse, as shown in Fig. 6.11.

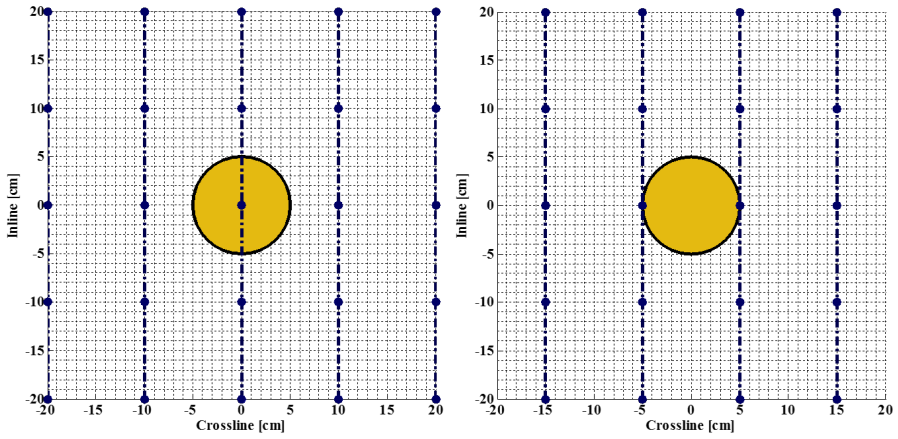

(a) Target axis profile. **(b)** Target edge profile.

Figure 6.11: Optimum sampling mesh analysis, $\Delta y = 10$ cm.

It is clear that ideally a spacing of 10 cm will be sufficient for detecting the diffraction hyperbola, even in the less favourable condition, as in such case there are two profiles crossing the target. However, this choice would require a very accurate acquisition to ensure that even when the profile is located on the border of the target the target would still be detected. The effects of being close to the target edges is depicted in Fig. 6.12.

It is implicit that when including the width of the radiation pattern, a profile located

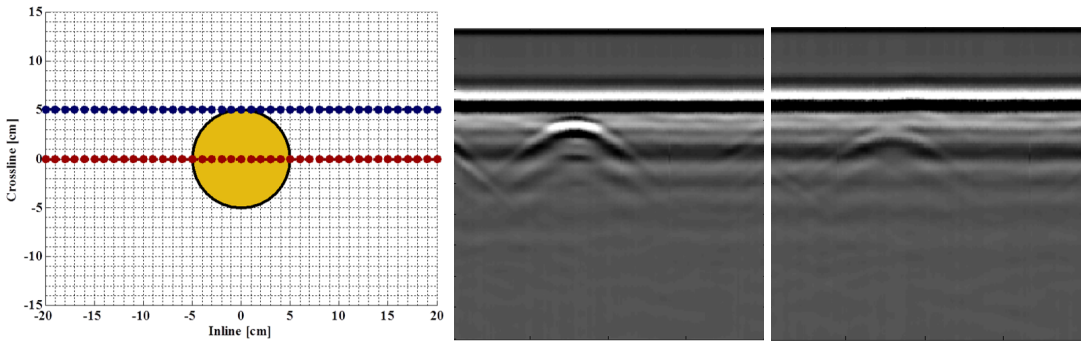

(a) Profile location. **(b)** Target axis profile. **(c)** Target edge profile.

Figure 6.12: Radar profile collection, effects of profile location.

on the border will include an increased scattering contribution from the target, reducing the risk of missing it (Fig. 6.12b). On the other side, it must be considered that uneven soil topography and surface obstacles and/or clutter may reduce the profile location accuracy during the survey.

Reducing the spacing between parallel profiles brings a more conservative situations, described in Fig.6.13.

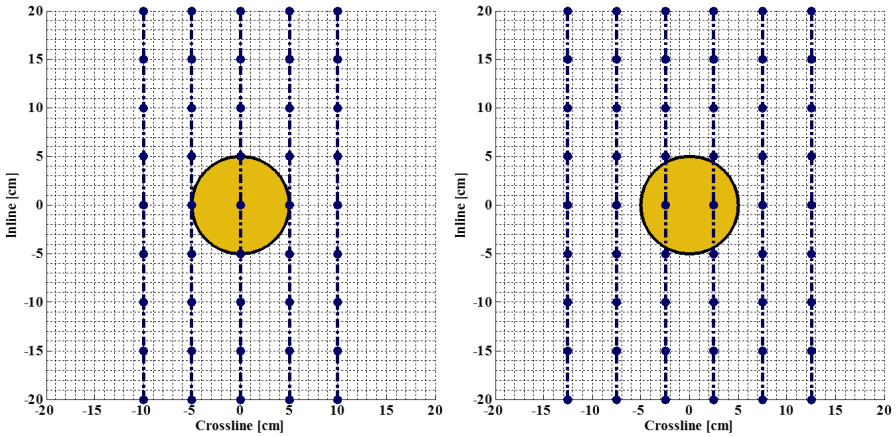

(a) Target axis profile. **(b)** Target edge profile.

Figure 6.13: Optimum sampling mesh analysis, $\Delta y = 5$ cm.

In this case, it can be seen that there is a higher probability of acquiring a profile crossing the target, therefore this scheme might be capable of better manage smaller and/or non-symmetrical targets, as well as inclined objects (which have a reduced radar signature).

Still, it is reasonable to reduce the total amount of data to be collected, i.e. inline direction, but it must be taken into account that a highly oversampled acquisition might not produce a clear hyperbola in the radar profile, therefore the detection step would be

based on a single signal, which clearly yields less information. A comparison between the two output is shown in Fig. 6.14, in which a conservative spacing of 1 cm is taken as a proper parameter.

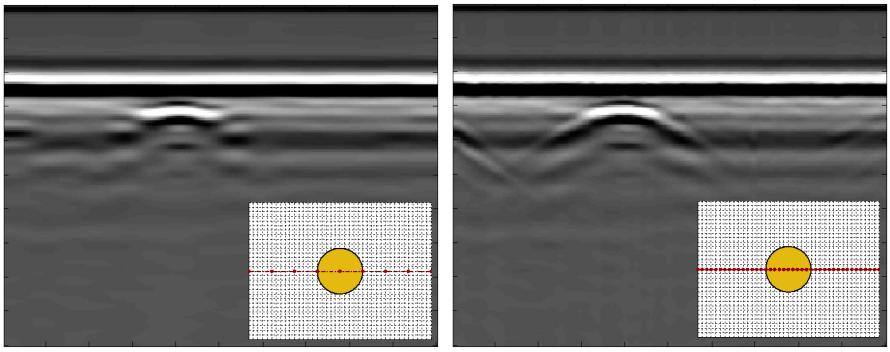

(a) $\Delta x = 5$ cm. **(b)** $\Delta x = 1$ cm

Figure 6.14: Data collection, effects of inline sampling on detection decision.

As can be seen, even with a sample spacing of 5 cm the resulting image still shows an hyperbolic pattern, but it is expected that a less cooperative soil will degrade the results, making the interpretation of the profile of Fig. 6.14a less intuitive.

When the system detects an hyperbola in the GPR image, through an automatic detection scheme or via human supervision, as well as through a combination of sensors response, the platform should search for the apex of the target in the neighbourhood of the profile to pick up the optimal geometry. This location can be easily found by acquiring an orthogonal GPR scan from the apex of the individuated hyperbola, obviously along the orthogonal direction along (the crossline one). This additional effort put in place for positioning the equipment precisely over the centre of the target is required to ensure a proper CMP profile collection. Then, the bistatic signatures collection can be performed, and the detected buried anomaly can be classified according to the collected results.

Search flow can be described as follows:

- **Area reduction** through a sparse survey to reduce the impact of non-contaminated sectors.
- **Target detection** from the GPR profile and surrounding regions.
- **Target characterisation** through a bistatic scheme.

Finally, it was described that the effects of the internal scattering are somehow independent of the antenna polarisation, in the sense that its contributions is visible

regardless the antenna orientation, hence there are no preferential directions to follow for the acquisition of the bistatic signatures.

6.4.1 Considerations on dual sensor equipment

Following the considerations of the previous Sections, an efficient way of performing the survey can be employing a combined GPR platform and a metal detector unit. In this way the metal detector can operate as a trigger for a GPR acquisition, taking into account also that there are still many metal mines and just a number of landmines are completely free of it. Therefore, in case of no alarms, the acquisition can be sparser, while once something is found by the MD unit, the GPR system will take control of the process and impose a more dense acquisition. Strictly theoretically, this way of surveying allows both methodology, the 3D imaging and the 2D bistatic, to be accomplished.

The use of an additional sensor as a trigger for the GPR survey could provide at the same time supplementary features that can be a valuable inclusion for the identification and recognition step. In addition, electing the MD rather than the GPR as the trigger for the acquisition also overcome the sampling issue of the radar sensor and the geometrical constraints for the hyperbola formation. Clearly, in situations in which the MD might become inefficient, the hierarchy can be inverted, thus promoting the GPR survey as the principal. In addition, the capability of MD sensors to accurately locate the target center of mass can bring additional advantage in the detection phase.

The great advantage of including the additional MD unit is however compensated by the increasing platform complexity, as a supplemental mounting and/or scanning platform need to be integrated. On a general perspective, there are mainly two possibilities:

- Robotic arm sweeping the terrain, equivalent to the operations carried out by a human operator.
- Multi-channel array, equivalent to the GPR array commonly mounted on vehicles.

Clearly, the effort required by the first option is the electro-mechanical structure that can allow for a precise sweep of the area in front of the platform, while the second solution forces the inclusion of an additional equipment with relevant physical dimensions (order of metres).

6.5 Summary

Conventional methods for demining operations works, but their efficiency and safety should be improved taking advantage of the evolving technology. To facilitate machine-based sensing in place of manual sensing, the intuitive way to ensure a precise area scanning, continuous operations and to allow efficient operations is to employ an autonomous and/or mechanical platform. Given the framework of application and the demanding constraints, the only probable solution is the development of a ground based equipment, due to the described limitations of aerial platforms.

This solution has the advantages of (1) being flexible, as it can be intended also for vehicle mounting, (2) maintaining a size and weight suitable for terrain robotic platforms, and (3) increasing the efficiency in area survey.

In several studies it has been noticed that a large amount of time is spent in surveying non contaminated areas, hence the first addressed feature has been the resources saving when there is no need of, meaning that the acquisition strategy will follow the sparsest scheme as possible in order to ensure the detection of the target.

To achieve the desired bistatic characterisation of the target, starting from the experimental trials experience, an electro-mechanical array is delineated, as the needed signature density almost preclude the use of a fixed system due to elements spacing constraints. This implementation substitutes the two single GPR platforms to maintain a reduced physical size.

The introduction of such a platform in the humanitarian demining market is clearly dependent from the cost of production and development, but it is clear that on a life-time scale consideration, these costs can challenge the current expenses.

Even if representing an acceptable compromise, the only parameter that does not match the current hand-held operations is the sweep velocity, which would be slower (tens of cm/s maximum) employing the designed platform. The reasons for this are mainly related to the motion planning in case of rugged topography and obstacle avoidance.

Finally, the inclusion of an additional sensor, in particular a metal detector unit, might notably increase the performance of the equipment and improve the productivity, clearly with the associated costs of inserting an additional sensor in the platform.

Chapter 7

Conclusions and future work

Collectively we have the knowledge, skill, and resources to achieve it, so let's make future generations proud.

Prince Harry of Wales KCVO, 2017, [309]

This thesis has addressed the challenge of characterising buried targets to enhance the performance of GPR as a landmine detection methodology. A key to improve performance is to identify, understand and extract the features of the landmine radar signature so that a discriminant plane between the landmine and clutter targets can be identified. A discriminant properties is expected to be the presence, in the target radar response, of scattering components that can most likely be attributed to the presence of the detonator and other internal mine structure. This feature can be ascribed only to man-made objects, thus, considering the variety of targets commonly found in a minefield scenario, its presence could be beneficial for removing a number of misleading detections.

A plastic landmine may be characterised by a number of scattering centres, each with its own angular radiation pattern, and therefore a landmine might be in principle considered as a multiple layered dielectric cylinder that interact with each other to produce multiple reflections.

The challenge is therefore to be able to effectively sense these internal reflections to achieve improved discrimination.

The first key aspect is the availability of representative inert landmines for the experimentation. As landmines are objects that are difficult to replicate, and given the research scope, it is essential that properly constructed inert landmines are used

for research and development, otherwise the results could be significantly affected or misleading. The employed devices were complete with all their external and internal components and were filled with a high explosive simulant commonly used to train the UK Ammunition Technical Officers; the substance has the same electrical and chemical properties of commonly employed explosive materials.

The impact that the internal assemblies of the landmine have on the resulting radar signature has been evaluated through a series of experimental campaigns, aiming at (1) confirming the validity of the research question, and (2) evaluating a suitable way to highlight these contributions and improve the efficiency of GPR.

In particular, the aim of this research has been to establish to what extent GPR technique is suitable for providing information on the design and composition of a buried target and the impact that a bistatic strategy may have on the characterisation and identification process. Considering that when a dielectric target is illuminated by an electromagnetic wave, energy is partially transmitted through the target, a variation in the transmitter and receiver separation will illuminate a different internal section of the target, which will scatter the energy accordingly to the features of that particular section. Therefore, it is expected to be able to highlight targets with composite structure and internal assemblies.

The novelty of this work arises from the demonstration of the valuable contribution that the internal structure yields to the radar results and the potential that a bistatic approach shows for target discrimination and identification.

7.1 Summary of findings

Investigation of radar signatures in the form of simulations and measurements has increased the understanding of the scattering mechanisms induced by the internal components of landmines.

The preliminary numerical analysis has shown that, at least theoretically, the presence of internal assemblies can be detected and recognise as an additional scattering contribution. This potential has been investigated considering design parameters (mainly system bandwidth and frequency) that are common to the majority of GPR equipment employed in demining operations to maintain a realistic operational configuration. In addition, the reliability of these scattering events has been tested by

changing both target geometrical properties and soil attenuation characteristics, assessments which have shown that the internal structure information can be retrieved even for deeper targets and in case of unfavourable propagation conditions.

Off the ground targets investigation showed a relatively strong multiple reflections that appears beneath the target space, confirming the outcomes of the numerical simulations and additionally highlight the importance of the relative geometry between the target and the antennas plane not only for the their detection but also for their recognition. This includes the antenna orientation, i.e. polarisation, and target inclination angle. Even if the experimental set up would hardly be suitable for a proper ground survey, as the employed frequencies would allow a very limited soil penetration, the results maintain a certain level of reliability due to a consistent central wavelength to target size ratio and a realistic bandwidth. The only phenomenon that the results did not consider, for obvious reasons, is the absorption due to the propagation in free space. However, for the purpose of this initial investigation the effect could be neglected.

The methodology has been replicated burying the targets in a sharp sand pit and employing a GPR platform already on the market, and the results confirmed what was found in the previous experiments. Effects of soil, even if in controlled conditions, appears as a reduction in the number detectable reflections, as only the prominent one were able to reach the receiver antenna. However, the scattering contributions can be easily identified. Despite the different propagation environments, a high degree of correlation has been achieved.

Analysis of the collected signatures demonstrated that the expected reflections generated by the detonator and other internal mine structure are detectable, thus providing a first hint on the significance that this feature can bear. In addition, as the internal components have their own radiation pattern, a change in the antenna orientation provides a clearer marking of their presence, as a solid dielectric object will show no variations.

A single, mono-dimensional scan, unfortunately, has the limitation of being dependent on the target aspect angle. As well, as landmines may not be perfectly symmetric a bi-dimensional profiles may not be able to properly characterise the internal components. Example of this can be found considering the two employed devices: if for the VS-50 landmine the structure covers the entire target extension, the SB-33 shows

some assemblies located in a precise sector of the landmine. Hence, their detection but especially their characterisation can be unreliable.

A logical step ahead can be increasing the dimensionality of the problem, hence evaluating the imaging performance of a 2D profile. Also in this case the results have shown some improvements, especially for inclined targets (VS-50 example), but they still present the critical limitation of not being able to properly delineate the structure for irregular targets (SB-33 example).

Therefore, a 3D acquisition is needed to extract valuable information on the spatial extent of the internal design of a landmine.

A set of dense and regular 3D GPR acquisition have been carried out, under the same set up of the previous experiments to maintain consistency. The produced images exhibit a very close correlation with the actual design of the investigated targets, confirming the ability of GPR to image and to precisely delineate the internal features of a landmine. In addition, the shortcomings highlighted from the 1D signatures and the 2D profiles are significantly mitigated. The overlay of the radar slices and the photograph of the target further demonstrates this capability. The innovative aspect of this section is that it is possible to produce images closely matched with the physical design of the landmine. To validate these outcomes, a surrogate of the VS-50 landmine has been investigated as well. The surrogate is accurately moulded from the actual landmine but it is substantially a solid explosive, with just a representative metallic inclusion. Furthermore, in comparison with an air gap, a small metal inclusion has a very weak effect on the target response. Therefore, the presence of an air gap notably facilitates the detection of buried plastic cased landmines with GPR.

Although not strictly within the scope of this work, results suggested the use of inert (otherwise known as neutralised) landmines for releasing the potential of GPR of detecting the internal structure of a target.

A discussion on the requirements for a proper 3D imaging has been provided as well, highlighting the demanding constraints on the density, i.e. the maximum affordable sample spacing, and the regularity, i.e. the precision in samples positioning, that the acquisition grid should have. Even if a relaxation is possible, the need for a sub-wavelength sampling still represents an obstacle for an effective employment of 3D methodologies.

This considerations gave birth to the main theme of the thesis, whether a bistatic approach could provide the same level of information but with a lower acquisition effort.

The chosen methodologies for the bistatic acquisition were a common receiver, fixing the receiver and moving the transmitter only, and a common mid point scheme, in which both the transmitter and receiver antenna move away from a common point in opposite direction. With the target located in the common point, both strategies allow to investigate the target internally, layer by layer, with little differences between them. The resulting bistatic signatures clearly show the potential of the approach, as information on the presence of internal assemblies can be extracted, and details on the complexity of such internal design can be easily obtained. Considering the investigated targets and their design, a consistent pattern has been found in case of regular structure (VS-50 example), while a more complex reflections pattern was generated by the irregular device (SB-33 example). This benefit becomes even more important considering that a demanding 3D volume is no longer needed. As before, the corresponding surrogate has been exploited as well to validate the outcomes. Bistatic characterisation has been proposed in the case of an inclined targets, showing robustness and consistency.

Based on the experimental results, a conceptual design of a possible bistatic GPR platform has been provided, highlighting advantages and limitations compared to the actually way of area scanning. In particular, two main aspects have been considered: (1) operator safety, and (2) acquisition efficiency. Clearly, the first aspect is of notable importance given the application and therefore the equipment must allow the the operator to stand in a 100% safe position. This can be achieved by designing an unmanned or a remotely controlled GPR platform, with all the consequences that arise, in terms of cost and complexity. The latter item has been addressed by considering that the landmine density per square metre can be very low, thus the system should save time and resources from non-contaminated areas (which represent the predominant situation). This can be achieved by following the sparsest grid as possible in order to ensure detection. The need for a dense bistatic characterisation logically not only precludes the use of an hand held platform, but also brings the need for electro-mechanical components to simultaneously perform the series of periodic motion. Considerations on a possible MD-GPR sensor combination have been provided as well. The described

architecture represents a suggestion to increase the efficiency, reliability and safety of demining operation where such an infrastructure can be employed.

7.2 Future work

This thesis has resulted in some key achievements summarised in the previous section. However, it has also opened up many possibilities for further work and improvements.

First of all, only three types of landmines have been investigated in this thesis. Even though it would not be practical to exploit all the devices spread around the world, a further step could be to increase its number in the light of a common landmine signature database. A significant advantage for its development might come from the high degree of correlation found between the numerical solutions and experimental trials, features which may suggest that the catalogue development can take advantage of the (ideally) infinite modelling possibilities. It has been found that for a given minefield, the possible number of different landmine models is limited, therefore this information can be used to infer a representative list of high priority targets to extend the work made in this thesis.

Similarly, other variables that strongly influence GPR efficacy are the soil conditions and electromagnetic properties, as GPR detection performance can bounce from optimal to unacceptably low depending on the propagation characteristics of the soil. Further validation of the proposed technique should be carried out in less favourable terrain conditions, in terms of texture homogeneity and absorption coefficients. It has been shown that the scattering contribution of the internal air layer is robust to the lossy attributes of the surrounding medium, thanks to a strong impedance contrast, but this must be verified considering the detection threshold of the system. As indicated for the landmine models, mine contamination has reached a worldwide scale, therefore also for this attribute, a prioritisation of the terrain models should be made.

It has been shown that the detection of internal components is somehow independent of antenna orientation, i.e. they scatter randomly, but only for co-polar configuration, therefore a detailed analysis of the radar signatures in the cross-polarisation domain could bring further indications of the presence of these components. In addition, the acquisition of both cross-polar and co-polar data allows for a fully polarimetric analysis of the target, reducing the number of unknown of the problem and increase the

accuracy of the results.

In this work, two regular geometries have been examined and evaluated. However, separating the transmitter and the receiver, and independently managing their operations can ideally produce an unlimited number of possible combinations. This practically means that there is plenty of space for investigating more complex acquisition geometries and survey methodology. Nevertheless, it must be taken into account that landmines are shallow targets, with a possibly weak RCS and with reduced dimensions. This means that the maximum separation between the antennas is limited, soil absorption included, as well the possibility of deploying elaborated acquisition geometries. The suggested autonomous platform, even if only a conceptual design, is firstly limited by these factors: close proximity to the ground, methodical area sweeping and regular relative geometry between the transmitter(s) and the receiver(s). Unleashing the true potential of a fully independent bistatic and polarimetric GPR system would clearly be of remarkable importance, even if the trade-off between the achievable results and the system complexity would then be a critical argument.

The aim of the work has been focused only to demonstrate the feasibility of determining the nature of a target from its internal structure contribution, therefore, concerning the possible dedicated processing schemes, there are several possible expansion of the work. The use of information on the internal structure of a target has been restricted to characterisation only, using the prior information on the buried target, but significant advantages can be achieved if employed in blind target recognition and identification scheme.

First of all, the majority of the current recognition algorithms are mostly based on the extraction of features related to the physical properties, i.e. dielectric characteristics or geometrical design, without accounting for the contributions from the internal structure. While there are a large number of useful automatic detection schemes for GPR data analysis, robust recognition and identification remain a challenge as the scale of the problem severely impacts the performance of certain features, lowering their discriminant properties. The capability of extracting the scattering contribution generated by the internal structure of a target, instead, it is theoretically independent of the boundary conditions of the problem, therefore representing a robust and valuable feature to rely on.

It has been demonstrated that this landmine feature brings quite a discriminant information on the nature of the target, hence a processing scheme driven by the presence of multiple reflection in the target signature need to be developed to fully exploit this GPR capability. As it has been showed, the potential level of accuracy may lead to identify the landmine model, as each family of landmines can be thought of being characterised by a similar structure. The close correspondence with the optical image further suggests also that a diagram, rather than a number of expensive experimental campaign, can be employed for finding the proper template match. This aspect is particularly important, as robustness of automatic recognition/identification schemes strongly relies on the amount of data available for training and learning, and overcoming the necessity of extensive data acquisition can fasten the development.

Bibliography

[1] Daniels D.J. *Ground Penetrating Radar*. Wiley Online Library, 2005.

[2] Croll M. *The History of Landmines*. Leo Cooper, 1998.

[3] The New York Times. http://www.nytimes.com/2018/03/07/opinion/the-danger-underfoot.html.

[4] United Nations Information Center. http://www.cinu.org.mx/temas/asun_hum/minas.htm.

[5] Vines A. and Thompson H. Beyond the mine ban: Eradicating a lethal legacy. Technical report, Research Institute for the Study of Conflict and Terrorism, London, 1999.

[6] Landmine and Cluster Munition Monitor. http://www.the-monitor.org/.

[7] Wurst J. Ten million tragedies, one step at a time. *Bulletin of the Atomic Scientists*, 49(6):14–21, 1993.

[8] United Nations International Children's Emergency Fund. http://www.unicef.org/press-releases/220000-children-threatened-by-mines-other-explosive-weapons-eastern-ukraine.

[9] Strada G. The horror of land mines. http://www.scientificamerican.com/article/the-horror-of-land-mines/, April 1996.

[10] United Nations. Convention on the prohibition of the use, stockpiling, production and transfer of anti-personnel mines and on their destruction. `http://www.icbl.org/en-gb/the-treaty/treaty-in-detail/treaty-text.aspx`, September 1997.

[11] International Campaign to Ban Landmines. `http://www.icbl.org/`.

[12] Geneva International Centre for Humanitarian Demining. `http://www.gichd.org/resources/publications/`.

[13] Blagden P.M. Kuwait: Mine clearing after iraqi invasion. *Army Quarterly & Defence Journal*, 126(1):4–12, 1996.

[14] International Standards for Humanitarian Mine Clearance Operations. `http://www.un.org/Depts/mine/Standard/glossary.htm`.

[15] Jol H.M. *Ground Penetrating Radar Theory and Applications*. Elsevier Science, 2008.

[16] Bello R. Literature review on landmines and detection methods. *Frontiers in Science*, 3(1):27–42, 2013.

[17] Gonzalez-Huici M.A., Catapano I., and Soldovieri F. A comparative study of gpr reconstruction approaches for landmine detection. *IEEE Journal of Selected Topics in Applied Earth Observations and Remote Sensing*, 7(12):4869–4878, 2014.

[18] Mendez-Rial R., Uschkerat U., Rial F.I., and Gonzalez-Huici M.A. Evaluation of landmine detection performance applying two different algorithms to gpr field data. In *Detection and Sensing of Mines, Explosive Objects, and Obscured Targets XVIII*, volume 8709, pages 8709 – 8709 – 10, 2013.

[19] Slob E., Sato M., and Olhoeft G. Surface and borehole ground-penetrating-radar developments. *GEOPHYSICS*, 75(5):75A103–75A120, 2010.

[20] Watson F.M. *Better imaging for landmine detection: an exploration of 3D full-wave inversion for ground-penetrating radar.* PhD thesis, The University of Manchester, 2016.

[21] Claerbout J.F. *Imaging the Earth's Interior*. Blackwell Publishers, 1985.

[22] Tarantola A. *Inverse problem theory and methods for model parameter estimation*. SIAM, 2005.

[23] Huxley A. *Ends and Means: An Inquiry into the Nature of Ideals*. Harper & Brothers, 1937.

[24] Roberts S. and Williams J. *After the Guns Fall Silent: The Enduring Legacy of Landmines*. Vietnam Veterans of America Foundation, 1995.

[25] New York Times. `http://www.nytimes.com/2017/09/06/world/americas/bangladesh-rohingya-land-mines.html`.

[26] Human Rights Watch. `http://www.hrw.org/news/2017/09/23/burma-landmines-deadly-fleeing-rohingya`.

[27] The Telegraph. `http://www.telegraph.co.uk/news/worldnews/europe/hungary/11867291/Fear-of-landmines-as-Hungarys-iron-curtain-forces-migrants-to-consider-new-routes.html`.

[28] The New York Times. `http://www.nytimes.com/1993/08/09/world/four-us-soldiers-are-killed-by-mine-in-somali-capital.html`.

[29] The New York Times. `http://www.nytimes.com/1993/08/09/world/four-us-soldiers-are-killed-by-mine-in-somali-capital.html`.

[30] Los Angeles Times. `http://www.latimes.com/archives/la-xpm-1992-08-17-mn-5167-story.html`.

[31] ANDMA. `http://www.apminebanconvention.org/fileadmin/APMBC/clearing-mined-areas/art5_extensions/countries/Afghanistan-2012/Afghanistan-ExtRequest-Received29Mar2012.pdf`.

[32] Ejercito Nacional. http://www.ejercito.mil.co/?idcategoria=437712.

[33] Danish Demining Group. http://danishdemininggroup.dk/news/two-national-employees-have-lost-their-lives-in-south-sudan.

[34] United Nations International statistical resources. http://research.un.org/en/mines/statistics.

[35] United Nations Mine Action. http://www.mineaction.org/.

[36] The Irrawaddy. http://www.irrawaddy.com/news/burma/3-civilians-reportedly-killed-landmines-shan-state-june.html.

[37] Reuters. http://www.reuters.com/article/us-colombia-landmines/colombia-aims-to-rid-country-of-landmines-by-2021-govt-idUSKBN15T2FM.

[38] Monin L. *The Devil's Gardens: The Story of Landmines*. Random House, 2011.

[39] History.net. http://www.historynet.com/wars-of-scottish-independence-battle-of-bannockburn.htm.

[40] Croll M. *Landmines in War and Peace: From Their Origin to Present Day*. Pen and Sword Military, 2008.

[41] Davis Waters W. "deception is the art of war": Gabriel j. rains, torpedo specialist of the confederacy. *The North Carolina Historical Review*, 66(1):29–60, 1989.

[42] Smithsonian Magazine. The historic innovation of land mines. http://www.smithsonianmag.com/innovation/historic-innovation-land-minesand-why-weve-struggled-get-rid-them-180962276/.

[43] History.net. http://www.historynet.com/new-art-war.htm.

[44] Sloan C.E.E. *Mine Warfare on Land*. Brassey's Defence, 1986.

[45] Maslen S. *Anti-personnel Mines Under Humanitarian Law: A View from the Vanishing Point*. Clarendon paperbacks. Intersentia, 2001.

[46] William C Schneck. The origins of military mines: Part ii. *Engineer*, 28(3):49–54, 1998.

[47] BBC News. `http://www.bbc.com/news/world-europe-40200305`.

[48] Howell M.L. Scatterable mines. *The Military Engineer*, 69(452):396–399, 1977.

[49] VV.AA. *Issues in Peace and Conflict Studies: Selections From CQ Researcher*. SAGE Publications, 2010.

[50] The Independent. `http://www.independent.co.uk/news/world/europe/landmine-kills-three-children-in-bosnia-279712.html`.

[51] BBC News. `http://www.bbc.com/news/world-latin-america-11980034`.

[52] Physicians for Human Rights. The coward's war: Landmines in cambodia. `https://www.hrw.org/news/1991/09/02/cowards-war-landmines-cambodia`, September 1991.

[53] Williams J. and Ensler E. *My Name Is Jody Williams: A Vermont Girl's Winding Path to the Nobel Peace Prize*. University of California Press, 2013.

[54] NATO Association of Canada. `http://natoassociation.ca/the-ottawa-process-two-decades-later/`.

[55] CNN World News. `http://edition.cnn.com/WORLD/9709/10/diana.angola/`.

[56] BBC News. `http://www.bbc.co.uk/news/special/politics97/news/08/0808/diana.shtml`.

[57] BBC Politics. `http://www.bbc.co.uk/news/special/politics97/news/06/0625/diana.shtml`.

[58] BBC News. http://www.bbc.com/news/uk-england-cumbria-41111012.

[59] CNN World News. http://edition.cnn.com/WORLD/9709/17/land.mines/.

[60] Nobel Prize Official Website. http://www.nobelprize.org/nobel_prizes/peace/laureates/1997/press.html.

[61] International Committee of the Red Cross. http://www.icrc.org/eng/resources/documents/misc/57jnr5.htm.

[62] AP Mine Ban Convention. Status of universalization of the anti-personnel mine ban convention. http://www.apminebanconvention.org/fileadmin/APMBC/MSP/16MSP/President-universalization-EN.pdf.

[63] Human Rights Watch. http://www.hrw.org/news/2017/04/20/yemen-houthi-saleh-forces-using-landmines.

[64] Amnesty International. http://www.amnesty.org/en/latest/news/2017/09/myanmar-army-landmines-along-border-with-bangladesh-pose-deadly-threat-to-fleeing-rohingya/.

[65] Reuters. http://www.reuters.com/article/us-nigeria-security-chad/boko-haram-landmine-kills-four-chadian-soldiers-idUSKCN1120KY.

[66] Bottigliero I. *120 Million Landmines Deployed Worldwide: Fact Or Fiction?* Fondation Pro Victimis, 2000.

[67] James Madison University. Cisr: Munitions reference guide. http://www.jmu.edu/cisr/_pages/research/munitions.shtml.

[68] NATO Standardization Office STANAG 2036. http://nso.nato.int/nso/.

[69] NATO Glossary of Military Terms and Definitions. http://standards.globalspec.com/std/13429635/aap-06.

[70] Lesser I., Arquilla J., Hoffman B., Ronfeldt D.F., and Zanini M. *Countering the New Terrorism*. RAND Corporation, 1999.

[71] Certini G., Scalenghe R., and Woods W.I. The impact of warfare on the soil environment. *Earth-Science Reviews*, 127:1 – 15, 2013.

[72] The Monitor Glossary of Terms. http://www.the-monitor.org/en-gb/the-issues/glossary.aspx.

[73] Habib M.K. Mechanical mine clearance technologies and humanitarian demining: Applicability and effectiveness. In *5th International Symposium on Technology and Mine Problem*, Monterey , CA, USA, 2002.

[74] Prada A.P. and Rodríguez M.C. Demining dogs in Colombia – a review of operational challenges, chemical perspectives, and practical implications. *Science & Justice*, 56(4):269 – 277, 2016.

[75] Bajic M., Ivelja T., Hadzic E., Balta A., Skelac G., and Grujic Z. Impact of flooding on Mine Action in Bosnia and Herzegovina, Croatia, and Serbia. *Journal of Conventional Weapons Destruction*, 19(1):43–49, 2015.

[76] Reuters. http://www.reuters.com/article/us-balkans-flood-landmines/balkan-floods-may-have-undone-years-of-landmine-detection-idUSBREA4J0K220140520.

[77] Geneva International Centre for Humanitarian Demining. http://www.gichd.org/resources/publications/.

[78] Keeley R. Understanding landmines and mine action. http://mit.edu/demining/assignments/understanding-landmines.pdf, September 2003.

[79] Habib M.K. Mine clearance techniques and technologies for effective humanitarian demining. *Journal of Conventional Weapons Destruction*, 6(1):62–65, 2002.

[80] Bruschini C. and Gros B. A survey of research on sensor technology for landmine detection. *Journal of Conventional Weapons Destruction*, 2(1):1–25, 2016.

[81] Schubert H. and Kuznetsov A. *Detection of Explosives and Landmines: Methods and Field Experience*, volume 66. Springer Science & Business Media, 2012.

[82] Daniels D.J. *EM detection of concealed targets*, volume 196. John Wiley & Sons, 2009.

[83] Acheroy M. Mine action: status of sensor technology for close-in and remote detection of anti-personnel mines. *Near Surface Geophysics*, 5(1):43–55, 2007.

[84] Collins L. and Gao P. Hypothesis testing for landmine detection with EMI images. In *IEEE International Conference on Fuzzy Systems Proceedings.*, volume 1, pages 237–240, Anchorage, AK, USA, 1998.

[85] Won I.J., Keiswetter D.A., and Bell T.H. Electromagnetic induction spectroscopy for clearing landmines. *IEEE Transactions on Geoscience and Remote Sensing*, 39(4):703–709, 2001.

[86] Sato M. Principles of mine detection by ground-penetrating radar. In *Anti-personnel Landmine Detection for Humanitarian Demining*, pages 19–26. Springer, 2009.

[87] Daniels D.J. A review of GPR for landmine detection. *Sensing and Imaging*, 7(3):90–123, 2006.

[88] Church P., McFee J.E., Gagnon S., and P P., Wort. Electrical impedance tomographic imaging of buried landmines. *IEEE Transactions on Geoscience and Remote Sensing*, 44(9):2407–2420, 2006.

[89] Metwaly M., El-Qady G., Matsushima J., Szalai S., Al-Arifi N.S.N., and Taha A. Contribution of 3-D electrical resistivity tomography for landmines detection. *Nonlinear Processes in Geophysics*, 15(6):977–986, 2008.

[90] Bowman A.P., Winter E.M., Stocker A.D., and Lucey P.G. Hyperspectral infrared techniques for buried landmine detection. In *2nd International Confer-*

ence on the Detection of Abandoned Land Mines, pages 129–133, Edinburgh, UK, 1998.

[91] McFee J.E., Anger C., Achal S., and Ivanco T. Landmine detection using passive hyperspectral imaging. In *Chemical and Biological Sensing VIII*, pages 655404–655404, 2007.

[92] Martinez P.L., Van Kempen L., Sahli H., and Cabello Ferrer D. Improved thermal analysis of buried landmines. *IEEE Transactions on Geoscience and Remote Sensing*, 42(9):1965–1975, 2004.

[93] Deans J., Gerhard J., and Carter L.J. Analysis of a thermal imaging method for landmine detection, using infrared heating of the sand surface. *Infrared Physics & Technology*, 48(3):202 – 216, 2006.

[94] Sabatier J.M. and Ning X. An investigation of acoustic-to-seismic coupling to detect buried antitank landmines. *IEEE Transactions on Geoscience and Remote Sensing*, 39(6):1146–1154, 2001.

[95] Scott W.R., Schroeder C.T., Martin J.S., and Larson G.D. Use of elastic waves for the detection of buried land mines. In *IEEE International Geoscience and Remote Sensing Symposium*, volume 3, pages 1116–1118, Sydney, Australia, 2001.

[96] Martin J.S., Larson G.D., and Scott Jr W.R. Surface-contacting vibrometers for seismic landmine detection. In *Detection and Remediation Technologies for Mines and Minelike Targets X*, volume 5794, pages 590–601, 2005.

[97] Petculescu A.G. and Sabatier J.M. Doppler ultrasound techniques for landmine detection. In *Detection and Remediation Technologies for Mines and Minelike Targets IX*, volume 5415, pages 30–35, 2004.

[98] Habib M.K. Controlled biological and biomimetic systems for landmine detection. *Biosensors and Bioelectronics*, 23(1):1 – 18, 2007.

[99] Poling A., Weetjens B., Cox C., Beyene N.W., Bach H., and Sully A. Using trained pouched rats to detect landmines: another victory for operant conditioning. *Journal of Applied Behavior Analysis*, 44(2):351–355, 2011.

[100] Steinfeld J.I. and Wormhoudt J. Explosives detection: a challenge for physical chemistry. *Annual Review of Physical Chemistry*, 49(1):203–232, 1998.

[101] Yinon J. Peer reviewed: Detection of explosives by electronic noses. *Analytical Chemistry*, 75(5):98 A–105 A, 2003.

[102] Gudmundson E., Jakobsson A., and Stoica P. NQR-based explosives detection; an overview. In *9th International Symposium on Signals, Circuits and Systems*, pages 1–4, Iasi, Romania, 2009.

[103] Garroway A.N., Buess M.L., Miller J.B., Suits B.H., Hibbs A.D., Barrall G.A., Matthews R., and Burnett L.J. Remote sensing by nuclear quadrupole resonance. *IEEE Transactions on Geoscience and Remote Sensing*, 39(6):1108–1118, 2001.

[104] Datema C.P., Bom V.R., and Van Eijk C.W.E. Landmine detection with the neutron backscattering method. *IEEE Transactions on Nuclear Science*, 48(4):1087–1091, 2001.

[105] McFee J.E., Faust A.A., Andrews H.R., Kovaltchouk V., Clifford E.T., and Ing H. A comparison of fast inorganic scintillators for thermal neutron analysis landmine detection. *IEEE Transactions on Nuclear Science*, 56(3):1584–1592, 2009.

[106] Harding G. X-ray scatter tomography for explosives detection. *Radiation Physics and Chemistry*, 71(3–4):869 – 881, 2004.

[107] Faust A.A., Rothschild R.E., Leblanc P., and McFee J.E. Development of a coded aperture X-ray backscatter imager for explosive device detection. *IEEE Transactions on Nuclear Science*, 56(1):299–307, 2009.

[108] DiFranco J. and Rubin B. *Radar detection*. SciTech Publishing Inc., 2004.

[109] Bach H. Scalable technical survey for improved land-release rates. *Journal of ERW and Mine Action*, 18(1):17–21, 2014.

[110] Bruschini C., Sahli H., Van Kempen L., Schleijpen R., and Den Breejen E. Achievements and bottlenecks in humanitarian demining EU-funded research: final results from the EC-DELVE project. In *Detection and Sensing of Mines, Explosive Objects, and Obscured Targets XIII*, volume 6953, page 69530E, 2008.

[111] Newnham P. and Daniels D.J. Market for advanced humanitarian mine detectors. In *Detection and Remediation Technologies for Mines and Minelike Targets VI*, volume 4394, pages 1213–1225. International Society for Optics and Photonics, 2001.

[112] Soumekh M., Ton T., and Howard P. 3D wavefront image formation for NIITEK GPR. In *Radar Sensor Technology XIII*, volume 7308, pages 73080J–1, 2009.

[113] Daniels D.J., Curtis P., Amin R., and Hunt N. MINEHOUND production development. In *Detection and Remediation Technologies for Mines and Minelike Targets X*, volume 5794, pages 488–495, 2005.

[114] Daniels D.J. and Curtis P. MINEHOUND trials in Cambodia, Bosnia, and Angola. In *Detection and Remediation Technologies for Mines and Minelike Targets XI*, volume 6217, page 62172N, 2006.

[115] Sato M., Fujiwara J., Kido T., and Takahashi K. ALIS evaluation tests in Croatia. In *Detection and Sensing of Mines, Explosive Objects, and Obscured Targets XIV*, volume 7303, page 73031B, 2009.

[116] Cremer F., Schutte K., Schavemaker J.G.M., and Eric E., Den Breejen. A comparison of decision-level sensor-fusion methods for anti-personnel landmine detection. *Information fusion*, 2(3):187–208, 2001.

[117] Frigui H., Zhang L., and Gader P.D. Context-dependent multisensor fusion and its application to land mine detection. *IEEE Transactions on Geoscience and Remote Sensing*, 48(6):2528–2543, 2010.

[118] Doheny R.C., Burke S., Cresci R., Ngan P., Walls R., and Chernoff J. Handheld standoff mine detection system (HSTAMIDS) field evaluation in Namibia. volume 6217, page 62172K, 2006.

[119] Daniels D.J. and Curtis P. MINETECT. In *2nd International Workshop on Advanced Ground Penetrating Radar*, pages 110–114, Delft, Netherlands, 2003.

[120] Daniels D.J., Curtis P., Amin R., and Dittmer J. An affordable humanitarian mine detector. In *Detection and Remediation Technologies for Mines and Minelike Targets IX*, volume 5415, pages 1185–1194, 2004.

[121] Sato M., Fujiwara J., and Kazunori K., Takahashi. The development of the hand-held dual-sensor alis. In *Detection and Remediation Technologies for Mines and Minelike Targets XII*, volume 6553, page 65531C, 2007.

[122] Leimbach G. and Löwy H. Verfahren zur systematischen erforschung des erdinnern grosserer gebiete mittels elektrischer wellen. Patent, DE 237944, Filed on 15 June 1910.

[123] Stern W. Versuch einer elektrodynamischen dickenmessung von gletschereis. *Gerlands Beitrage zur Geophysik*, 27:292–333, 1929.

[124] Waite A.H. and Schmidt S.J. Gross errors in height indication from pulsed radar altimeters operating over thick ice or snow. *Proceedings of the IRE*, 50(6):1515–1520, 1962.

[125] Ciarletti V. A variety of radars designed to explore the hidden structures and properties of the solar system's planets and bodies. *Comptes Rendus Physique*, 17(9):966–975, 2016.

[126] Gene Simmons. The surface electrical properties experiment. 1972.

[127] Conyers L.B. *Interpreting ground-penetrating radar for archaeology*. Routledge, 2016.

[128] Rotter A.J. *Light at the End of the Tunnel: A Vietnam War Anthology*. SR Books, 1999.

[129] Nilsson B. *Two Topics in Electromagnetic Radiation Field Prospecting*. PhD thesis, University of University of Luleå, 1978.

[130] Ruffell A. and McKinley J. *Geoforensics*. John Wiley & Sons, Ltd, 2008.

[131] BBC News. http://news.bbc.co.uk/2/hi/uk_news/1019682.stm.

[132] BBC News. http://news.bbc.co.uk/2/hi/uk_news/7103836.stm.

[133] Benedetto A. and Pajewski L. *Civil engineering applications of ground penetrating radar*. Springer, 2015.

[134] González-Huici M.A., Catapano I., and Soldovieri F. A comparative study of GPR reconstruction approaches for landmine detection. *IEEE Journal of Selected Topics in Applied Earth Observations and Remote Sensing*, 7(12):4869–4878, 2014.

[135] Nuzzo L., Alli G., Guidi R., Cortesi N., Sarri A., and Manacorda G. A new densely-sampled ground penetrating radar array for landmine detection. In *15th International Conference on Ground Penetrating Radar*, pages 969–974, Brussels, Belgium, 2014.

[136] Bruschini C., Gros B., Guerne F., Pièce P.Y., and Carmona O. Ground penetrating radar and imaging metal detector for antipersonnel mine detection. *Journal of Applied Geophysics*, 40(1):59 – 71, 1998.

[137] Webb A., Havens T.C., and Schulz T.J. GPR imaging with mutual intensity. In *Detection and Sensing of Mines, Explosive Objects, and Obscured Targets XXII*, volume 10182, page 101821B, 2017.

[138] Igel J. The small-scale variability of electrical soil properties–influence on GPR measurements. In *12th International Conference on Ground Penetrating Radar*, pages 16–19, Birmingham, UK, 2008.

[139] Nicolaescu I. and Van Genderen P. Performances of a stepped-frequency continuous-wave ground penetrating radar. *Journal of Applied Geophysics*, 82:59 – 67, 2012.

[140] Bleistein N. and Gray S.H. From the hagedoorn imaging technique to kirchhoff migration and inversion. *Geophysical Prospecting*, 49(6):629–643, 2001.

[141] Ton T., Wong D., and Soumekh M. Alaric forward-looking ground penetrating radar system with standoff capability. In *2010 IEEE International Conference on Wireless Information Technology and Systems*, pages 1–4. IEEE, 2010.

[142] Persico R., Leucci G., Matera L., de Giorgi L., Soldovieri F., Cataldo A., Cannazza G., and De Benedetto F. Effect of the height of the observation line on the the diffraction curve in GPR prospecting. *Near Surface Geophysics*, 13(3):243–252, 2015.

[143] Pramudita A.A., Kurniawan A., Suksmono A.B., and Lestari A.A. Effect of antenna dimensions on the antenna footprint in ground penetrating radar applications. *IET Microwaves, Antennas Propagation*, 3(8):1271–1278, 2009.

[144] Diamanti N. and Annan A.P. Characterizing the energy distribution around GPR antennas. *Journal of Applied Geophysics*, 99:83–90, 2013.

[145] Hines M.J., Piers A., Du K., Gonzalez-Valdes B., Martínez-Lorenzo J.Á., and Rappaport C.M. Localization of anti-personnel landmines using multi-bistatic ground-coupled ground penetrating radar. In *Radio Science Meeting (Joint with AP-S Symposium)*, pages 241–241, 2014.

[146] Eide E., Våland P.A., and Sala J. Ground-coupled antenna array for step-frequency GPR. In *15th International Conference on Ground Penetrating Radar*, pages 756–761, Brussels, Belgium, 2014.

[147] Diamanti N. and Annan A.P. Air-launched and ground-coupled GPR data. In *11th European Conference on Antennas and Propagation*, pages 1694–1698, Paris, France, 2017.

[148] Zhang Y., Orfeo D., Burns D., Miller J., Huston D., and Xia T. Buried nonmetallic object detection using bistatic ground penetrating radar with variable antenna elevation angle and height. In *Nondestructive Characterization and Monitoring of Advanced Materials, Aerospace, and Civil Infrastructure*, volume 10169, page 1016908, 2017.

[149] Lopera O., Milisavljević N., and Lambot S. Clutter reduction in GPR measurements for detecting shallow buried landmines: a Colombian case study. *Near Surface Geophysics*, 5(1):57–64, 2007.

[150] Paglieroni D.W., Chambers D.H., Mast J.E., Bond S.W., and Beer N.R. Imaging modes for ground penetrating radar and their relation to detection performance. *IEEE Journal of Selected Topics in Applied Earth Observations and Remote Sensing*, 8(3):1132–1144, 2015.

[151] Bernstein R., Oristaglio M., Miller D.E., and Haldorsen J. Imaging radar maps underground objects in 3-D. *Computer Applications in Power*, 13(3):20–24, 2000.

[152] Grasmueck M. and Weger R. 3D GPR reveals complex internal structure of pleistocene oolitic sandbar. *The Leading Edge*, 21:634–639, 2002.

[153] Lualdi M. and Zanzi L. 2D and 3D experiments to explore the potential benefit of GPR investigations in planning the mining activity of a limestone quarry. In *10th International Conference on Ground Penetrating Radar*, pages 613 – 616, Delft, the Netherlands, 2004.

[154] Lorenzo H., Novo A., Rial F.I., and Solla M. Three dimensional ground-penetrating radar strategies over an indoor archaeological site convent of Santo Domingo (Lugo Spain). *Archaeological Prospecting*, 17:213–222, 2010.

[155] Zhao W.K., Tian G., Wang B.B., Shi Z.J., and Lin J.X. Application of 3D GPR attribute technology in archaeological investigations. *Applied Geophysics*, 9:261–269, 2012.

[156] Groenenboom J., Van der Kruk J., and Zeeman J.H. 3D GPR data acquisition and the influence of positioning errors on image quality. In *63rd EAGE Conference & Exhibition*, pages 1–4, Amsterdam, Netherlands, 2001.

[157] Lualdi M., Zanzi L., and Binda L. Acquisition and processing requirements for high quality 3D reconstructions from GPR investigations. In *International Symposium Non-Destructive Testing in Civil Engineering*, pages 1–13, Berlin, Germany, 2003.

[158] Lehmann F. and Green A.G. Semiautomated georadar data acquisition in three dimensions. *Geophysics*, 64(3):719–731, 1999.

[159] Grasmueck M., Weger R., and Horstmeyer H. How dense is dense enough for a 'real' 3D GPR survey? In *73rd SEG Annual lntemational Meeting*, pages 1180–1183, Dallas, TX, USA, 2003.

[160] Yilmaz Ö. *Seismic Data Analysis*. Society of Exploration Geophysicists, 2001.

[161] Nyquist H. Certain topics in telegraph transmission theory. *Transactions of the American Institute of Electrical Engineers*, 47(2):617–644, 1928.

[162] Doerksen K. Improved optical positioning for GPR-based structure mapping. In *9th International Conference on Ground Penetrating Radar*, pages 503–507, Santa Barbara, CA, USA, 2002.

[163] Sato M., Gaber A., Yokota Y., Grasmueck M., and Marchesini P. Ccd camera and igps tracking of geophysical sensors for visualization of buried explosive devices. In *International Conference on Indoor Positioning and Indoor Navigation*, pages 1–4, Zurich, Switzerland, 2010.

[164] Forte E. and Pipan M. Review of multi-offset GPR applications: Data acquisition, processing and analysis. *Signal Processing*, 132:210 – 220, 2017.

[165] Berard B.B. and Maillol J.M. Multi-offset ground penetrating radar data for improved imaging in areas of lateral complexity — application at a Native American site. *Journal of Applied Geophysics*, 62(2):167 – 177, 2007.

[166] Sule S.D. and Paulson K.S. A comparison of bistatic and multistatic handheld ground penetrating radar (GPR) antenna performance for landmine detection. In *IEEE Radar Conference*, pages 1211–1215, Seattle, WA, USA, 2017.

[167] Diamanti N., Annan A.P., and Redman J.D. Anisotropy effect on gpr signals. In *8th International Workshop on Advanced Ground Penetrating Radar*, pages 1–5, Firenze, Italy, 2015.

[168] Forte E., Dossi M., Pipan M., and Colucci R.R. Velocity analysis from common offset GPR data inversion: theory and application to synthetic and real data. *Geophysical Journal International*, 197(3):1471–1483, 2014.

[169] Lavoué F., Brossier R., Métivier L., Garambois S., and Virieux J. Two-dimensional permittivity and conductivity imaging by full waveform inversion of multioffset GPR data: a frequency-domain quasi-newton approach. *Geophysical Journal International*, 197(1):248–268, 2014.

[170] Roberts R.L. and Daniels J.J. Analysis of GPR polarization phenomena. *Journal of Environmental and Engineering Geophysics*, 1(2):139–157, 1996.

[171] Borghese F., Denti P., Saija R., and Cecchi-Pestellini C. On the polarization and depolarization of the electromagnetic waves. *Journal of Physics: Conference Series*, 6(1):59–72, 2005.

[172] Leckebusch J. Problems and solutions with GPR data interpretation: Depolarization and data continuity. *Archaeological Prospection*, 18(4):303–308, 2011.

[173] Balanis C.A. *Advanced engineering electromagnetics*. John Wiley & Sons, 1989.

[174] Van der Kruk J., Arcone S.A., and Liu L. Fundamental and higher mode inversion of dispersed GPR waves propagating in an ice layer. *IEEE Transactions on Geoscience and Remote Sensing*, 45(8):2483–2491, 2007.

[175] Arcone S.A., Peapples P.R., and Liu L. Propagation of a ground-penetrating radar (GPR) pulse in a thin-surface waveguide. *Geophysics*, 68(6):1922–1933, 2003.

[176] Baker G.S. Applying AVO analysis to GPR data. *Geophysical Research Letters*, 25(3):397–400, 1998.

[177] Skolnik M.I. *Introduction to Radar Systems*. McGraw-Hill Education, 2 edition, 1981.

[178] Boniger U. and Tronicke J. Subsurface utility extraction and characterization: Combining GPR symmetry and polarization attributes. *IEEE Transactions on Geoscience and Remote Sensing*, 50(3):736–746, 2012.

[179] Radzevicius S.J. and Daniels J.J. Ground penetrating radar polarization and scattering from cylinders. *Journal of Applied Geophysics*, 45(2):111 – 125, 2000.

[180] Tsoflias G.P., Van Gestel J.P., Stoffa P.L., Blankenship D.D., and Sen M. Vertical fracture detection by exploiting the polarization properties of ground-penetrating radar signals. *Geophysics*, 69(3):803–810, 2004.

[181] Chi-Chih Chen, Matthew B Higgins, Kevin O'Neill, and Richard Detsch. Ultrawide-bandwidth fully-polarimetric ground penetrating radar classification of subsurface unexploded ordnance. *Geoscience and Remote Sensing, IEEE Transactions on*, 39(6):1221–1230, 2001.

[182] Peichl M., Schreiber E., Heinzel A., and Dill S. Novel imaging radar technology for detection of landmines and other unexploded ordnance. *European Journal for Security Research*, 2(1):23–37, 2017.

[183] Cihlar J.B. and Bray J.R. Radar cross section modeling and measurement of electric detonators. In *IEEE Radar Conference*, pages 1–4, Ottawa, ON, Canada, 2013.

[184] Soldovieri F., Brancaccio A., Leone G., and Pierri R. Shape reconstruction of perfectly conducting objects by multiview experimental data. *IEEE Transactions on Geoscience and Remote Sensing*, 43(1):65–71, 2005.

[185] Giannakis I., Giannopoulos A., and Yarovoy A. Model-based evaluation of signal-to-clutter ratio for landmine detection using ground-penetrating radar. *IEEE Transactions on Geoscience and Remote Sensing*, 54(6):3564–3573, 2016.

[186] Reichman D., Morton K.D., Malof J.M., Collins L.M., and Torrione P.A. Target signature localization in GPR data by jointly estimating and matching templates. In *Detection and Sensing of Mines, Explosive Objects, and Obscured Targets XX*, volume 9454, page 945416, 2015.

[187] Borgatti L., Forte E., Mocnik A., Zambrini R., Cervi F., Martinucci D., Pellegrini F., Pillon S., Prizzon A., and Zamariolo A. Detection and characterization of animal burrows within river embankments by means of coupled remote sensing and geophysical techniques: Lessons from river panaro (northern italy). *Engineering Geology*, 226:277 – 289, 2017.

[188] Webb A., Havens T.C., and Schulz T.J. Spectral diversity for ground clutter mitigation in forward-looking GPR. In *Detection and Sensing of Mines, Explosive Objects, and Obscured Targets XXI*, volume 9823, page 98231M. International Society for Optics and Photonics, 2016.

[189] Metwaly M., Ismail A., and J. Matsushima. Evaluating some factors that affect feasility of using ground penetrating radar for landmine detection. *Applied Geophysics*, 4(3):221–230, 2007.

[190] Asimov I. and Shulman J.A. *Isaac Asimov's Book of Science and Nature Quotations*. Blue Cliff, 1988.

[191] Bucci O.M. and Isernia T. Electromagnetic inverse scattering: Retrievable information and measurement strategies. *Radio Science*, 32(6):2123–2137, 1997.

[192] Tellez O.L.L. and Scheers B. Ground-penetrating radar for close-in mine detection. In *Mine Action-The Research Experience of the Royal Military Academy of Belgium*. InTech, 2017.

[193] McGrath R. *Landmines And Unexploded Ordnance: A Resource Book*. Pluto Press, 2000.

[194] Daniels D.J. An assessment of the fundamental performance of GPR against buried landmines. *Detection and Remediation Technologies for Mines and Minelike Targets XII*, 6553:65530G, 2007.

[195] Savelyev T.G., van Kempen L., Sahli H., Sachs J., and Sato M. Investigation of time-frequency features for GPR landmine discrimination. *IEEE Transactions on Geoscience and Remote Sensing*, 45(1):118–129, 2007.

[196] Savelyev T.G. and Sato M. Optimal GPR bandwidth for time-frequency landmine discrimination. In *Detection and Remediation Technologies for Mines and Minelike Targets X*, volume 5794, pages 435–447, 2005.

[197] Sai B. and Ligthart L.P. GPR phase-based techniques for profiling rough surfaces and detecting small, low-contrast landmines under flat ground. *IEEE Transactions on Geoscience and Remote Sensing*, 42(2):318–326, 2004.

[198] Nasif A.O. and Hintz K.J. Observations on syntactic landmine detection using impulse ground-penetrating radar. In *Detection and Sensing of Mines, Explosive Objects, and Obscured Targets XVI*, volume 8017, page 80171M, 2011.

[199] Schofield J., Daniels D.J., and Hammerton P. A multiple migration and stacking algorithm designed for land mine detection. *IEEE Transactions on Geoscience and Remote Sensing*, 52(11):6983–6988, 2014.

[200] Carevic D., Craig M., and Chant I.J. Modeling GPR echoes from land mines using linear combinations of exponentially damped sinusoids. In *Detection and Remediation Technologies for Mines and Minelike Targets II*, volume 3079, pages 568–581, 1997.

[201] Roth F. *Convolutional Models for Landmine Identification with Ground Penetrating Radar*. PhD thesis, Delft University of Technology, 2005.

[202] Roth F., van Genderen P., and Verhaegen M. Processing and analysis of polarimetric ground penetrating radar landmine signatures. In *2nd International Workshop on Advanced Ground Penetrating Radar*, pages 70–75, Delft, Netherlands, 2003.

[203] Jacob R.W. and Urban T.M. Ground-penetrating radar velocity determination and precision estimates using Common-Midpoint (CMP) collection with hand-picking, semblance analysis and cross-correlation analysis: A case study and tutorial for archaeologists. *Archaeometry*, 58(6):987–1002, 2016.

[204] Booth A.D., Linford N.T., Clark R.A., and Murray T. Three-dimensional, multi-offset ground-penetrating radar imaging of archaeological targets. *Archaeological Prospection*, 15(2):93–112, 2008.

[205] Muller W. Self-correcting pavement layer depth estimates using 3D multi-offset ground penetrating radar (GPR). In *15th International Conference on Ground Penetrating Radar*, pages 887–892, Brussels, Belgium, 2014.

[206] Schennen S., Tronicke J., Wetterich S., Allroggen N., Schwamborn G., and Schirrmeister L. 3D ground-penetrating radar imaging of ice complex deposits in northern east siberia. *Geophysics*, 81(1):WA195–WA202, 2016.

[207] Ojowu Jr O., Wu Y., Li J., and Nguyenb L. SIRE: A MIMO radar for land-mine/IED detection. In *Radar Sensor Technology XVII*, volume 8714, page 87140O, 2013.

[208] Shaw D., Ho K.C., Stone K., Keller J.M., Popescu M., Anderson D.T., Luke R.H., and Burns B. Explosive hazard detection using MIMO forward-looking ground penetrating radar. In *Detection and Sensing of Mines, Explosive Objects, and Obscured Targets XX*, volume 9454, page 94540Z, 2015.

[209] Burkholder R.J., Gupta L.J., and Johnson J.T. Comparison of monostatic and bistatic radar images. *IEEE Antennas and Propagation Magazine*, 45(3):41–50, 2003.

[210] Pauli M., Fischer C., and Wiesbeck W. Mine-detection using a multistatic antenna setup and non-linear inversion. In *10th International Conference on Ground Penetrating Radar*, volume 1, pages 83–85, Delft, The Netherlands, 2004.

[211] Counts T., Gurbuz A.C., Scott W.R., McClellan J.H., and Kangwook K. Multi-static ground-penetrating radar experiments. *IEEE Transactions on Geoscience and Remote Sensing*, 45(8):2544–2553, 2007.

[212] Lloyd D. and Longstaff I.D. Ultra-wideband multistatic SAR for the detection and location of landmines. *IEE Proceedings - Radar, Sonar and Navigation*, 150(3):158–164, 2003.

[213] Kim K., Gurbuz A.C., Scott Jr W.R., and McClellan J.H. A multi-static ground-penetrating radar with an array of resistively loaded vee dipole antennas for

landmine detection. In *Detection and Remediation Technologies for Mines and Minelike Targets X*, volume 5794, pages 495–507, 2005.

[214] Ashtari A., Flores-Tapia D., Thomas G., and Pistorius S. A method for combining focused monostatic and bistatic GPR to reduce multipath effects. In *1st International Workshop on Computational Advances in Multi-Sensor Adaptive Processing*, pages 28–31, Puerto Vallarta, Mexico, 2005.

[215] Jin T., Lou J., and Zhou Z. Extraction of landmine features using a forward-looking ground-penetrating radar with MIMO array. *IEEE Transactions on Geoscience and Remote Sensing*, 50(10):4135–4144, 2012.

[216] Fischer C. and Wiesbeck W. Multistatic GPR for antipersonnel mine detection. In *International Geoscience and Remote Sensing Symposium*, volume 6, pages 2721–2723, Sydney, Australia, 2001.

[217] Fischer C. and Wiesbeck W. Multistatic antenna configurations and image processing for mine-detection GPR. In *3rd Demining Technology Information Forum workshop*, pages 23–24, Ispra, Italy, 2002.

[218] Zeng Z., Li J., Huang L., Feng X., and Liu F. Improving target detection accuracy based on multipolarization MIMO GPR. *IEEE Transactions on Geoscience and Remote Sensing*, 53(1):15–24, 2015.

[219] Dumanian A.J. and C.M. Rappaport. Enhanced detection and classification of buried mines with an uwb multistatic GPR. In *Antennas and Propagation Society International Symposium*, volume 3B, pages 88–91, Washington, DC, USA, 2005.

[220] Fischer C., Herschlein A., Younis M., and Wiesbeck W. Detection of antipersonnel mines by using the factorization method on multistatic ground-penetrating radar measurements. *IEEE Transactions on Geoscience and Remote Sensing*, 45(1):85–92, 2007.

[221] Fischer C., Younis M., and Wiesbeck W. Multistatic antennas and non-linear inversion for mine-detection GPR. In *2nd International Workshop onAdvanced Ground Penetrating Radar*, pages 212–215, Delft, Netherlands, 2003.

[222] Stiles J.M., Apte A.V., and Beh B. A group-theoretic analysis of symmetric target scattering with application to landmine detection. *IEEE Transactions on Geoscience and Remote Sensing*, 40(8):1802–1814, 2002.

[223] Hayashi N. and Sato M. 3D subsurface visualization by suppressing ground reflection and direct wave with bistatic GPR. In *International Geoscience and Remote Sensing Symposium*, pages 4592–4595, Honolulu, HI, USA, 2010.

[224] Hayashi N. and Sato M. Fk filter designs to suppress direct waves for bistatic ground penetrating radar. *IEEE Transactions on Geoscience and Remote Sensing*, 48(3):1433–1444, 2010.

[225] van Zyl J.J., Zebker H.A., and Elachi C. Imaging radar polarization signatures: Theory and observation. *Radio Science*, 22(4):529–543, 1987.

[226] Born M. and Wolf E. *Principles of optics*. Cambridge Univ. Press, 1999.

[227] Deschamps G.A. Techniques for handling elliptically polarized waves with special reference to antennas: Part II - geometrical representation of the polarization of a plane electromagnetic wave. *Proceedings of the IRE*, 39(5):540–544, 1951.

[228] Huynen J.R. *Phenomenological theory of radar targets*. PhD thesis, Delft University of Technology, 1970.

[229] Huynen J.R. Measurement of the target scattering matrix. *Proceedings of the IEEE*, 53(8):936–946, 1965.

[230] Sinclair G. The transmission and reception of elliptically polarized waves. *Proceedings of the IRE*, 38(2):148–151, 1950.

[231] Kennaugh E.M. and Sloan R.W. Effects of type of polarization on echo characteristics. Technical report, DTIC Document, 1952.

[232] Heath G.E. Properties of the linear polarization bistatic scattering matrix. *IEEE Transactions on Antennas and Propagation*, 29(3):523–525, 1981.

[233] Bickel S.H. Some invariant properties of the polarization scattering matrix. *Proceedings of the IEEE*, 53(8):1070–1072, 1965.

[234] Shanmugan K.S., Narayanan V., Frost V.S., Stiles J.A., and Holtzman J.C. Textural features for radar image analysis. *IEEE Transactions on Geoscience and Remote Sensing*, GE-19(3):153–156, 1981.

[235] Ulaby F.T., Kouyate F., Brisco B., and Williams T.H.L. Textural infornation in sar images. *IEEE Transactions on Geoscience and Remote Sensing*, GE-24(2):235–245, 1986.

[236] Copeland J.R. Radar target classification by polarization properties. *Proceedings of the IRE*, 48(7):1290–1296, 1960.

[237] Daniels J.J., Wielopolski L., Radzevicius S., and Bookshar J. 3D GPR polarization analysis for imaging complex objects. In *16th Symposium on the Application of Geophysics to Environmental and Engineering Problems*, pages 1–13, San Antonio, TX, USA, 2003.

[238] Roberts R.L., Daniels J.J., and Peters Jr L. Improved GPR interpretation from analysis of buried target polarization properties. In *Symposium on the Application of Geophysics to Engineering and Environmental Problems*, pages 597–611, Oakbrook, IL, USA, 1992.

[239] Zhao W., Tian G., Forte E., Pipan M., Wang Y., Li X., Shi Z., and Liu H. Advances in GPR data acquisition and analysis for archaeology. *Geophysical Journal International*, 202(1):62–71, 2015.

[240] Radzevicius S.J., Guy E.D., and Daniels J.J. Pitfalls in GPR data interpretation: Differentiating stratigraphy and buried objects from periodic antenna and target effects. *Geophysical Research Letters*, 27(20):3393–3396, 2000.

[241] Radzevicius S.J., Daniels J.J., Guy E.D., and Vendl M.A. Significance of crossed-dipole antennas for high noise environments. In *Symposium on the Application of Geophysics to Environmental and Engineering Problems*, pages 407–413, Washington, DC, USA, 2000.

[242] Guy E.D., Daniels J.J., Radzevicius S.J., and Vendl M.A. Demonstration of using crossed dipole GPR antennae for site characterization. *Geophysical Research Letters*, 26(22):3421–3424, 1999.

[243] Stiles J.M., Parra-Bocaranda P., and Apte A. Detection of object symmetry using bistatic and polarimetric GPR observations. In *Detection and Remediation Technologies for Mines and Minelike Targets IV*, volume 3710, pages 992–1002, 1999.

[244] Chun E.H.Y. and Chun C.S.L. Polarimetric invariants for detection by forward-looking ground penetrating radar. In *IEEE Radar Conference*, pages 185–188, Kansas City, MO, USA, 2011.

[245] Villela A. and Romo J.M. Invariant properties and rotation transformations of the GPR scattering matrix. *Journal of Applied Geophysics*, 90:71–81, 2013.

[246] O'Neill K. Discrimination of uxo in soil using broadband polarimetric GPR backscatter. *IEEE Transactions on Geoscience and Remote Sensing*, 39(2):356–367, 2001.

[247] Alawneh I., Beine C., and Edenhofer P. Calculation of fingerprints of typical antipersonnel landmines by varying the observation point and incidence angles of excitations. In *6th European Conference on Antennas and Propagation*, pages 1068–1071, Prague, Czech Republic, 2012.

[248] Carin L., Kapoor R., and Baum C.E. Polarimetric sar imaging of buried landmines. *IEEE Transactions on Geoscience and Remote Sensing*, 36(6):1985–1988, 1998.

[249] Rosenberg D. and Stephens M. *Use Case Driven Object Modelling with UML. Theory and Practice*. Apress, 2007.

[250] Balanis C.A. *Antenna theory: analysis and design.* John Wiley & Sons, 2005.

[251] Yarovoy A.G., Savelyev T.G., Aubry P.J., and Ligthart L.P. Array-based GPR for shallow subsurface imaging. In *4th International Workshop on Advanced Ground Penetrating Radar*, pages 12–15, June 2007.

[252] Reynolds J.M. *An introduction to applied and environmental geophysics*. John Wiley & Sons, 2011.

[253] Grote K., Crist T., and Nickel C. Experimental estimation of the gpr groundwave sampling depth. *Water Resources Research*, 46(10), 2010.

[254] Topp G.C., Davis J.L., and Annan A.P. Electromagnetic determination of soil water content: Measurements in coaxial transmission lines. *Water Resources Research*, 16(3):574–582, 1980.

[255] Hunt A.G. Continuum percolation theory and archie's law. *Geophysical Research Letters*, 31(19):1–4, 2004.

[256] Friedman S.P. Soil properties influencing apparent electrical conductivity: a review. *Computers and Electronics in Agriculture*, 46(1):45 – 70, 2005.

[257] Peplinski N.R., Ulaby F.T., and Dobson M.C. Dielectric properties of soils in the 0.3-1.3-GHz range. *IEEE Transactions on Geoscience and Remote Sensing*, 33(3):803–807, 1995.

[258] Trang A.H. Simulation of mine detection over dry soil, snow, ice, and water. In *Detection and Remediation Technologies for Mines and Minelike Targets*, pages 430–441, 1996.

[259] Borchers B., Hendrickx J.M.H., Das B.S., and Hong S.H. Enhancing dielectric contrast between land mines and the soil environment by watering: modeling, design, and experimental results. In *Detection and Remediation Technologies for Mines and Minelike Targets V*, pages 993–1000, 2000.

[260] Wang P., Hu Z., Zhao Y., and Li X. Experimental study of soil compaction effects on GPR signals. *Journal of Applied Geophysics*, 126:128 – 137, 2016.

[261] Guillemoteau J., Bano M., and Dujardin J.R. Influence of grain size, shape and compaction on georadar waves: examples of aeolian dunes. *Geophysical Journal International*, 190(3):1455–1463, 2012.

[262] Igel J., Takahashi K., and Preetz H. Electromagnetic soil properties and performance of GPR for landmine detection: How to measure, how to analyse and how to classify? In *6th International Workshop on Advanced Ground Penetrating Radar*, pages 1–6, Aachen, Germany, 2011.

[263] Igel J., Preetz H., Takahashi K., and Loewer M. Landmine and UXO detection using EMI and GPR–limitations due to the influence of the soil. *First Break*, 31(8):43–51, 2013.

[264] Cassidy N.J. A review of practical numerical modelling methods for the advanced interpretation of ground-penetrating radar in near-surface environments. *Near Surface Geophysics*, 5(1):5–21, 2007.

[265] Cai J. and McMechan G.A. Ray-based synthesis of bistatic ground-penetrating radar profiles. *Geophysics*, 60(1):87–96, 1995.

[266] Taflove A. and Hagness S.C. *Computational Electrodynamics: The Finite-Difference Time-Domain Method.* Artech house, 2005.

[267] Dmitry B Avdeev. Three-dimensional electromagnetic modelling and inversion from theory to application. *Surveys in Geophysics*, 26(6):767–799, 2005.

[268] Scheers B., Acheroy M., and Vander Vorst A. Time-domain modeling of uwb gpr and its application to land mine detection. In *Detection and Remediation Technologies for Mines and Minelike Targets V*, volume 4038, pages 1452–1460. International Society for Optics and Photonics, 2000.

[269] Warren C., Sesnic S., Ventura A., Pajewski L., Poljak D., and Giannopoulos A. Comparison of time-domain finite-difference, finite-integration, and integral-equation methods for dipole radiation in half-space environments. *Progress In Electromagnetics Research*, 57:175–183, 2017.

[270] Rodriguez-Hervas B., Flores B.C., Pappu C., von Borries R.F., and Debroux P.S. Testing a transmission line model for homogeneous subsurface media using ground penetrating radar. In *Radar Sensor Technology XVI*, volume 8361, page 836104. International Society for Optics and Photonics, 2012.

[271] Ratto C.R., Morton K.D., Collins L.M., and Torrione P.A. Analysis of linear prediction for soil characterization in gpr data for countermine applications. *Sensing and Imaging*, 15(1):86, 2014.

[272] Harrington R.F. *Field Computation by Moment Methods*. Wiley-IEEE Press, 1993.

[273] Kunz K.S. and Luebbers R.J. *The finite difference time domain method for electromagnetics.* CRC Press, 1993.

[274] Box G.E.P. Robustness in the strategy of scientific model building. In Launer R.L. and Wilkinson G.N., editors, *Robustness in Statistics*, pages 201 – 236. Academic Press, 1979.

[275] Giannopoulos A. *The investigation of Transmission-Line Matrix and Finite-Difference Time-Domain Methods for the Forward Problem of Ground Probing Radar*. PhD thesis, University of York, 1997.

[276] Yee K. Numerical solution of initial boundary value problems involving maxwell's equations in isotropic media. *IEEE Transactions on Antennas and Propagation*, 14(3):302–307, 1966.

[277] Sadiku M.N.O. *Numerical techniques in electromagnetics with MATLAB*. CRC press, 2018.

[278] Courant R., Friedrichs K., and Lewy H. On the partial difference equations of mathematical physics. *IBM Journal of Research and Development*, 11(2):215–234, 1967.

[279] Bérenger J.P. Theoretical investigation of the reflection from impedance absorbing boundary conditions. *IEEE Microwave and Wireless Components Letters*, 28(7):543–545, 2018.

[280] Mur G. Total-field absorbing boundary conditions for the time-domain electromagnetic field equations. *IEEE transactions on electromagnetic compatibility*, 40(2):100–102, 1998.

[281] Bérenger J.P. A historical review of the absorbing boundary conditions for electromagnetics. In *Forum for Electromagnetic Research Methods and Application Technologies*, volume 9, 2015.

[282] Yuan X., Borup D., Wiskin J.W., Berggren M., Eidens R., and Johnson S.A. Formulation and validation of berenger's pml absorbing boundary for the fdtd simulation of acoustic scattering. *IEEE Transactions on Ultrasonics, Ferroelectrics, and Frequency Control*, 44(4):816–822, 1997.

[283] Mur G. Absorbing boundary conditions for the finite-difference approximation of the time-domain electromagnetic-field equations. *IEEE transactions on Electromagnetic Compatibility*, (4):377–382, 1981.

[284] Sankaran K. Are you using the right tools in computational electromagnetics? *Engineering Reports*, 1(3):e12041, 2019.

[285] Warren C., Giannopoulos A., and Giannakis I. gprMax: Open source software to simulate electromagnetic wave propagation for ground penetrating radar. *Computer Physics Communications*, 209:163 – 170, 2016.

[286] Giannopoulos A. Modelling ground penetrating radar by gprMax. *Construction and Building Materials*, 19(10):755 – 762, 2005.

[287] Wang Y. Frequencies of the ricker wavelet. *Geophysics*, 80(2):A31–A37, 2015.

[288] Marsland T.P. and Evans S. Dielectric measurements with an open-ended coaxial probe. *IEE Proceedings on Microwaves, Antennas and Propagation*, 134(4):341–349, 1987.

[289] Database of Demining Accidents. `http://www.ddasonline.com/index.html`.

[290] Doswald-Beck L., Herby P., and Dorais-Slakmon J. Basic facts: the human cost of landmines. Technical report, International Committee of the Red Cross, 1995.

[291] Maathuis B.H.P. and van Genderen J.L. A review of satellite and airborne sensors for remote sensing based detection of minefields and landmines. *International Journal of Remote Sensing*, 25(23):5201–5245, 2004.

[292] Cramer E.A. The mineseeker airship: 'supporting the U.N.'. *Journal of Mine Action*, 5(1):108–113, 2001.

[293] Mineseeker Foundation. http://www.airships.narod.ru/mineseeker/dera.html.

[294] Horizon magazine. http://horizon-magazine.eu/article/how-speed-landmine-clearance.html.

[295] García Fernández M., Álvarez López Y., Arboleya Arboleya A., González Valdés B., Rodríguez Vaqueiro Y., Las-Heras Andrés F., and Pino García A. Synthetic aperture radar imaging system for landmine detection using a ground penetrating radar on board a unmanned aerial vehicle. *IEEE Access*, 6:45100–45112, 2018.

[296] Colorado J., Devia C., Perez M., Mondragon I., Mendez D., and Parra C. Low-altitude autonomous drone navigation for landmine detection purposes. In *2017 International Conference on Unmanned Aircraft Systems (ICUAS)*, pages 540–546, June 2017.

[297] Dorn A.W. Eliminating hidden killers: How can technology help humanitarian demining? *Stability: International Journal of Security and Development*, 8(1), 2019.

[298] Cornelis J. and Sahli H. International conference sheds light on mine action trends and concerns. *Journal of Conventional Weapons Destruction*, 8(1):24, 2004.

[299] Diakonia Lebanon International Humanitarian Law Resource Desk. http://www.diakonia.se/contentassets/710fe542e0e141d38baa1620c429161a/legal-brief_humanitarian-demining-as-a-form-of-humanitarian-assistance-under-ihl.pdf.

[300] Geneva International Centre for Humanitarian Demining. A study of socio-economic approaches to mine action. http://www.gichd.org/fileadmin/GICHD-resources/rec-documents/Socio_Economic_Study_2001.pdf.

[301] Bach H. Mine action technology now and in the future: Is it realistic to expect great leaps forward in technology? *Journal of Conventional Weapons Destruction*, 6(1):12, 2002.

[302] Geneva International Centre for Humanitarian Demining. Manual mine clearance costings and sensitivity analysis. http://www.gichd.org/fileadmin/GICHD-resources/info-documents/Manual-mine-clearance-Aug2005/Manual_Mine_Clearance_Book5.pdf.

[303] Peyton A. and Daniels D.J. http://www.ingenia.org.uk/Ingenia/Articles/2f67b8a4-4fee-4fc2-88d7-f0c535b0dc89.

[304] MacDonald J., Lockwood J.R., McFee J., Altshuler T., and Broach T. Alternatives for landmine detection. Technical report, DTIC Document, 2003.

[305] Fritzsche M. and Löhlein O. Sensor fusion for the detection of landmines. *Subsurface Sensing Technologies and Applications*, 1(2):247–267, 2000.

[306] Daniels D.J., Braunstein J., and Nevard M. Using MINEHOUND in Cambodia and Afghanistan. *Journal of Conventional Weapons Destruction*, 18(2):14, 2015.

[307] Sharma P., Gaba S.P., and Singh D. Study of background subtraction for ground penetrating radar. In *2015 National Conference on Recent Advances in Electronics Computer Engineering (RAECE)*, pages 101–105, Feb 2015.

[308] Cagnoli B. and Ulrych T.J. Singular value decomposition and wavy reflections in ground-penetrating radar images of base surge deposits. *Journal of Applied Geophysics*, 48(3):175 – 182, 2001.

[309] VV. AA. Landmine free world 2015. http://www.landminefree2025.org, April 2017.